Final Report

Save the Earth from Asteroids

DSE Group 1

Delft University of Technology

TU Delft

This page left intentionally blank.

Final Report

Save the Earth from Asteroids

by

DSE Group 1

Name	Abbreviation	Student Number
Anwar-Hameed, Amir	AAH	4452291
Burr, Zachary	ZIB	4659821
Chin A Foeng, Luke	LGTC	4609972
de Lange, Pieter	PDL	4678362
Petit dit de la Roche, Nicolaas	NPDDLR	4556135
Sanders, Andres	AKS	4559142
Stebbins Dahl, Nathaniel	NPSD	4667018
van Eil, Tijn	TVE	4471423
Welzel, Lukas	LLW	4551486

Tutor	Dr. J. Guo
Coaches	Dr. A. Bombelli; ir. C. Jux
Teaching Assistant	C. Immerzeel, MSc

TUDelft Faculty of Aerospace Engineering

AE3200 - Design Synthesis Exercise

January 27, 2021

TU Delft

Contents

Nomenclature

Acronyms

CPC	Compound Parabolic Concentrator
MF	Margin Factor
OAP	Off-Axis Parabolic (Reflector)
ADCS	Attitude Determination and Control System
BER	Bit Error Rate
BWG	Beam-Waveguide
C&DHS	Command and Data Handling System
CA	Close Approach
CAD	Computer Assisted Drafting & Design
CMG	Control Moment Gyroscope
CNC	Computer Numerical Control
COPV	Carbon Fiber Over-wrapped Pressure Vessel
DR	Data Rate
DSN	Deep Space Network
EIRP	Effective Isotropic Radiated Power
EOL	End Of Life
EPS	Electrical Power System
ESA	European Space Agency
EU	Electronic Unit
FAA	Federal Aviation Administration
FEM	Finite Element Methods
FPGA	Field Programmable Gate Array
GNC	Guidance, Navigation & Control
H/K	Housekeeping
HGA	High-Gain Antenna
HPGP	High-Performance Green Propulsion
I/O	Input/Output
LEO	Low Earth Orbit
LGA	Low-Gain Antenna
LV	Launch Vehicle
LVA	Launch Vehicle Adapter
MLI	Multilayer Insulation
MOC	Means Of Compliance
MOID	Minimum Orbit Intersection Distance
MTTF	Mean Time To Failure (MTBF, MTBE)
N	No
NASA	National Aeronautics and Space Administration
NEA	Near Earth Asteroid
OBC	On-Board Computer
OH	Optical Head
PCDU	Power Control and Distribution Unit
PRA	Probabilistic Risk Assessment
QPSK	Quadrature Phase Shift Keying
RCS	Reaction Control System
ROM	Rough Order-of-Magnitude
SI	Solar Irradiance
SSR	Solid-State Recorder
SWOT	Strengths, Weaknesses, Opportunities & Threats
SWOT	Strengths, Weaknesses, Opportunities and Threats
TBD	To Be Determined
TCS	Thermal Control System
TID	Total Ionizing Dose
TM/TC	Telemetry/Telecommand
TT&CS	Telemetry, Tracking and Command System
V&V	Verification & Validation
WBS	Work Breakdown Structure
WFD	Work Flow Diagram
Y	Yes

Greek Symbols

α	Absorptivity	[-]
ϵ	Emissivity	[-]
ϵ	Spacing	$[m]$
η	Viscosity	$[Ns/m^2]$
γ	Incidence angle	$[Rad]$
γ	Isentropic coefficient	$[-]$
λ	Failure rate	$[-]$
λ	Wavelength	$[m]$
Ω	Solid Angle	$[sr]$
Ψ	Lagrange invariant	$[m\ Rad]$
ρ	Density	$[kg/m^3]$

Σ	Surface	$[m^2]$
σ	Resistance	$[\Omega]$
θ	Angle	$[Rad]$
θ_0	Maximum OAP angle of divergence	$[Rad]$
θ_{slew}	Slew angle	$[Rad]$

Latin Symbols

$\bar{u}$	Chief ray angle	$[Rad]$
$\bar{y}$	Chief ray height	$[m]$
ΔV	Change in velocity required for orbital maneuvers	[m/s]
A	Area	$[m^2]$
a	Semi-major axis	$[m]$
B	Bandwidth	$[byte/s]$
b	Semi-minor axis	$[m]$
C	Data capacity	$[byte]$
c	Speed of light in vacuum	$[m/s]$
CF	Compression factor	$[-]$
D	Diameter	[m]
d	Distance	$[m]$
E	Electric field	$[V/m]$
E	Young's Modulus	$[GPa]$
E_b	Energy per bit	$[Ws]$
F	Failure Probability	$[-]$
F	Force	$[N]$
F	True Focal Length	[m]
F	View Factor	$[-]$
f_n	Natural frequency	$[1/s]$
G	Etendue	$[m^2]$
G	Gravitational Constant	$[6.674E-11m^3/kgs^2]$
H	Absolute magnitude	$[W]$
H	True Depth of a Parabolic Reflector	[m]
h	Height	$[m]$
I	Second moment of inertia	$[m^4]$
I_{sp}	Specific Impulse	$[s]$
J	Moment of inertia	$[kgm^2]$
K	Spring constant	$[N/m]$
k	Boltzmann constant	$[1.380649E-23Ws/K]$
L	Length	$[m]$
m	Mass	$[kg]$
N	number (ϵ $\mathbb{N}$)	$[-]$
n	Refractive index	$[-]$
P	Aggregated probabilities	$[-]$
P	Power	$[W]$
p	Probability	$[-]$
P_1	Buckling failure load	$[N]$
Q	Heat flux	$[W/m^2]$
q	Particle charge	$[C]$
R	Radius	[m]
R	Reliability	$[-]$
S	Surface	$[m^2]$
s	Distance	$[m]$
SF	Sustainability Factor	$[-]$
T	Disturbance Force	$[N]$
T	Temperature	$[K]$
t	Thickness	$[m]$
t	Time	$[s]$
T_D	Disturbance torque	$[Nm]$
T_{RW}	Reaction wheel torque	$[Nm]$
u	Marginal ray angle	$[Rad]$
V	Volume	$[m^3]$
v	Speed of light in a medium	$[m/s]$
V_e	Exit velocity	$[m/s]$
W_f	Flux density	$[W/m^2]$
X	Reference length of a polygon	$[-]$
x, y, z	Cartesian coordinates	$[m]$
y	Marginal ray height	$[m]$
g	Acceleration due to Gravity	$[m/s^2]$

Other Symbols

^{T}	Transposes

Summary

This report presents a novel concept for a swarm of solar concentrator satellites for rapid deflection of small asteroids. With 32 satellites each with a 60 $[m]$ radius parabolic reflector, the system will be able to redirect 45% of asteroids $10 - 100$ $[m]$ in diameter which are detected two years before impact. The system is modular and can easily be scaled up by increasing the number of spacecraft, if it is desirable to be able to deflect asteroids larger than 100 $[m]$.

Each satellite will concentrate sunlight on the asteroid, heating it up and sublimating material. The resulting gas jet will produce thrust to redirect the asteroid. The primary reflector concentrates incoming sunlight. This light will be collimated and projected onto a flat secondary reflector. The secondary reflector then aims the beam of concentrated sunlight onto the asteroid. The spacecraft does not expose the primary reflector to the ejecta, preventing its degradation. The secondary reflector will be actively cleaned using an electrodynamic screen to remove ejecta and maintain a high efficiency. This optical arrangement combined with active cleaning is a novel solution to solar concentrator design. This fixes the problem of reflector degradation faced by previous designs. The mirrors themselves will be deployable structures which will be folded up for launch into space.

The system can be stationed in low Earth orbit for up to five years. This removes the need to wait for launch vehicle integration and launch from Earth, enabling redirection within a much shorter period. When a threatening asteroid is detected, the system can begin to intercept immediately. Upon arrival the swarm will be deployed. The reflectors will unfold so the swarm can begin redirection.

Asteroids $10 - 100$ $[m]$ in size have not been discussed much in previous redirection concept research. However, they can still have devastating effects upon impact with Earth. These pose extra risks as they impact more frequently and are more difficult to detect. It is therefore necessary to design a system which can respond to and deflect these asteroids within a short time period. This paper presents one potential solution for this problem. This concept is a completely novel idea for deflection, enables redirection in a shorter period than previous concepts, and represents a new approach to solar concentrator spacecraft design.

1 Executive Overview

This report presents the detailed design of a swarm of solar concentrator spacecraft for asteroid deflection. The report is structured in two main parts. Part I: Project Overview gives information on the mission and the project itself, as well as a brief overview of the high-level characteristics of the spacecraft (such as layout, mass budget, etc.). Then Part II: Detailed Design delves into the design of the spacecraft on a subsystem level, and goes more in depth on some other features of the mission such as budget and sustainability.

This chapter summarizes the most important details of each chapter of the report, and is structured in the same way as the larger report.

1.1 Project Overview

Design Overview

The design makes use of concentrated sunlight to sublimate part of the asteroid. This produces a vapor stream which acts like a thruster on the asteroid. In order to produce sufficient thrust, a large mass flow of vapor has to be sustained. This requires a large heat flux into a small area of the asteroid. This heat flux is archived by a swarm of 32 spacecraft which concentrating sunlight onto the asteroid. The entire swarm is launched and transported to the asteroid with SpaceX Starship.

Each spacecraft is equipped with 3 deployable reflectors:

- A primary reflector which concentrates the light onto the collimator
- A collimator which collimates the incoming concentrated light and reflects this collimated beam onto the secondary reflector. The collimator is shielded by the main reflector
- A secondary reflector which has limited gimbaling capabilities and can be actively cleaned.

The design solves a until now unsolved problem for solar concentrators. Past concepts have a limited lifetime due to reflector degradation from the vapor deposition. This design uses an optical train geometry which only exposes the secondary reflector to the vapor stream. Additionally, the secondary reflector can be actively cleaned using a single-phase electric curtain. This electric curtain limits the degradation of the reflector to 98% at a maximum. Compared to past design which have operational periods between some hours to 10 days the operational period of this design is mainly limited by the overall failure rate of the spacecraft. This is a significant performance increase over past designs.

As the system is a swarm of actively redundant satellites the total failure probability of the system, once at the asteroid is very low. Furthermore, this design can be scaled up or down to respond to different threats.

At end of life the spacecraft can either be safely de-orbited or used to de-orbit space debris before de-orbiting themselves. With this the design can contribute to the different initiative like the the ”Clean Space” initiative of ESA.

Mission Operations

The overall mission profile begins with production of the system, following which it will be integrated into the launch vehicle and launched into space. It will wait in low Earth orbit for up to five years, until a threatening asteroid is detected. At that point, the system will rendezvous with the asteroid and begin deflection. At various stages of the mission, notably production and deployment, robust verification and validation procedures will be employed to ensure everything is running smoothly.

Once the system arrives at the asteroid in question, the system will have to exit the fairings of the Starship and the pallets within which the satellites are located. These satellites would first exit the Starship while still connected together in their pallet configuration through the use of the RCS thrusters already incorporated into the satellites individually. This would avoid the use of a propulsion system incorporated into the support structure

of each pallet.

These satellites are positioned in such a way so as to provide a buffer space between each of them in the case of a required correction thrust on any of them. The satellites are also positioned in this manner so as to prevent the impingement of any one satellite's subsystems on the exhaust of the thrusters of any repositioning satellite surrounding any other satellite. This in turn maximizes the efficiency of the reflectors by preventing any unnecessary residue from forming on any of the surfaces.

Once the pallet is positioned in the correct location, the satellites belonging to said pallet disperse, with the satellites at the top positioning themselves the furthest away from the Starship so as to prevent any impingement issues. This process then continues until the entire system is deployed. After this stage, the satellites unravel their collimator arms, followed by the primary reflector and lastly the secondary reflectors, preventing the creation of large moments in doing so. Contingency plans are in place in the case of a failed start-up of any of the satellites. This results in a drop in the total amount of thrust able to be induced on the asteroid, but would otherwise not cause a loss of the mission due to the modularity of the system. Throughout the mission the satellites will be in communication with each other and the ground station, in case of any errors.

Market Analysis

The mission to save the earth from asteroids is not about creating profit. The mission will still need to work within the forces of the space industry. A mission SWOT analysis, Five Forces analysis and market segmentation were performed in Chapter 6. The strengths and opportunities found in the SWOT analysis aligned well with the driving forces in the market. Buyers and suppliers have very high bargaining power over the industry. The mitigation for these two forces require innovative business models and large investments in vertical integration of the supply chain. The mission strengths that compliment these mitigation strategies are the budget and the clear mission goal as we are not working with the main goal of producing profit.

Porter's Five Forces analysis provided a useful insight into the internal dynamics of the satellite industry. Many of the large incumbents are vulnerable to fast innovation as they have high corporate inertia and have not had fierce competition for many years.

Finally it was identified that the launch mass of the system is only about half the capacity of Starship. The launch vehicle is very much volume limited and not mass limited. However, there are still small spaces between the spacecraft that could be used for CubeSats. This allows for some revenue to be made by opening up the launch to ride-shares. It was also identified that there was a possibility to ride-share to the asteroid. This could provide upwards of $\$100M$ of revenue.

1.2 Detailed Design

Mission Geometry

While the system is waiting for a threatening asteroid to be detected, it will be stationed in low Earth orbit for up to five years. A parking orbit with $0\,\mathrm{deg}$ inclination and an orbital altitude of $900\ [km]$ was chosen. This leaves the spacecraft below the Van Allen radiation belts, so it will not be exposed to a high level of harmful radiation, but also high enough so there will be very little atmospheric drag and no orbital maintenance will be required. In addition, this orbit gives plenty of time for communication with the ground.

From the parking orbit, the system will then transfer to the asteroid. High energy transfers will be used to get to the asteroid in a short time span. However, reaching asteroids with such high energy transfers requires a high amount of ΔV. The best performing current or proposed launch vehicle is the SpaceX Starship, which would be able to give this system a ΔV of $8\ [km/s]$ from low Earth orbit.

With the ΔV goal known it is possible to compute the envelope of possible asteroids that can be reached. A list was compiled of all currently known near-Earth asteroids 10-100 $[m]$ in size, then transfer orbits were calculated and optimized to reach each one one year or half a year before an Earth close approach (CA). This resulted in being able to reach 29.8% of the asteroids at least one year before CA, and a further 18.1% at least half a year before CA.

Mission Implementation

The main function of this system is to produce the concentrated, collimated sunlight beam which sublimates the asteroid. It consists of three reflectors which for its optical train. With a diameter of $120\ [m]$ and an aperture of more than $11000\ [m^2]$ the primary reflector concentrates the incoming sunlight by a factor of 399. The light is then collimated and projected onto the asteroid. Every reflector as well as the supporting structures are deployable. The reflectors consists of a Kapton substrate which is coated by an aluminum layer with a combined thickness of $200\ [\mu m]$. The total reflectively of the reflectors are between 96% and 98% with a total optical efficiency of $\approx 94\%$. Due to the Kapton substrate and the low thickness all reflectors can be towed during launch in a folded configuration.

The optical train is designed to only expose the secondary reflector to the vapor stream. The secondary reflector can be actively cleaned using a single-phase electric curtain which is embedded into the substrate of the reflector. The active cleaning allows the total reflectively of the secondary reflector to remain above 96% even for operational times longer than multiple months.

The deployable support structure is shaped like a an regular polygon. The actuation is driven by constant torque springs. To avoid excess momentum in the system a small electrical motor is used along with a system of cables and pulleys. The main reflector support structure has 162 sides while both the collimator and the secondary reflector supports have 48 sides.

The reflector itself is tensioned using a net on the backside of the reflector. The support is made of either Tungsten of Molybdenum woven into a net. The net must have the correct tension at the correct temperature when the reflector is fully deployed. Otherwise the shape of the reflector will not be correct. The netting is completely supported on the two smaller reflectors but due to the depth of the large reflector it was required to extend the mast out behind the mirror to provide support for the $11\ [m]$ deep mirror.

Attitude Determination and Control System

This subsystem will be able to manage large perturbations through the use of both reaction control wheels and reaction control, monopropellant thrusters. This combination of reaction control systems is easily able to generate maximum torques of $260\ [Nm]$ around the x-axis, $89\ [Nm]$ around the y axis, and $175\ [Nm]$ around the z-axis, allowing for quick rotations in the event of large misalignments. Allowing the system to not waste any time on initially configuring itself for the execution of the mission. However, with large moments come large remnant torques, which stem from the minimum thrust each of these thrusters is able to generate. These reaction wheels are then able to correct these remnant torques, maintaining a maximum error of $0.0755°$, generated while the system is correcting for the residual torque around the z-axis.

An ion engine was also included to mitigate the effects of the gravitational and solar forces that the asteroid and concentrated sunlight would exert on the satellite, respectively. The gravitational force on the satellite was calculated to not exceed $0.00793\ [N]$, which, although quite small, would still cause the satellite to collide with the asteroid after 3.7 hours spent with no corrections made. This force, however, would be negated by the photon pressure force generated on the secondary reflector. This force was found to be $0.135\ [N]$, causing the satellite not only to moving towards the asteroid, but rather away from it. Therefore, the ion engine was incorporated into the design, behind the secondary reflector, to maintain the satellite's position relative to the asteroid. However, this would create a moment, as the gravitational force was assumed to be acting through the center of gravity of the asteroid, and this throttled ion engine creates a difference in forces acting on the secondary reflector. This moment would then be mitigated by the reaction wheel system, with the thrusters dumping the momentum once the reaction wheels become saturated.

Communications and Data Systems

In order to manage the systems onboard the satellite a command and data handling block diagram was constructed showing the connection required in order to relay commands to the subsystems that require commands. Three different control boards were required, those being the H/K board, the TT&C board, and the I/O board. The H/K board would be responsible for the data coming from the heat sensors, structural integrity sensors, tank sensors, ADCS sensors, component statuses, and battery statuses. The TT&C board would be responsible for the transponders and antennas. The I/O board would be responsible for the propulsion valves, the reflector deployment mechanism, the reflector pointing mechanisms, the reflector cooling mechanism, the

reflector cleaning system, the heat pipes and radiators, the reaction wheels, and the solar array pointing mechanism. The data rates required were totaled, resulting in a total 5450 $[bps]$ into the on-board computer (OBC) and a total 90250 $[bps]$ out of the OBC. This computer was selected to be the LEON3FT-RTAX processor used on the Ariane 6 launch vehicle and is developed by Aeroflex Gaisler. This processor is immune to the effects of radiation and can handle speeds of up to 20 $[MIPS]$. A solid-state recorder was selected to be the Basic Airbus DS Solid-State Recorder, with a preference to having the flash memory option. The data bus was selected to be the SpaceWire which was designed for ESA applications, and can support data rates of up to 400 Mb/s and is a highly reliable bus, and is also fully compatible with the OBC and SSR selected previously.

The telemetry, tracking and command system was also sized, with two hemispherical antennas being chosen to be placed on opposite ends of the bus. However, during the transfer period, the system will make use of the Starship's communication system. The ground stations were selected to be the REdu-1 Antenna operated by ESA, and the DSN Madrid BWG operated by NASA. A high gain and low gain antenna were selected for use once the system reached its destination. The low gain antenna was sized to be 0.052 $[m]$ in diameter, with a bandwidth of 126438 $[Hz]$ with a data rate of 12797 $[bps]$ while in a parking orbit, while the high gain antenna was sized to be 3.86 $[m]$ as it would require a capacity of 50575 $[bps]$ and a bandwidth of 126438 $[Hz]$.

The total mass of the telemetry, tracking and command system was found to be 26.7 $[kg]$, requiring a total volume of 246 $[L]$, with only 9.6 $[L]$ of that required within the space bus. This system would also consume a total of 28 $[W]$.

Electrical Power System

The electrical power system was sized in accordance with the needs of the subsystems. This system was sized with the total 5.425 $[kW]$ of power required for the entire system in mind. After conducting a brief trade-off, a solar array was selected to be the power source due to the collapsability and weight of the panels required. These panels were sized to be 20 $[m^2]$ which included a safety margin of 25%. These solar panels were to be arranged in a 10 2x1 $[m]$ configuration in strings of 75 $[V]$. After these panels were sized, their total mass came out to be 82 $[kg]$.
Calculations were conducted that would require a total energy storage potential of around $850,000$ $[J]$. Due to this large energy storage requirement, lithium-ion batteries were to be used, resulting in the total mass of the batteries coming out to be 10.3 $[kg]$. These batteries would drop 3% in storage every month, which would result in a total reduction of capacity of 43% over the course of 1.5 years.

A power control and distribution unit is also included in the report to manage the supply of power to the different subsystems. This required an off-the-shelf product to be selected in order to meet the demands of the system. Since the system was considered as having a medium power level, the Medium Power from Thales Alenia was selected. This system added an extra 10.45 $[kg]$ to the total mass of the electrical power system.

Thermal Control System

The thermal control system must monitor and regulate the temperatures of the other subsystems included in the system, since the subsystems would experience both extremely high and extremely low temperatures in space. The surviving and operational temperature ranges for each of the subsystems was determined, with the reflectors and collimator being able to operate in maximum temperatures of up to 673 $[K]$. The power control and distribution unit had the lowest operation temperature range, only being able to tolerate maximum temperatures of up to 308 $[K]$. Ultimately the thermal control system required the ability to reduce the emissivity of the bus, as well as a heat source in order to keep the systems cool. In order to retain heat, the use of multilayer insulation blankets was required, commonly used in the space industry. Ten patch heaters were also required in order to maintain a certain temperature within the bus. These space heaters would maintain an operation temperature of 280 $[K]$, would weigh a total of 9.74 $[kg]$, and would consume a total of 86.4 $[W]$.

Structures

The structures of the spacecraft were analyzed under the various load cases to ensure that they are strong enough to withstand the loading. The critical load cases and parts where determined, then analyzed with a combination of analytical and finite element methods. The structures were analyzed for both the deployed and undeployed configurations of the spacecraft. The result was that the structures are deemed to be strong enough to withstand the loads that will be place on them during the operation of this mission.

In addition the bus of the spacecraft was sized. This will contain the batteries, reaction wheels, computers, etc. of the spacecraft. The sizing was done by listing all the components that need to fit inside the bus, and placing them all within 3D space. Then a central support column was designed, which will be able to withstand the loads during launch and transfer them to the rest of the structures. The result is a bus which is $1.2\ [m]$ in diameter and $1\ [m]$ in height, with a roughly conical shape. The shell of the bus will be made of aluminum, and the central support, which is $0.15\ [m]$ in diameter, is constructed out of Kevlar-49.

Risk Engineering

Technical risk of the space segment was assessed using probabilistic risk assessment. The total probability of mission failure due to spacecraft failure is below 0.4% with a certainty of more than 99.6%. The mission failure probability of the space segment depends heavily on the performance of the launch vehicle (Starship) and is conservatively estimated to be below 3.41%. This risk is acceptable.

Satellite Production

Producing 32 satellites reliably and cost effectively requires the strategic use of automation and hands on production. The deployable structures have hundred of repeating parts and can make good use of production level automation such as computer numerically controlled machining. The reflectors on the other hand will only need to be made 32 two time which can be a lot more labor intensive.

For further analysis parts were split into three categories. High volume components, low volume components and commercially available components. Key features about the production process are identified for each. Finally a serialized production process is provided similar to what is seen on large aircraft production lines.

Cost Analysis

For the cost analysis of this mission, further research was done for the costs of recurring and non-recurring events. Material and labor costs for the production of the spacecraft are considered to be the recurring costs. Other costs, such as costs for research and development, testing and launch were considered to be non-recurring costs. Next to that, a budget for any contingencies was accounted for.

Summed up, the total cost for all recurring costs was estimated to be $€156M$. The non-recurring costs were estimated to be $€533M$. Lastly, the total budget for contingencies was assumed to be $€207M$. In total, a mission cost of $€896M$ was estimated.

Sustainability Engineering

The sustainability of this project and mission, as a whole, reflect on four pillars: Human, Social, Environmental and Economic. Both Human and Social correlate with the teamwork environment, the applicability of new technology and the desire to work harmoniously with the goal of developing strong alliances as a species, which in turn will benefit future generations. On a mission level, the development of such a novel system can easily deplete resources if left unchecked. Therefore a sustainability analysis is performed on the selected system materials as well as chosen propellants. Furthermore, with the rapid development of more sustainable Launcher Systems, the level of care which can be placed on a sustainable mission approach is possible. Beyond the initial phases, due to the time-frame of this mission, the sustainability approach can be applied throughout all phases, such as the Ground Segment. This can have a crucial impact on the surrounding environments, therefore choices related to this must be taken with care.

In total, during the production of each of the satellite's subsystems, a total of 419037.4 $[kg]$ of CO_2 was used, with the ADCS subsystems contributing the largest amount of CO_2 emissions due to the production of the xenon gas used to propel the ion engine. The propellant LMP-103S was used as a replacement for hydrazine due to hydrazine's noxious qualities. This new green propellant is also more energy dense than hydrazine leading to it becoming the obvious choice for RCS thruster propellant. Launchers were also compared, even though a launch provider was already decided on due to size constraints. Even having already chosen a launch provider, the Starship still ends up being more sustainable than the other launchers when looking at the launch costs and propellant mass required per payload mass. As for the ground segment, Boca Chica was chosen due to its proximity to the equator requiring less propellant to be burned to achieve orbit. After a successful FAA Environmental Assessment, the Starship can beginning launching from this site. If this assessment does not work, the Kennedy Space Center would have to be made use of, where they make use of carbon-neutral facilities, a

1 $[MW]$ photo-voltaic system and electric personal transport vehicles.

The sustainability goals that were set up in the Baseline Report were all but four achieved. This resulted in a total sustainability factor of 0.844, a higher value than was initially expected in the Midterm Report. Therefore, the team has done a good job throughout the design to incorporate the four pillars of sustainability

Performance Analysis

To confirm whether the system is indeed capable of deflecting asteroids as per requirements **AD-SH-PFM-1** and **AD-SH-RISK-1** performance analysis was carried out. It should be noted that asteroids vary greatly in both composition and orbit making it extremely difficult to say anything definitive about the effectiveness of deflection of a yet unknown asteroid. Nevertheless, the system was tested against a collection of just under a thousand known asteroids that would hopefully be similar to our target asteroid so to find an indication of the chance of a successful deflection. Assumptions had to be made for the asteroids albedo and density, the assumptions made are purposefully limiting as to get a worst case estimate.

Each asteroid in the envelope was simulated using the solar system model developed for this purpose, information on this model can be found in the midterm [4]. The simulation was ran three times for each asteroid, simulating an undeflected case, a case where the system's force was applied along the velocity vector of the asteroids thus speeding it up and a case where the system's force was applied along the velocity vector of the asteroids thus slowing it down. The greatest difference in closest approach with Earth compared to the undeflected case was taken as the deflection the system can deliver onto the asteroid. The system was able to deflect at least 97% of the asteroids at least one Earth radius and 83% of the asteroids at least ten Earth radii, some asteroids were deflected far greater amounts. Actual percentages could be higher due to an underestimation of the deflection caused by the asteroid returning closer to Earth at a later date however to confirm this each asteroid must be looked at at an individual basis.

Additionally an effort was made to get a general idea of what type of asteroids are most suitable for deflection. Unsurprisingly the size of the asteroids had a large impact on their deflection. Asteroids with a high absolute magnitude, and thus small size, were usually deflected far further. Asteroids with an Earth like semi-major axis and to a lesser degree a low eccentricity are also more suitable for deflection. These are however extremely general trends barely suitable as 'rule of thumb' and actual deflection can vary greatly depending on the individual asteroid.

I

Project Overview

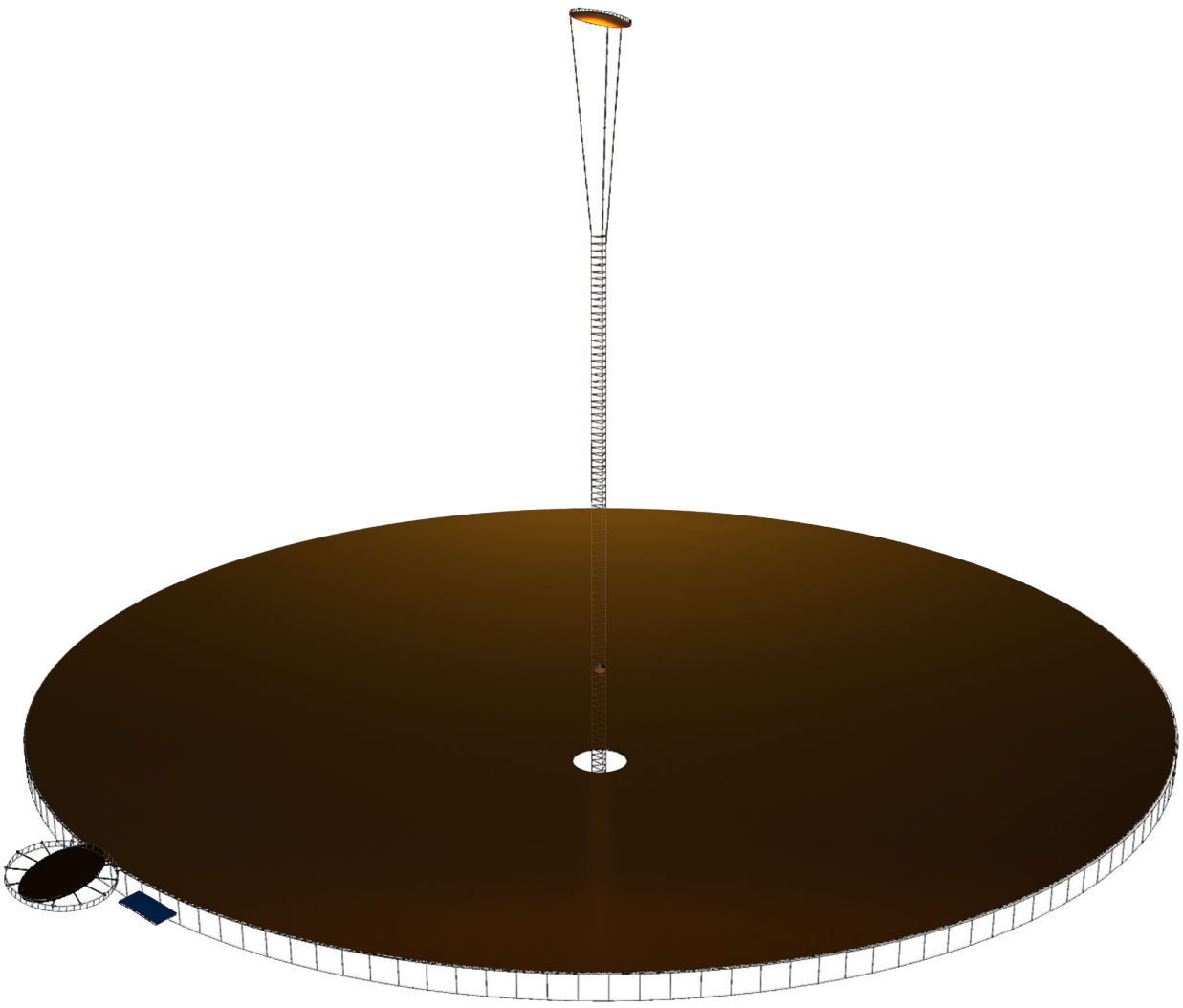

2 Project Objectives

Asteroid impacts pose a substantial threat to the Earth and the people on it. Asteroids of several kilometers can cause full scale extinction events, and even asteroids of only tens to hundreds of meters can cause a great amount of damage and loss of life. These smaller asteroids pose a particular challenge as they are difficult to detect, and consequently do not give an advanced warning before a potential collision. It is of importance for programs to be put in place to keep the Earth safe from such threats. [37]

This DSE team aims to fulfill part of that need and help protect the Earth from such asteroids. As such, the team has defined the following Mission Need Statement:

"Provide a system which can deflect asteroids that are an imminent threat to the Earth."

Following from this Mission Need Statement, the Project Objective Statement has also been defined:

"Design a deflection system for asteroids up to $\mathbf{100}$ $[\mathbf{m}]$ ***in any dimension, within ten weeks by nine students, with the goal of preventing collisions with the Earth."***

Following the trade-off in the previous phase of the design a swarm of solar concentrator satellites was chosen to be used for redirecting asteroids [4]. This report goes over the final detailed design of this system. Here the exact details of how such a system could be constructed are investigated. In this way the Project Objective Statement will finally be fulfilled by presenting the design of the deflection system. Following from this detailed design, the system could be manufactured and begin redirecting real asteroids, thus fulfilling the Mission Need Statement as well.

3 Requirements

This chapter presents the stakeholder requirements in Table 3.1 and the performance requirement in Table 3.2. For both, the means of compliance (MOC) is given, as well as whether or not the system meets the requirement (shown with Yes (Y), No (N) or To Be Determined (TBD)). Requirements for specific subsystems will be listed and analyzed in the respective chapter of that subsystem. All the stakeholder requirements are met by the chosen design. From the user requirements, all are met by this system except one: requirement AD-PFM-4 is not applicable anymore as no assembly will be required in space.

Table 3.1: Stakeholder Performance Requirements

Identifier	Requirement	MOC	Compliance
AD-SH-PFM-1	The system shall be able to deflect an asteroid of a size up to 100 meters in any dimension.	Analysis	Y
AD-SH-PFM-1.1	The system shall be able to raise the closest approach of the asteroid by no less than $10\ 000\ [km]$ with at least 3 σ confidence	Analysis	Y
AD-SH-PFM-1.2	The system shall decrease the probability of impact below 2%.	Analysis	Y
AD-SH-PFM-2	The system shall prevent an asteroid collision trajectory with the Earth.	Analysis	Y
AD-SH-PFM-3a	The redirection period shall be two years.	Analysis	Y
AD-SH-PFM-4	The system shall be able to operate in space for at least five years.	Analysis	Y
AD-SH-PFM-5	The system shall be ready for asteroid redirection missions before November 2030.	Analysis	Y
AD-SH-PFM-6	The system shall be able to perform a controlled deorbit maneuver such that no debris land outside a determined area of $1000\ [km]$ radius on Earth.	Analysis & Inspection	Y
AD-SH-PFM-7	The system shall be able to communicate using NOAA ground stations.	Inspection	Y
AD-SH-PFM-8	The system shall not make use of explosives as its primary deflection or destruction method.	Inspection	Y

Table 3.2: Performance Requirements

Identifier	Requirement	MOC	Compliance
AD-PFM-1	The system shall be able maintain its parking orbit during its operational lifetime.	Analysis	Y
AD-PFM-2.1	The system shall be able to dodge space junk during its operational lifetime.	Analysis	Y
AD-PFM-3	The system shall be maintainable for its operational lifetime.	Inspection	Y
AD-PFM-4	Individually launched system components shall be assembled in orbit.	Not applicable	Not applicable
AD-PFM-5	The system shall be able to deflect asteroids with a mass of at least $42\ 000\ 000\ [kg]$.	Analysis	Y
AD-PFM-7.1	The system shall be able to report on its health.	Inspection	Y
AD-PFM-7.2	Each subsystem shall be able to report on its health.	Inspection	Y

4 Design Overview

This chapter gives an overview of the previous, preliminary phase of the design and explains the approach to the current phase of the design. Section 4.1 goes over the preceding phase of the project, where a trade-off was performed to determine the steps to be taken towards the final design. Then in Section 4.2, a brief explanation will be given of the design that was chosen and that will be further explained in detail in the rest of this report. Finally, the details of how the group approached the detailed design phase will be given in Section 4.3.

4.1 Trade-off Summary

In the previous phase of the design, a trade-off was performed to determine the method of asteroid deflection that would be used for the final design. This section will detail the different concepts investigated, the process used for the trade-off and the outcome.

4.1.1 Concepts

For the trade-off, three main groups of concepts were analyzed: pusher concepts, which attach directly to the asteroid and impart force over time; impactors, which collide with the asteroid and impart momentum; and heater concepts, which heat up the asteroid and produce thrust by sublimating material. Each group is briefly explained below. For more in depth analysis of all the concepts, the reader is referred to the Midterm Report. [4]

Pusher Concepts

The pusher concepts are those which attach directly to the asteroid and produce thrust, thereby ”pushing” the asteroid. Two main methods were identified for this group: attaching an engine (ion or chemical) to the asteroid and attaching mass drivers to the asteroid, which produce thrust by drilling into the asteroid and propelling pieces of it away. The mass driver concept was identified as being more feasible as the engine(s) would require too much propellant.

Impactor Concepts

Impactors directly impact the asteroid and impart momentum to change its orbit. To get the maximum amount of force a high relative velocity and a high spacecraft mass are needed. Toward that end, there are multiple methods of acquiring the large mass required. Classic kinetic impactors bring as much mass into orbit from launch, however, this is expensive as it requires a large amount of propellant to launch a large amount of mass into orbit. Enhanced kinetic impactors aim to collect extra mass in space, either by collecting defunct satellites or space debris in Earth orbit, or by grabbing other small NEAs. All of these options were considered for the Midterm Report, however gaining mass by collecting small NEAs was deemed the best.

Heater Concepts

Heater concepts aim to heat the asteroid and sublimate material on it, producing thrust. There are two main ways to go about heating the asteroid: with lasers and with solar concentrators. Lasers are high energy beams which could be aimed at the asteroid. However, too much energy is required for powerful enough lasers to sufficiently heat the asteroid, so lasers were decided to not be an option. Solar concentrators work by using large mirrors to focus sunlight on the asteroid. Several spacecraft can be used to further increase the amount of sunlight focused on the asteroid.

4.1.2 Trade-off Methodology

Five trade-off criteria were identified to compare the concepts. The criteria and their relative weights are given in Table 4.1. These weights were determined via an analytical hierarchy process, whereby several team members and knowledgeable outsiders ranked the criteria relative to each other.

Table 4.1: Trade-off criteria with their respective weights.

Criteria	Explanation	Weight
Risk	Chance of loss of mission	40.5%
CA Ratio	How much the asteroid is deflected by (deflected CA distance/undeflected CA distance)	38.8%
System Efficiency	Total ΔV supplied to an asteroid divided by total system mass	9.7%
Sustainability	How well the system meets the sustainability goals (see [3])	5.6%
Cost	Whether the mission is under the €1 billion Euro budget (per **AD-SH-CST-01**)	5.3%

The mass driver, enhanced kinetic impactor, and solar concentrator were all evaluated on these criteria. Then the potential options were weighed against each other. Sensitivity analysis was performed on the trade-off by systematically varying the weights of the various criteria, as well as the values for each of the specific concepts. This was done with normal distributions based on the uncertainties for the values. The trade-off was run 100,000 times with these varying weights and values.

4.1.3 Trade-off Result

The result of the trade-off was that the solar concentrator design won in 100% of the trade-offs. This is due to the fact that it can impart the largest force to the asteroid and has a low risk because of the large number of spacecraft. The only variation was between different versions of the solar concentrator concept: a concept with a swarm of 18 spacecraft won in 10% of the trade-offs, and a concept with a swarm of 43 spacecraft won 90% of the time. It can be determined with a high level of confidence that the solar concentrator is the best concept for this mission.

Therefore the solar concentrator was selected to be designed in the detailed design phase, which is outlined in this report. Further iteration on the exact number of spacecraft in the swarm was performed during the detailed design. For a more in-depth explanation of the trade-off process, the reader is referred to the Midterm Report. [4]

4.2 Overview of Chosen Design

4.2.1 Concept Description

The selected concept uses a method in which an area of the the asteroid is heated, evaporating the material. This evaporation will produce a thrust similar to a hot-gas thruster so that the asteroid will experience an acceleration [47]. For an in-depth explanation and analysis of this method the reader is referred to the Midterm Report. [4]

The concept consists of a swarm of 32 solar concentrator spacecraft, each equipped with a primary reflector with a radius of 60 $[m]$. The number of spacecraft was reduced following the trade-off, as the amount of force produced by 43 spacecraft was significantly larger than needed and the 43 spacecraft could not fit in a launcher together. The incident flux is concentrated and redirected towards the asteroid. All spacecraft focus on the same point of the asteroid. Existing concepts have a limited lifetime due to the degradation of their reflectors [47]. The proposed design solves this problem by angling the main reflector away from the asteroid and actively cleaning the reflector which faces towards the asteroid. This is a novel solution.

The optical train of the spacecraft consists of:

- A primary reflector which concentrates the light onto the collimator.
- A collimator which collimates the incoming concentrated light and reflects this collimated beam onto the secondary reflector. The collimator is shielded by the main reflector.
- A secondary reflector which has limited gimbaling capabilities and can be actively cleaned.

4.2.2 System interface chart

The individual subsystems present within the spacecraft are all linked to each other. In order to do a proper design, it should be clear what information a certain system needs from another system and vice-versa. In order to obtain a clear overview of this, the N2-chart presented in Figure 4.1 has been created before the start of the detailed design phase. In this way, each team member was aware of the information he had to gather in order to start designing his subsystem.

Mission geometry		Delta-V Budget	Day/Night in orbit, solar flux, orbital inclination	Mission geometry			Spacecraft distance	Earth distance
	ADCS / GNC	Position vectors	Power req. gimballing, operational temp.	Repositioning / Station keeping, pointing		Applied attitude correction vector	Applied attitude correction	S/C attitude data
Thrust	Thrust vectors	**Propulsion**	Operational temperature			Applied thrust vector	Available proplusion	Propulsion data
			Power & Thermal	Thermal control				Power input, power system data
Recquired positioning	Hot spot, photon pressure			**Mission implementation**				Deployment data, system data
					Instrumentation			Sensor data
	Provide connection	Connection points		Mounting, vibration, stability		**Structures**		Structural integrity data
							Ground segment & operations	Ground communication & data
Geometry comms	S/C attitude comms	Propulsion feedback comms	Power feedback comms	Deployment commands			S/C communication & data	**Comms & Data**

Figure 4.1: N2-chart of the subsystem interface relations.

On the diagonals, all individual subsystems are presented along with the sensors. On the verticals, the inputs to the subsystems are given, so for example for the propulsion subsystem, the delta-V budget is necessary for its sizing. Along the horizontals, the output of the subsystems are given, the ADCS for example provides information on the applied attitude correction to the ground station. With this chart, the detailed design of the individual subsystems could be started.

4.2.3 Layout

System Reference Frame

In order to generate the positions of all of the subsystems as well as the moments and forces generated by the attitude determination and control system, a coordinate system was agreed upon.

This coordinate system was required to be fixed as this would mitigate the propagation of errors throughout the design of the subsystems. This automatically removed the center of gravity position from the list of possible origins due to its constantly shifting location as the systems were being sized. This left either a location on the exterior circumference of the primary reflector, or on either end of the collimator arm. Since the primary reflector was circular in nature, it was deemed to be too confusing on where to position the origin were it to

be decided that it would be positioned on the circumference. This left only the ends of the collimator arm as possible locations. Since the collimator at the end of the collimator arm was still being sized, the opposite end of this arm was selected, particularly the center of area of the cross section of the arm, due to its unchanging position as the design was iterated upon. This coordinate system is shown in Figure 4.2, where the long grey beam is the collimator arm, the small yellow bar being the collimator.

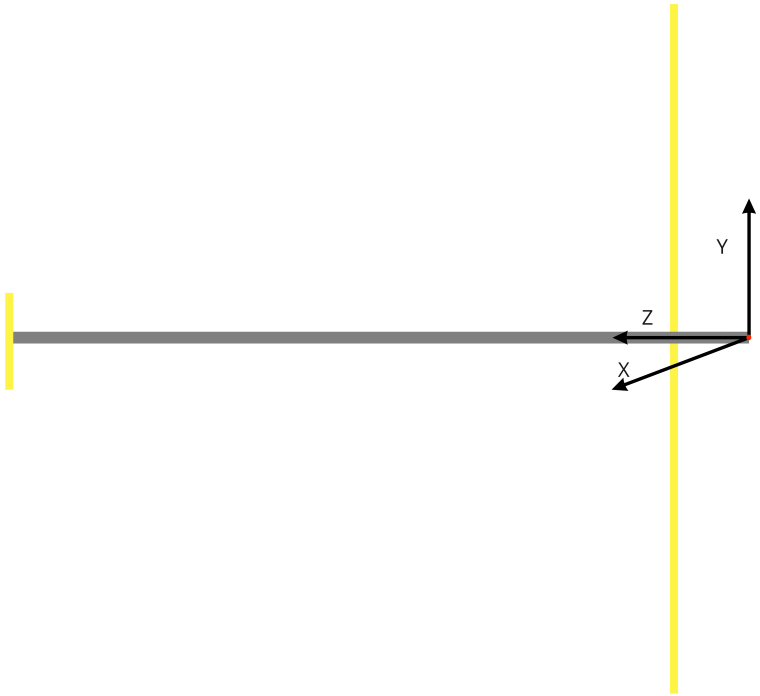

Figure 4.2: The location of the origin and the selected coordinate system to go along with it.

External Layout

The system as a whole consists of a primary reflector, a secondary reflector, a collimator, the bus, solar panel, as well as several thruster blocks located on the exterior of the satellite. The locations of these external systems are shown in Figure 4.3.

Internal Layout

The internal layout comprises of the bus structure and the necessary subsystems which must be housed inside. The details of the bus structure design will be presented in Section 13.2. As for the individual subsystems, they are discussed in the detailed design segment, along with the sizing of each subsystem (which is also summarized in Section 13.2).

Figures 4.4, 4.5 & 4.6 show a visual representation of the bus design. There are various approaches to choosing a bus interior; in this case, a shelf design was chosen to accommodate for the subsystems which interact with one-another. Figure 4.5 houses the ADCS subsystems and the Power subsystems. The upper shelf, as shown in Figure 4.6, houses the TT&C subsystems due to their need to interact with external components of the system.

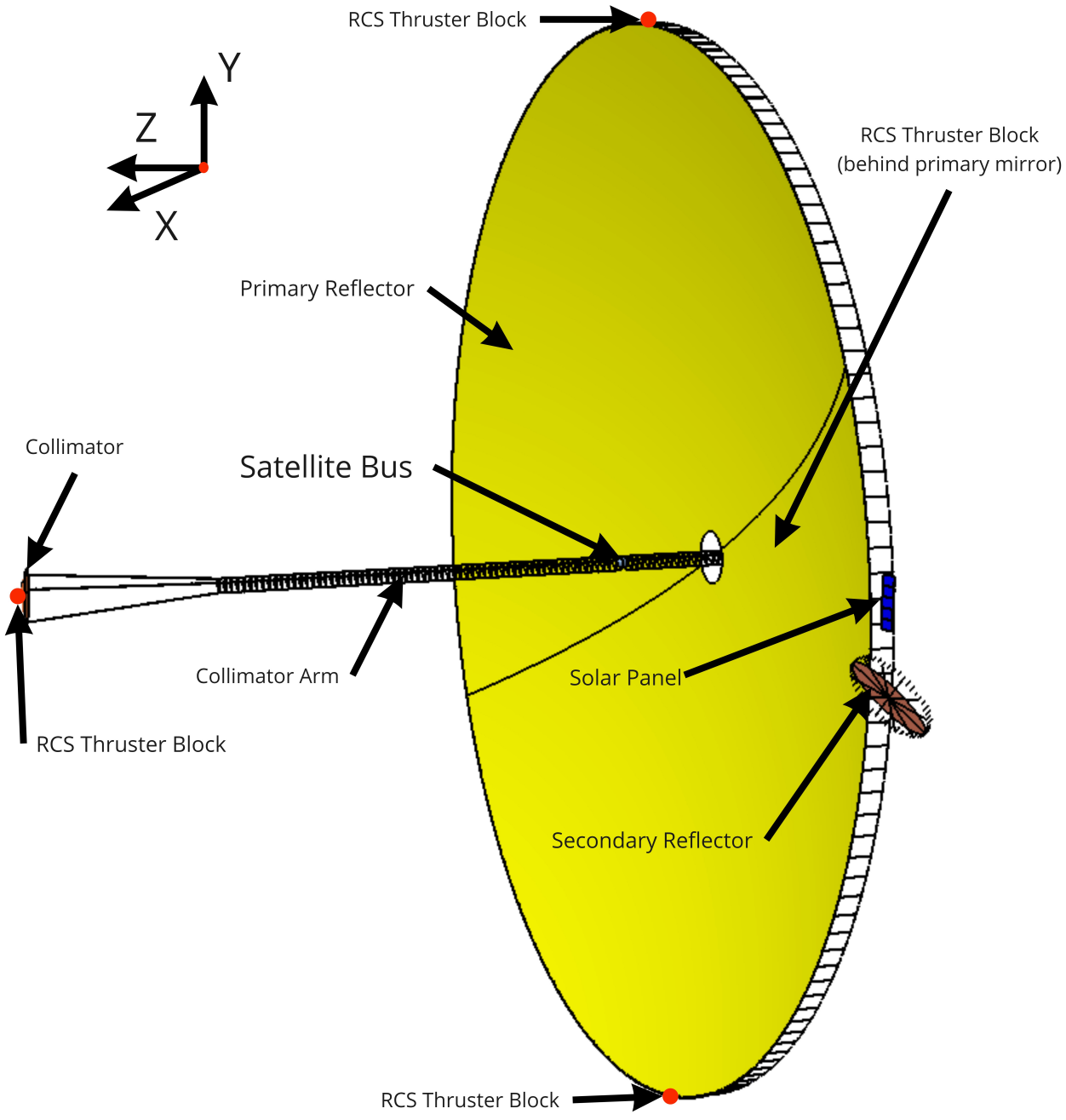

Figure 4.3: A depiction of a single satellite in the constellation with the locations of certain externally visible subsystems labeled.

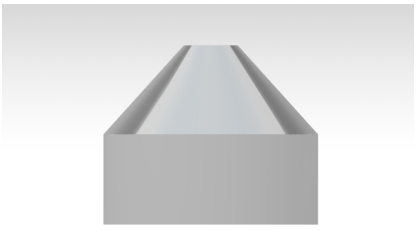

Figure 4.4: External depiction of the bus.

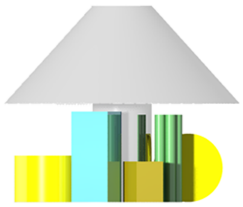

Figure 4.5: A lower-side view of the subsystems within the bus structure.

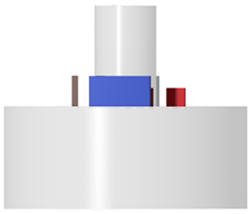

Figure 4.6: An upper-side view of the subsystems within the bus structure.

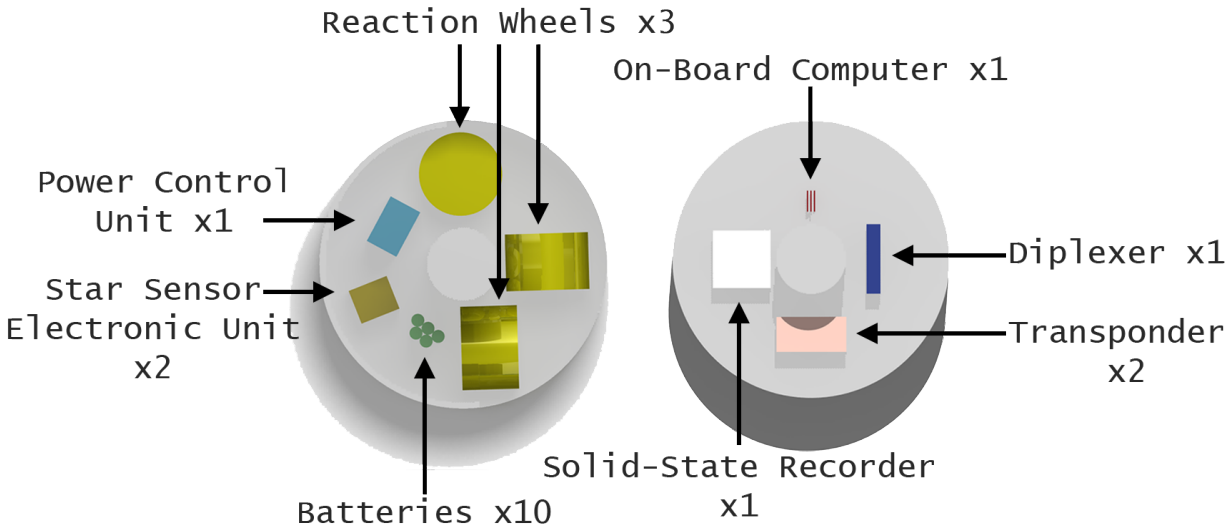

Figure 4.7: Bus structure containing the incorporated subsystems. The left is the base level, the right is the first level.

Figure 4.7 shows the lower and upper shelves with their respective labeled subsystems. It is clear that there is a large excess volume available within the bus, on both levels. Steps were taken to mitigate this, such as designing the bus for the minimum critical dimension of any subsystem (discussed in Section 13.2). But due to the stages of development for each subsystem, a more generic design was initiated to account for any discrepancies that may occur during sizing the subsystems. Furthermore, what is shown in Figure 4.7 does not show all sub-system components; such as the heater and cables & connections for data transfer within the bus. These are assumed to occupy a significant amount of the available volume, especially considering there will be wiring from external spacecraft subsystems to the Bus. Therefore, it is justified to leave a necessary amount of excess volume for this. But for further iterations of the bus layout and design, a more tailored approach would be taken to house each included subsystem with a margin of excess space. This would result in a more distinct shape and structure of the Bus design.

4.2.4 Budget Breakdown

During the previous design phase, some mass, power and cost budgets were estimated based on statistical data. At this point, after finishing the detailed design phase, more precise budgets could be constructed. All values present in Table 4.2 will be discussed in the second part of this report. To be specific, the power, mass and cost budget will be discussed in Chapter 11, Chapter 13 and Chapter 16 respectively.

Table 4.2: Budget Breakdown per subsystem per spacecraft.

Subsystem	**Mass [kg]**	**Power [W]**	**Cost** $[k\,€]$
Mission Implementation	845.0	92	156
ADCS	61.1	559	846
Propulsion	82.8	4,400	1,459
C&DHS	22.1	45.5	231
TT&CS	24.7	28	120
EPS	103.3	NA	58
TCS	9.7	300	32
Structures	27.9	NA	NA
Total	1176.6	5424.5	2902

4.3 Project Management

The project is split up into 3 project phases: a project orientation completed by the Project Plan, the conceptual design phase completed by the Midterm Report and the detailed design phase completed by this Final Report. [4, 5]

4.3.1 Team Organization

A couple of changes have been made in the team organization after the conceptual design phase. The GNC & ADCS Engineer and the Propulsion Engineer positions were merged. The design responsibility for the GNC was moved to the Comms & Data Engineer. The Instrumentation Engineering role was not used and therefore removed. An updated organogram was made to incorporate these changes and is presented in Figure 4.8. The general responsibilities for each role and a detailed explanation of the team structure can be found in the Project Plan report. [5]

Figure 4.8: An organogram visualizing the organizational structure of the project and the role division among team members. Note that team member names between brackets indicate backup roles and the arrows indicate the reporting hierarchy.

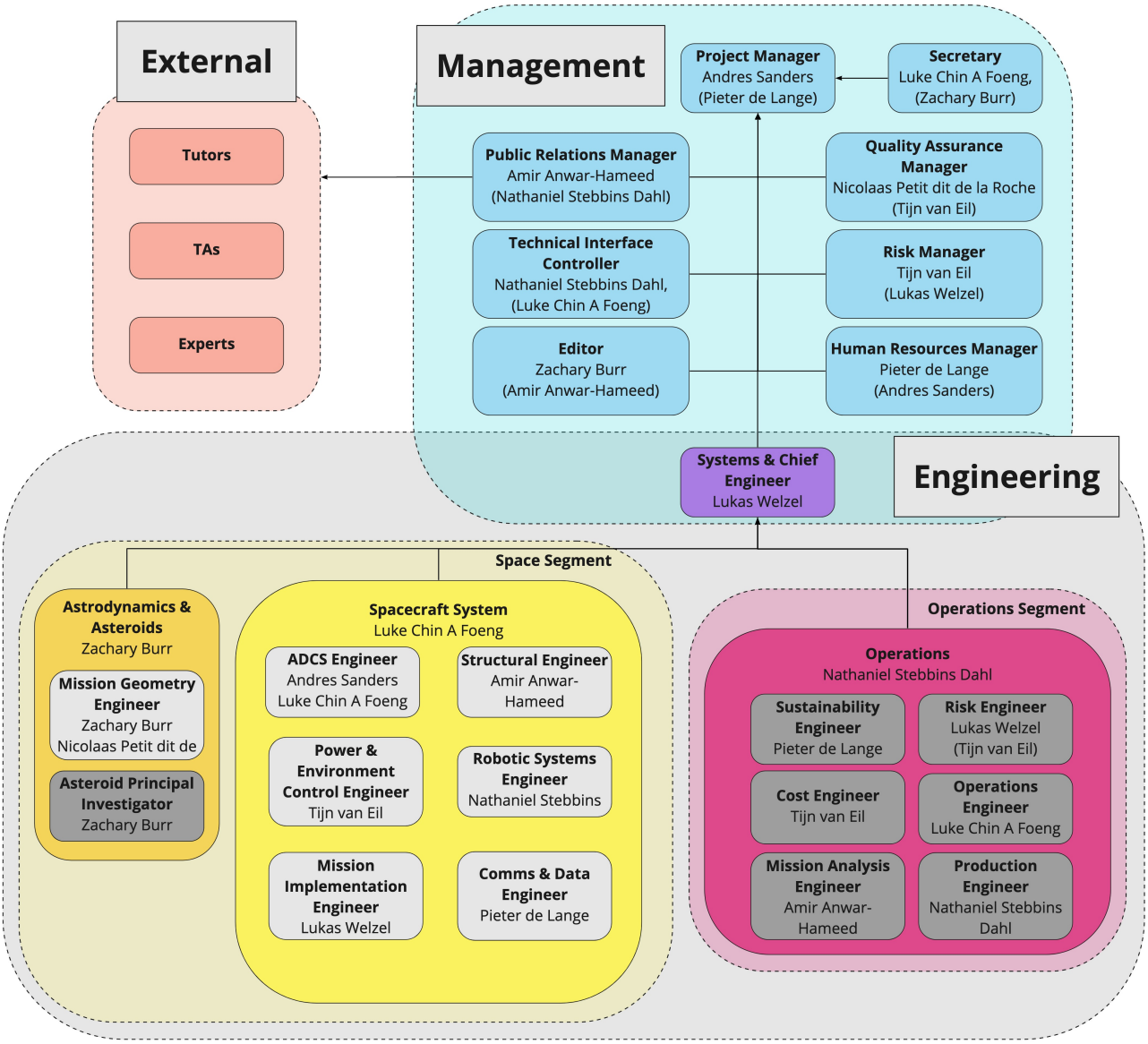

4.3.2 Project Planning

The timeline and plan of the project have been set during the orientation phase. Several visualizations of the planning have been created to ensure the team is on track. These were continuously updated over the coarse of the project. One of these visualizations is a Work Flow Diagram, which depicts the chronological order of tasks that needed to be fulfilled. A Work Breakdown Structure was also included, which follows from the WFD and includes an extra level of detail. This extra specification included all the task that need to be performed in the given schedule. More details about the WFD and the WBS can be found in the Project Plan report and the Midterm report. [4, 5]

In order to make the use of the planning more practical, the project management software ClickUp was used[1]. This software allows for easy task assignment, time tracking and compiling of Gantt charts, which can be found in Section A.1.

[1]URL `https://clickup.com/` [accessed 19 January 2021]

5 Mission Operations

This chapter outlines all the operational details of how the mission will be carried out. Section 5.1 goes over the steps of how the satellites get into position and become operational upon arrival at the asteroid. Then Section 5.2 gives insight into the communications that need to take place throughout the mission. Following which Section 5.3 will go over the logistics and steps of the larger mission, from production to deflection. Finally the validation and verification procedures are given in Section 5.5; these will be used throughout the operations to check everything is going correctly.

5.1 System Deployment

For the system to redirect an asteroid, it must first get into position. The deployment of such a large swarm of spacecraft is an in depth process with a lot of steps. This section goes over all the steps of deployment, from how the spacecraft will be placed in relation to each other and how they will exit the LV, to how the individual satellite structures will be deployed.

5.1.1 Constellation Formation

The satellite constellation was determined to require a tight formation. This is to avoid the exhaust of the thruster blocks, so as not to damage the collimator, primary, or secondary reflectors of each of the satellites. This would provide for optimal maneuverability, while maintaining as little exhaust plume impingement as possible. Creation of this formation will also require the spacecraft to be spaced far enough apart to allow for repositioning when necessary.

Constellation Model

In order to create an accurate model of the exhaust plumes of the RCS subsystem, it was assumed that all of the exhausts for all of the RCS thruster blocks were cones of exhaust with half angles of 15° as defined in Chapter 9. The positioning of the nozzles of these systems flat against the attachment surface would not only prevent the impingement of the satellite's systems in its own exhaust plumes, but would also aid other satellite systems in avoiding impingement as well.

The model begins with a singular satellite node at the center of the constellation plane. The model then continues to place four satellites around this central satellite, maintaining a minimum distance found through the Equation 5.1. These distances are measured from the centers of each of the primary reflectors.

$$dist_{tot} = 2l_{collimator} + dist_{bumper} \tag{5.1}$$

These four satellites are positioned in 90° increments around the central satellite starting at 45° relative to the central satellite's coordinate system. This process is then repeated for each of the satellites surrounding this central satellite until there are no satellites left to be placed. The satellites are placed in this manner so as to make sure that both the distances in the X and Y axes are accounted for. The positioning in the Z axis was generated based on the length of the collimator arm. This generates a formation that can be seen in Figure 5.1, where the red spheres indicate the exclusion zone where no other exclusion zone is allowed to impinge upon. This is simply a sphere surrounding the center point of the primary reflector with radius equal to the length of the forward mast, as this is the minimum distance before the possibility of a collision. The spacing between these exclusion zones allows for small maneuvers that have little effect on the surrounding satellites. This space was set to be a further $100\ [m]$ in all directions of all of the satellites, leaving a total of $200\ [m]$ to be used for maneuvers and re-positioning.

Furthermore, this spacing would also allow for the satellites within the constellation to rotate both as they are in formation, so as to maintain a 90° incidence angle to keep the surface area facing the sun as large as possible. This amount of spacing would also allow for small translational thrusts to be exerted to rotate the constellation as a whole around an axis to avoid the satellites from also impinging on each others shadows, keeping the amount of reflected sunlight at as high of a level as possible. This would be possible given the secondary reflector's ability to gimbal around two axes, leaving only one axis unaccounted for.

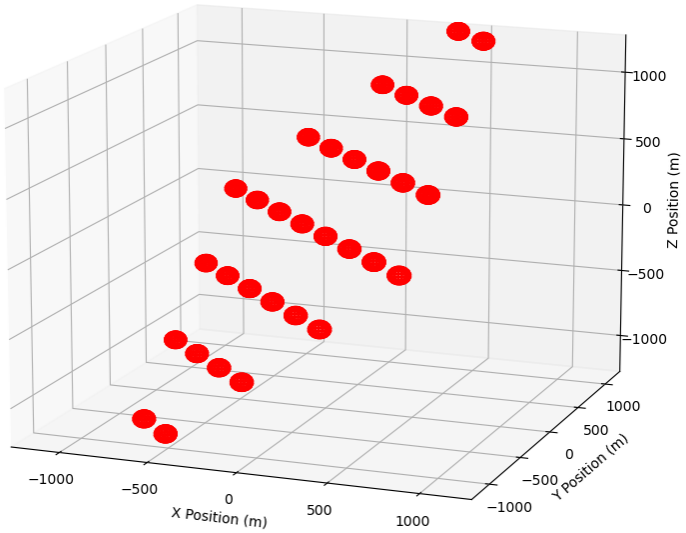

Figure 5.1: This figure shows the spacing of the satellites when fully deployed. The red spheres surrounding the satellites indicate the exclusion zone.

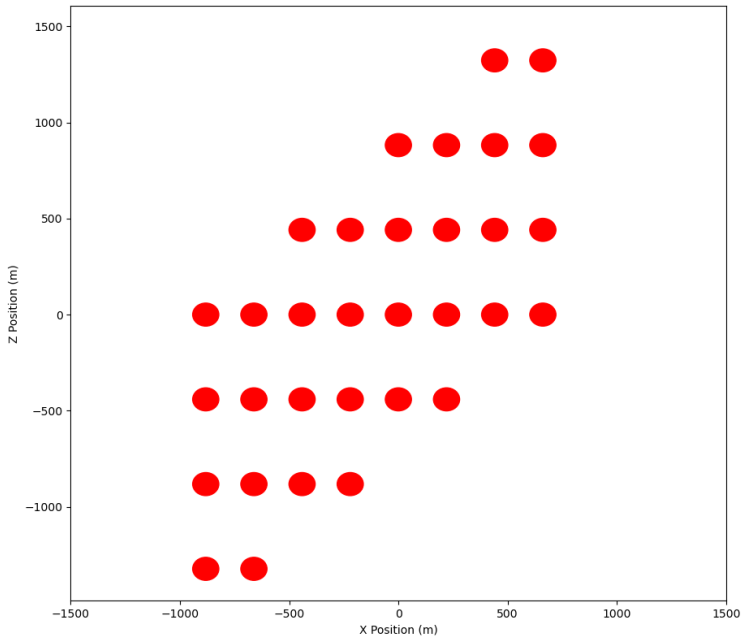

Figure 5.2: This is a 2-dimensional representation of the satellite constellation positioning with the included exclusion zones shown in red, with the asteroid being located approximately 3000 meters in the positive Y direction.

5.1.2 Constellation Deployment

The satellite constellation must be deployed in such a way so as to avoid collision of not only the individual satellites, but also the collections of satellites exiting the fairings of the Starship as well. In normal rideshare procedures, these groups of satellites, known as pallets, exit the fairings of the final stage by means of a propulsion system independent of the satellites themselves. This is done to spare the individual satellites from requiring extra on-board propellant mass [24]. This deployment strategy, although efficient for small satellites taking part in rideshare programs, would not be suitable for a system of this size and mass. Instead, pallets would be required to maneuver as a unit to their required position before dispersing. In order to mitigate collisions between the pallets, pallets that leave the fairings first must travel the farthest away from the ship. This process is further detailed in the Figure 5.3, where the pallets are labeled 1 to 6 depending on the order in which they exit the fairings of Starship. This configuration was generated with the assumption that the Starship comes to a full standstill at a position greater than $2\ [km]$ in the positive X direction and $2\ [km]$ in the positive Z direction on the provided coordinate system from the origin.

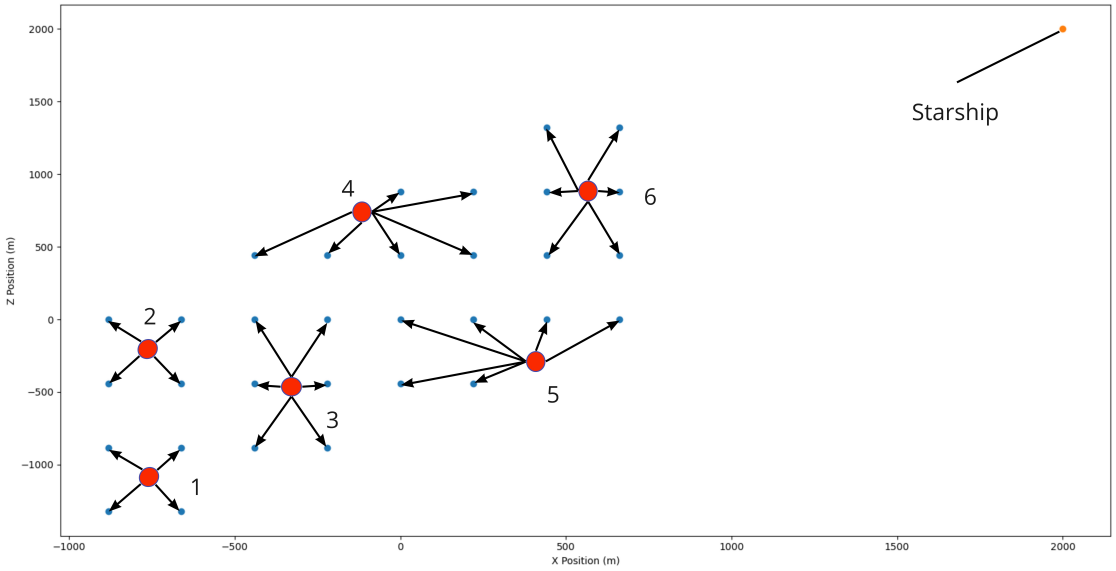

Figure 5.3: The distribution procedure for the satellite constellation, preventing pallet collisions.

The deployment strategy is further outlined in Figure 5.4. This block diagram was generated with Level 2 autonomy in mine. The mission makes use of a large constellation of satellites in close proximity, where on-board systems would have to be quarantined based on their level of functionality following a failure [93]. Initially, a start-up procedure is conducted for each satellite in the pallet. If there is a failure, the satellite will then check for issues with each subsystem, followed by a possible reboot if an issue can be fixed. If there is not a possible fix on-board the satellite, the high gain antenna is deployed, directly relaying the issue to ground control. If the high-gain antenna is unable to be deployed, the low-gain antenna is used to relay the issue to another satellite in the constellation in order to make use of their high gain antenna. A safe state is only re-entered if there is no correction found via the ground control. The verification and validation procedures for checking this are given in more detail Section 5.5.

The pallet initially makes use of the satellite thruster blocks positioned on the extremities of the pallet to exit the fairings with a purely translational motion. The RCS thrusters will only make use of one singular thrust impulse of a maximum of $0.14\ [Ns]$,determined by multiplying the minimum impulse bit of the thrusters by two, as that would be the minimum number of thrusters in the proper orientation for this maneuver to take place, causing a minor acceleration to occur, only to be counteracted by another singular thrust impulse to stop this translational motion once the pallet has exited the fairings [1]. Additional corrections will be made by the reaction control system of the Starship itself so as to combat any reactionary forces causing any unstable motions to occur such as a downward pitching moment on the Starship. After this maneuver, the pallet moves into its deployment position and then decouples the satellites from their support structure by making use of the RCS thrusters to induce a small thrust vector to induce a rotation. After this rotation is initiated there will be a small reverse thrust induced, followed by the decoupling of the satellites so as to push the support structure away from the satellites being deployed.

5.1.3 Satellite Deployment

As with the pallet deployment method, the satellite system deployment would have to be conducted with a Level 2 level of autonomy due to the complexity of the subsystems as well as the spacing of the constellation [93]. This level of autonomy would allow for the system to run uninterrupted without having to wait for special commands, unless an unaccounted for issue were to be detected. After the satellites reach their intended deployment locations shown two-dimensionally in Figure 5.3, the satellite deployment procedures can begin. These procedures are outlined in Figure 5.5. This block diagram addresses the available options if there were to be a mechanical error during deployment. The deployment process begins with the extension of the collimator arm. This is to provide stability during the deployment of the primary reflector. The deployment process would only continue onto the deployment of the primary reflector in the case of a successful collimator arm deployment. After a successful collimator deployment, the primary reflector initiates its own deployment process. After a successful primary reflector deployment, the secondary reflector is deployed. The deployment

[1] URL `https://www.ecaps.space/products-overview-ecaps.php` [accessed 25 January 2021]

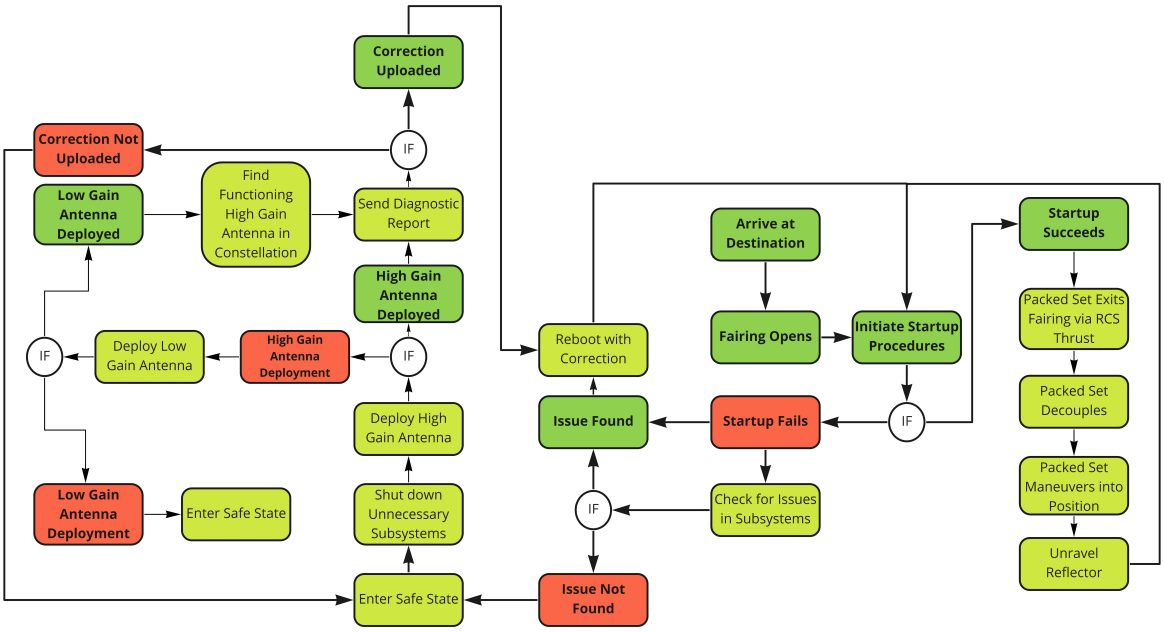

Figure 5.4: This block diagram describes the process of deploying a single pallet of satellites.

procedure is conducted in this order to as to prevent large moments from being generated, which would result in the use of large amounts of unnecessary RCS thruster corrections.
After this block flow diagram process is completed, the satellite should be in its final position, however, it may have incorrect pitch, roll, and yaw Euler angles. This is where the RCS system would have to come into use. Due to the massive moment arms of the system, the RCS system would be the first system to be used in order to re-position the satellites. This would be followed by the reaction wheels for a better pointing accuracy.

5.2 Communications Operations

This section will detail the communications operations required for satellite to satellite information exchange as well as ground station to satellite information exchange as well. While satellites only require small amounts of information to be transferred between one another in order to avoid collisions, the ground station must maintain a larger connection due to the extent of telemetry required to make sure that no human intervention is required.

5.2.1 Satellite to Satellite Communications

In order to have a self-sufficient constellation, the satellites within the constellation must communicate with one another in order to remain safely spaced out. This is to be done by separately interpreting the positioning of each individual satellite. These positions are then subsequently relayed to each satellite through the use of the low gain antenna. This antenna would then also be used to receive the positions of the four satellites positioned the closest. Once the information is received by the satellite, it then must determine whether or not it must re-position itself. This comes down to whether or not it is within $200\ [m]$ of another satellite's exclusion zone. If the satellite deems itself to be too close to another system and it is not currently being re-positioned, it will begin a re-positioning maneuver in order to maintain the $200\ [m]$ distance. However, while committing this maneuver, the satellite will also announce its maneuver and planned final position to surrounding satellites, thus creating a chain reaction of small maneuvers and adjustments until all satellites remain at least $200\ [m]$ apart from their respective exclusion zones. This procedure is detailed in Figure 5.6.

5.2.2 Ground to Satellite Communications

While the system is relatively self-sufficient, data must still be transmitted to the ground station. This allows the possibility of a manual systems check by the ground crew in order to correct any unforeseen errors during the mission that are not correctable on-board. This results in an extension to the possible lifespan of the satellite

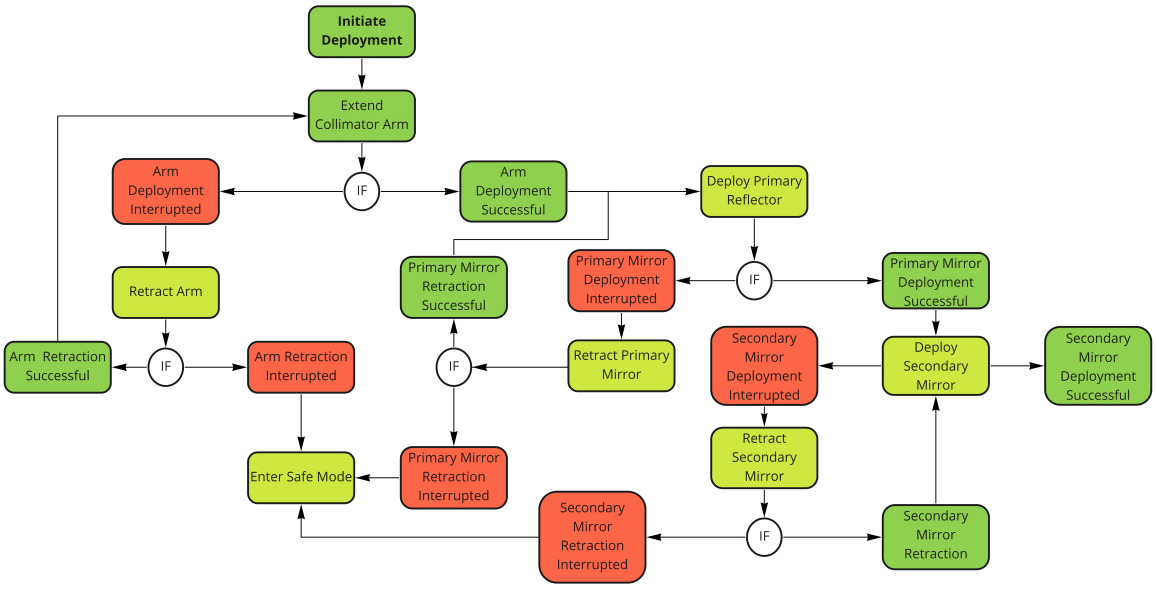

Figure 5.5: This block diagram describes the deployment procedures for an individual satellite.

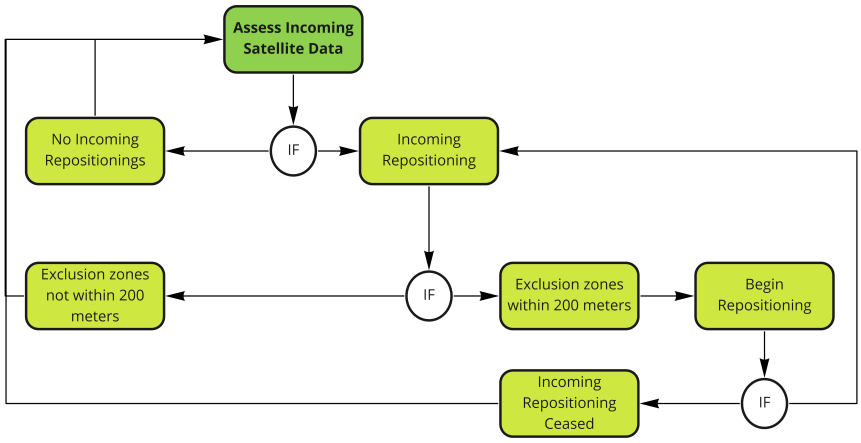

Figure 5.6: The block diagram describing the re-positioning procedures if a satellite in the system were to require a translational correction.

as well as the mission as a whole.

The satellite must send down several state vectors in order to account for the position, velocity, and acceleration of the satellite. These vectors allow for the validation of the system's actions in order to make sure that the satellite is still operating nominally, and that it is still interpreting all incoming data as it is supposed to be interpreted. Some other values that must be transmitted include the fuel levels of all the RCS thruster blocks as well as the xenon tank levels, the thermal values of the entire system, as well as the power consumption and power production values. These values would then be checked against values calculated on the ground after certain operations are executed in order to determine whether or not the system is still nominal. If an issue within an on-board subsystem is detected and the satellite fails to shutdown said subsystem, a shutdown command would need to be sent to the satellite in order to maintain the possibility of nominal operation after a correction, so as to prevent further damage being done to that subsystem, and any surrounding subsystems. A total safe state initiation could also be implemented if the situation is deemed to be irreparable. This exchange of information is detailed in Figure 5.7.

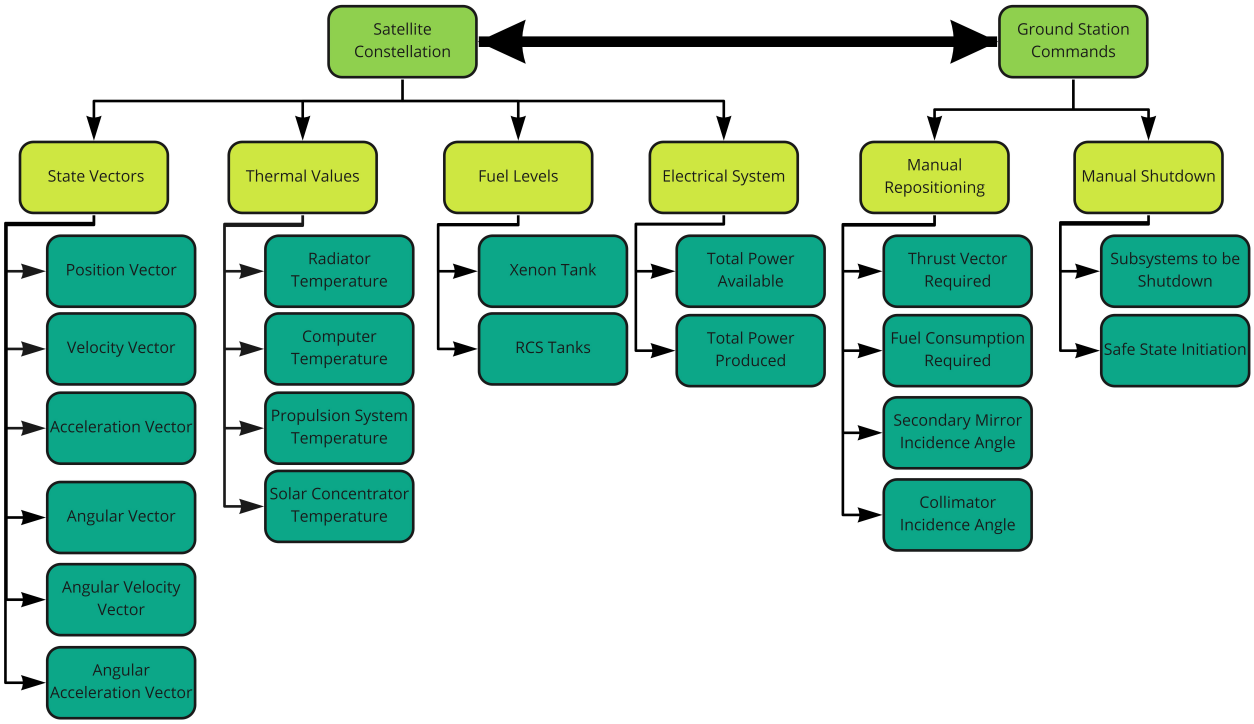

Figure 5.7: This communication flow diagram displays the information exchanged between the ground control and the satellite constellation in order to ensure nominal operation.

5.2.3 Fault Detection, Isolation and Recovery

This section will detail the process of handling issues involving the loss of certain portions of any on-board subsystems or the subsystems as a whole. Such a system would have to be created in order to ensure the proper steps are taken to attain the safe mode when necessary, or to circumvent a faulty subsystem if there is some level of redundancy in place. Alarms must also be in place in order to notify the ground station of any potential issues occurring within subsystems. These alarms would have to be configured in a manner so as to attach certain levels of urgency and severity to them in order for the ground control to distinguish between which alarms will and will not require some form of human intervention [46]. The levels of severity are shown in Figure 5.8.

Level 4: To be addressed by the ground station-Required when there are communication interruptions or deployment failures
Level 3: To be addressed by the on-board computer-Required when there are hardware failures
Level 2: To be addressed by the system software-Required when the system fails
Level 1: To be addressed by the subsystem software-Required when a subsystem fails or fails to relay correct information to other subsystems
Level 0: To be addressed by the component itself- Can be corrected within an instant shut-down and restart sequence of the component

Figure 5.8: This figure shows the levels of severity errors that may arise in the system [46].

Any level zero error management can be assumed to already be built into the off-the-shelf components constructed by any third party supplier. These include certain sensor thresholds to initiate a quick restart in the case of values outside of the performance domain as well as electronic protections such as circuit breakers to protect from any overload scenarios. Higher level error management relies on more complex fault detection and handling routines. A large degree of level one failure still are not critical and can be handled locally. Errors which persist or escalate to higher system levels are escalated to more advanced fault recovery systems. Both level three and four will require either oversight or handling by the ground system. Due to the potentially large distance and low data rate between the space craft and earth, much of the fault detection, isolation and recovery shall be designed to happen below level four. This will require extensive testing of the units.

For the risk requirement AD-RISK-OP-1.2, the digital systems implemented shall have a triple modular redundancy so as to vet the information being output by a subsystem. This type of error management could be implemented to handle all issues on levels one and two. On a system level, this same vetting procedure could be implemented to correct for errors in other systems by using the data output by the systems surrounding it. This would be a further layer of security added to the level two and three error types. For example, in the case of a satellite relaying its position incorrectly, and surrounding satellites relaying an alternative position interpreted of that satellite, a sensor check could be perform whereby the sensors of the surrounding satellites could be used to correct the incorrect sensors on-board the satellite relaying incorrect values. This type of system architecture is inline with a decentralized system, where the information is not relayed through a central satellite, but instead relayed among the entire system. The system as a whole could be considered dynamic, where not only the information sent between the systems could be used for redundancy, but the characteristics of the signals sent could also be used for redundancy [64].

In accordance with the risk requirement AD-RISK-OP-1.1, critical systems require a level of redundancy of at least one. This type of redundancy would be implemented so as to accommodate for any level three errors. Furthermore, values would be checked against a model and a redundant sensor in order to generate residuals for which the system would check for diverging values, which would then set off an alarm in the case of diverging values. This process is depicted in Figure 5.9.

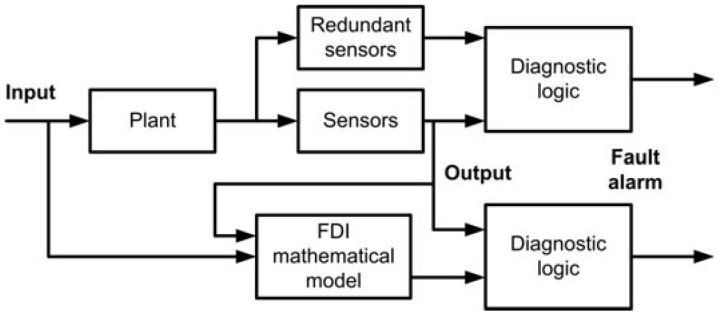

Figure 5.9: An example of the FDIR system to be used to check for inconsistencies in the subsystems [64].

Issues that cannot be resolved by a simple reconfiguration, such as a system unable to be deployed, would be deemed a level four error and would be handed off to the ground control [64]. Within the Figure 5.5, the mission implementation segment Level 4 error management can be seen, where the system will make use of its OBC in order to ensure a proper deployment in the case of a deployment issue.

5.3 Logistics

This section details the steps required in order to properly organize the mission so as to avoid delays induced during various phases of the mission. This starts off with sourcing the materials required for the production phase, followed by the production phase itself, and then followed by the launch, transfer, deployment, and deflection phases required.

5.3.1 Ground Station and Production Logistics

Before the start of production, the materials required for production must be sourced and transported to the production facilities. This is normally outsourced to a 3rd party by the companies responsible for for the production of the subsystems. Once the materials are sourced by these third parties, they must begin their production phases, something which will be described in further detail in Chapter 15. After the components are produced and subsequently tested by these third party subsystem providers, they are then integrated into the system. After this integration is completed, integration tests will commence. This is where the system as a whole is tested in order to check whether the correct data is transferred to the correct systems. This is when the subsystems are verified as properly relaying information as operating nominally together. After this occurs, the satellites are to be transported to the launch site, where they are then integrated with the launcher. After this integration, the system will undergo a second round of testing so as to check whether or not the satellites are relaying their information through the launcher nominally.

However, before the launch even begins, the launch must be planned well in advance of the launch itself. This planning period would occur roughly two to three years before the launch due to the complexity and size of the system [93]. A team must also be assigned to address the acquisition of the launcher as well. This team would also nominally begin operations at the same time the launch date planning team would start operations as well. A team must also be assigned to inspection and operation of the launch facility before and during the launch of the system as well.

After this the system is launched, a parking orbit is established, during which a skeleton crew would remain at the ground station to monitor the satellites as they await an oncoming asteroid. While the system remains in a parking orbit within the Starship, an asteroid localization team would commence operations. This team would work on discovering the most consequential asteroids, selecting the one that both poses the largest risk to the planet as well as one that has the highest potential to be redirected. Once the asteroid is located, a larger crew assumes the role of spacecraft localization team. This crew will be responsible for interpreting the telemetry of the Starship and the satellites on board, making sure that the system stays on course. This team would also be assisted by a team responsible for the analysis of the ΔV remaining, to make sure that the system does not overshoot or undershoot the required rendezvous point.

Once the system successfully reaches the asteroid, a team will be dispatched to the ground station in order to start the deployment phase. This team will then be joined by a deployment finalization team to verify that the system has been deployed correctly. After the system is deployed, a team dedicated to the alignment of the systems will be required to monitor the deflection process. This group will also address any issues that may arise pertaining to subsystem errors and system inefficiencies, such as a sudden drop in reflectivity of one of the satellites. There will also be a secondary team on stand-by, in case any subsystem specific issues arise. While the deflection process is being executed, the asteroids positioning will also be monitored by another team by not only analyzing incoming system telemetry, but also analyzing the shift in positioning of the asteroid on Earth through the use of data obtained from Earth and space-based observatories. This team will also be in charge of re-calculating the trajectory of the asteroid as well. A block diagram detailing the staffing required is shown in Figure 5.10.

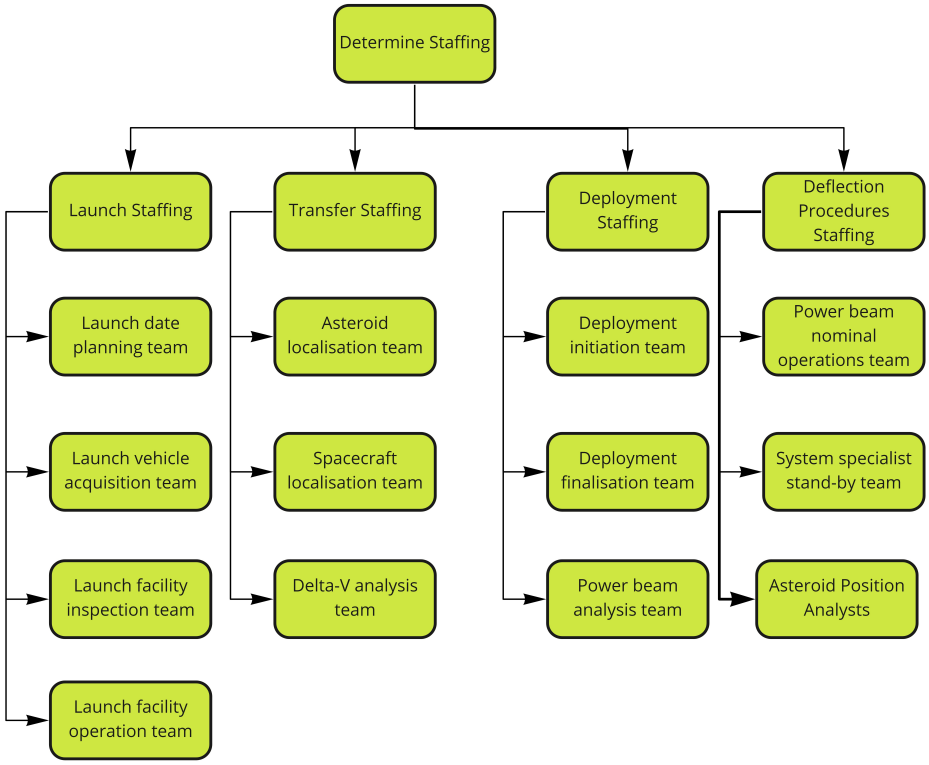

Figure 5.10: This block diagram shows the breakdown of the staff required during each phase of the mission.

5.3.2 Functional Flow Diagram

The functional flow diagram gives a graphical overview of operations and logistics of the entire operation. This is given in Section A.2. The functional breakdown structure is given in Section A.3 and goes one level deeper

than the functional flow diagram.

5.4 Post-DSE planning

The mission is divided into four phases, namely the Research and Development, Production, Launch and the Mission Execution phase. For this planning, the user requirements **AD-SH-PFM-3a**, **AD-SH-PFM-4** and **AD-SH-PFM-5** should be met. These requirements state that the system should be ready for asteroid redirection before November 2030 and the system should be able to operate for at least five years.

With the current planning, the Research and Development phase will be finished in 2027. The Production phase will already start when the Research and Development phase is not fully executed and will end in 2029. This phase will be further discussed in Chapter 15. When all components are manufactured, assembled and tested, the system will be made ready for the Launch phase. Note that a maximum of five years is planned for the system to maintain in the parking orbit. The Mission Execution phase is rather short and also contains the EOL disposal of the spacecraft, which should be further researched. The mission planning can be found in Figure 5.11.

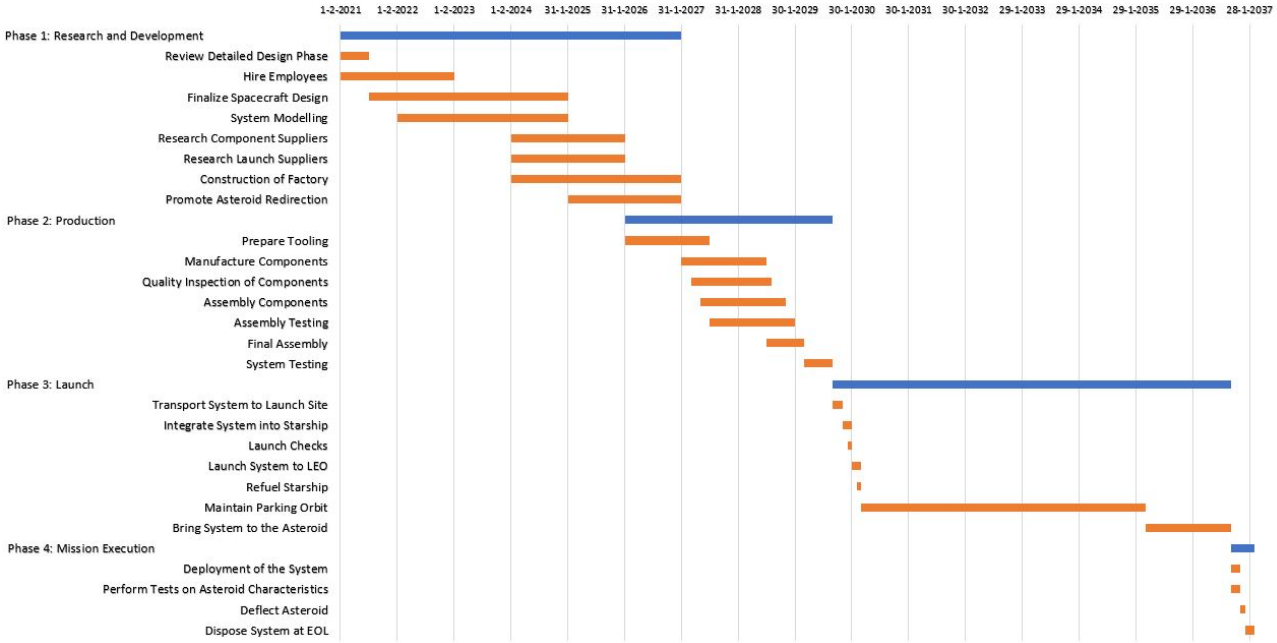

Figure 5.11: Gantt chart containing future activities.

5.5 Verification and Validation Procedures

In this section, the verification and validation methods that were described in the Midterm Report are further elaborated upon. It explains how the steps taken in the detailed design phase, and also during the testing of the actual system afterwards, are verified and validated [4]. After all of these procedures have been completed, the mission should be completely ready for launch.

5.5.1 V&V Implementation

As presented in the Midterm Report, a V&V process timeline has to be adhered to in order for all subsystems and requirements to be verified and validated. First of all, the requirements presented in the Baseline Report have to be validated, this process is explained in Subsection 5.5.2. Secondly, the models and scripts that have been used for each subsystem have to be verified an validated. Taking the Solar Concentrator as an example, the code used for the system needs to be verified. The script for the sizing of this subsystem was programmed in Python, then the model itself had to be verified. A unit test has been performed to make sure the units are right, along with a consistency test with different varying inputs. For model validation, peer review and comparison have been used to assure that the model is valid.

The next step in the V&V procedures is product verification, a process not actually performed by the team because no physical product will be constructed. However, in case the Solar Concentrator is realized, the computer analysis performed will indicate whether the model may work. Also, a test with incoming light, equivalent to the solar flux at asteroid distance, can indicate whether the system will work. In this setup, demonstration and inspection are also possible.

The procedure explained above can be applied to all subsystems. In product verification, some subsystems might not be as viable as the Solar Concentrator, so only analysis can be performed for example. Once all subsystems are verified in this manner, the spacecraft is completely suitable to perform its tasks.

5.5.2 Subsystem verification

Mission geometry and performance

For the mission geometry, the python packages pykep and pygmo (developed by ESA) were utilized to find the optimal trajectories to get to the asteroids. The implementation of these was checked by examining a reference case given in the pykep documentation, and the resulting values matched up. Additionally, the ΔV and transfer time to get to the asteroids is in line with values given by literature on asteroid redirection, so these tools can be said to be validated.

Additionally, for the geometry and the performance analysis, a numerical model of the solar system was constructed to model the asteroid trajectory, and assess deflection. This model was first of all verified by performing unit and consistency tests. The model was then validated against high-precision ephemerides from JPL to check that the results lined up. The model does drift from the JPL data over time, but it was only run for simulations of at most two years at a time, which resulted in a maximum error in the order of 10^5 $[km]$ for the asteroid position, which is accurate enough for the purposes of this project. Figure 5.12 shows the error over time for a simulation of the asteroid Bennu, whose orbit is very well known, with a time step of 10 $[s]$. For more in depth information on the verification and validation of the model, see [4].

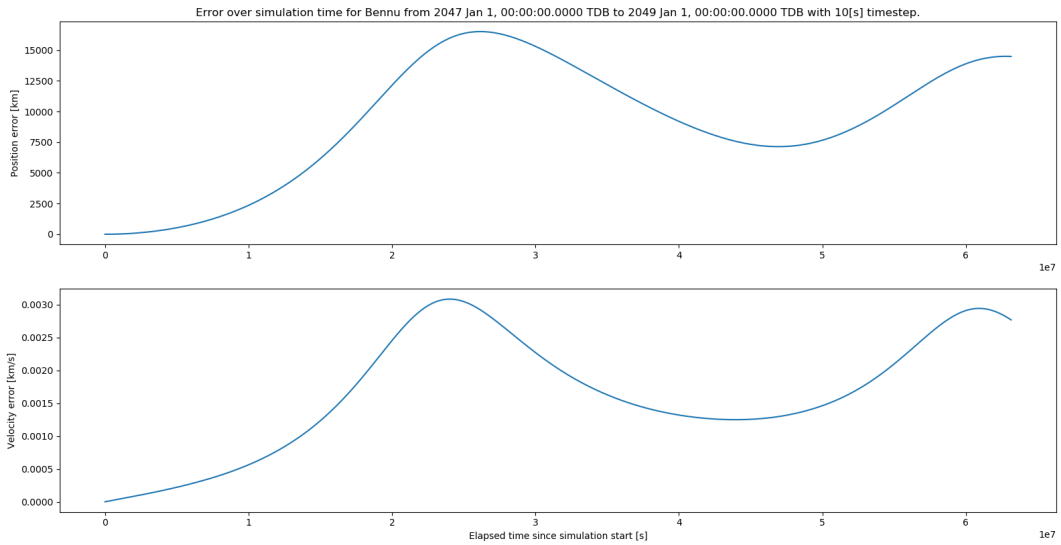

Figure 5.12: Error over time for a simulation of asteroid Bennu over two years with a time step of 10 $[s]$

ADCS

In order to verify the models used during the ADCS sizing, different methods were used based on the type of model. To verify the moment calculations generated by the RCS thruster system, calculations were conducted by hand, considering that the moments simply required multiplying the force generated by the thruster by the distance it was positioned from the center of gravity. The model generated for the pointing error was verified through the use of the SMAD pointing error estimates which rely on statistical data generated from systems

already in operation [93].

While the system is constructed, tests could be conducted on each of the thrusters used in order to check if the thrusts generated were those specified within the specifications sheet of the thrusters. These tests could be conducted by connecting a thruster to a fuel source and attaching the thruster to a load cell, and then varying the flow of the propellant to the thruster. The minimum impulse bit could be verified by sending a pulse signal to the valve of the thruster, timing how long the valve remains open and how much force is generated while this burst of propellant is released.

The torsion generated by the reaction wheels could be verified through the use of a camera and a script written to calculate the angular velocity of the reaction wheel while inducing a certain momentum onto it [53]. This, as well as weighing the wheel and noting its dimensions would provide enough values that could be used to calculate the amount of momentum that could be stored in this wheel.

Communications and data system

For the C&DHS and TT&CS, estimations were primarily used. These estimations were validated by comparison to existing missions and displayed in literature [93]. When the actual system will be built, the On-Board Computer can be tested on its data rate requirements, along with both antenna types. Therefore, all four product verification methods are possible. Furthermore, link budgets have been set up using basic telemetry equations, which are automatically validated based on the literature they were displayed in, meaning face validity is applied. [93]

Electrical power system

Different methods were used to verify the model that was used to size the solar arrays and batteries. Firstly, a zero value for the required power was used as input. As expected, this also resulted in a required solar array area of $0[m^2]$. Next to that, the models used for the sizing of the solar area and batteries were also checked by doing calculations by hand. Small errors in the model were found and adjusted. Next to that, the model was validated with the use of data from reference missions. The results from the model were in line with the solar panel area of those spacecraft. Future product verification can be done via demonstration or testing.

Thermal control system

The model that was used for the TCS design should also be verified. As the model is relatively simple, hand calculations were done in order to verify the results from the model. As there were no errors found, the model was considered to be verified. For future product verification, the system can be tested in different environments, such as vacuum. Next to that, the performance of the subsystems can be tested for varying temperatures.

Structures

The structures were analyzed using finite element methods in Catia. This was validated by checking the output of the analysis on the simple case of a cantilever beam, for which the analytical solution is know. The error from these tests was approximately 30%, but the results were in the correct order of magnitude, and should be small enough for this case. For more information on the results of the validation, see Subsection 13.1.1. In the future, when production of the spacecraft is done, extensive vibration and load tests will be done. This will ensure that the structures can indeed carry the launch loads.

5.5.3 Mission V&V

After the detailed design phase has been finished, the actual system can be developed and brought to practice. The steps that have to be taken in order to bring the system in a fully functioning state should all be validated so that nothing can malfunction or in any other way can go wrong during the mission itself.

First of all, a prototype of the system will be built. This can either be a to-scale prototype, with a $1:120$ scale so that the the reflector diameter will only be $1\ [m]$, or an actual-size system. Tests can be performed with the scaled version by casting light upon the reflector with the same density flux as the light would be at the asteroid location. In this manner, some extrapolations can be made towards the performance of the eventual system. A real-life prototype will also be built, where the same experiments can be performed on as well as structural and thermal assessments. The deployment mechanism can be tested if the system is suspended with cables by

using cranes for example. Also, the secondary reflector cleaning mechanism can be tested by mimicking the asteroid ejecta plume on the ground. The results from these various tests lead to the re-iteration of the design and further improvement on the reflector's performance.

In the next stage of the mission preparation, the spacecraft has been completely validated and improved upon but the mission implementation itself still needs to be validated. For this, a prototype will be sent in a parking orbit so that its functioning and communication capabilities can be tested from here. The launch vehicle selected here is also Starship, since ride-sharing can be applied with other space missions so that launch costs can be limited. The system can then also be deployed from the launcher, so that the concentrator deployment mechanism of only one spacecraft can be tested. After this deployment, the spacecraft will de-orbit and its remaining parts may be reused. In later testing stages, more spacecraft may be launched to the parking orbit so that the deployment of multiple systems from Starship at the same time may be tested, along with the pointing of the solar concentrators. The latter is of utmost importance since they need to be aligned in such a way during the deflection phase so that their power beams are focused on the same points. Re-iteration of the ADCS may be a result of these findings. Also, the communications system (TT&CS) may be tested in this situation as well, leading to further improvements on the subsystem.

After all of these tests have been performed and the entire mission has been validated, the first spacecraft can be launched to parking orbit as a start of the mission. Having tested all aspects, the entire mission is sufficiently reliable and can effectively deflect impending asteroids.

6 Market Analysis

The mission to redirect asteroids and possibly save millions of lives is at its heart not about making a profit. To achieve the mission goals it is important to understand the environment that the asteroid redirect mission will operate in. The physical world is not the only environment that the mission will need to survive in. Ensuring the mission can operate in its market increases the chance of success along with opening the possibility of creating value for more customers in the long run. The mission itself must be analyzed to find a complimentary fit in current or future markets. To that end a SWOT analysis was done on the mission as shown in Figure 6.1.

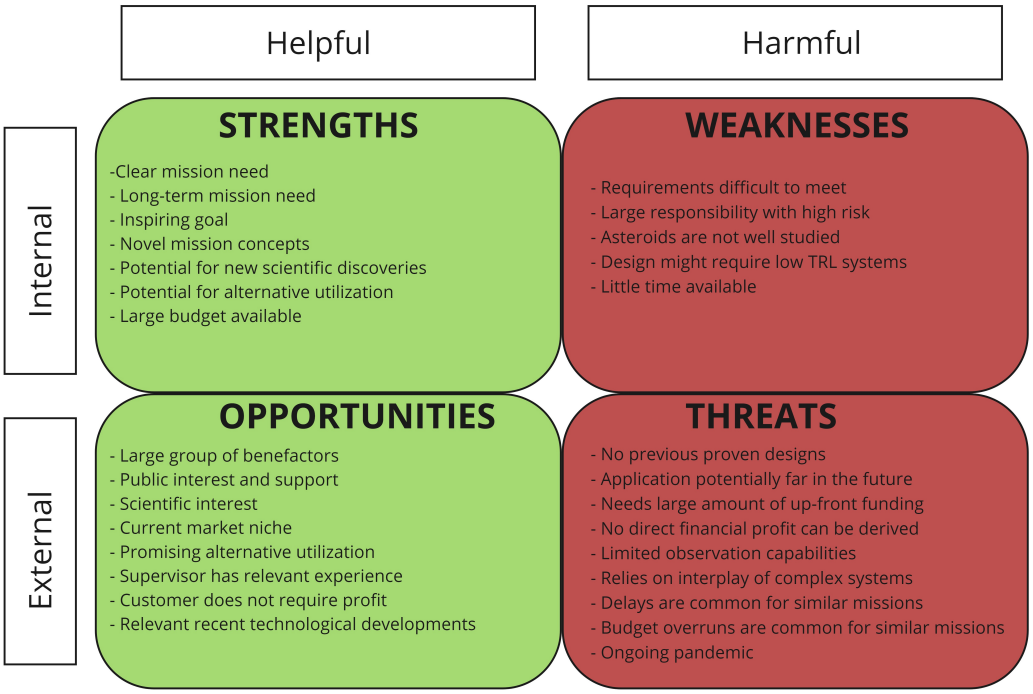

Figure 6.1: Mission SWOT analysis.

This chapter delves into the Satellite industry by making use of Porter's Five Forces in Section 6.1. Then the chapter is concluded by identifying the key market drivers and constraints in Section 6.2.

6.1 Porter's Five Forces Analysis

Porter's Five forces is a tool used to develop insight into the profitability and the competitiveness of an industry [70]. The first of the five forces is the bargaining power of the buyer. This is dictated by how easily the buyer can find a different supplier or how smart they are and thus how much power they have to determine your product or the price they will pay for your product.

The second force is the power of the suppliers. The relationship here is very similar to the buyer relationship. The number of suppliers and level of service they provide can have a large impact on their bargaining power.

The third force is the threat of new entrants into the market. If it is easy for new companies to enter a market then it can be difficult to defend a competitive position and thus drive down the profitability. This force also takes into account the difficulty to leave the market. If there is a high sunk cost then companies will fight hard to not have to leave the market, reducing profits for everyone.

The threat of substitution refers to the ability for your product or service to be replaced or substituted for another option. This limits the longevity of the market and can hamper profits.

Porter's fifth force is the competition within the market itself. High competition can lead to larger development costs and lower profit margins.

6.1.1 Bargaining Power of Buyers

The space industry has buyers with high bargaining power. Most satellites are made to custom order and the sums of money involved are generally large. Buyers are also very knowledgeable about what they are purchasing. This is the case as most buyers are in the space industry themselves. This is less the case when it comes to market segments like telecommunication. These segments either sell directly to consumers or customers who are only knowledgeable about the service itself.

In contrast there are also not a huge number of companies working in the space industry thus reducing the buyer power as they cannot simply turn to a different supplier. For example, Thales Alenia Space is one of if not the only company that provides human rated pressurized containers. In the end though as most parts are made to order this does not reduce the bargaining power of the buyer by a significant margin. The take-away is that the customer must be taken as one of the if not the most important stakeholder.

6.1.2 Bargaining Power of Suppliers

The bargaining power of the suppliers is also high in the space industry. Here the example given in the final paragraph of Subsection 6.1.1 holds again. There are very few providers of off the shelf components and most will be made to customer order. This means that in the long run to reduce costs it is important to bring as much development and knowledge in-house as possible. This also mitigates the risk of smaller specialty providers going bankrupt and causing large delays and cost over-runs. The cost of raw materials is relatively cheap but the knowledge that is held by suppliers is of extremely high value.

6.1.3 Threat of New Entrants

The threat of new entrants into the space business is increasing but still low compared to other industries. While it is possible that companies come in and disrupt the market like SpaceX has done, it is hard to say that this is a large threat. It is more likely that new industries will open up by new entrants bringing new technologies like how micro-launchers have improved the market for micro-satellites. The availability of more off the shelf systems such as ADCS or communication systems is also allowing for smaller companies to enter the space industry with more specialized systems and lower budgets.

These small companies are not likely to cause large market disruptions as access to space is still expensive and limited in supply.

6.1.4 Threat of Substitution

The threat of substitution is low. The services provided by satellites are not easily replaceable by terrestrial services. Most space based services would be much more expensive if not impossible if they were to only utilize terrestrial systems.

6.1.5 Competitive Rivalry

There is significant competition in the space industry. While the market has not been saturated, there are already many strong competitors with immense resources behind them, such as Lockheed Martin, Airbus SE, and SpaceX. There are many more specialty providers that already have strong relationships with suppliers and customers. This means that entering the market from the outside is difficult. To ensure a competitive advantage and a business level a strong technological improvement or business model must be present as shown by SpaceX. Another way to improve chances in this market is to follow a highly differentiated business strategy. This means finding a small niche and dominating it, then expanding from there.

The other notable weakness for these large companies is that they have high overhead and large corporate inertia. They can be beaten by fast paced and cheap innovation. However this is not historically easy to do in the space industry due to the high entry requirements to afford a launch into space.

6.2 Market Drivers and Constraints

The driving forces and constraints of the market can be summarized from the above analysis. Porter's Five Forces analysis shows that the driving factors are the buyers, suppliers, and incumbents. These forces can be

mitigated by selling services to outside of the space industry and bringing development of spacecraft subsystems in-house. The incumbents can be bypassed with fast and cheap innovation. One of the main constraints of the space industry is the high cost to orbit and the long development times.

Comparing the above drivers and constraints to the SWOT analysis in the beginning of this Chapter shows that the Strengths and Opportunities coincide well with the market. The Weaknesses and Threats can be overcome through proper planning and good use of the the Opportunities available. This leads to the conclusion that the mission can be a success in the current market and could lead in the creation of new markets in the space industry.

For the spacecraft design it was decided that it would be best to use as many commercially available components as possible to save on development costs and meet the timeline requirements. As the mission does not aim to produce direct profit, the mission can also benefit from the aggressive innovation from companies in the space market.

6.3 Follow-on Markets and Return on Investment

The most promising market to exploit given the mission profile is the possibility of ride-sharing. As will be discussed in Section 8.2, the volume is the limiting factor for the launch vehicle and not the mass. This means that the Starship has a significant amount of mass budget available to lift into orbit. As the Starship will be used as a kickstage it is also possible to bring scientific missions along to the asteroid. These types of launch services are quite expensive; for example the NASA Psyche mission spent 117 Million dollars on launch services [1]. This may enable the mission to recoup some of the launch costs.

Again it is important to emphasize that the mission does not aim to create a profit but if the mission successfully redirects an asteroid then it will clearly have provided sufficient return on investment. The aim of the market analysis is to ensure the mission stays within budget and possibly provide secondary value other than the primary mission.

[1] URL `www.nasa.gov/press-release/nasa-awards-launch-services-contract-for-the-psyche-mission` [accessed 26 January 2021]

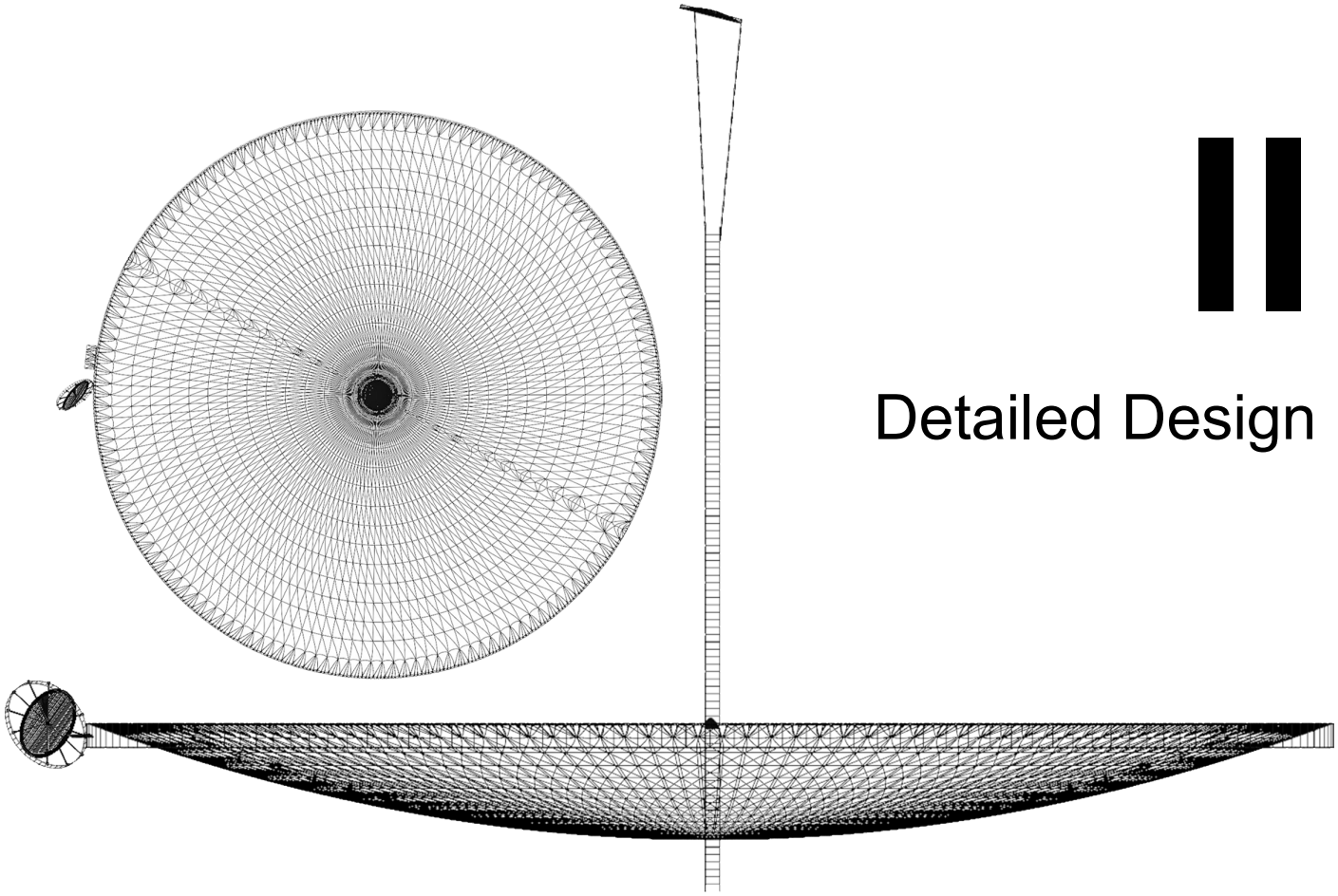

II

Detailed Design

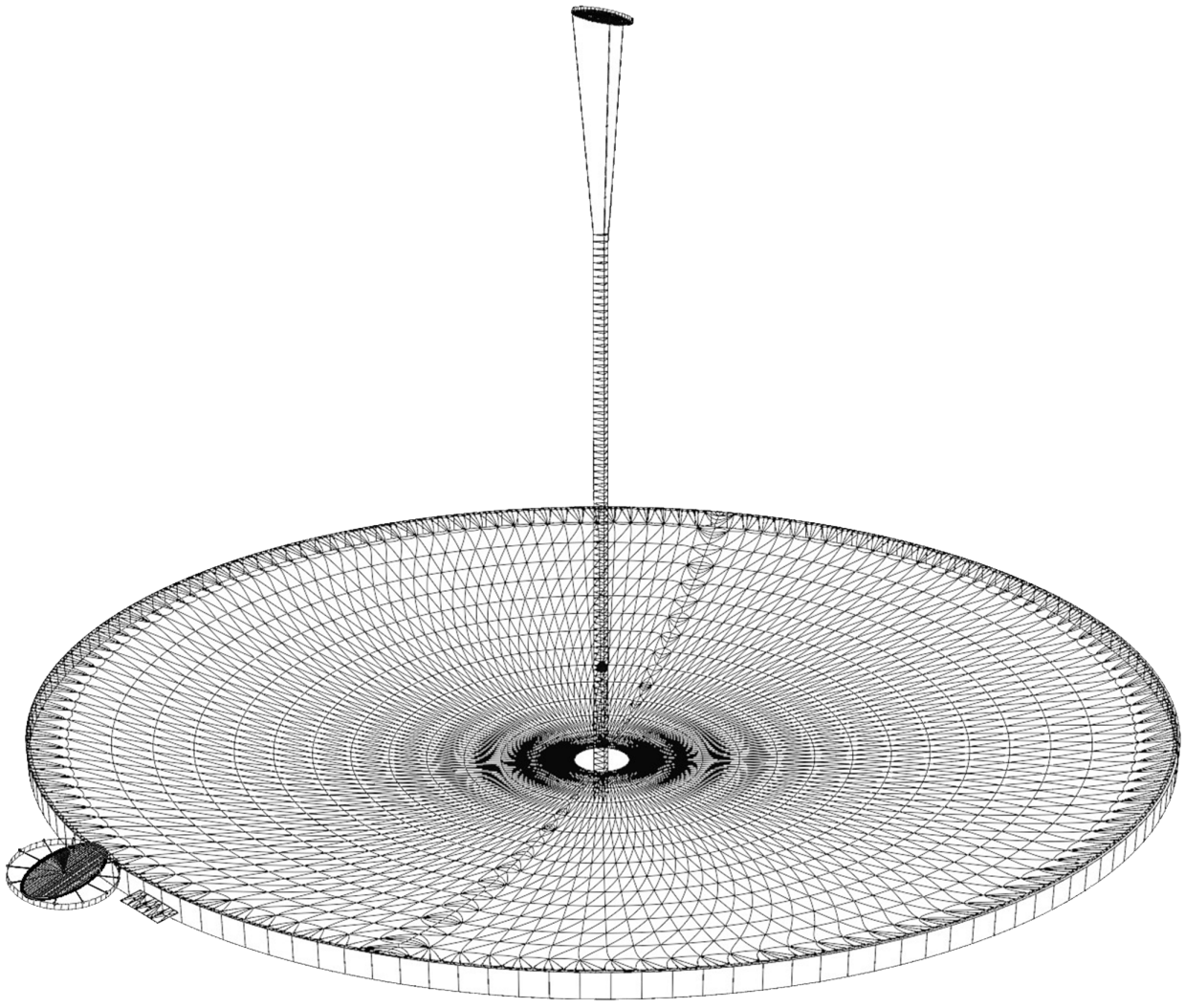

7 Mission Geometry

This project focuses on redirecting asteroids. In order to conduct the mission, it is therefore necessary to rendezvous with the asteroid. This chapter details the plan for this mission to arrive at the asteroid, as well as the geocentric parking orbit that will be used before a threatening asteroid has been detected.

7.1 Parking Orbit

The aim for this mission is to redirect asteroids within two years. Integrating a system with a launch vehicle and launching it in to space takes a long time. Therefore, the system will wait in space—for up to five years—for an asteroid, in order to be able to respond as quickly as possible. While in space, the system will wait in a ”parking orbit” around Earth. While in this orbit the satellites will remain inside the Starship, which will function as a kick-stage to get to the asteroid.

This parking orbit was set at an altitude of $900\ [km]$. This is a Low Earth Orbit (LEO), such that the SpaceX Starship (the chosen launch vehicle for this mission) will be able to launch the required mass to this altitude, and rendezvous here to refuel in orbit before launching on to the asteroid. Furthermore, the orbit is high enough to where the orbital decay rate should not be too high.

The inclination of the orbit was chosen at $0\,\mathrm{deg}$. This ensures that the spacecraft has the same groundtrack every orbit, giving more time in contact with the ground station. The spacecraft will be launched from SpaceX's Boca Chica launch site, which is at $18.45\,\mathrm{deg}\,N$. This is relatively close to the desired orbital inclination, so less energy will be needed to reach the desired orbit. There are launch sites on the equator that could be used, further reducing the energy needed to reach orbit. However, as the spacecraft will be refueled in orbit, this will not increase the total amount of ΔV that the system will have from LEO, and launching from a location outside the US would make the logistics of transporting the launch vehicle to the launch site significantly more difficult. For these reasons Boca Chica was determined to be the best launch site.

At this altitude, the spacecraft will have an orbital period of $103\ [min]$, with approximately $35\ [min]$ of eclipse time per orbit. As the spacecraft will be communicating with an omni-directional antenna, the spacecraft only needs to be in view of the ground station to communicate. This orbit should allow for $16.5\ [min]$ of communication time with the ground station every orbit. While in holding orbit, a minimal amount of data will need to be transferred back and forth and not as much power will be needed, so this should be sufficient. The chapters on communications and data handling (Chapter 10), as well as environmental control (Chapter 12) will go more in depth on these subjects.

In LEO, cosmic rays will also not be a problem like they would be in higher altitude orbits. As the spacecraft will be below the Van Allen belts, the amount of radiation in the orbit will be much lower. Inside the kick-stage there will also be an extra layer of stainless steel in front of the individual spacecraft, in addition to the skin of the satellites themselves, meaning any sensitive instruments will be exposed to far less radiation than while flying to the asteroid, so radiation concerns in the parking orbit are negligible.

7.1.1 Orbit Maintenance

In LEO, there is often a need for regular orbit maintenance. Even at $900\ [km]$ altitude there may be some atmosphere that will cause drag on the spacecraft and push it to a lower orbit. This can be calculated with the equation:

$$a = \frac{0.5\rho V^2 C_D S}{m} \tag{7.1}$$

Where a is the acceleration, ρ is the atmospheric density, V is the velocity, C_D is the drag coefficient, S is the cross-sectional area, and m is the mass.

The Starship upper stage can be approximated by a cylinder with a rounded nose. For such a shape, the C_D is proportional to the ratio of length/diameter, which in this case is $\frac{50[m]}{9[m]} = 5.56$. This results in $C_D \approx 0.2$.[42] The

cross sectional area is: $S = \pi r^2 = 63.6\ [m^2]$. The total mass of the Starship with the payload is approximately $176,000\ [kg]$. And the velocity in orbit should be $V = \sqrt{gr} \approx 8.445\ [km/s]$.

The most difficult quantity to estimate is the atmospheric density, as this fluctuates with solar activity, which is impossible to predict. However, taking the value at peak solar activity gives a worst case scenario, which means the drag should always be less than the estimated value. At peak solar activity, the atmospheric density at $900\ [km]$ altitude is $4.03E-13\ [kg/m^3]$[1].

Plugging in all the values to Equation 7.1, results in an acceleration of $1.039E-9\ [m/s^2]$. Integrated over the five years the system is potentially stationed in orbit, this results in a ΔV of $0.01\ [m/s]$. This is a negligible amount of drag at this altitude. Any other perturbations will be similarly negligible over the five year span. This means that for the holding orbit no orbital maintenance will be required.

7.2 ΔV Budget

In order to rendezvous with the asteroid a certain ΔV is needed. How much depends on the specific orbit of the asteroid in relation with earth. Added complexity comes from the time constraints set by the requirements of the mission. This makes it so that the spacecraft cannot be launched during the most efficient transfer window, resulting in the need for high energy transfers and further increasing the required ΔV.

The ΔV required depends heavily on the specifics of each asteroid's orbit. It was therefore decided to take a large sample of know asteroids and compute the ΔV required to reach these. This should serve as a good indication of the required ΔV to reach yet unknown asteroids.

A database of a few thousand asteroids was established. Data was taken for all asteroids within the relevant size limit (an absolute magnitude (a measure of how bright the asteroid appears) of 22.5 < H < 27.5, which roughly translates to $10 - 100\ [m]$ in diameter as per requirements AD-SH-PFM-1 & AD-SH-RISK-1), with an MOID with Earth of less than 0.05 [AU]. The asteroid data was acquired from the JPL small-body database[2], with SPK files generated from the JPL Horizons system[3].

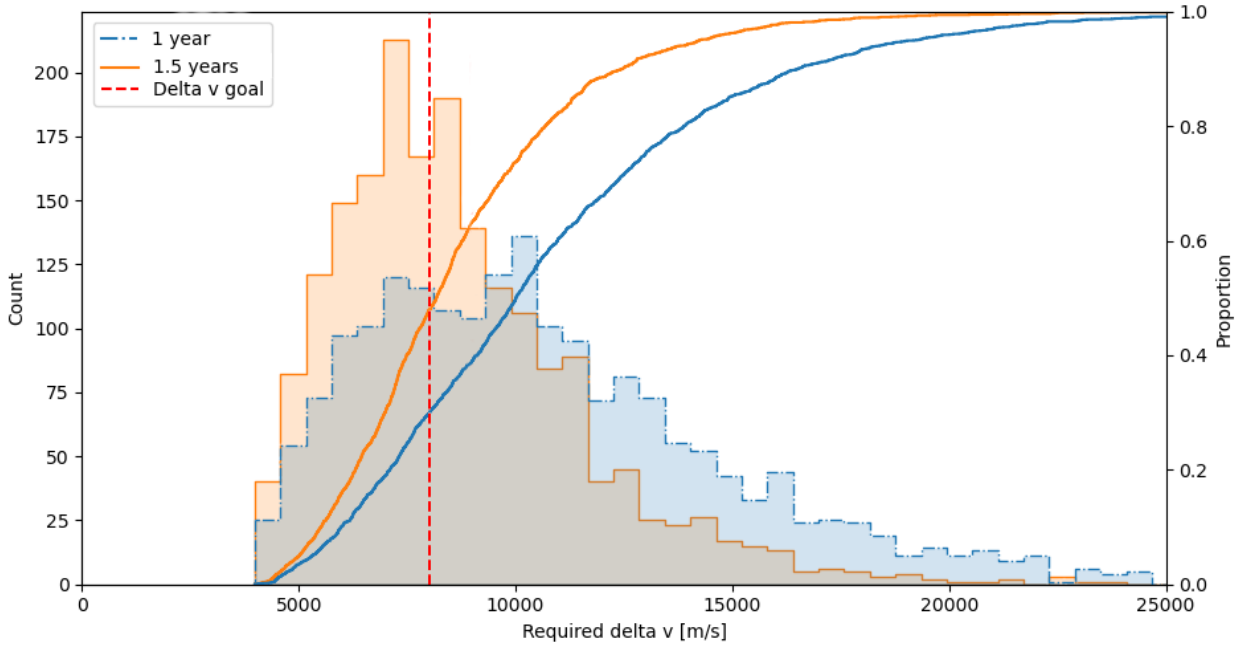

Figure 7.1: The required ΔV for reaching asteroids with a transfer window of 1 and 1.5 years starting 2 years before the asteroid's closest approach with Earth.

[1] URL `http://www.braeunig.us/space/atmos.htm` accessed 6 January 2021
[2] URL `https://ssd.jpl.nasa.gov/sbdb_query.cgi` accessed 2021-01-02
[3] URL `https://ssd.jpl.nasa.gov/x/spk.html` accessed 2021-01-04

Transfer orbits for each asteroid were calculated and optimized using pykep[4] and pygmo[5]. This resulted in a distribution of ΔV values for all asteroids. A restriction was placed on the transfer window: the window opens two years before the specific asteroids closest approach with Earth and lasts either a year or a year and a half. This allows for at least a year or half a year to deflect the asteroid. Finally the first burn of the transfer was adjusted to account for escaping Earth's gravity using Equation 7.2. Here V_1 is the required ΔV for the first burn after adjustment, V_∞ is the required ΔV for the first burn before adjustment, μ_{earth} is the standard gravitational parameter of earth and r is the distance from the earth's center of gravity to the spacecraft in it's parking orbit. The results can be seen in Figure 7.1.

$$\Delta V_1 = \sqrt{V_\infty^2 + \frac{\mu_{earth}}{r}} - \sqrt{\frac{\mu_{earth}}{r}} \tag{7.2}$$

Many of the asteroids required ΔV in excess of $10\ [km/s]$. This is infeasible with any currently existing launcher. It was therefore determined to set an upper limit on the ΔV available, and reduce the system's capabilities slightly.

A maximum ΔV was set at $8\ [km/s]$ (assuming using the SpaceX Starship with refueling in Earth orbit). This allows the system to arrive at 29.8% of asteroids within one year, and a further 18.1% of asteroids within 1.5 years. Thus the sytem will be able to reach 47.9% of the asteroids within 1.5 years See Figure 7.1.

[4]URL `https://esa.github.io/pykep/` accessed 2021-01-05
[5]URL `https://esa.github.io/pygmo/` accessed 2021-01-05

8 Mission Implementation

8.1 Optical Train

The main function of the Mission Implementation System is to concentrate and redirect sunlight. The Mid-Term Report [4] explores the solution space for a solar concentrator design. The further analysis in this report lead to a significant departure from the theoretical optimum system configuration presented in the Mid-Term Report. This departure is mainly due to the launch vehicle constraints. A major unsolved problem for solar concentrators has been the degradation of reflectors [4, 47]. The proposed optical train resolves this problem. The optical geometry is shown in Figure 8.3 and Figure 4.3 shows the spacecraft in its operational state.

8.1.1 Overview & Layout

The optical train consists of three major optical components:

1. Primary Reflector: Concentrates the incoming sunlight and reflects it toward the collimator
2. Collimator: Reflector that collimates the light and reflects it onto the secondary reflector
3. Secondary Reflector: Reflects the light towards the asteroid.

Figure 8.1 shows the simplified, flattened optical train.

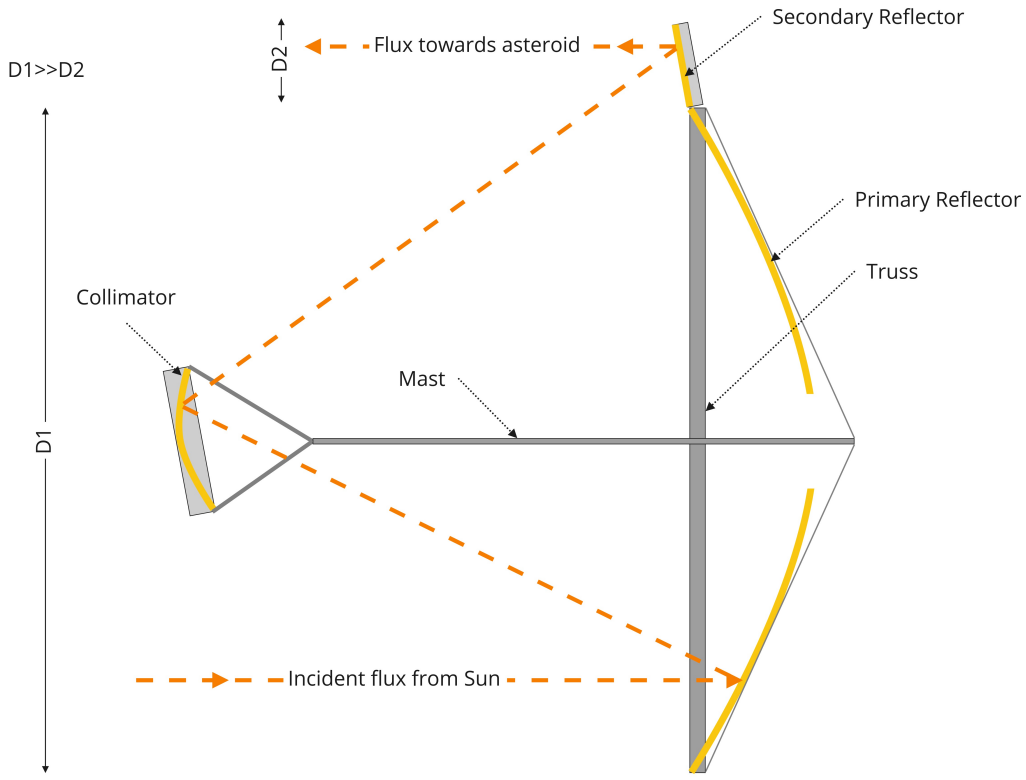

Figure 8.1: Simplified, flattened optical train with main supporting elements.

The radius of the collection area of a single spacecraft is $60\ [m]$ which is concentrated onto roughly circular area with radius of $3\ [m]$ on the asteroid which coincides for all spacecraft. All reflectors can be considered to be effectively non-imaging optics and the concentration ratio of a single space craft is 399. For normal, imaging concentrators this high concentration ratio would be impossible due to thermodynamic constraints. However, since the proposed system can be non-imaging and the temperature of the irradiated area is constrained not only by the radiative heat flux but also by the heat flux associated with the vapor mass [7, 39] this concentration

ratio is possible for this design.

The masses of the reflectors are given in Table 8.1.

Table 8.1: Masses of the reflectors. (Mass percentage is given as proportion of spacecraft total mass.)

Name	Total Mass [kg]	Mass [%]
Primary Reflector	610.72	51.874
Collimator	1.993	0.169
Secondary Reflector	2.5	0.212

8.1.2 Primary Reflector

The primary reflector is a parabolic dish reflector with a radius of $R = D/2 = 60\ [m]$ and a focal length of $80\ [m]$. The true depth H of the primary reflector is:

$$H = \frac{R^2}{4F} \tag{8.1}$$

The maximum angle between incoming and reflected ray θ_0 is:

$$\theta_0 = arctan\left(\frac{R}{F}\right) = 36.87° \tag{8.2}$$

Since the primary reflector is symmetric about its optical axis its geometry is fully described. Assuming perfect incidence, the light collection area, or aperture, of the space craft is thus:

$$A = \pi R^2 \approx 11310\ [m^2] \tag{8.3}$$

In the worst case, assuming the maximum pointing error of the ADCS the aperture is reduced by less than 0.07% which is acceptable.

The diameter of the primary reflector is constrained by the space available for the primary reflector truss in the payload bay of the launch vehicle, which is discussed in Subsection 8.2.1. The focal length is determined as a compromise between the mass of the mast holding it and the optical properties and mass of a deeper parabolic reflector. Additionally, the maximum mast length is limited by the space available in the payload bay: it was assumed that in no case a folded mast length of more than the collapsed height of the primary reflector truss is acceptable. Other types of concentrating reflectors, such as compound parabolic concentrators (CPC), have been considered, however their advantages are heavily outweighed by their larger mass or other structural considerations [39, 56, 65, 71, 92].

8.1.3 Collimator

Due to the mast holding the collimator, the incoming light cannot be reflected towards the center of the primary reflector where the main bus is stored. Different concepts for reflection along the central axis have been considered, however none were deemed feasible either due to payload bay constraints or insufficient mast stiffness. Hence, the collimator needs, additionally to collimating the incoming light, also reflect it to the side of the primary reflector. The angle between the optical axis of the primary mirror and the true optical axis of the collimator can be determined using Equation 8.2 where R is now

$$R = R_{primary} + R_{secondary} = R_{primary} + a_{semi\ major,\ secondary} \tag{8.4}$$

since, while the secondary reflector is not necessary circular, the expanding truss structure supporting it will have to be. This means that the collimator needs to be necessary an off-axis collimating reflector. Similar reflector concepts as for the primary reflector were considered. However, since a CPC would require a mechanism to transport a high powered beam towards the secondary reflector all concepts but an off-axis parabolic reflector (OAP) were deemed infeasible.

An OAP is a section of a parent parabolic reflector. The properties of the parent parabola will be referred to with the prefix ”true” while the OAP will use the prefix ”apparent” or ”off-axis”.

The radius of the OAP mus be the same as the radius of the intended illuminated area on the asteroid which is held constant at $3\ [m]$ [4]. The true focal length is then completely defined by the angle of divergence θ_0 of the primary reflector using Equation 8.2. The true depth of the parabola is then given by Equation 8.2. θ_0 is also the angle the apparent optical axis of the OAP makes with the true optical axis which intersect at the focal point. The OAP is then defined by the intersection of a circle with a radius of $3\ [m]$ projected on the optical axis of the OAP onto the true parabola.

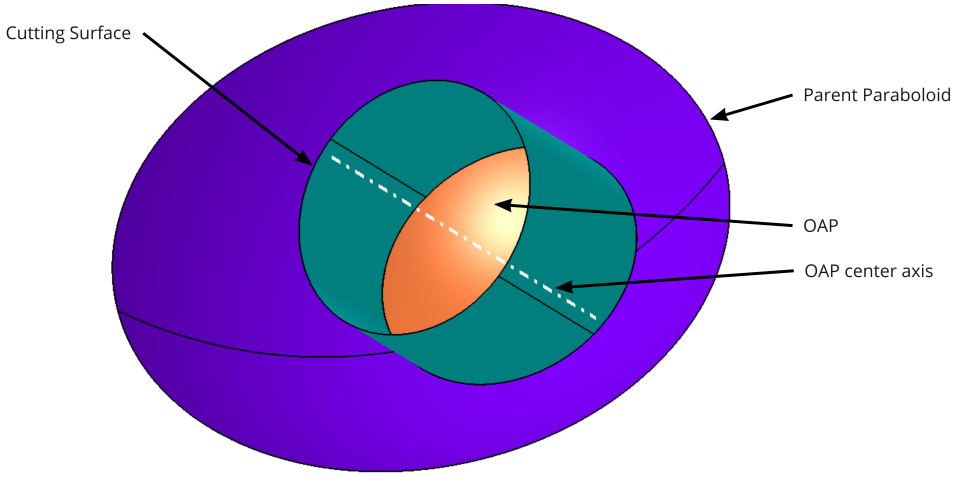

Figure 8.2: Sketch of the OAP construction.

8.1.4 Secondary Reflector

The secondary reflector can be a simple flat reflector since the light has already been collimated after being concentrated. The incoming light needs to be reflected towards the asteroid for a number of positions in 3 dimensional space around the asteroid. Hence the secondary reflector must be able to gimbal slightly and the shape of the reflector must be an elongated ellipse. The semi-major axis of this ellipse is $a = 4.5\ [m]$ and its semi-minor axis $b = 3.2\ [m]$. Furthermore the secondary mirror needs to be able to gimbal around two axis to adjust its exact pointing. This allows each spacecraft to be positioned in the whole space spanned by the constellation as shown in Chapter 5. See Figure 8.3 for an example optical geometry of one space craft.

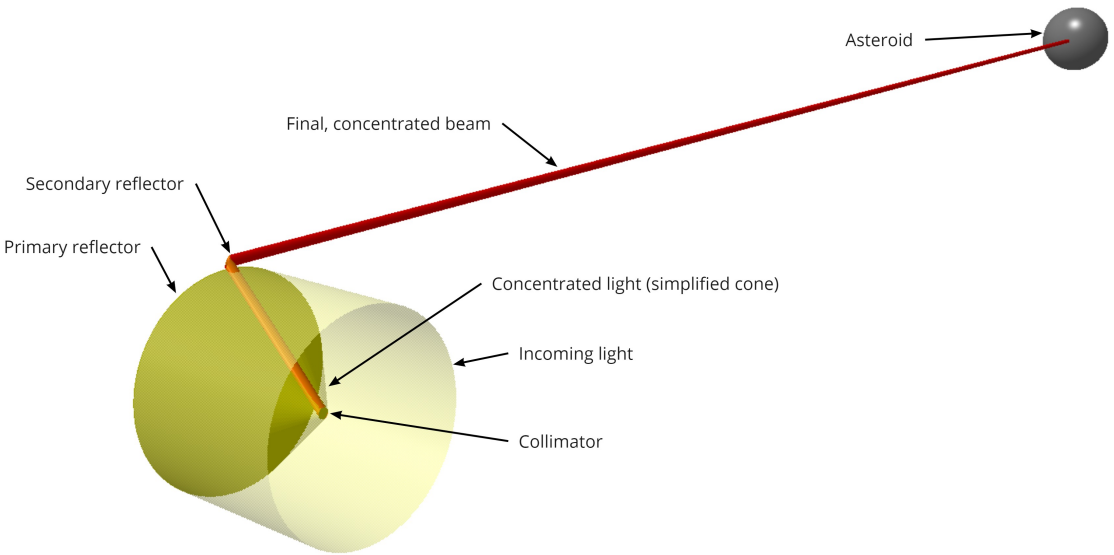

Figure 8.3: Sketch of the optical geometry of a single spacecraft.

8.1.5 Optical Properties

Reflectors

The reflectors need to reflect sunlight. The incident sunlight can be approximated as black body radiation with a temperature of $T \approx 5777\ [K]$. The amount of energy that can be reflect is constrained by the maximum wavelength that can be reflected by a given reflector. In order for an ideal thin reflector to reflect photons with wavelength λ the reflector's thickness t needs to be much larger than the wavelength of the photons $t >> \lambda$. A thickness of at least $3\ [\mu m]$ allows for a reflection of the super-majority of the usable solar flux. [44]

All reflectors are fabricated out of a polyimide film substrate that has been coated on one (or for the collimator both) sides with aluminum or silver. Kapton has seen wide use in space application and was selected for the substrate due to its high temperature stability, mechanical properties and technology readiness level [30, 91, 95]. Other promising substrates that have been considered are Mylar, carbon fiber mesh, carbon fiber nano-tubing and lithium [76, 95]. Kapton sheets can be manufactured with thicknesses starting from $2\ [\mu m]$ [95]. Furthermore, Kapton substrate has sufficiently low decomposition when exposed to radiation [66]. Nevertheless, extremely thin Kapton sheets are susceptible to rupturing under small loads and large sheets might rupture completely when punctured by a small object [40]. Furthermore, while Kapton sheets can be folded efficiently, precautions need to be made along the fold lines to inhibit the creation of fault lines [27]. Hence it was determined that the substrate shall have a minimum thickness of $100\ [\mu m]$.

It is possible the deposit metal coating with minimum thicknesses of $16\ [\mu m]$ for a total reflectively of 95% using vacuum vapor deposition [2]. However, even higher reflectively values are desirable and required for increased optical efficiency and to reduce thermal stresses as can be seen in Chapter 12. Coatings with a thickness of $20 - 100\ [\mu m]$ can reach up to a total reflectivity of 98% and are more resistant to degradation [2, 95]. The material of the coating was chosen to be high-purity aluminum due to its lower density, easier production and almost equivalent optical performance to silver [2, 43]. Furthermore, this aluminum coating has acceptable thermal properties, see Chapter 12 for more details. This results in a thickness of the reflectors of $200\ [\mu m]$. For comparison, the James Webb Space Telescope will use a Kapton sheet with a thickness of $500\ [\mu m]$ for its sun shield [61, 77].

The resultant total optical efficiency of the system is $\approx 0.94\%$.

Beam Divergence

Calculating final beam divergence is difficult for beams with a high energy flux per area. The ideal, classical focal point radius of the primary reflector is given by [7] as:

$$R_{focal\ point} = \frac{R_{sun} F_{primary\ reflector}}{d_{sun\ -\ asteroid}} \tag{8.5}$$

At $1\ [AU]$ this radius is $\approx 0.38\ [m]$. With a total of more than 11200 times the standard solar irradiance concentrated into this spot it is difficult to assess weather a classical treatment of the beam is sufficient to estimate the beam divergence. A classical treatment of the divergence of the image beam of the optical system uses the etendue of the incoming light and its imagine. Without having to fulfill the Abbe sine condition the rays of the optical system are Smith-Helmholtz invariant and the system can be analyzed using Fourier optics. With that and assuming optical power is conserved the Lagrange invariant and thus the etendue are conserved. The Lagrange invariant Ψ is a function of y and $\bar{y}$ the marginal and chief ray height respectively and u and $\bar{u}$ the marginal and chief ray angle, respectively, and n, the ambient refractive index. It is then given by [63] as:

$$\Psi = n\bar{u}y - nu\bar{y} \quad where \quad n = \frac{c}{v} \tag{8.6}$$

Assuming a perfect vacuum the local speed of light in the medium is equal to the speed of light $c = v$ and then $n = 1$. With this the etendue dG of light crossing some observer S with a cross section dS normal to the optical axis of the system (in this case the collimator or focal point) can then be expressed as:

$$dG = dScos(\theta)d\Omega \tag{8.7}$$

where θ is the angle of the solid angle $d\Omega$ of the incoming light (in this case the collimator angle θ_0).
In free space with the view factor F of differential areas A_1 and A_2 at distance s, with the ray - surface normal vectors angle θ:

$$F_{1\to 2} = \frac{1}{A_1}\int_{A_1}\int_{A_2} \frac{\cos\theta_1 \cos\theta_2}{\pi s^2}\, \mathrm{d}A_2\, \mathrm{d}A_1 \tag{8.8}$$

the etendue can be shown to be:

$$dG = d\Sigma \cos\theta_\Sigma \frac{\mathrm{d}S \cos\theta_S}{d^2} = \pi \, \mathrm{d}\Sigma \left(\frac{\cos\theta_\Sigma \cos\theta_S}{\pi d^2} \, \mathrm{d}S \right) = \pi \, \mathrm{d}\Sigma \, F_{\mathrm{d}\Sigma \to \mathrm{d}S} \tag{8.9}$$

where Σ is the light source and $d\Sigma$ is the surface of the light source (in this case the primary reflector). For reflections it can be shown that $dG_\Sigma = dG_S$ and hence the etendue of the system is conserved. [36, 50]

With this analysis an upper bound for the distance that the space craft can have from the asteroid can be estimated to be smaller than $5000[m] \pm 500[m]$ depending on the actual optical performance.

Nevertheless, this analysis of the optics of the system is purely classical, apart from the empirical values for the reflector properties. This might lead to an overestimation of the performance or might miss critical factors that would become clear when it, especially the reflector interaction with the incoming light and the optical geometry, is analyzed using either a more accurate classical or non-classical approach. Lastly, this analysis is can be applied whether the optical system is imaging or non-imaging. [7, 63]

8.2 Deployable Structure Design

Deployable structures are a key feature needed to meet the mission goals. The concept calls for many spacecraft with three large reflectors. No launch vehicle in the foreseeable future will have a payload bay large enough to fit the main reflector or collimator. The number of spacecraft directly impacts the effectiveness of the system. As the system uses the Starship as a kick-stage it is thus of high importance to ensure the maximum packing density to avoid having to launch multiple Starships into deep space. Not only do the reflectors need to become small enough to fit in the launcher payload bay, the entire spacecraft needs to become small enough to fit a large number of them together in the payload bay.

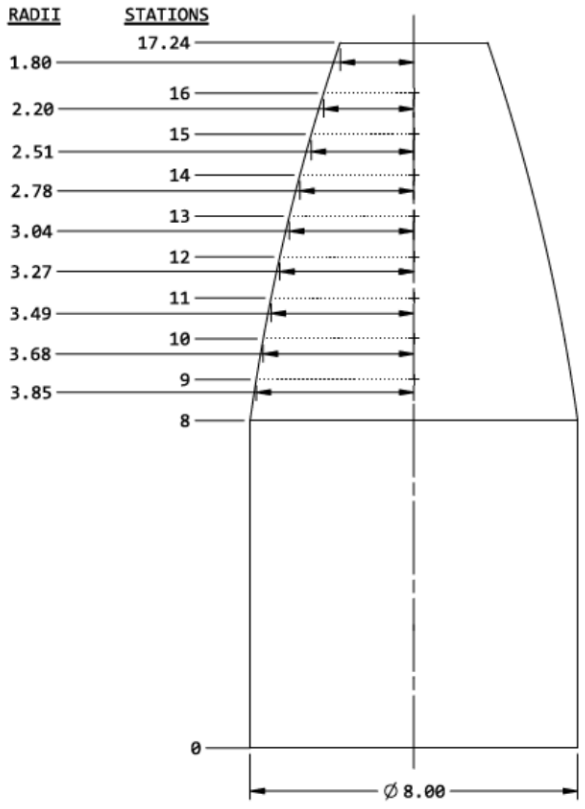

Figure 8.4: Dimensions of the 17 $[m]$ Starship payload bay. The payload bay length can be extended to 22 $[m]$. The dimensions are provided in meters. [1]

The team approached this problem by finding the optimal reflector and spacecraft size, allowing for a high packing density and volume utilization in the payload bay. For the initial iteration the team used literature values for how small the support structures could fold. After the sizing of the reflectors had been completed, the support structure was designed. The primary and secondary reflector and the collimator must be folded to fit into the payload bay. To keep development, testing and production costs low, one deployable structure design was used for all three reflectors. Due to size differences there will be differences in some components but the majority of the validation testing and production methods can be applied to all three.

8.2.1 Payload Packing

Each spacecraft consists of a large expanding structure that has a volume expansion fraction of $V_{expanded}/V_{folded} \approx 2300$. However, the large size of the deployed structure means that even with this efficient packing the stowed spacecraft is still large. Hence, the number of spacecraft that can be launched is limited by the volume available in the launch vehicle. The only launch vehicle powerful enough for the mission is the Starship (see Section 7.2). This is also the launch vehicle with the largest payload bay of any existing or in-development launch vehicles. The dimensions of the payload bay are taken from the Starship Users Guide[2] and can be seen in Figure 8.4.

[1] URL https://www.spacex.com/media/starship_users_guide_v1.pdf [accessed 26 January 2021]
[2] URL https://www.spacex.com/media/starship_users_guide_v1.pdf [accessed 26 January 2021]

The payload bay diameter of $8\ [m]$ can theoretically fit seven space craft on the same layer as can be seen in Figure 8.5. However, this would require that each space craft will have to support multiple other space craft which are positioned over it. Considering the maximum acceleration of the Starship during launch, this would require a significantly stronger spacecraft design. Hence, the central spacecraft will have to be replaced by a truss which can support the spacecraft further up the payload bay.

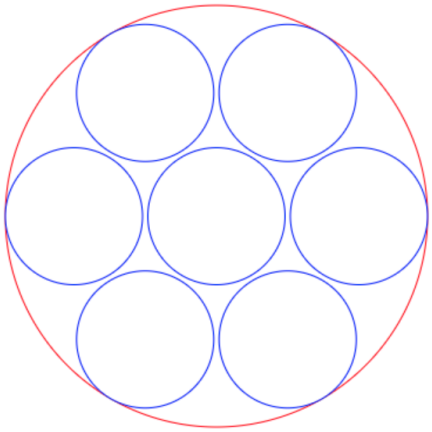

Figure 8.5: Maximum packing of spacecraft into Starship payload bay. The diameter of the large circle is $8\ [m]$ and the diameter of the small circles is $2.6\ [m]$.

Due to the diameter of the payload bay decreasing towards the end only four layers of six spacecraft each can be accommodated. In the smaller section of the payload bay four space craft will be stored per layer. This leads to four layers of six spacecraft each and two layers of four spacecraft. In total, the payload bay holds 32 spacecraft with sufficient space for a support structure and some space left over for ride-share options. See Figure 8.6 and Figure 8.7 for a visualization of the payload bay layout.

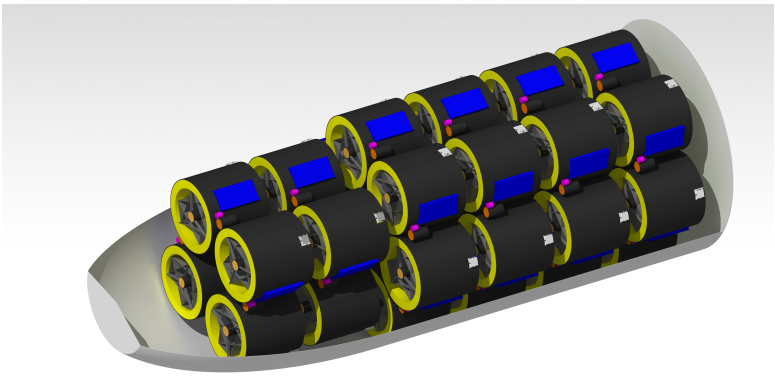

Figure 8.6: Starship payload bay cutaway showing the layout of all 32 spacecraft.

8.2.2 Reflector Folding

Fitting over $11,000\ [m^2]$ of reflector between the furled structure and the spacecraft bus requires that it is packed very densely. This cannot be accomplished by forcing the delicate reflector film into a small form factor. Instead the reflector must be folded in such a way that reduces the chance at tearing and tangling upon deployment while increasing packing density. Two folding patterns were analyzed that could be adjusted to fit the volume to depending on the height to diameter ratio.

The first pattern is know as the inverted cone pattern. The folding pattern is shown in Figure 8.8. The height to diameter ratio of the folded surface can be adjusted by changing the number of peaks. The major issue with this folding technique is that the folding density is not very high due to the chaotic nature as shown in Figure 8.8b. When collapsed the pattern still allows for voids to be present between layers. The advantage of the inverted cone is that it is very simple to construct.

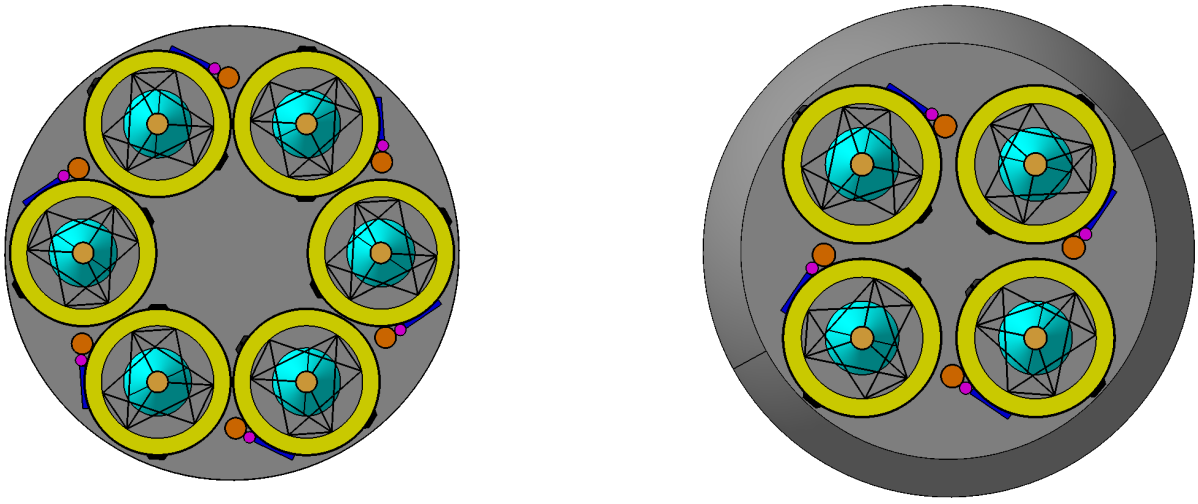

(a) Bottommost layer with six spacecraft.

(b) Topmost layer with four spacecraft. The lower layers are hidden.

Figure 8.7: Payload bay layout cross section

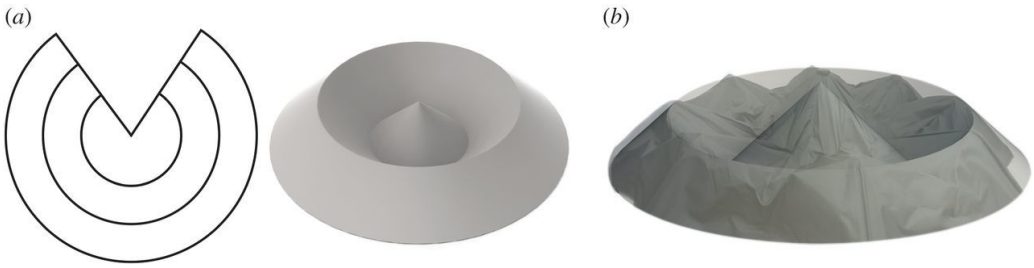

Figure 8.8: Inverted Cone Folding Pattern [10]

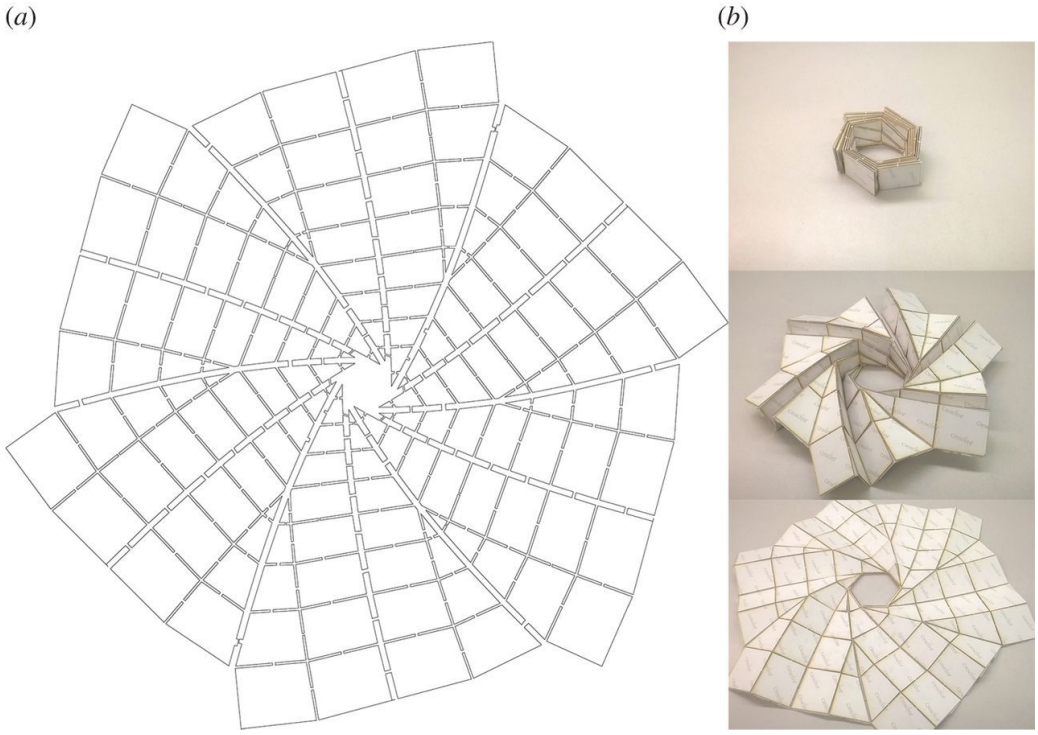

Figure 8.9: Flasher pattern [10]

The second pattern is known as the Flasher pattern and is shown in Figure 8.9. The Flasher pattern allows for a very tight packing density by having the surface of the sheet be very carefully folded which reduces the number of voids present. Achieving the flasher pattern is more difficult than the inverted cone as the folding lines need to be precise and the outer edge needs to rotate with respect to the inner edge during the fold. The rotation can be dealt with as the deployable structure does not need to be rigidly connected to the bus in the center. The Flasher pattern has been used before in spacecraft designs however it has not been flown yet [99].

Either pattern is suitable for the application. However due to the extremely large size difference needed between the deployed and furled reflector it was decided to use the Flasher pattern. This also allows for strategic use of reinforcement in case the reflector material is weakened due to folding. Folding Kapton in this pattern is feasible and the unfolding characteristics can be accurately predicted to ensure a suitable final reflector shape [27].

8.2.3 Reflector Support Structure

The support structure for the reflectors is required to have a very large volume ratio between the unfurled and furled configuration. It also must sufficient structural rigidity and strength that the deployed structure can be accurately pointed. The primary role however, is to support the reflecting sheets. The size of each of the reflectors in the optical train means that each must be supported by an expanding structure. The driving structure is the support for the main reflector so it will be discussed in more detail in this section. The other support structures follow the same design just at different scales and are shown in Table 8.2

The design of the support structure had three driving requirements. First the structure must meet the volume ratio and size requirements discussed in Subsection 8.2.1. The furled diameter of the structure must be smaller than $2.6\ [m]$ and the unfurled diameter must be $120\ [m]$ to support the main reflector[3]. To achieve this diameter a grid structure was designed that folds out to approximate the circle with a polygon as shown in Figure 8.10a. D is the diameter of the circle that describes the outer parameter of the polygon and N is the number of sides.

The deployable structure is made up of a number of rods and joints that are repeated for each section of the polygon. This structure can be seen in Figure 8.10b. The vertical rod AB must be longer than the length of one polygon section to ensure the structure can collapse. The rods BC, CD, AF and FE must each be half the length of one polygon section. The length of a polygon section is given by Equation 8.10.

$$X = D \cdot \sin \frac{\pi}{N} \tag{8.10}$$

The consequence of the the vertical rod AB having to be at least double the length of the polygon side is that the number of sides needs to be large enough that the vertical beams of the structure fit within the packing requirements. Another driving criteria for the number of sides that most mesh designs used to hold the reflector in the correct shape require the polygon to have sides that are a multiple of six [82]. Together these two factors led to the main reflector structure having 162 sides with a Section length of $2.327\ [m]$.

Table 8.2: Basic Dimensions of the reflector supports

Dimension	Value
Main Mirror Support Structure	
Radius	$60\ [m]$
Polygon number	$162\ [-]$
Polygon section length	$2.33\ [m]$
Undeployed diameter	$2.58\ [m]$
Rod element diameter	$0.01\ [m]$
Collimator\Secondary Reflector Support Structure	
Radius	$4.5\ [m]$
Polygon number	$48\ [-]$
Polygon section length	$0.6\ [m]$
Undeployed diameter	$0.382\ [m]$
Rod element diameter	$0.005\ [m]$

[3] $120\ [m]$ is the projected diameter of the parabolic reflector.

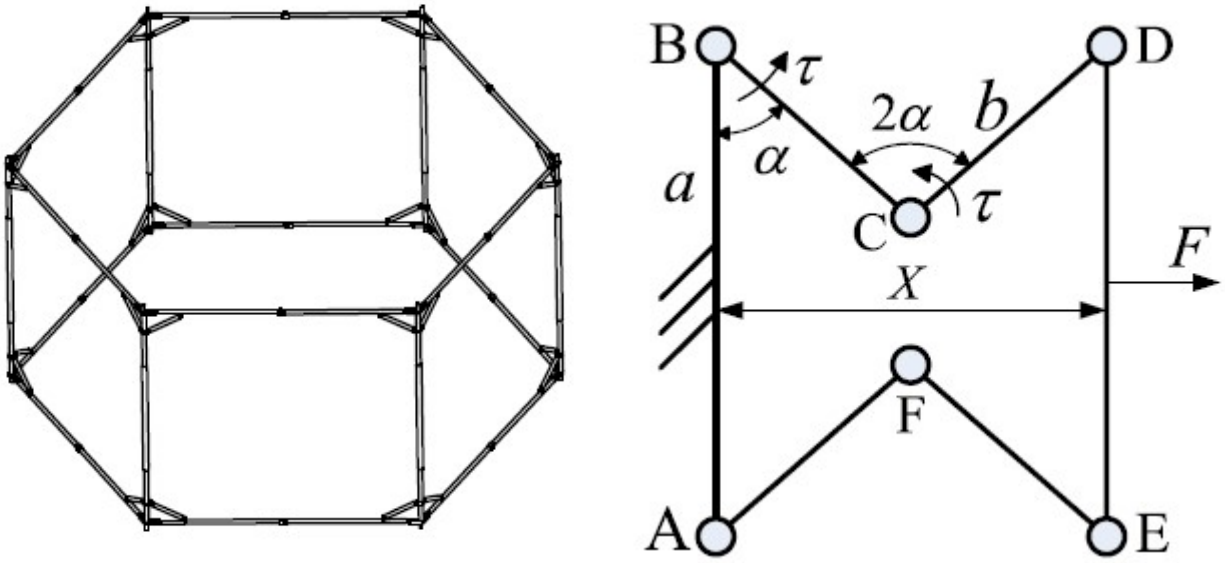

(a) Deployable Structure with $n = 6$ [72]

(b) Partially folded section of the deployable structure [72]

Figure 8.10: Geometry of the deployable structure

The mechanics of the deployable structure can be seen in Figure 8.10b and Figure 8.11. When full furled the system is limited in size but the diameter of the rods and the number sides. As the rods can be relatively small this allows for a small furled diameter even at high N numbers.

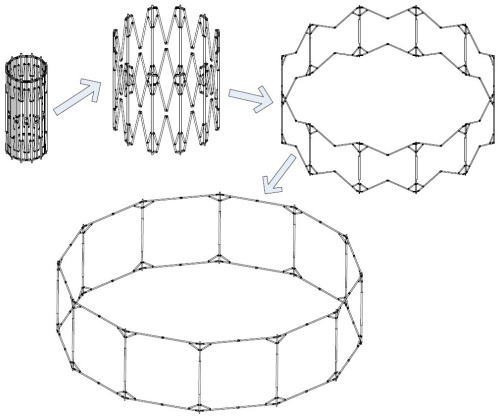

Figure 8.11: Multiple Stages of deployment of the deployable structure [72]

Driving the expandable structure is done via constant torque springs. The springs are located at A, B, C and D in Figure 8.12 or more generally the springs are located at between every short rod. The springs are supported on small rods as as shown in Figure 8.13. Pulleys and wires were used to the structure from building significant momentum during deployment. The wires are run as shown in Figure 8.12. A small electric motor is used to hold back the springs. In case of an electrical failure on the motor there is still a reasonable chance the reflector will successfully deploy.

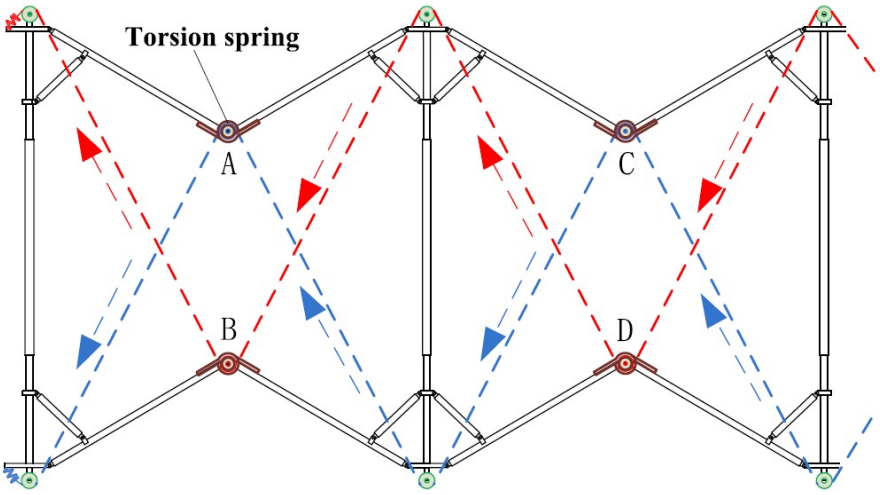

Figure 8.12: Spring driven system for deploying the reflector supports [72]

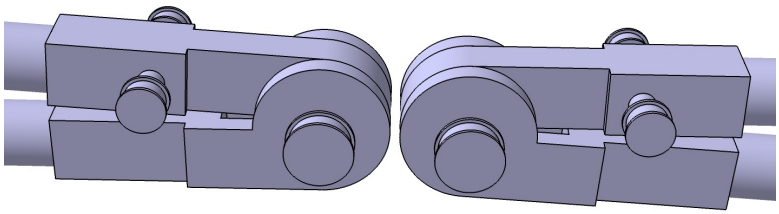

Figure 8.13: Close up of the Connectors that support the constant torque springs

8.2.4 Reflector Mesh Support

The second part of the support structure for the reflectors is the net on the back. This is to help pull the sheet into the correct shape. The mesh forms triangular sections and is designed such that at full deployment the array is tensioned into the correct shape. On both the secondary reflector and the collimator the mesh is support as shown in Figure 8.14. On these smaller reflectors the mesh is fully and only supported by the deployable grid structure.

The primary reflector requires a more intricate solution due to the very large depth of the reflector. The reflector requires a depth of $11\ [m]$ while the structure is only $2.327\ [m]$ high. Instead the mesh is connected at the center to the deployable mast. This allows the deployable structure to be small but also allows the main reflector to be shaped correctly.

The mesh will be made out of thin metal strands and will be braided to ensure that it holds its shape correctly and does not deteriorate over time [82]. The mesh also needs to be able to deal with high temperature fluctuations as the temperature will not be actively regulated. Tungsten or Molybdenum are both suitable choices for material [82].

Figure 8.14: Shape support mesh/net of an antenna in a deployable structure [82].

8.3 Cleaning of the secondary reflector

The secondary reflector allows for the primary reflector to stay out of the ejecta cloud thus maintaining its efficiency and increasing its longevity. Naturally this only moves the problem as now the secondary reflector is inside of the ejecta cloud and thus will collect dust particles over its operational lifetime. Thus it is still essential for some kind of cleaning method to be employed. However due to the much smaller size and the straightness of the secondary reflector this is a much more manageable task compared to cleaning the primary reflector.

While some research was done into multiple cleaning methods there was one method which was deemed by far the most promising and hence this method was selected. The method being cleaning the secondary mirror by ejecting particles using electrostatic and dielectrophoretic forces generated by a 'curtain' of electrodes inside a strong polymer layer placed on top of the secondary reflector.

8.3.1 Working principle

The basic principle of the curtain is having a series of parallel electrodes, embedded in a strong dielectric layer, generating an electric field and thus exerting a force on any charged particles lying on top of it. Figure 8.15 (left) shows the basic working principle of the curtain. An AC voltage source generates an electric field which direction oscillates as the polarity of the electrodes change. Any charged particles are pushed along the electric field either away from the surface and slightly to the side or towards the electrode within the curtain surface. Any particles charged so that they would be pulled towards the electrode would be pushed away and ejected as the polarity of the electrode changes. [11]

The technology is originally developed for use in the dusty environments of the martian or the lunar surface. Here due to the presence of gravity particles pushed away from the surface in an oscillating sideways direction would simply fall back on top of the surface. Hence the technology employs a three-phase curtain, Figure 8.15 (right), where a traveling wave pushes the particles along or against the wave and thus sideways and eventually off the curtain. For the application in deep space where there is no gravity, it is not needed to have this three-phase curtain as any particle pushed away from the curtain will not return to the curtain as long as the ejecta cloud is sparse enough that the particles from the ejecta do not hit the particles pushed away by the curtain. For our application this is the case and hence a single-phase electric curtain will be used as, besides simplicity, this has the benefit of creating no sideways thrust due to the particles being ejected in quickly alternating sideways directions. Equation 8.11 describes the motion of the particles where m is the particle mass, r is the particle's position, E is the electric field, q is the particle charge, η is the viscosity of the fluid in which the particles move and g is the acceleration due to gravity. Note that due to the lack of significant gravity and atmosphere the two right most terms reduce to zero.

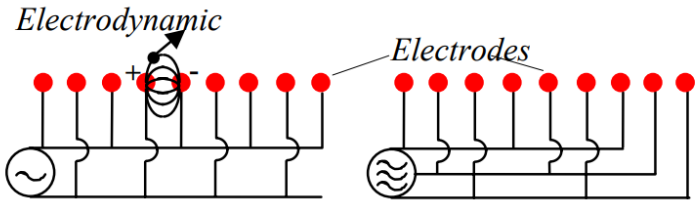

Figure 8.15: :(Left) Single-phase electric curtain. (Right) Three-phase electric curtain [81]

$$m\frac{d^2r}{dt^2} = qEcos(\omega t) - 6\pi\eta\frac{dr}{dt} - mg \tag{8.11}$$

As can be seen from Equation 8.11 the motion of the particles is highly dependent on their charge. A concern would be whether this system is able to clear out uncharged particles. Luckily it has been observed that these uncharged particles clear out from the curtain as well. This is due to two factors. Larger neutrally charged particles carry both positive and negative charges on their surface, albeit in equal amounts, these particles can still be lifted by the curtain [13]. Similarly particles with intrinsic electric dipole moments or containing polar materials will also experience this so called dielectrophoretic force as long as they have a different dielectric constant than that of the surrounding medium [13]. This force will either push or pull the particles away or towards the electrodes. In the case of the particles being pulled towards the electrodes will travel along the insulated curtain as the electrodes polarity changes and would as a result of this triboelectrically acquire a charge after which it will be lifted from the curtain by the stronger qE force [13]. Hence the presence of neutral particles is of no concern.

8.3.2 Design and implementation

In this section the major design choices are explained for the application of this technology in our specific use case. An overview of the design choices can be found in Table 8.3.

The electrodes should be embedded in some kind of polymer with high heat resistance as the secondary reflector will heat up, a high dielectric voltage breakdown as then a high voltage can be run through the electrodes, and a high resistivity so little power is consumed during operation. It happens that the Kapton used as reflector material fits these requirements perfectly. Naturally the secondary reflector is designed to withstand the heat it operates in so heat is not an issue. It has an extremely high dielectric breakdown voltage of $154\ [kV/mm]$ allowing for a voltage well beyond what is necessary. Finally it has sufficient resistivity in the range of $10^{10} - 10^{17}\ [\Omega \cdot cm]$. The electrodes can thus be printed straight on the back of the secondary reflector,

no additional dielectric material is needed for embedment saving weight.[4]

As for the electrode material it must be able to resist the same heat as the secondary reflector, must be a good conductor and most constraining it must be flexible enough to be folded up as the secondary reflector is. For this stretchable silver nanowire conductors are chosen. These are silver nanowires embedded in the surface layer of a polydimethylsiloxane wire. The result is a highly flexible and stretchable wire with a very high conductivity of $5285\ [S/cm]$ [96]. Furthermore it also satisfies the heat requirement as polydimethylsiloxane is capable of withstanding heats upwards of $400\ [^{\circ}C]$ [15].

The spacing between the electrodes is set to be $0.67\ [mm]$. This value was chosen as changing the spacing of the electrodes in the range of $0.48 - 0.67\ [mm]$ had no major effect on the performance as all tested values were able to clear particles such that over 98% of the solar energy went through [14]. However larger electrode spacing in excess of one millimeter will negatively affect the performance [11].

Initially the electrode lay-out was a spiral design similar to those tested in [12–14]. The advantage being that in a three-phase design the particles would be ejected evenly in all directions and thus creating no net sideways thrust and no moment. This spiral design however has a few significant disadvantages. Mainly that due to the large size of the reflector the electrodes would become extremely long (several thousand meters) resulting in the resistance along the electrode increasing to levels so high it would rival that of the dielectric polymer. Additionally with only two or three very long electrodes present having one break would mean the reflector cleaning system would largely no longer function. Hence this idea was discarded and multiple straight electrodes connected in parallel along the semi-minor axis of the reflector were chosen instead. This way electrode length is no longer an issue. In case of one electrode breaking only a very minor part of the reflector will no longer be able to be cleaned. Also it is possible to connect both sides of the electrodes to the voltage source making it that an electrode has to break in two separate places to cease functioning.

The AC power source must be able to provide a high voltage. The higher the voltage the greater the force on the particles. A combination of $0.67\ [mm]$ electrode spacing and a voltage of $1500\ [V]$ is capable of cleaning over 98% of simulated lunar dust [13, 14]. These tests however were done in a gravity environment and thus levels of cleaning of over 98% should easily be possible in the no gravity environment the cleaner will operate in. Additionally for the tests the electrodes had a layer of polymer on top thicker than the secondary reflector, hence with the dust closer to the electrodes in our case even better results should be achievable. While $1500\ [V]$ should be a more than sufficient operating voltage ideally one would like to have an optical sensor on the reflector so that the operating voltage can be adjusted dynamically to achieve the desired cleaning at a minimum power use. As for the frequency of the AC source it is shown that a frequency in the range of $10 - 100\ [HZ]$ has no significant effect on the effectiveness of the curtain [11]. The frequency is then chosen to be $100\ [HZ]$ as it makes sense to choose a frequency on the higher end of the range as a higher frequency gives the dielectric material increased resistance and thus reduces the power consumed.

Table 8.3: An overview of the design choices made for the electrostatic curtain responsible for the cleaning of the secondary reflector.

Design Choice	**Chosen Option**	**Reasoning**
Electric curtain type	Single-phase electric curtain	Sufficient for zero-gravity environments.
Dielectric material for electrode embedment	Directly onto the back of the secondary reflector	The secondary reflector has sufficient dielectric properties, no need for additional material.
Electrode material	stretchable silver nanowire conductor	Highly flexible conductor with sufficient heat resistance.
Electrode spacing	$0.67\ [mm]$	Biggest spacing that is still proven to be over 98% effective.
Electrode voltage	$1500\ [V]$	Proven to be over 98% effective.
AC frequency	$100\ [HZ]$	Highest frequency proven to still be effective.

[4]URL http://www.matweb.com/search/datasheet_print.aspx?matguid=338573ad1bdf4586aa17fab95f3a57d7 [accessed 11 January 2021]

8.3.3 Power estimate

A power estimate was done on the curtain. The power dissipated comes from the voltage over the dielectric material which acts as a resistor. Equation 8.12 gives the equation used to calculate the power dissipated. Here P_{max} is the power dissipated while the curtain is turned on, n is the number of electrodes on the curtain, V is the voltage running through the electrodes, R is the resistance provided by the dielectric material in between the electrodes, L_i is the length of the electrode, σ is the resistivity of the dielectric assumed as a worst case to be 10^{10} and ε is the spacing in between the electrodes. The power dissipated while the curtain is turned on was estimated to be $44.16\ [W]$.

$$P_{max} = \sum_{i=1}^{n} \frac{V^2}{R} = \sum_{i=1}^{n} \frac{V^2 \cdot L_i h}{\sigma \varepsilon} \tag{8.12}$$

8.4 Mast

The mast is the central truss along the optical axis of the primary reflector. It is split into two sections which are separated by the spacecraft bus: the front mast and the aft mast. The function of the front mast is to support the collimator and it is the largest part of the mast. The function of the aft mast is to provide support for the primary reflector.

The collimator is positioned roughly $84\ [m]$ from the deepest point of the primary reflector. The spacecraft bus is positioned at the height of the rim of the primary reflector. This means that the total length of the front mast must be $l_{mast} = d_{collimator\ -\ primary\ reflector} - H_{primary\ reflector} \approx 72.75\ [m]$. The collimator can either be connected to the mast via the center or along the outside diameter of its support structure. Connecting the mast via the center of the support structure means that some part of the reflector is occluded by the mast. Connecting the collimator via the outside diameter also partly occludes the reflector, however this is much less severe as the occlusion occurs far from the focal point.

Typically antennas making use of deployable structures hold their shape by using a mesh extending from the opposite side of the support structure as shown in Figure 8.14. This is not possible for the primary reflector since its depth is much larger than the depth (or height) of its support truss. Hence a different structure needs to hold the shape of the reflector. The lightest possible structure accomplishing that task is a central mast that extends far enough behind the primary reflector that cables can be panned between it and the outside diameter of the truss holding the primary reflector. From these spoke-like cables more cables can be run towards the reflector, holding it in shape. Since the forces acting on the reflector are very small, the cables can be extremely light. This allows the folded aft mast to be only $0.2\ [m]$ in length instead of $12\ [m]$ at the same mass.

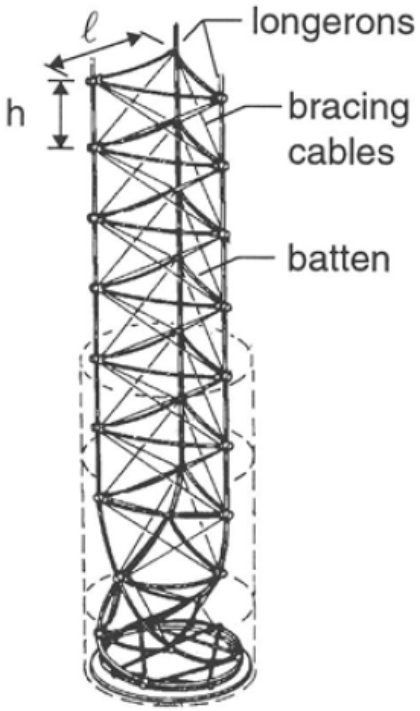

Figure 8.16: Deployable boom structure using a repeating 3-sided prism as its basic element [68].

The mast itself can be subject to complex loading cases during slewing of the spacecraft. These complex loading cases necessitate a structure with a significant cross section. Additionally, as is discussed before, the length of each part of the mast is significant, hence its packing needs to efficient as well. Typically deployable boom (mast) structures make use of a repeating elements which consist of longerons and batten (see Figure 8.16) which are joined by some kind of joint. These designs make use of either 3-sided prisms or cubes as their elements [8, 68]. The most efficient packing of

large cube-based booms flattens its elements and then rolls them up into a drum. This drum needs to oriented with its center axis perpendicular to the extension direction as can be seen in Figure 8.17. This is extremely inconvenient for the proposed spacecraft since it wastes space inside the folded primary reflector. Furthermore, the total length of this structure is limited by the diameter of the inside of the folded primary mirror as can be seen in Figure 8.18. However, structures using a 3-sided prism as their basic element can be folded up into a cylinder shape which expands along its center axis. This allows the structure to stowed inside the spacecraft and leaves some space for the spacecraft bus. Furthermore, this configuration allows the collimator to be stowed inside the envelope of the folded primary reflector, reducing the overall length of the spacecraft.

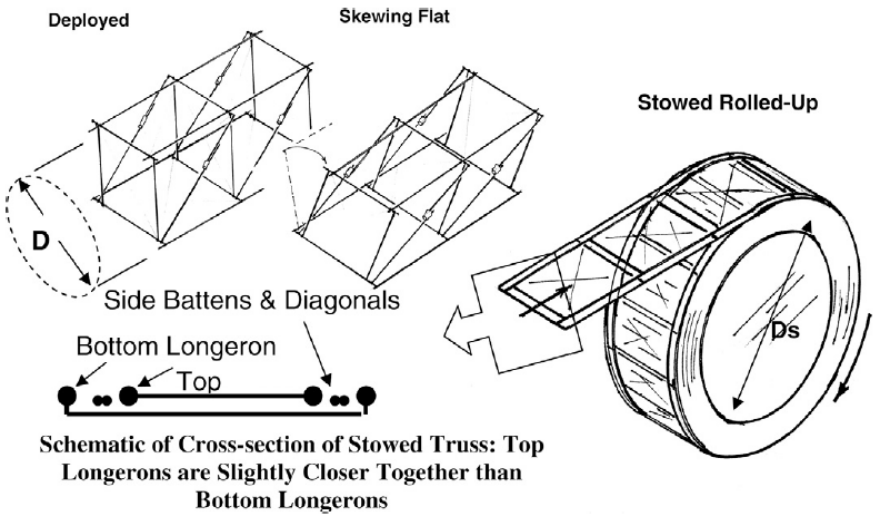

Figure 8.17: Deployable boom structure using a repeating cube as its basic element [8]

In order to archive high stiffness cables need to be spanned on each side of each element. The battens must be in a buckled state, which pretensions the cables without reducing compression stiffness of the overall structure [68]. The batten must be stored inside the folded primary reflector so their length is constrained as can be seen in Figure 8.19.

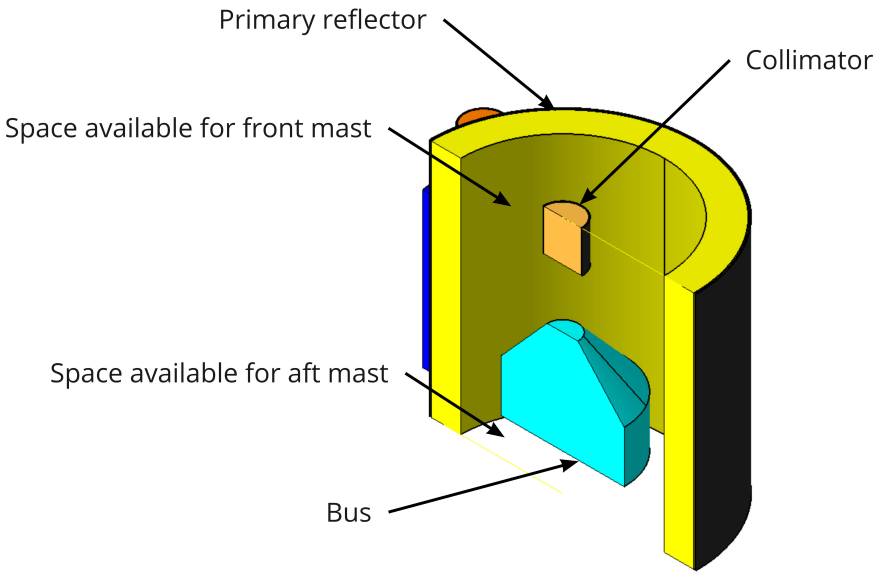

Figure 8.18: Cross-section of the simplified, folded spacecraft showing the available space for the folded mast.

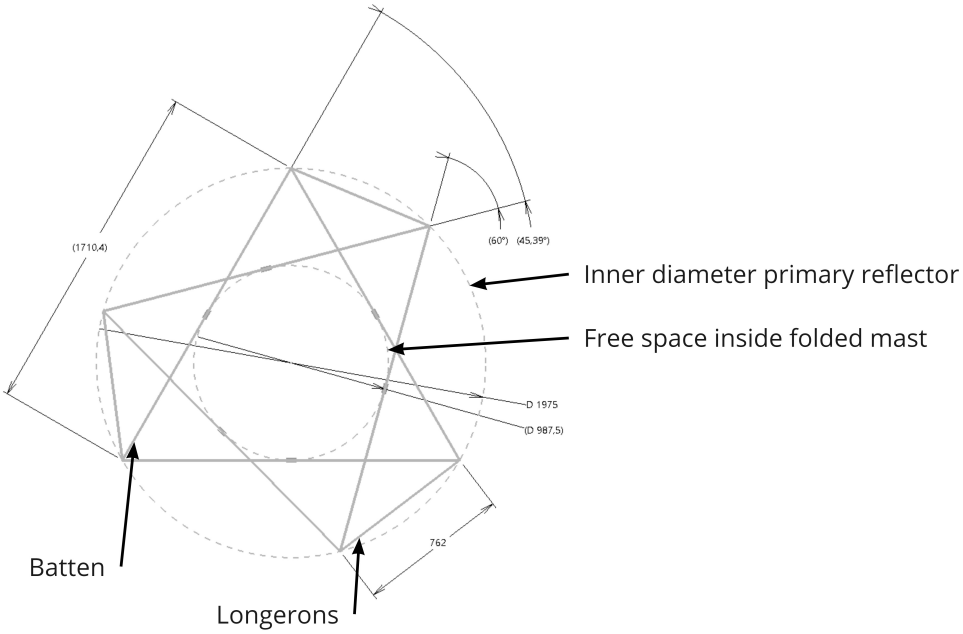

Figure 8.19: Geometry of the flattened mast with dimensions.

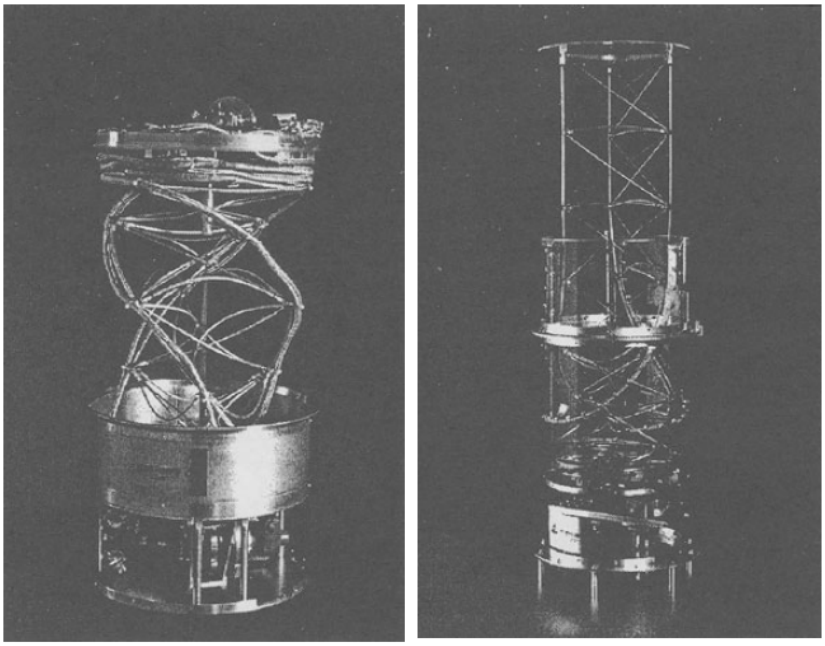

Figure 8.20: Zig-zag laying of the mast [68].

The most reliable type of prism deployable booms make use of joints that are preloaded and return to their deployed state when the boom is released [68]. Additionally, these joints need to be self-locking once deployed. This significantly increases the stiffness of the structure and inhibits a failure mode where the truss twists itself out of its deployed state when under compression and slewed around the x-Axis (see Figure 9.4 for the reference frame) [97]. This design has minimal risk compared with active deployment by multiple motors or actuators [85].

The front and aft mast have cables running to the support truss of the primary reflector. Hence, the mast needs to be folded without continues rotation but rather using zig-zag laying, depicted in Figure 8.20. This inhibits the cables tangling up during deployment. This leads to a helix-like stacking which reverses direction every two elements. The efficiency of this kind of folding is slightly less than that of a pure helix. The efficiency can be increased by altering the angles between the flattened battens of one element to the next. However, this is not necessary as the folded structure is already small enough for the spacecraft and would increase production costs because of the dissimilar joints required. [68]

This structure can be idealized as a Euler strut so that the buckling failure load is:

$$P_1 = \frac{\pi^2 E I_C}{L^2} \tag{8.13}$$

for the entire structure, where I_C is the combined second moment of inertia of the longerons, E is the Youngs modulus of the longerons and L is the total length of the mast. Additionally, bucking of each element needs to be considered, assuming all three longerons buckle simultaneously:

$$P_1 = \frac{\pi^2 E I_L}{l^2} \tag{8.14}$$

where I_L is the the second moment of a single longeron and l is its length. [68] Each the longerons and batten have the same cross section; an outside diameter of $10\ [mm]$ and a wall thickness of $1\ [mm]$. They are made out of a carbon fiber composite. The analysis in Chapter 13 shows that the masts are fit-for-purpose. Table 8.4 gives an overview of the resulting masses of the mast components.

Table 8.4: Masses of the elements of the mast. Includes cables, joints, batten and longerons. (Mass percentage is a proportion of the total spacecraft mass.)

Name	Total Mass [kg]	Mass [%]
Mast Front	81	6.43
Mast Collimator Holder	12	0.857
Mast Aft	23	1.715

8.5 Requirements

Table 8.5 shows the requirements on the MI system and its compliance with them.

Table 8.5: Mission Implementation Requirements

Identifier	Requirement	MOC	Compliance
AD-SYS-TECH-MI-1	The mission implementation system shall concentrate sunlight by at least a factor of $375[-]$.	Test	Y
AD-SYS-TECH-MI-2	The beam of emitted light shall have a diameter of less than $6\ [m]$ at the asteroid.	Inspection	Y
AD-SYS-TECH-MI-3	The primary collector aperture shall be $11300\ [m^2] \pm 10\%$.	Analysis	Y
AD-SYS-TECH-MI-4	The mass of the primary reflector shall be less than $625\ [kg]$.	Inspection	Y
AD-SYS-TECH-MI-21	The mass of the collimator shall be less than $5\ [kg]$.	Inspection	Y
AD-SYS-TECH-MI-22	The mass of the secondary reflector shall be less than $10\ [kg]$.	Inspection	Y
AD-SYS-TECH-MI-5	The primary reflector shall have a depth of less than $15\ [m]$.	Inspection	Y
AD-SYS-TECH-MI-6	The apparent depth of the collimator shall be less than the length of its support truss.	Inspection	Y
AD-SYS-TECH-MI-7	The collimator shall produce a collimated beam.	Test	Y
AD-SYS-TECH-MI-8	The collimated beam of the collimator shall be redirect by a secondary reflector.	Test	Y
AD-SYS-TECH-MI-9	The secondary reflector shall be able to gimbal around 2 axes.	Demonstration	Y
AD-SYS-TECH-MI-10	The MI system shall be able to utilize at least 90% of the incoming solar flux.	Analysis	Y

Table 8.5 – *Continued on next page*

Table 8.5 – *Continued from previous page*

Identifier	Requirement	MOC	Compliance
AD-SYS-TECH-MI-11	The MI system shall be able to reflect wavelengths below $3\ [\mu m]$.	Test	Y
AD-SYS-TECH-MI-12	The total optical efficiency of the MI system shall be at least 90%.	Test	Y
AD-SYS-TECH-MI-13	The reflectors of the MI system shall have a combined rupture probability of no more than 0.5%.	Analysis	Y
AD-SYS-TECH-MI-14	32 spacecraft shall fit into the $22\ [m]$ payload bay of Starship.	Demonstration	Y
AD-SYS-TECH-MI-14.1	Each spacecraft shall have a height of less than $2.5\ [m]$ when stowed.	Inspection	Y
AD-SYS-TECH-MI-14.2	Each spacecraft shall have an average diameter of less than $2.6\ [m]$ when stowed.	Inspection	Y
AD-SYS-TECH-MI-14.3	Each spacecraft shall protrude outside the diameter given by AD-SYS-TECH-MI-14.2 at no more than one place.	Inspection	Y
AD-SYS-TECH-MI-14.4	The protrusion specified by AD-SYS-TECH-MI-14.3 shall span less than $25\ [°]$ around the x-axis.	Inspection	Y
AD-SYS-TECH-MI-14.5	The layout of the stowed spacecraft in the payload bay of the LV shall allow for a support truss.	Analysis	Y
AD-SYS-TECH-MI-14.6	Between each layer of spacecraft there shall be no less than $0.5\ [m]$ vertical space.	Analysis	Y
AD-SYS-TECH-MI-16	The reflectors shall be able to expand to its deployed state.	Test	Y
AD-SYS-TECH-MI-17	The support truss of the primary reflector shall be no higher than $2.5\ [m]$ when stowed.	Inspection	Y
AD-SYS-TECH-MI-18	The support truss of the primary reflector shall have a diameter of no more than $2.6\ [m]$ when stowed.	Inspection	Y
AD-SYS-TECH-MI-19	The reflectors shall not deviate more than 1% from its intended shape during nominal operation.	Test	Y
AD-SYS-TECH-MI-19.1	The primary reflector shape shall be supported along at least 16 lines when deployed.	Inspection	Y
AD-SYS-TECH-MI-19.2	The collimator shape shall be supported along at least 6 lines when deployed.	Inspection	Y
AD-SYS-TECH-MI-19.3	The secondary reflector shape shall be supported along at least 6 lines when deployed.	Inspection	Y
AD-SYS-TECH-MI-20	The secondary reflector shall not degrade below 95% efficiency at at EOL.	Analysis	Y
AD-SYS-TECH-MI-20.1	The secondary reflector shall be actively cleaned.	Test	Y
AD-SYS-TECH-MI-20.2	The secondary reflector shall withstand a temperature of at least $400\ [C]$ without performance decrease.	Test	Y
AD-SYS-TECH-MI-20.3	The secondary reflector shall use less than [TBD] [W] during operation.	Inspection	TBD
AD-SYS-TECH-MI-24	The front mast shall support the collimator.	Test	Y

Table 8.5 – *Continued on next page*

Table 8.5 – *Continued from previous page*

Identifier	Requirement	MOC	Compliance
AD-SYS-TECH-MI-24.1	The front mast shall have a length of 84 $[m]$ when deployed.	Inspection	Y
AD-SYS-TECH-MI-24.2	The position of the tip of the front mast shall vary no more than 5 $[mm]$ in any direction during nominal operation.	Test	Y
AD-SYS-TECH-MI-24.3	The front mast shall have a length of no more than 1.2 $[m]$ when stowed.	Inspection	Y
AD-SYS-TECH-MI-24.4	The front mast shall not occlude any concentrated beam within 5 $[m]$ of the focal point.	Inspection	Y
AD-SYS-TECH-MI-25	The aft mast shall support the primary reflector.	Test	Y
AD-SYS-TECH-MI-25.1	The aft mast shall have a length of 14.2 $[m]$ when deployed.	Inspection	Y
AD-SYS-TECH-MI-25.2	The aft mast shall have a length of no more than 0.3 $[m]$ when stowed.	Inspection	Y
AD-SYS-TECH-MI-27	The mast shall permanently self-lock when fully deployed.	Test	Y
AD-SYS-TECH-MI-28	The mast shall withstand a compression load of at least 100 $[N]$ when deployed.	Test	Y
AD-SYS-TECH-MI-29	The secondary reflector shall be mounted at the rim of the primary reflector.	Inspection	Y
AD-SYS-TECH-MI-30	The MI system shall point the collimated, concentrated beam within a 5 $[^\circ]$ half-angle cone.	Test	Y

9 Attitude Determination and Control System

In order to focus the concentrated beams of sunlight focused by the primary reflector and aimed with the secondary reflector, a precise attitude determination and control system is necessary. This allows the system to focus with pointing errors specified by the requirements, but also allows for the system to focus a set distance away from the asteroid in order to maintain the efficiencies outlined in the midterm report solar concentrator concept [4]. With higher pointing accuracies, the system was able to maintain larger distances from the asteroid, thus making less use of the cleaning systems on-board. This chapter will discuss the processes required in sizing and selecting the required reaction control wheels, RCS thrusters, and an ion engine, as well as the fuel containers and fuel required for the systems to operate nominally. This will culminate in the torque generation and pointing accuracy models, which were used to calculate the values that ultimately influence the structural and mission implementation subsystems, respectively.

ADCS Considerations

Table 9.1: ADCS considerations during various mission phases

Mission Phase	ADCS Considerations
Launch & Preperations	None
Standby in Leo	The attitude and altitude will be maintained by Starship for at least five years. Additionally Starship might need to perform maneuvers to avoid collisions with space debris in Earth's orbit. The spacecrafts will be put into a hibernation mode in order to minimize the risk of failures.
Transfer	During this phase additional payload could be brought with us to reduce cost by ridesharing. These extra activities will require a certain attitude performance for Starship. An advanced deep space transponder is used to track Starship and communicate potential course correction. The deflection spacecrafts will be put into a hibernation mode in order to minimize the risk of failures.
Rendezvous	In order to ensure a successful rendezvous the main thrusters from Starship will need to be oriented precisely. Some additional maneuvers might be necessary in order to acquire the required attitude and altitude for which Starship will be responsible for.
Deployment	During deployment the still undeployed spacecrafts will need to be positioned and oriented to the sun by using the capabilities of the ADCS. The spacecraft will use it's thrusters for positioning, optical navigation and low gain communication system to determine it's position relative to already deployed spacecraft.
Deflection	During deflection a constant alignment of the mirror, the ion thruster, the solar panels and the high gain antenna will be required. Due to disturbances the ADCS will constantly need to perform maneuvers using it's full capabilities. These are the thrusters, the ion engine, star and sun sensors.
End of Life	The ADCS will operate until it runs out of propellant for the RCS thruster or the Ion engine. After which the spacecraft will be lost in space

9.1 Attitude Determination

In order to determine the attitude of the spacecraft ADCS sensors were used. The main sensor performance criteria that need to be taken into account were the desired spacecraft orientation and the attitude accuracy. Different kind of sensors exist and were listed in Table 9.2

Table 9.2: Typical ADCS Sensors [93]

Sensor	**Performance Range**	**Mass** $[kg]$	**Power** $[W]$
Gyroscopes	Drift rate = 0.003 to 1 deg/hr	0.1 to 15	1 to 200
Sun Sensors	Accuracy = 0.005 to 3 deg	0.1 to 2	0 to 3
Star Sensors	Accuracy = 0.0003 to 0.01 deg	2 to 5	5 to 20
Horizon Sensors (scanner)	Accuracy = 0.05 to 1 deg	1 to 4	5 to 10
Horizon Sensors (static)	Accuracy = 0.1 to 0.25 deg	0.5 to 3.5	0.3 to 5
Magnetometer	Accuracy = 0.5 to 3 deg	0.3 to 1.2	1

Horizon sensors and magnetometers can be discarded as options as they are optimally used in Earth orbit where there is a reliable horizon and a strong magnetic field. This is different from asteroids who generally do not have a mapped magnetic field and are not well-defined oblate spheroids like Earth. Gyroscopes and inertia measurement units are viable options, but are subjected to gyro drift and are not able to obtain an accurate attitude position after a loss in space scenario. Inertia measurement units have therefore not a substantial advantage with respect to Sun sensors and Star sensors which will be used as attitude determination sensors.

9.1.1 ADCS Sensor Selection

A list of available Sun and Star sensors can be found in Table 9.3.

Table 9.3: Considered sensors available on the market

Sensor	**Accuracy** $[deg]$	**Mass** $[kg]$	**Power** $[W]$
Hydra-TC (Star sensor) [1]	0.0031	5.3	8
Hydra-CP (Star sensor) [2]	0.0031	1.4	1
Hydra-M (Star sensor) [3]	0.0031	2.75	8
Hydra-HP (Star sensor) [4]	0.0031	3.2	8
Fine Sun Sensor [5]	0.3	0.375	0.25
Mini Fine Sun Sensor [6]	1.5	0.05	passive
Coarse Sun Sensor [7]	3	0.215	passive
Cosine Sun Sensor [8]	3	0.024	passive

From the sensor comparison, star sensors were the clear winner if only the accuracy was considered. However, star sensors were subjected to a couple of limitations which makes them not viable as stand-alone options. The main limitation being that star sensors have a limited slew tracking rate, generally around $5[deg/s]$ during acquisition and $8[deg/s]$ during tracking. This means that if the spacecraft exceeds a certain slew rate, attitude determination becomes impossible. Sun sensors do not have this limitation but do not meet the angular precision requirements on all control axis such as **AD-SYS-TECH-ADCS-11.1**. Therefore, a combination of Star and Sun sensors will be used. The sun sensors will provide a coarse attitude determination after which the Star sensors can provide an accurate attitude position. Star sensors consist of two parts, the Optical Head and an Electronic Unit which processes the images obtained by the Optical Head and calculates the attitude of the spacecraft. From the considered Star sensors the Hydra-CP is the lightest and uses the least power and therefore seems the best option. However, the Hydra-CP or Centralized Processing does not come with an EU and the image processing needs to take place in the spacecraft's on-board computer. This adds complexity and more development time to the data handling system of the spacecraft. Therefore, the Hydra-M [9] or Minimal Power from Sodern Ariane Group was the preferred option due to the low mass. All the considered sun sensors were considered to be light and power-efficient. The Fine Sun Sensor [10] from Bradford Space provides the best accuracy and will therefore be used.

[1]URL `https://bit.ly/2Mlce8i` [accessed 26 January 2021]
[2]URL `https://bit.ly/3pkI7MW` [accessed 26 January 2021]
[3]URL `https://bit.ly/2NFQhBH` [accessed 26 January 2021]
[4]URL `https://bit.ly/3sUGA29` [accessed 26 January 2021]
[5]URL `https://bit.ly/3qRwbm3` [accessed 26 January 2021]
[6]URL `https://bit.ly/3opYQNG` [accessed 26 January 2021]
[7]URL `https://bit.ly/3a892oy` [accessed 26 January 2021]
[8]URL `https://bit.ly/3odFnQ0` [accessed 26 January 2021]
[9]URL `https://bit.ly/3iQcsk6` [accessed 14 January 2021]
[10]URL `https://bit.ly/2MsiMBT` [accessed 14 January 2021]

9.1.2 ADCS Sensor Configuration

In order to ensure redundancy, four Optical Heads will be connected to two Electronical Units and form two separate systems. The optical heads have a sun exclusion angle of 26 degrees but should be placed in the shade for maximum performance. The optical heads will be positioned behind the primary mirror angled 45 degrees from the z-axis in a pyramid configuration as seen in Figure 9.1a. The EU's will be placed in the spacecraft bus. The sun sensors have a field of view of 128x128 degrees and a total of eight sun sensors will be configured in pairs in a tetrahedral configuration as seen in Figure 9.1b angled with 109x109 degrees with respect to each other in order to cover a full 360x360 degrees field of view. Positioning the sun sensors on the spacecraft in a perfect tetrahedral configuration where the distances between the sensors are equal might prove to be impossible. This was not an issue as long as the sensors were angled 109 degrees from each other.

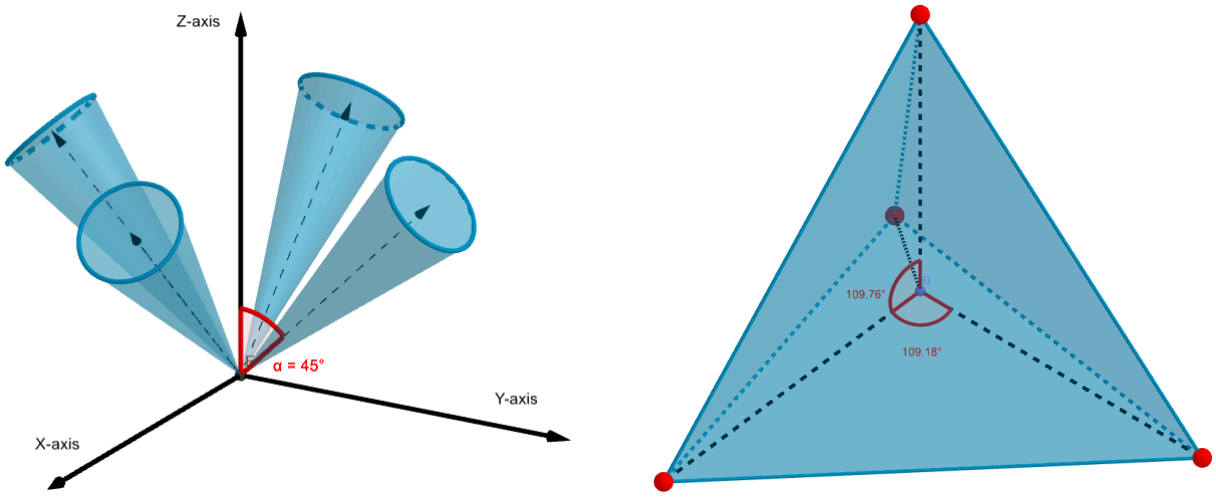

(a) Configuration of the star sensors.

(b) Configuration of the sun sensors.

Figure 9.1: Star and sun sensor configuration

9.2 Disturbances

During the mission, various forces will affect the attitude and altitude of the spacecraft. These forces were called disturbances and can come from internal and external sources. The disturbances need to be accounted for by the ADCS subsystem. Originally, gravitational and solar pressure perturbations were inspected, and it was determined that the gravitational force exerted on the satellites within the constellation does not create a large enough disturbance to the system to require any corrections through the use of the ADCS system.

9.2.1 Gravitational Disturbance Forces

In order to determine the magnitude of the forces applied to the systems in the constellation, a simple calculation involving the gravitational force equation was conducted. The equation used can be seen in Equation 9.1.

$$F = G\frac{m_1 m_2}{r^2} \tag{9.1}$$

It was assumed that the asteroid has a mass of $2.2E10\ [kg]$, while the satellite has a total mass of $1350\ [kg]$. These two bodies were spaced 500 m apart, generating a force of $7.93\ [mN]$. This force causes the satellite constellation to collide with the asteroid within 3.7 hours. This gravitational attraction, however, was easily mitigated through the solar pressure applied to the solar mirror by throttling down the ion drive to account for this. This was due to the fact that the secondary reflector will be directly facing the asteroid during nominal operation. This practice is also employed through the use of solar sails in statite satellites, which maintain a certain orbit through the balance of solar pressure and perturbation forces [34]. However, a moment was generated due to this imbalance. This moment came to $0.4758\ [Nm]$, due to the position of the secondary reflector. This moment was counteracted by the ADCS system, which will be described in greater detail later in this section.
Furthermore, the magnitude of the gravitational disturbance torque applied on the satellites by the asteroid was also calculated, in order to determine whether or not this was a significant disturbance. Equation 9.2 was used

to have a rough order of magnitude estimate of this disturbance. This is where G is the gravitational constant, assumed to be $6.672E-11\ [\frac{m^3}{kgs^2}]$. The mass of the asteroid, or M, was taken to be $2.2E10\ [kg]$ [93].

$$T_g = \frac{3GM}{2R^3}\left|I_z - I_y\right| sin(2\theta) \tag{9.2}$$

A worst case scenario was accounted for by assuming a θ of $45°$. This resulted in a maximum perturbation torque of $0.0138\ [Nm]$. This torque was counteracted through the use of the reaction wheels. These wheels, once saturated, require the RCS thrusters to dump the momentum. This will be discussed in greater detail later in the chapter.

9.2.2 Solar Perturbation Torques

In order to assess the solar perturbation induced on the satellite, an equation was used in order to best account for the torsion generated by the solar pressure. This is seen in Equation 9.3 [62]. In Equation 9.3, r_0 is the average distance between the Earth and the Sun, r_1 is the distance between the satellite and the Sun, A is the area of the satellite facing the Sun, SI_0 is the solar irradiance, c is the speed of light, α is the reflective efficiency of the surface, γ is the incidence angle of the incoming solar rays, $\mathbf{cg_{press}}$ is the vector position of the center of solar pressure of the reflective surface, and $\mathbf{cg_{mass}}$ is the center of mass of the satellite.

$$\mathbf{T_{solar}} = -(\frac{r_0}{r_1})^2 \frac{AS_0}{c}(1+\alpha)cos(\gamma)(\mathbf{cg_{press}} - \mathbf{cg_{mass}}) \tag{9.3}$$

This torque generated by the solar pressure creates a maximum moment of $0.2573\ [Nm]$ when at the perigee of the asteroid with the closest approach to the Sun in the dataset, around either the x, y or z axis depending on the orientation of the spacecraft relative to the sun. This moment created by the solar pressure was negated however, as due to the reflection of the photons off of the primary mirror onto the collimator and onto the secondary mirror.
However, due to the reflection of the photons off of the secondary mirror, a torque was still generated. In order to counteract this torque, an ion engine capable of gimballing will be positioned behind the secondary mirror.

9.3 Actuator Sizing

In order to counteract the before mentioned disturbances, a set of different actuators can be used[93]. The actuators considered were reaction wheels, RCS thrusters and ion drives. Another option for three-axis control were control moment gyroscopes or CMG's which were also used for high torque applications in which fine control is needed and may be used as an alternative to reaction wheels. The use of CMG's requires complex control laws and careful momentum dumping, which is also the case for reaction wheels. However, CMG's make use of a more complex mechanism that suffer a great deal of wear and tear. The lifetime is therefore much shorter compared to reaction wheels, who already provide a sufficient accuracy and were therefore the better option. The loss in available torque compared to CMG's can be mitigated by the use of RCS thrusters and ion drives. Another option for three-axis control is the use of magnetic torquers who make use of a magnetic field to control the spacecrafts attitude. It is not sure that the to be deflected asteroid will have a magnetic field and it Will certainly not be mapped. Magnetic torquers were therefore also discarded as an option.

9.3.1 Reaction Wheel Selection

Reaction wheels can rotate in two directions. The acceleration or deceleration of these wheels will generate a torque that, by Newton's third law, is opposed by the spacecraft in order to conserve angular momentum. A reaction wheel is therefore a momentum storage device with a certain angular momentum capacity and a defined torque range. In Table 9.4 an overview is presented of available reaction wheels on the market.

Table 9.4: Considered reaction wheels available on the market

Name	**Momentum Capacity** $[Nms]$	**Max torque** $[Nm]$	**Mass** $[kg]$	**Peak power** $[W]$
RSI 68-75/60 [11]	68	0.075	8.5	90
RSI 25-75/60 [12]	25	0.075	6.3	90
RSI 30-280/30 [13]	30	0.280	8.5	150
RSI 18-220/45 [14]	18	0.220	6.3	150
RW-10NMS [15]	10	0.190	5	110
RW1000 [16]	15	1	11.5	160
W45E [17]	45	0.248	7.45	168
W45 [18]	40	0.248	6.7	168
W18ES [19]	25	0.265	6.02	168
HR0610 [20]	12	0.055	5	80

In order to select the best reaction wheel, the sizing method from SMAD was used [93]. To verify if a considered reaction wheel was able to counteract the disturbances obtained in Section 9.2, Equation 9.4 can be used. Where T_{RW} is the required torque of the reaction wheel, T_D the disturbance torque and MF a margin factor. The only disturbance torque that can be accounted for by the reaction wheels is the gravitational disturbance torque of 0.00138 $[Nm]$. This is below the max torque of all the considered reaction wheels.

$$T_{RW} = T_D \cdot MF \tag{9.4}$$

The performance of the reaction wheel can be quantified by the slew maneuverability θ_{slew} in Equation 9.5 with I the mass moment of inertia of the to be considered axis, T_{RW} again being set to the max torque of the reaction wheel and t_{max} the max time the reaction wheel can accelerate before saturation occurs, which if multiplied by the max torque results in the momentum capacity.

$$\theta_{slew} = \frac{T_{RW} t_{max}^2}{4I} \tag{9.5}$$

The driving factor for the slew performance of the reaction wheels according to Equation 9.5 is the momentum capacity of the reaction wheel. From the considered reaction wheels in Table 9.4 the RSI 68-75/60[21] from Rockwell Collins was the best option to be used. A single RSI 68-75/6 was able to perform a no resisting momentum maneuver of 0.48 degrees on the most demanding z-axis which was obviously not sufficient. Therefore maneuvering will be performed by the RCS thrusters. The reaction wheels were however still needed in order to comply with the accuracy requirements such as **AD-SYS-TECH-ADCS-11.1** as proven in Subsection 9.4.2.

9.3.2 Reaction Wheel Configuration

A reaction wheel can provide torques around a single axis. Therefore, a minimum of 3 reaction wheels are needed to have three-axis control, one for each axis. Reaction wheels have a high failure rate compared to the other subsystems. In order reduce this risk, four reaction wheels can be configured in a tetrahedral configuration. This was the most efficient way to have no single points of failure. This configuration however has proved to be hard to model. Therefore, two reaction wheels were used on each principle axis as shown in Figure 9.2 during the remainder of the design.

[11] URL `https://bit.ly/39g7vxM` [accessed 26 January 2021]
[12] URL `https://bit.ly/39g7vxM` [accessed 26 January 2021]
[13] URL `https://bit.ly/3a3348B` [accessed 26 January 2021]
[14] URL `https://bit.ly/3a3348B` [accessed 26 January 2021]
[15] URL `https://bit.ly/39ixYdV` [accessed 26 January 2021]
[16] URL `https://bit.ly/3qQvw4d` [accessed 26 January 2021]
[17] URL `https://bit.ly/3iMsYS0` [accessed 26 January 2021]
[18] URL `https://bit.ly/36czJHO` [accessed 26 January 2021]
[19] URL `https://bit.ly/3oieBpL` [accessed 26 January 2021]
[20] URL `https://bit.ly/3qKgnSa` [accessed 26 January 2021]
[21] URL `https://bit.ly/3oZqjGM` [accessed 18 January 2021]

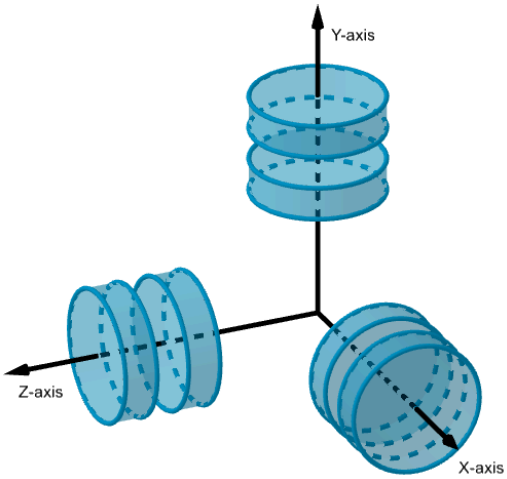

Figure 9.2: Reaction Wheel Configuration

9.3.3 RCS Thruster Selection

In order to account for the large disturbance forces and large maneuvers required of the system in the case of any re-positioning, an RCS thruster system was required. This thruster system was designed with efficiency and redundancy in mind, as these impact both the size of the thrusters required as well as the amount of propellant required for the mission duration as well.

Thruster selection ultimately depended on the fuel type required, as well as the moment arms given to the system in both the packed and unpacked configurations, as the system is released from the launcher some distance away from the asteroid. This required the system to maneuver into place before being fully deployed in order to avoid collisions. This criteria, plus a simple versatility check, were the factors used to decide on a proper RCS thruster.

Originally, due to the high TRL of hydrazine-based propulsive systems, the monopropellant hydrazine thruster family was the initial group of thrusters inspected for potential use [22]. However, this family of thrusters was quickly ruled out due to the dangers of hydrazine, as well as the complications of transporting systems that require its use [69]. This, on top of the environmental risk requirement **AD-RISK-ENV-3**, disqualified the use of hydrazine aboard the satellite. This disqualification led to research into the potential use of LMP-103S, a hydrazine alternative with a higher density impulse than traditional hydrazine [69]. This monopropellant was selected due to these reasons. This type of monopropellant is used and by a class of thrusters known as the HPGP Thrusters [23]. This thruster class consisted of several variable thrust RCS thrusters. However, due to the large moment arms of the satellite, only the two smallest thrusters available were considered, the 0.1 $[N]$ and the 1 $[N]$ thrusters, as only small forces were required to generate large moments in this system.

The two viable thruster types were compared based on several aspects deemed important to the efficiency and longevity of the mission. The thrust range was chosen as an important criteria due to the variance in required correction necessary throughout the mission, but also the thrust potentially required during the insertion of the systems into the proper orbital plane. Propellant throughput was chosen to analyze how long the thrusters could fire for. This was also why the firing sequences and pulses were also included in the analysis. The specific impulse was included to assess the efficiency of the engine.

Table 9.5: An overview of the specifications of the HPGP 1 N and HPGP 0.1 N engines[24].

Thruster Type	**Thrust Range** $[N]$	**Isp** $[s]$	**Firing Sequences** $[-]$	**Pulses** $[-]$	**Propellant Throughput** $[kg]$
HPGP 1 N	0.25-1	204-231	1500	60000	24
HPGP 0.1 N	0.03-0.1	196-209	150	2000	1

[22] URL `https://www.space-propulsion.com/spacecraft-propulsion/hydrazine-thrusters/index.html` [accessed 11 January 2021]
[23] URL `https://www.ecaps.space/products-overview-ecaps.php` [accessed 13 January 2021]
[24] URL `https://www.ecaps.space/products-overview-ecaps.php` [accessed 13 January 2021]

From these criteria, it can be seen that although the HPGP 0.1 N engine can create thrusts as low as 0.03 N, thrusts of this resolution were not as useful to the system, as the torsions created by thrusts are small, this resulted in rotational corrections that could easily be created by the reaction wheels instead. This, as well as the relatively low specific impulse values, eliminate the 0.1 N engine from the possible RCS thrusters, leaving only the HPGP 1 N engine, seen in Figure 9.3. This engine has a minimum impulse bit of 0.07 $[Ns]$ which not only minimized the amount of angular momentum to be dispersed, but also resulted in less momentum dumping maneuvers and less fuel consumption because of how little angular momentum the reaction wheels account for. This, along with its Technology Readiness Level of nine, were deciding factors in its selection . This configuration and thruster type combination resulted in a maximum remnant torque of 0.6 $[Nm]$ around the z axis, and a maximum remnant torque around the x and y axes of 0.06 $[Nm]$ with the thruster block layout discussed in Subsection 9.3.4. These remnant torques were calculated by simply multiplying the smallest thrust available from the thrusters by the smallest moment arm. This was done for each axis.

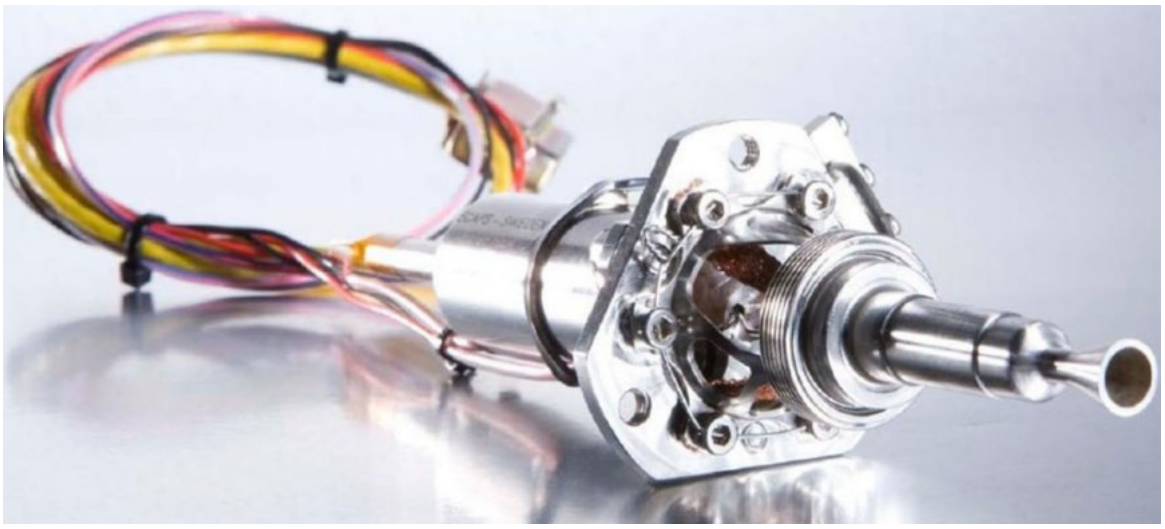

Figure 9.3: An image of the selected 1N thruster, capable of making use of the green propellant replacement for hydrazine [25].

9.3.4 Thruster Block Configuration

In order to fulfill the requirements set out for the ADCS system, particularly requirements **AD-SYS-TECH-ADCS-11.4**,**AD-SYS-TECH-ADCS-11.7**, and **AD-SYS-TECH-ADCS-11.8**, large moment arms were required. This required the placement of thruster sets in positions 1, 2, 3, and 4 as is depicted in Figure 9.4.

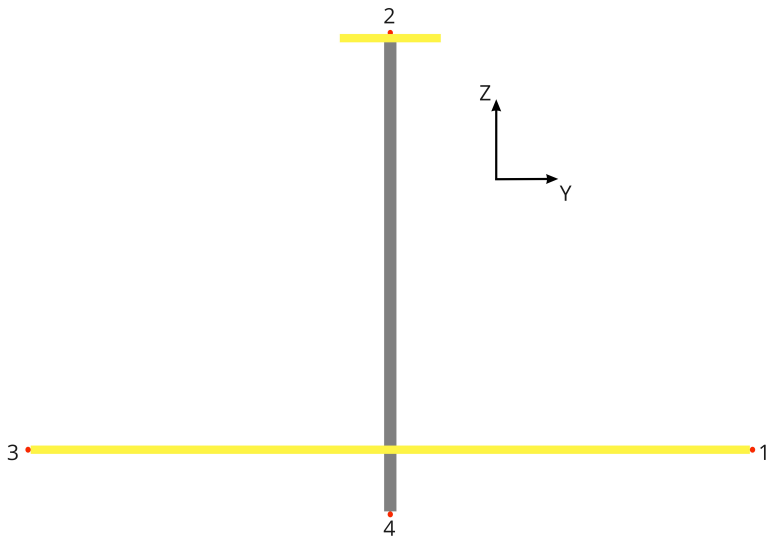

Figure 9.4: Locations of the RCS thruster blocks, where the origin of this reference was set to be at the center of the end of the collimator arm behind the primary reflector.

[24]URL `https://www.ecaps.space/products-1n.php` [accessed 19 January 2021]
[25]URL `https://www.ecaps.space/products-1n.php` [accessed 19 January 2021]

This placement scheme of the primary RCS thrusters allowed for each thruster to have as large of a moment arm as possible, with the longest moment arm for any of the thrusters being the length of the collimator arm for thruster block two, which was found to be $79.02\ [m]$. This thruster assists in the pitch and roll rotations. Furhtermore, thruster blocks one and three assist in the yaw rotation of the system. Thruster block four was included to assist in the pitch and roll rotations. This block has the ability to make corrections to the rotations created by thruster block two, as this block four had a moment arm of $9.75\ [m]$.

Thruster block two, however, required a slight offset from the z-axis to generate moments around the z axis. This allowed for more precise yaw rotations with no sacrifices having to be made to the amount of torque the thrusters located within block two could provide around the x and y axes.

These large moment arms allow for extremely large moments to be creating, resulting in the relatively swift rotation of the system, which are put to good use in asteroid redirection situations where time is of the essence, or if large perturbations are encountered.

In order to prevent the satellites from impinging the RCS thruster ejecta, a certain placement angle had to be determined. This angle depended on the diverging nozzle half angle, which was assumed to be $15°$ due to the nozzle of the thruster being conical [54].

9.3.5 RCS Fuel & Tank Sizing

The RCS fuel sizing and tank sizing were required in order to properly create an operational envelope of the system. Since the determination of the exact amount of ΔV required for this mission required estimates that involve the accuracy of the launch provider (Starship) as well as the orbit required to reach the target asteroid, ΔV statistics of previous missions and the respective maneuvers required for the missions were used to generate a rough estimate on the amount of propellant required for a nominal amount of LMP-103S. It was found from the data that the system required a ΔV of $10.3\ [m/s]$ [58]. This amount of ΔV was then multiplied by the assumed total mass of the system, giving a total of $11610\ [Ns]$ of impulse. To obtain the liters of fuel required, this can then be divided by a density impulse of 2860 Ns/l, the LMP-103S impulse density [1]. This amount of fuel was split amongst four of the RCS fuel containment units. After this, a 1.5 safety factor was introduced to account for any re-positioning uncertainties. In order for all of the thrusters to maintain access to the same amount of fuel at the start of the mission, each tank must contain a minimum of 7.3 kg of fuel, leading to a total fuel mass of 29.2 kg. After this, a SMAD method was used to size the tanks [93]. Given a fuel density of $1244.44\ [\frac{kg}{m^3}]$, it was found that a volume of 5.86 L per tank was necessary to contain the required fuel. This volume, along with the required 22 bar, were then used to find the estimated mass of the tank [1]. The line of best fit equation used is shown in Equation 9.6 where P is the pressure of the tank in bar and V is the volume of the tank in m^3.

$$M_{tank} = 0.7266(PV)^2 + 2.5119PV + 2.9826 \tag{9.6}$$

This led to an assumed COPV tank mass of $3.3\ [kg]$ per tank.

After this sizing procedure was conducted, a valve layout was designed in order to check the required bandwidth as well as amount of risk associated with this portion of the ADCS system. Initially, some research into valve layouts was conducted in order to get a better understanding of the required amount of redundancy and components necessary to create a working thruster block [88]. A tank of nitrogen gas was used to pressurize the propellant tanks for each thruster block. Nitrogen was chosen to be the pressurant due to its inert qualities. The feed pipe from the nitrogen to the propellant tank has a valve to be used for venting in the case of an issue with the nitrogen tank, as well as a feed valve to control the flow of nitrogen from the nitrogen tank to the propellant tank. Fuel level sensors were used for both the nitrogen and propellant tanks in order to check the amount of both still in the system. A pressure sensor is used to sense the amount of pressure in both the feed line going from the nitrogen tank to the propellant tank as well as the feed line going from the propellant tank to the four thrusters within the thruster block. A drain valve was also included in the feed line leading from the propellant tank to the four thrusters so as to allow for the venting of the propellant tank in the case of an issue with sadi tank. There was also a feed valve attached to this feed line. There was also one valve per thruster so as to allow for control over the amount propellant exhausted by each of the thrusters. This system is shown in Figure 9.5.

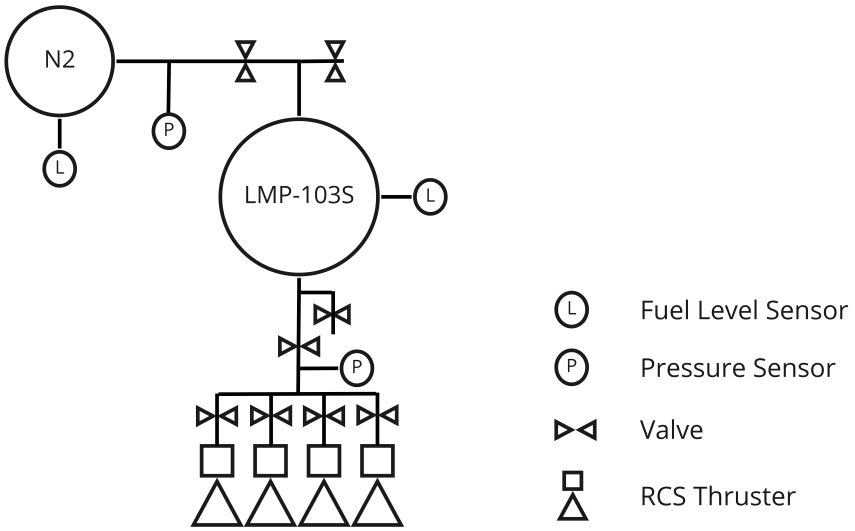

Figure 9.5: A schematic detailing the layout of a valve system to be used for each RCS thruster block on the satellite.

Center of Gravity Envelope

In order to calculate the bounds within which the center of gravity was, an assumption was made that the fuel containers for the satellite were to be located where the thrusters blocks were located. It was also assumed that each tank contained exactly one quarter of the contents of all of the fuel allotted to the satellite. A simple weighted average was conducted, and scenarios were generated to create the three dimensional center of gravity plots. First four different scenarios were generated where all of the tanks were full but one. This same process was conducted for two empty tanks, then three, resulting in Figure 9.6.

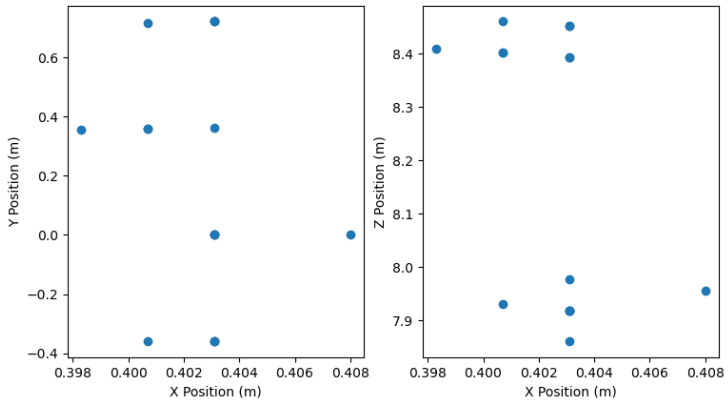

Figure 9.6: The center of gravity positions for various fuel load configurations.

The maximum x position resulted from a dry mass center of gravity. This was ultimately due to the secondary reflector being extremely far out along the x axis. The maximum y position was estimated to be under any circumstance when the tanks for thruster blocks three and four were both empty. The largest z position occurred when tank four was set to be empty. Ultimately, due to the configuration of the thruster blocks, increases in the x position of the center of gravity resulted in increases in moments around the y and z axes generated by the thruster blocks three and four. However, this was already accounted for in the moment equations as this makes use of the original center of gravity assumed to be from the dry mass, and thus introduced no increases to the critical moments. Increases in the y position of the center of gravity resulted in increases in moments around the x and z axes generated by the thruster block three and block two. However, since these blocks generate couple moments with blocks one and four, there were no increases or decreases in the critical moments around that axis from the moment calculations conducted with the original center of gravity. An increase in the z position of the center of gravity increased the moment around the x axis generated by the thruster block four and decreased the moment created by thruster block two around that axis as well. This also had a similar effect when calculating moments around the y axis. However, since this was an investigation

of the changing center of gravity position's effects on the critical moments, the critical moment values did not change due to the couple moments generated by the blocks two and four. However, the change in center of gravity altered the resolution of the moments generated by the thrusters, as a larger moment arm reduced the resolution of these thrusters. However, due to the minute changes in the center of gravity due to the draining of certain fuel tanks, the changes in the moment resolution of the thrusters system was disregarded.

9.3.6 Ion Drive and Tank Sizing

In order to counteract the forces and moments generated by the solar pressure, an ion engine placed behind the secondary mirror was considered the proper precaution as ion engines create the required amount of force over the course of a long period of time. The inclusion of this ion thruster significantly prolongs the potential deflection period, as it removes the largest perturbation from the system, without having to account for it with the RCS thruster system.

The ion drive was selected based on the total solar pressure applied to the secondary reflector. An altered version of Equation 9.3 equation was used to calculate the solar pressure. This equation was created by simply removing the moment arm vector. This led to a force of $0.135\ [N]$ to be counter-acted by the engine. The force required, along with a high specific impulse, were the two main criteria on which an engine was selected. A SMAD chart was then consulted to determine the engine required, which ultimately led to the selection of an ion engine [93]. This led to the selection of the NEXT-C engine, due to its extremely high specific impulse of $4190\ [s]$ and ability to throttle down to $17.1\ [mN]$ and up to as high as $236\ [mN]$. This ion drive was throttled down to $0.135\ [N]$ in order to counteract the solar pressure. In order to size the required fuel mass of the system, one must first calculate the mass flow required. This was obtained by consulting Equation 9.7, where F_T is the thrust force of the engine and V_e being the exit velocity of the propellant.

$$\dot{m} = \frac{F_T g_0 I_{sp}}{V_e^2} \tag{9.7}$$

This ultimately resulted in a mass flow of $3.467E-3\ [\frac{kg}{s}]$ and a required thrust force of $0.135\ [N]$. For a worst case scenario, this thrust force had to be applied over the course of 100 days. This required a total of $29.95\ [kg]$ of xenon propellant to be exhausted. A COPV tank was then sized to contain this amount of xenon, to be held under a pressure of 150 bar [87]. Through the use of the Equation 9.6, the required volume was calculated with the use of Equation 9.8, where γ is the isentropic coefficient, found to be 1.6495.

$$\frac{P_2}{P_1} = (\frac{V_1}{V_2})^{\gamma} \tag{9.8}$$

This led to a calculated volume of $0.185\ [m^3]$ for the xenon gas. When consulting the line of best fit located in Equation 9.6, the mass of the required COPV tank was found to be $4.0683\ [kg]$.

9.4 ADCS Model

In order to assess the moments generated by the RCS system as well as the pointing accuracy of the system as a whole, a model was developed. This model was then used to determine the critical moments generated by the thruster configuration, but also the maximum pointing error generated by the system.

9.4.1 Moment Model

A moment model was determined in order to assess the maximum amount of moment loading the system experienced in the roll, pitch and yaw directions. These values were then made use of in the bending tests for the structural analysis of the system, as the activation of a combination of these thrusters generated the critical moments. In order to first start generating this model, however, a reference frame was selected. The origin was set to be at the base of the collimator arm, behind the primary reflector, with the z axis pointing towards the collimator arm, and the y axis pointing towards the "top" of the satellite, shown in Figure 9.4.

After the thrusters were positioned, their coordinates were then used to determine the maximum moments generated by the system. This was done with the assumption that the thrusters fired at their maximum amount,

[25] URL `https://www1.grc.nasa.gov/space/sep/gridded-ion-thrusters-next-c/#factsheets` [accessed 14 January 2021]

which was a thrust of $1\ [N]$, with a half-angle of $15°$, resulting in a thrust of $0.9659\ [N]$. In reference to Figure 9.4, thruster block 1 was taken to be the initial thruster vector matrix. This thrust vector matrix was then multiplied by a $-90°$ rotation matrix to obtain the thrust vector matrix of the thruster block two. This process was then repeated until all four required thruster block matrices were generated. This process is illustrated in Equation 9.9 where the first matrix is the thrust block one matrix and the second matrix is the rotation matrix. The variable θ_{eject} describes the half-angle of the nozzle, T_{RCS} describes the thrust of the engine, and θ_{rot} is the angle of rotation.

$$\mathbf{T_{B1}} = \begin{bmatrix} -T_{RCS}cos(\theta_{eject}) & T_{RCS}sin(\theta_{eject}) & 0 \\ 0 & T_{RCS}sin(\theta_{eject}) & T_{RCS}cos(\theta_{eject}) \\ T_{RCS}cos(\theta_{eject}) & T_{RCS}sin(\theta_{eject}) & 0 \\ 0 & T_{RCS}sin(\theta_{eject}) & -T_{RCS}cos(\theta_{eject}) \end{bmatrix} \times \begin{bmatrix} 1 & 0 & 0 \\ 0 & cos(\theta_{rot}) & -sin(\theta_{rot}) \\ 0 & sin(\theta_{rot}) & cos(\theta_{rot}) \end{bmatrix} \tag{9.9}$$

These thrust matrices were then transposed, multiplied against a moment arm matrix, and then transposed again, to determine the moments generated around the x, y, and z axes for each thrust vector. This is displayed in Equation 9.10 where the first matrix details the moment arm matrix where x_{pos} is the x position of the moment arm, y_{pos} is the y position of the moment arm, and z_{pos} is the z position of the moment arm.

$$\mathbf{M} = \left(\begin{bmatrix} 0 & -z_{pos} & y_{pos} \\ z_{pos} & 0 & -x_{pos} \\ -y_{pos} & x_{pos} & 0 \end{bmatrix} \times \mathbf{T_{B1}}^{T} \right)^{T} \tag{9.10}$$

This generated a matrix of moments relative to the amount of thrust applied by each of the thrusters. Once this was obtained, the thrusters generating the largest moments around the x,y, and z axes were selected and summed, leading to the critical moments the structure encountered.

9.4.2 Pointing Error Model

In order to fulfill the pointing error requirements **AD-SYS-TECH-ADCS-11**, **AD-SYS-TECH-ADCS-11.1**, **AD-SYS-TECH-ADCS-11.2**, and **AD-SYS-TECH-ADCS-11.3**, a pointing model was required. This model had to display how the reaction control wheels handled the maximum remnant torques generated by the thruster system. These were the thrusts that could not be mitigated by the thruster system without inducing even more torque into the system. These were initially determined to be $1.9875\ [Nm]$ around the x and y axes, whereas with the remnant torque around the z axis was determined to be $15\ [Nm]$. These initial torsions were found after simply multiplying the minimum amount of thrust the thrusters could provide by the moment arms available to them. However, after running these disturbance torques through the system, it was discovered that they exceeded the requirements set out for the pointing accuracy, and ultimately had to be re-positioned slightly to avoid large remnant torques.

Reaction Wheel Transfer Function

Since the reaction wheel had to be controlled by a brushless DC motor [49], a set of differential equations had to be derived through the use of both Newton's second law for the reaction wheel and Ohm's law for the DC motor. A diagram of the motor's electrical layout can be seen in Figure 9.7.

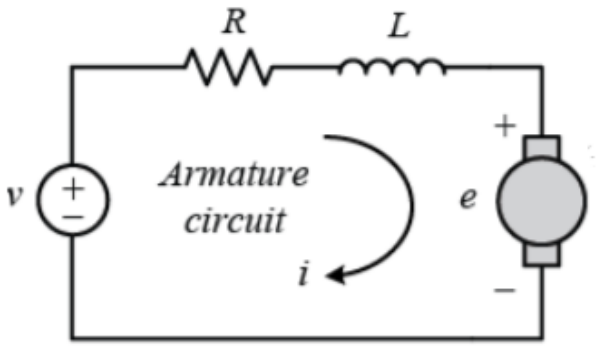

Figure 9.7: A circuitry layout of a DC motor [73].

This circuit can be represented as in Equation 9.11 where the total voltage induced is equal to the inductance from the inductor multiplied by the change in current over time added to the resistance times the current. This is in accordance with Ohm's law for an inductor and the relationship between the resistance and voltage.

$$v(t) = L\frac{di}{dt} + Ri \tag{9.11}$$

However, one must also consider the back electromotive force generated when running a current through a wire. This can be added to Equation 9.11, giving Equation 9.12, where K is considered to be a spring constant, resisting the motion of the DC motor on the reaction wheel.

$$v(t) = L\frac{di}{dt} + Ri + K\frac{d\theta}{dt} \tag{9.12}$$

The equation for the reaction wheel can be found by simply creating a differential equation for a rotating body seen in Equation 9.13 where J is the moment of inertia of the system around a certain axis and b is the rotational dampening constant of the wheel. The T value is the total torque of the wheel.

$$J\frac{d^2\theta}{dt^2} + b\frac{d\theta}{dt} = T \tag{9.13}$$

The torque value can be set equal to $T = K_t i$ where K_t is a constant relating the amount of current passing through the DC motor to the amount of torque induced on the wheel [73]. This value can be assumed to be the same as the spring constant resisting the motion of the DC motor [73]. The equations 9.12 and 9.13 can then be Laplace transformed into Equation 9.14 and Equation 9.16 respectively.

$$V(s) = LsI(s) + RI(s) + Ks\Theta(s) \tag{9.14}$$

$$V(s) = (Ls + R)I(s) + Ks\Theta(s) \tag{9.15}$$

$$Js^2\Theta(s) + bs\Theta(s) = KI(s) \tag{9.16}$$

$$s(Js + b)\Theta(s) = KI(s) \tag{9.17}$$

Equation 9.15 and Equation 9.17 can be combined by setting Laplace function of the wheel equal to $I(s)$ and replacing it within Equation 9.15. The $\Theta(s)$ value becomes $\dot{\Theta}(s)$ by removing the s value, leaving Equation 9.18.

$$V(s) = ((Ls + R)(\frac{(Js + b)}{K}) + K)\dot{\Theta}(s) \tag{9.18}$$

This can be converted into an open loop transfer function by taking the output to be the rotational speed ($\dot{\Theta}(s)$) and the input to be the total voltage $V(s)$. This left the complete DC motor and reaction wheel transfer function shown in Equation 9.19 [73].

$$\frac{\dot{\Theta}(s)}{V(s)} = \frac{K}{K^2 + (Ls + R)(Js + b)} \tag{9.19}$$

Satellite Transfer Function

The satellite transfer function was derived from the same equation as the reaction wheel torque equation shown in Equation 9.13. However, instead of the moment of inertia and dampening value being that of the wheel, they were taken from the satellite instead. The Laplace transform of this equation was found to be Equation 9.20 where the torque was the input value and the output was the angle of the satellite around a certain axis.

$$\frac{\Theta(s)}{T(s)} = \frac{1}{Js^2 + bs} \tag{9.20}$$

These two transfer functions were then arranged in a closed loop, separated by a disturbance torque dependent on the axis on which each loop was set. A PID controller was included at the beginning of the loop in order to tune the system and to make sure the reaction control wheels respond optimally. A block diagram of one axis of the system created can be seen in Figure 9.8.

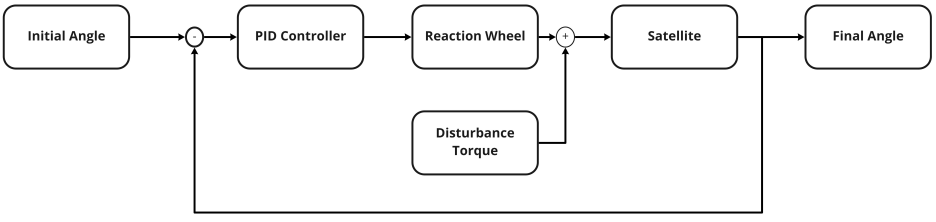

Figure 9.8: The close loop system devised to model the effects of the disturbance torques.

This transfer function was used for all three Euler angles with $1.9875\ [Nm]$ as the disturbance torque for the roll angle, $0.6\ [Nm]$ for the pitch angle, and $15\ [Nm]$ was used as the disturbance torque for the yaw angle. The PID controller was tuned through the use of the Simulink Tune option [28] which allowed for the creation of the optimum reaction time. This tuning resulted in gains of $K_p = 40158.28$, $K_I = 25.349$, and $K_D = 9539049.02$. These gain values were the same across all of the axes. After this tuning, the system was ran with the structural values such as the moment of inertia and the dampening values obtained from Chapter 13. The values required for the reaction wheel transfer function such as the inductance (L), the resistance (R), the spring constant (K), and the moment of inertia (J) were all calculated or found through the use of the specifications sheet of the specific reaction wheel [26]. The initial error values can be seen in Figure 9.9. Note that the input pitch, input roll, and input yaw angles were all $0°$, which was why the input yaw was the only angle to show up in the figure out of the input angles.

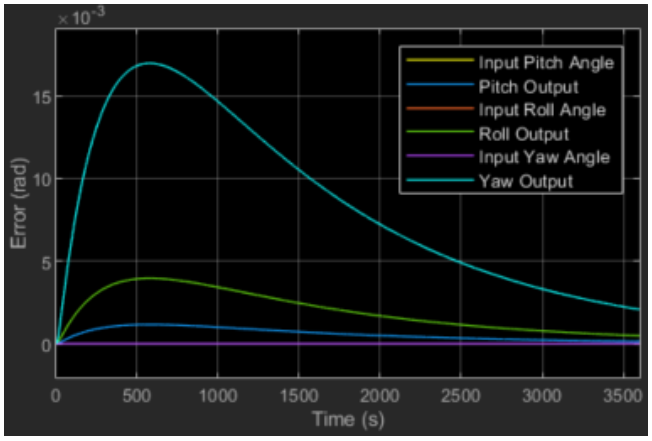

Figure 9.9: This figure displays the change in angle over the course of time when using the reaction wheels to correct for the disturbance torques generated by the thruster system.

This figure shows that the maximum pointing error experienced by any of the axes was the yaw axis with an error of $0.01696\ [rad]$ which converts to $0.9717°$, which was far greater than the required $0.08°$. Furthermore, the roll rotation had a pointing error of $0.2267°$. This was also far higher than the requirements. This ultimately required slight repositioning of the RCS thrusters in order to reduce the maximum errors that the system encountered. The pitch axis had a pointing error of $0.0319°$, which made it the only axis with no adjustments required.

In order to refine the pointing errors generated by the system, the amount of disturbance torque within the system must be minimized. In order to do this, small moment arms were required. This led to the decision to move the thruster block located at the end of the collimator more to the positive x direction in order to generate the small moments required in order to prevent the generation of disturbance torques. The model was then used to determine the minimum amount of disturbance torque tolerated in order to still achieve the requirement of having a pointing error of no more than $0.08°$. A moment arm of $2.65\ [m]$ was found to be the correct length necessary to generate maximum disturbance torques of $0.64\ [Nm]$ around the yaw axis with the thruster block placed behind the collimator. This resulted in a pointing error of just below the required maximum, with an error of $0.0755°$. In order to address the large pointing errors around the pitch and roll axes, a certain offset value was also determined. Since the RCS thurster blocks one and three were placed on the y axis going through the center of gravity, a slight offset from the y axis allowed for the generation of smaller moments that could be used to refine the amount of disturbance torque generated. It was therefore determined that these blocks could be placed a maximum of $1.16\ [m]$ in either the positive of negative z direction due to the overall depth of the truss structure used to support the main mirror being $2.327\ [m]$ deep. This type of maximum placement style not only ensures that the additional moments generated were as large as possible if necessary, but also ensures a refined pointing error. This moment arm generated a maximum of $0.28\ [Nm]$ torque, which translated to a pointing error of $0.0319°$. The Figure 9.10 displays the results of the adjustments, with the peak error occurring near 570 seconds, before diminishing. Note that the input pitch, input roll, and input yaw angles were all $0°$, and hence they overlap in Figure 9.9 and Figure 9.10.

[26] URL `http://www.electronicnote.com/RCG/RSI%2068_A4.pdf` [accessed January 15, 2021]

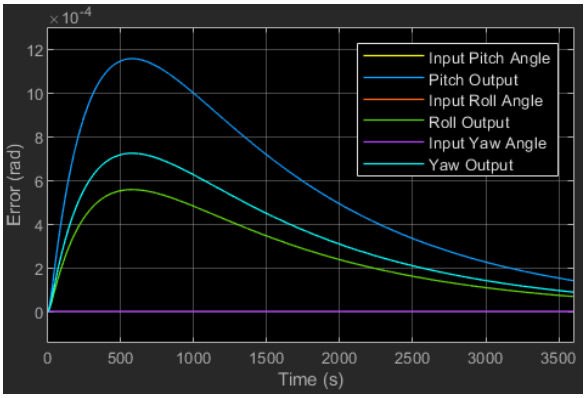

Figure 9.10: The maximum pointing errors around each of the angles after the moment arm adjustments.

9.5 Requirements

The requirements that the ADCS was designed for are given in Table 9.6. Based on the analysis done in this report, the system meets all of the requirements.

Table 9.6: ADCS Requirements

Identifier	Requirement	MOC	Compliance
AD-SYS-TECH-ADCS-11	The attitude control system shall control the pointing of the spacecraft.	Analysis	Y
AD-SYS-TECH-ADCS-11.1	The space system shall be able to control its pitch with an angular precision of 0.08 degrees.	Analysis	Y
AD-SYS-TECH-ADCS-11.1.1	The space system shall be able to control its pitch with an angular precision of 0.08 degrees during its standby phase.	Analysis	Y
D-SYS-TECH-ADCS-11.2	The space system shall be able to control its roll with an angular precision of 0.08 degrees.	Analysis	Y
AD-SYS-TECH-ADCS-11.2.1	The space system shall be able to control its roll with an angular precision of 0.08 degrees during its standby phase.	Analysis	Y
AD-SYS-TECH-ADCS-11.3	The space system shall be able to control its yaw with an angular precision of 0.08 degrees.	Analysis	Y
AD-SYS-TECH-ADCS-11.3.1	The space system shall be able to control its yaw with an angular precision of 0.08 degrees during its standby phase.	Analysis	Y
AD-SYS-TECH-ADCS-11.4	The attitude control system shall generate a minimum slew rate of 0.008 radians per second in the x axis.	Analysis	Y
AD-SYS-TECH-ADCS-11.5	The attitude control system shall be able to generate a load of 1 N.	Analysis	Y
AD-SYS-TECH-ADCS-11.6	The attitude control system shall be able to determine the pitch, roll and yaw positions of the space system with an accuracy of 0.08 degrees	Inspection	Y
AD-SYS-TECH-ADCS-11.7	The attitude control system shall generate a minimum slew rate of 0.008 radians per second in the y axis.	Analysis	Y
AD-SYS-TECH-ADCS-11.8	The attitude control system shall generate a minimum slew rate of 0.008 radians per second in the z axis.	Analysis	Y
AD-SYS-TECH-ADCS-11.9	The attitude control system shall weigh no more than 165 kg.	Analysis	Y
AD-SYS-TECH-ADCS-11.10	The attitude control system shall use no more than 5.5 kW.	Analysis	Y

10 Communications and Data Systems

In order for the mission to be successful, communication and data exchange between the space system and the ground system has to be possible. Within space missions, data is being generated on-board the spacecraft that has to be processed and sent back to Earth, data that for example is important in determining the spacecraft position and attitude. Also, commands have to be sent to the spacecraft by mission control, so that certain actions are being performed by the bus, for example the deployment or activation of the payload. The spacecraft bus should therefore contain components that make this data exchange and communication possible. Two general subsystems have been developed that facilitate these processes: the Command and Data Handling System (C&DHS) and the Telemetry, Tracking and Command System (TT&CS). In Section 10.1, the design of the C&DHS of the mission at hand will be elaborated upon and the same is done for the TT&CS in Section 10.2. Finally in Section 10.3 the requirements for the two subsystems are listed and compliance is checked.

10.1 Command and Data Handling System

The Command and Data Handling System acts as the neural network of the spacecraft with the central computer as its brain; it receives, validates, decodes and distributes commands to the other subsystems present in the spacecraft bus and it gathers, processes and formats spacecraft internal housekeeping and mission status data to either send back to the ground station or process within the On-Board Computer (OBC). Nowadays, these processes are all handled by the software printed in the OBC, creating an autonomous system for all different subsystems. In this section, the design steps for the C&DHS of the mission at hand are presented. [93]

10.1.1 Architecture

Sizing of the C&DHS begins with determining which components are all connected with each other in the spacecraft and especially with the On-Board Computer. The components should be exchanging data with the OBC at certain data rates. These data rates determine the performance necessary from the OBC and therefore give an indication of what type of OBC is required. Different types of components exist and they can be divided in different control boards, namely the housekeeping (H/K) board, the telemetry/telecommand (TM/TC) board and the input/output (I/O) board. When all subsystem components were determined, a high-level component list had been set up along with the information that has to be sent to the OBC and the information that has to be recieved from the OBC. With this list, a high-level C&DHS block diagram has been set up, which is presented in Figure 10.1 below. In this figure, the exact architecture of the C&DHS with all connections between components and the OBC is presented, containing arrows to indicate the direction of data transfer. It should be noted that data transfer will not take place for all components at the same time: further specification on thi will be presented later in this chapter.

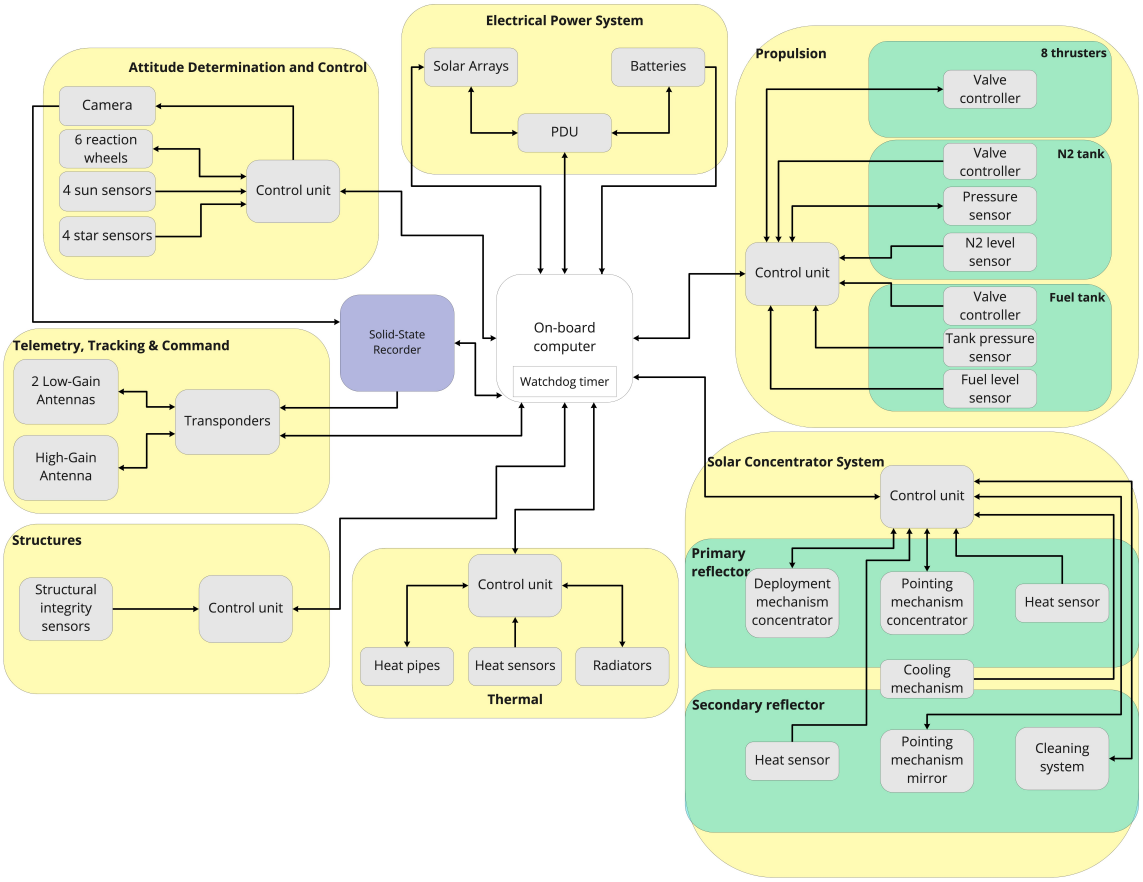

Figure 10.1: High-level C&DHS block diagram

Each subsystem has a control unit for its internal process control. All of these control units are directly linked to the OBC and send all data that they receive back and forth in this link. A Solid-State Recorder (SSR) and watchdog timer are also present. The SSR serves as a data storage location for situations where the computer cannot cope with the data rates that it is receiving and also as a storage location for the images taken by the ADCS camera, which will be explained later in this subsection. The watchdog timer is a device directly integrated with the OBC in order to detect and recover from computer malfunctions, therefore being the back-up component for computer failure. Direct links between the OBC and these two components are present so that regular and swift data transfer can take place.

Solar Concentrator system

A crucial subsystem within the spacecraft is the Solar Concentrator system. The control unit is connected to heat sensors that are present in both the primary and secondary reflector, so that overheating can be detected quickly and the performance of the power beam can be assessed. Furthermore, pointing mechanisms for both reflectors are present so that they will at any time be properly aligned and commands can adjust their attitude. Next to this, a deployment mechanism has to be commanded that is present in the primary reflector and a cooling mechanism is present for both reflectors and collimator. Finally, a cleaning system is connected in the secondary reflector for contamination removal.

Once the control unit assesses that the data coming from the heat sensors indicates that the components rise above a certain temperature, the cooling mechanism will be initiated until this temperature has been reduced under the threshold again. The control unit will send commands coming from the ground station through to the deployment mechanisms and pointing mechanisms, until the heat sensors indicate that the power beam is fully operational. If the heat sensors indicate a loss of power during the deflection of the asteroid, the cleaning mechanism is initiated until the heat sensors provide data that indicate regaining of the power.

ADCS

The ADCS consists of 4 sun sensors, 4 star sensors, 6 reaction wheels and a camera that all send data and status updates back to the control unit. Also, the control unit transmits sensitivity alterations, reaction wheel and camera activation commands back, ensuring correct spacecraft attitude. The camera present will not send its images back directly to the OBC, since these images will have a data rate of 20 $[Mbps]$, being excessively larger than the other component data rates. More information on data rates will be provided in Subsection 10.1.2. These images will therefore be stored in the SSR, from where they are periodically sent to the OBC directly for processing. After being processed, useful attitude information about relative position to the asteroid is created and ready for downlink transmission. In this way, the OBC will not be loaded as much as direct data transfer would induce.

Propulsion

The control unit of the propulsion system is connected to valve controllers within the fuel tank, nitrogen tank and thrusters and pressure and fuel/nitrogen level sensors are present so that information on the environment of the tanks is directly put through to the OBC. The ADCS and propulsion subsystem are in close connection via the OBC, due to the swift response needed when ADCS sensors require an alteration of the spacecraft attitude. Sensor sensitivity and valve status updates are directly sent to the control unit as well.

TT&C

Within the TT&C system, which will be discussed in Section 10.2, two transponders are present that transmit data to the on-board antennas. Therefore, all data to be transmitted to the ground station and the other spacecraft in the constellation is sent through them from the OBC and SSR. Also, received commands are immediately sent to the OBC for distribution among the subsystems. Next to this, transponders also receive commands themselves for activation/stand-by and the antennas receive pointing commands, integrated within their structures.

EPS

The electrical power system consists of solar arrays, batteries and a power distribution unit, which in this subsystem acts as the control unit. The PDU makes sure the OBC receives direct electrical power, provided from the solar arrays or stored energy in the batteries. Solar array pointing commands are transmitted directly by the OBC to the arrays and battery degradation status is also directly transmitted to the OBC. The PDU also delivers updates on the entire power system.

Thermal and structures

The thermal control system consists of a control unit that uses feedback loops with heat sensors, heat pipes and radiators in order to keep the temperatures of the spacecraft within acceptable ranges and provides information on all component temperatures and cooling/heating activation status. The computer itself has to be heated and this is also managed throughout the thermal control unit. Heat sensors within all subsystems are interconnected with each other to effectuate swift response from the thermal components.

Finally, throughout the entire spacecraft structure, structural integrity sensors have been placed that transmit updates on cracks, fatigue and other structural deficits for the ground station. These updates are sent to the OBC via the structures sensor control unit and sensitivity commands are transmitted to the sensors.

As mentioned previously, all components connected to the C&DHS can be linked to three different boards. These boards have not been displayed individually in Figure 10.1 since they are integrated parts within the central computer. A rough indication of what component data is connected to which board is presented in Table 10.1.

Table 10.1: Component division based on data processing within OBC by the three different control boards.

H/K board	TT&C board	I/O board
Heat sensors	Transponders	Propulsion valves
Structural integrity sensors	Antennas	Reflector deployment mechanism
Tank sensors		Reflector pointing mechanisms
ADCS sensors		Reflector cooling mechanism
Component status		Reflector cleaning system
Batteries		Heat pipes and radiators
		Reaction wheels
		Solar array pointing mechanism

10.1.2 Data rates

In Table 10.2 below, all connected subsystems are displayed with their respective data rates that transfer from their components into the OBC and the command data rates that come from the OBC into their components, all in bits per second $[bps]$. [93]

Table 10.2: Data rates transferring into the OBC and command data rates transferring out of the OBC during maximum occupation.

Subsystem (-)	Data rate into OBC (bps)	Data rate out of OBC (bps)
Mission implementation	2,550	24,500
ADCS	900	12,250
Propulsion	700	22,000
TT&C	400	12,000
EPS	400	7,250
Thermal	300	9,750
Structures	200	2,500
TOTAL	**5,450**	**90,250**

Above values have been derived from estimations in SMAD. The bit rates displayed are the maximum values that can be present within the spacecraft, meaning it would be fully operational with all components active. These maximum values are used so that the total process power of the OBC can be determined, aiding in the selection of an existing OBC. For TT&C, only the commands and data rates from the components themselves are considered, not the data rates for the transmission to the ground station.

The bit rates were derived from estimations in SMAD. The data rates going into the OBC from the different components are significantly smaller than the command rates out of the OBC. For commands, it was considered that a typical C&DHS complexity is present in the spacecraft and this implies that on average 50 commands per second are transmitted through the OBC. Each command has a size of either 50, 65 or 80 $[bps]$, depending on their accuracy needs. Therefore, commands per component could either require 2500, 3250 or 4000 $[bps]$ and adding all of them results in Table 10.2.

The data rates coming from each component are based on preliminary SMAD estimations, ranging from 100 to 500 $[bps]$ per component, dependent on for example sensor data size. The images made by the ADCS camera are converted into text data with a bit rate of 200 $[bps]$. All of the individual component data rates are rough estimations and can vary in real life. The total data rates the OBC ultimately has to deal with are also presented

in the table, From which it is evident that the command throughput is a factor 17 larger than the component data throughput. Keeping these requirements in mind, the final OBC can be selected along with the SSR.

One specific scenario that has to be taken into account is the time in which the spacecraft is in LEO and waiting until an asteroid is detected. At this point, not all data has to be transferred back to Earth and a number of components are shut down, namely ADCS, propulsion and solar concentrator components, with the exception of their sensors. The total data rate going into the OBC is at that point $2050\ [bps]$ and the command transmission out of the OBC is $43,250\ [bps]$, adding up to a total data throughput of $45,300\ [bps]$. Considering the orbital period in parking orbit of $103\ [min]$ and with that the ground contact time of $16.5\ [min]$, the total amount of data that has to be stored when the spacecraft is not in contact with the ground station can be calculated using the following equation.

$$Data\ gathered\ per\ orbit = DR_{in} * (T_{orbit} - T_{ground}) \tag{10.1}$$

This results in a total data size of $10.6\ [Mb]$ to be stored in the SSR in this parking orbit per orbit. During ground contact time, the data will be transmitted back to the ground station, so SSR memory will be cleared again.

10.1.3 Components

Three different types of components were selected: an OBC, an SSR and a data bus. A data bus is the communication system between the computer and the components in which the data is exchanged. Physically, this consists of the wires and potentially connecting devices.[1]

OBC

The On-Board Computer selected is the LEON3FT-RTAX Processor. It is a microcontroller also used on the Ariane 6 launch vehicle and it is part of a large processor family developed by Aeroflex Gaisler. Due to fault tolerant design and radiation tolerant FPGA (Field Programmable Gate Array) technology, the processor is completely immune to radiation effects. Its key specifications are tabulated in the left table in Table 10.3 below, where all values have been specified by Aeroflex Gaisler. As can be seen, its handling speed is up to 20 Mega Instruction Per Second (MIPS), which is sufficient considering the command data rate of $50 - 80\ [bps]$ per command mentioned previously.[2] [3]

SSR

The Solid-State Recorder selected is the Basic Airbus DS Solid-State Recorder. These recorders come in two memory forms: SD-RAM and Flash memory. The latter would be preferred, since no data is lost during loss of power. However, the performance of the Basic SSR is sufficient for the C&DHS design and using flash memory would only increase the mass of the SSR further without any other useful improvement of performance. The Airbus DS SSR is also widely used by ESA missions. In the right table in Table 10.3 below, key specifications for the selected recorder are presented, all provided by Airbus.[4]

Table 10.3: LEON3FT-RTAX Processor (left) and Airbus DS Basic Solid-State Recorder (right) key specifications.

Specifications	Value
Handling speed	Up to 20 $[MIPS]$
System frequency	Up to 25 $[MHz]$
Instruction cache	8 $[kByte]$
Data cache	4 $[kByte]$
Total Ionizing Dose (TID)	300 $[krad]$ (Si, functional)
Power supply	1.5 $[V]$ & 3.3 $[V]$
Power consumption (max)	500 $[mW]$
Mass	0.58 $[kg]$
Size	5 x 91 x 91 $[mm]$

Specifications	Value
SSR Type	Basic
Memory technology	SD-RAM
Capacity	512 $[Gbit]$
Input interface	SpaceWire
Data rate	500 $[Mbps]$
Power consumption	45 $[W]$
Mass	15 $[kg]$
Size	250 x 250 x 150 $[mm]$

[1] URL `https://bit.ly/3qNnVUj` [accessed 6 January 2021]
[2] URL `https://www.gaisler.com/doc/leon3ft-rtax-product_sheet.pdf` [accessed 6 January 2021]
[3] URL `http://www.cpushack.com/space-craft-cpu.html` [accessed 6 January 2021]
[4] URL `https://bit.ly/3izLlJU` [accessed 7 January 2021]

Data Bus

The data bus selected is SpaceWire, specifically designed for applications by ESA. It is a point-to-point system, meaning it connects components directly with each other or with a router, which can connect multiple components with each other or with other data buses. It supports data rates up to 400 Mb/s and the bus is typically implemented in FPGA architectures. Also, it can simply reroute data in case of single link failures, which makes it a highly reliable bus for modern spacecraft. The OBC and SSR selected above are fully compatible with the SpaceWire infrastructure and can therefore easily be connected. As for sizing, the mass of the entire wiring system is estimated to be $5\ [kg]$ and the size has been estimated by the assumed bus mass density of $0.5\ [kg/L]$, resulting in a total bus size of $0.01\ [m^3]$. These estimations are all based on SMAD and the system size indicate how much space the wires take up. On a final note, the system latency is heavily dependent on the selected data bus and for a typical SpaceWire system the longest target latency is $50\ [\mu s]$.[5] [23, 93]

The Command and Data Handling System will in the end have a total mass of $20.058\ [kg]$, a total volume size of $19.42\ [L]$ and has a total power consumption of $45.5\ [W]$. Both requirements on the CD&HS, **AD-SYS-TECH-COMM-10.6** and **AD-SYS-TECH-COMM-13**, have also been met, since the maximum latency between subsystems is $50\ [\mu s]$ and all on-board processes are handled by this system along with the TT&C subsystem.

10.1.4 Hardware and software diagrams

On a final note, the hardware and software diagrams are presented in Figure 10.2 and Figure 10.3. In the hardware diagram, the high-level placement of each subsystem with respect to the spacecraft bus is shown. Exact interrelations have not been presented since it should be obvious that for example the thrusters are connected with the fuel tanks via fuel pipes with valves in them, that are in their way controlled by the OBC. The PDU distributes electricity to all active components and the TCU will make sure the heat pipes and radiators supply heat to all components that require heating. The data and command layout has already been presented in Figure 10.1, from which the connection of the data bus with all components is evident and the structure of the TT&CS is also clear.

In the software diagram, the distribution of the OBC software among all components is shown. This diagram is still very high-level, since this has in principle already been completely described in Figure 10.1. Software needs to be present in each component that provides data or handles commands, which are all the components present in that figure. The specific software chosen is dependent on the suppliers or, in case of the OBC, taken from comparable missions, such as New Horizons[6].

10.2 Telemetry, Tracking and Command System

The need for communication between ground system and spacecraft in any space mission is evident; commands have to be sent towards the spacecraft so that certain actions can be taken and spacecraft data should be transmitted back to Earth for ground station processing. Next to this, the location of the spacecraft should be known at any time during the mission, which can be achieved by for example a Doppler tracker. The Telemetry, Tracking and Command System, also known as the communication system, consists of all components necessary for this communication link.

10.2.1 General infrastructure

As explained in Subsection 10.1.2, two mission phases can be distinguished. The first one is the spacecraft waiting in parking orbit until an asteroid is detected. In this phase, the entire system will be a payload within one of SpaceX's Starship launch vehicles. SpaceX will provide an interface for data exchange between ground station and the spacecraft in this scenario, but there might still be a malfunction within this system that requires the spacecraft to communicate by itself. This is why Low-Gain Antennas (LGA) will be designed for communication in this parking orbit with the ground station. The maximum distance between spacecraft and ground station during contact time is $3504\ [km]$, based on basic trigonometry and the orbital height of $900\ [km]$. Two hemispherical antennas will be chosen, to be placed on opposite sides of the spacecraft bus, so that pointing is not necessary for these components.[7] [93]

[5] URL `https://bit.ly/360I54X` [accessed 6 January 2021]
[6] URL `https://go.nasa.gov/2YiYXQ9` [accessed 8 January 2021]
[7] URL `https://www.spacex.com/media/starship_users_guide_v1.pdf` [accessed 26 January 2021]

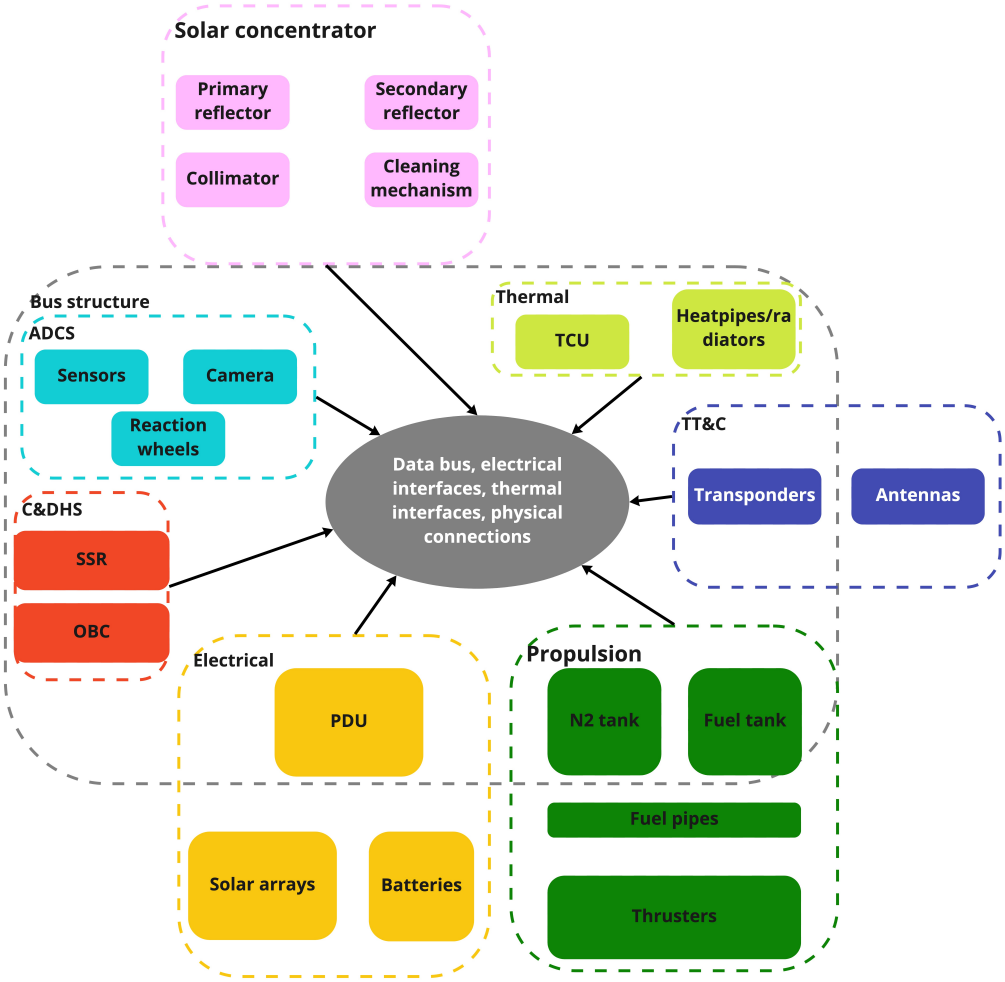

Figure 10.2: High-level Hardware diagram.

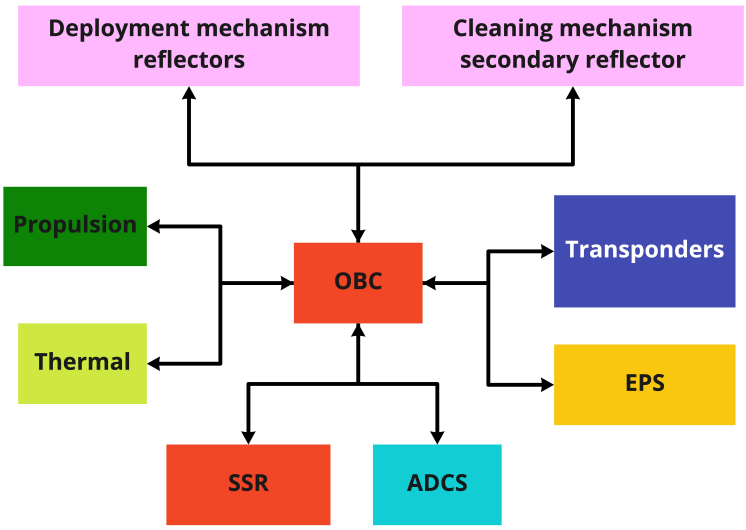

Figure 10.3: High-level Software diagram.

The other phase consists of the transfer to the asteroid and actively deflecting the asteroid. During transfer, the spacecraft will still be attached to the payload fairing so communication with the ground station can still take place via a Starship launch vehicle. When the spacecraft has been separated from the launch vehicle and is active, a High-Gain Antenna (HGA) is necessary for communication with the ground system, considering a maximum distance from Earth of $4\ AU$. The antenna will be parabolically-shaped, increasing its gain and narrowing its beam, which makes such long-distance communication easily possible.

Since a constellation of spacecraft will be used, communication among these different systems will be crucial. The LGA described above will also be used for that, so that constant accurate pointing is not necessary and there can be a constant link between the different spacecraft. The LGAs will make use of an S-Band frequency band, having a frequency range of $2-4\ [GHz]$, and the HGA will make use of an X-Band frequency band, which is typical for deep-space missions and has a frequency range of $8-12\ [GHz]$. [93]

Ground stations

In order to initiate the sizing of the TT&CS, existing ground stations have to be selected. For the S-Band communication link, ESA's Redu-1 Station in the Belgian Ardennes is selected[8] [9]. For the X-Band communication link, NASA's Deep Space Network (DSN) has been selected, more specifically the 34-meter diameter Madrid-based Beam-Waveguide (BWG) antenna[10]. Key specifications for both of these ground stations have been presented in Table 10.4 below.

Table 10.4: ESA Redu-1 Antenna and NASA DSN Madrid BWG key specifications. [75]

Redu-1 Antenna	
Specification	**Value**
Antenna diameter	15 [m]
S-Band TX band	2,025 - 2,120 [MHz]
S-Band RX band	2,200 - 2,300 [MHz]
Antenna efficiency	70 [%]
S-Band transmission bit rate	2.00 [Mbps]
S-Band EIRP	102.5 [dBm]
Half-power beamwidth	0.3 [degrees]
Pointing offset angle	0.08 [degrees]
Noise figure	1.5 [dB]

DSN Madrid BWG	
Specification	**Value**
Antenna diameter	34 [m]
X-Band TX band	7,145 - 7,235 [MHz]
X-Band RX band	8,400 - 8,500 [MHz]
Antenna efficiency	70 [%]
X-Band transmission bit rate	256 [kbps]
X-Band EIRP	109.5 [dBW]
Half-power beamwidth	0.079 [degrees]
Pointing offset angle	0.06 [degrees]
Noise figure	1.5 [dB]

10.2.2 Antenna sizing

In order to perform the on-board antenna sizing, multiple communication relations from SMAD were used and applied to the selected ground stations and antenna requirements. Using the results from Section 10.1, the required bit data rates that have to be transmitted or received in parking orbit and during deflection respectively can be determined and used for the antenna sizing. These two scenarios are once again considered, since they impose the limiting values regarding the data rates on these antenna systems. [93]

Low-Gain Antenna

First of all, the required LGA data rate capacity has to be derived from the C&DHS data rates present in parking orbit. It is assumed all data rates coming into the OBC are also transmitted to the ground station and all commands are transmitted for maximum operation. For the commands, this results in the same total uplink command data rate of $43,250\ [bps]$ presented previously. For the downlink data rate, the contact time with the ground station needs to be taken into account, represented by the following equation.

$$DR_{downlink,\,parking\ orbit} = \frac{DR_{in} * T_{orbit}}{T_{ground}} \tag{10.2}$$

[8] URL https://bit.ly/3sTNOna [accessed 8 January 2021]
[9] URL https://bit.ly/3ca1e8O [accessed 8 January 2021]
[10] URL https://go.nasa.gov/2Mjpdrd [accessed 8 January 2021]

Filling in these numbers results in a required downlink data rate for parking orbit of $12,797\ [bps]$. The total required LGA data capacity C will thus be $56,047\ [bps]$, which can then be used in the Shannon-Hartley theorem, expressed in the equation below.

$$C = B * log_2(1 + SNR) \tag{10.3}$$

B is the channel bandwidth in $[Hz]$ and SNR is the signal-to-noise ratio of the LGA. The bandwidth can easily be calculated using the fact that the data has to be compressed and digitized in order for it to be able to be transmitted. The following equation represents this process.

$$B = \frac{C}{CF * Spectrum\ Utilization} \tag{10.4}$$

C is here the total data rate required for the LGA, CF is the data compression factor and the $Spectrum\ Utilization$ is a measure for number of bits transmitted per unit of frequency, in $[bits/Hz]$. CF value is taken to be 5 and $Spectrum\ Utilization$ is taken to be $1.5\ [bits/Hz]$, both taken from SMAD estimations. Using these values, the bandwidth B per spacecraft LGA is computed to be $126.4\ [kHz]$.

The SNR can be rewritten to the total received signal power S in $[W]$. To do this, the noise density N_0 has to be calculated with the Boltzmann Constant k and the LGA system noise temperature T_s.

$$N_0 = k * T_s \tag{10.5}$$

This can then be related to the total received signal power using the following equations.

$$SNR = \frac{E_b}{N_0} \tag{10.6}$$

$$E_b = S/R \tag{10.7}$$

E_b is the energy per bit in $[J/bit]$ and R is the transmission bit rate of the antenna in $[bps]$. The total received signal power by the LGA is computed to be $1.49 * 10^{-10}\ [W]$.

Next, the power radiated by the ground station has to be considered. The Effective Isotropic Radiated Power ($EIRP$) of the REdu-1 Antenna was found to be $102.5\ dBm$[11], which converts to $17,782,794\ [W]$, and using the maximum distance between the spacecraft and ground station in parking orbit, the power flux density W_f at the spacecraft can be computed with the following equation.

$$W_f = \frac{EIRP}{4\pi r^2} \tag{10.8}$$

This power flux density can then be related to the total received signal power, the antenna area and the antenna efficiency by the following equation.

$$S = W_f * A_{antenna} * \eta_{antenna} \tag{10.9}$$

Computation resulted in a required Low-Gain Antenna diameter of $0.052\ [m]$.

High-Gain Antenna

For the HGA sizing, the same approach as for the LGA has been used. For the HGA, however, the maximum operation data rates need to be considered along with a maximum contact distance of $4\ [AU]$. The total required HGA capacity is assumed to be $50,575\ [bps]$, where nominal operation is assumed to consist of 50% of the total commands possible. The required bandwidth per satellite is $126,438\ [Hz]$ and the $EIRP$ of the ground station is assumed to be $109.5\ [dBW]$. Along with the other known parameters, a total HGA dish diameter of $3.86\ [m]$ is required for data transmission when actively deflecting an asteroid.

[11] URL `https://bit.ly/39bZtpA` [accessed 8 January 2021]

10.2.3 Link budget

For the LGAs and HGA, a downlink link budget has also been constructed using telemetry theory, considering the spacecraft antennas as the transmitters and the ground station as the receivers. Results for both antenna types are presented in Table 10.5.

Table 10.5: HGA (left) and LGA (right) downlink link budgets. [16, 17, 51, 93]

High-Gain Antenna		
Parameter	**Symbol**	**Value**
RF output power	P	$3\ [W]$
Effective Isotropic Radiated Power	$EIRP$	$191,982\ [W]$
Transmitter to antenna loss	L_l	$0.8\ [-]$
Transmitter gain	G_t	$49\ [dBi]$
DSN receiver gain	G_r	$68.2\ [dBi]$
Transmission path losses	L_a	$0.035\ [-]$
Space loss	L_s	$2.60 * 10^{-29}\ [-]$
Antenna pointing loss	L_{pr}	$2.03 * 10^{-1}\ [-]$
Reception feeder loss	L_r	$1\ [-]$
Reference noise temperature	T_0	$290\ [K]$
DSN system noise temperature	T_s	$500\ [K]$
Signal-to-Noise Ratio	SNR	$-18.14\ [dB]$

Low-Gain Antenna		
Parameter	**Symbol**	**Value**
RF output power	P	$12\ [W]$
Effective Isotropic Radiated Power	$EIRP$	$60.57\ [W]$
Transmitter to antenna loss	L_l	$0.8\ [-]$
Transmitter gain	G_t	$8\ [dBi]$
Redu-1 receiver gain	G_r	$49.23\ [dBi]$
Transmission path losses	L_a	$0.035\ [-]$
Space loss	L_s	$9.58 * 10^{-18}\ [-]$
Antenna pointing loss	L_{pr}	$0.82\ [-]$
Reception feeder loss	L_r	$1\ [-]$
Reference noise temperature	T_0	$290\ [K]$
Cable noise temperature	T_{cable}	$32.22\ [K]$
Amplifier noise temperature	T_n	$119.6\ [K]$
Redu-1 system noise temperature	T_s	$251.9\ [K]$
Signal-to-Noise Ratio	SNR	$37.6\ [dB]$

10.2.4 Components

The entire TT&C system consists of two transponders, two Low-Gain Antennas, one High-Gain Antenna and a diplexer. Two transponders are chosen since these are the only active components within the entire system and therefore have to be redundant as to lower the chances of system failure. The diplexer takes care of the frequency-domain multiplexing. Existing components and components under development have been chosen for the subsystem.

In recent literature, the development of a new Advanced Deep Space Transponder is presented, which is capable of having a direct communication link with Earth as well as a spacecraft-to-spacecraft link [22]. The design is based upon the Small Deep Space Transponder, present on multiple missions such as the Mars Reconnaissance Orbiter. Furthermore, multiple ranging tools, such as a Doppler shift device and a differential one-way ranging device, are present so that accurate navigation can be accomplished. The transponder is compatible with X-band as well as S-band frequency bands within the bandwidth selected for the mission. An RF amplifier is also present, which was chosen to be a solid-state amplifier since these are more reliable, lighter and smaller than the also popular traveling wave tube amplifiers. A Quadrature Phase Shift Keying (QPSK) is also part of the transponder so that signals can be modulated. The Bit Error Rate (BER) associated with this type of modulation is approximately $10^{-6}\ [-]$, a typical value for such antenna systems.

The transponder will have a total mass of $2.6\ [kg]$, which is comparable to the mass of the Small Deep Space Transponder. Along with an average transponder density (estimation taken from SMAD) of $0.75\ [kg/L]$, the total transponder volume is estimated to be $3.47\ [L]$ each. The transponders are the only active components present in the TT&CS and require an inlet power of $14\ [W]$ each.

For the HGA, the diameter of 3.86 $[m]$ was found with which the total mass can be estimated. Considering a dish thickness of 0.02 $[m]$, the total volume will be 234 $[L]$ and considering a density of 1.62 $[kg/m^2]$, typical for light-weight parabolic antennas, the total HGA mass becomes 18.9 $[kg]$[12]. [80]

For the LGAs, an existing component is chosen, namely the RUAG Space S-Band Patch Excited Cup Antennas[13]. Having a diameter of 0.14 $[m]$ and a height of approximately 0.069 $[m]$, its total volume is 1.06 $[L]$. It has a total mass of 0.28 $[kg]$ per antenna. Last but not least, the diplexer is chosen to be a compact, high-power diplexer used on the Mars Orbiter Mission. Its mass is assumed to be 2 $[kg]$ and its size is 2.7 $[L]$, considering typical dimensions of 15 x 30 x 6 $[cm]$. [86]

The total mass of the Telemetry, Tracking and Commands System will in the end be 26.7 $[kg]$, its total volume will be 246 $[L]$, with only 9.6 $[L]$ present inside the spacecraft bus. The total TT&CS power consumption is 28 $[W]$. The placement of the antennas will be on the outside of the bus so that clear communication with the Earth is possible.

10.3 Requirements

Looking back at the requirements set up in the Baseline Report and once more presented in Table 10.6, it can be observed that all of them have been achieved. For example, **AD-SYS-TECH-COMM-10.5** is satisfied since the total bit rate possible is $50,575$ $[bps]$, which is well below the value presented in the requirement itself. Therefore, the TT&CS will make sure the mission is viable and makes missions success realistic. The Measure of Compliance used for these requirements are either test, inspection or analysis. Most of them can be tested once a prototype of the actual system has been built, analysis has to be applied to **AD-SYS-TECH-COMM-10.7** and **AD-SYS-TECH-COMM-12** because for both requirements, the actual situation can not be mimicked, calling for specific computer analysis. For the total weight, inspection of the prototype or final system should be applied.

[12]URL `https://go.nasa.gov/3svdPsV` [accessed 15 January 2021]
[13]URL `https://bit.ly/38UdxEc` [accessed 15 January 2021]

Table 10.6: Communications and Information Processing Requirements

Identifier	Requirement	MOC	Compliance
AD-SYS-TECH-COMM-10	The communication system shall communicate with the ground station.	Test	Y
AD-SYS-TECH-COMM-10.1	The ground station shall provide $150\ [MHz]$ amount of bandwidth for the transfer of data from the space subsystem.	Test	Y
AD-SYS-TECH-COMM-10.2	The ground communication system shall provide a connection to the space system when it is at a maximum distance of $4\ [AU]$ from the Earth.	Test	Y
AD-SYS-TECH-COMM-10.3	The position of the space system shall be known by the ground station with an accuracy of $20\ [m]$ meters.	Test	Y
AD-SYS-TECH-COMM-10.4	The transmission system shall have an accuracy of 10^{-6} bit rate error when transmitting information.	Test	Y
AD-SYS-TECH-COMM-10.5	The transmission system shall have a bit rate of $50,575\ [bps]$ when transmitting information.	Test	Y
AD-SYS-TECH-COMM-10.6	The latency between subsystems, from input to output, shall not exceed $100\ [\mu s]$.	Test	Y
AD-SYS-TECH-COMM-10.7	The communication system shall alert the ground station to errors occurring on-board the space system.	Analysis	Y
AD-SYS-TECH-COMM-7	The communication system on the space system shall make use of no more than $35\ [W]$ over the course of the mission.	Test	Y
AD-SYS-TECH-COMM-11	The communication system shall weigh no more than $30\ [kg]$.	Inspection	Y
AD-SYS-TECH-COMM-12	The communication system shall revert a subsystem to a sleep state if a malfunction is detected within it.	Analysis	Y
AD-SYS-TECH-COMM-13	The communication and information processing system handle all on-board processes.	Test	Y

11 Electrical Power System

Most subsystems require power to stay operative during the mission. An Electrical Power System (EPS) was designed in order to generate power and to supply the subsystems with this generated power. This chapter discusses the design of the EPS. First, Section 11.1 discusses the design of the power source and Section 11.2 will present the design of the Power Control and Distribution Unit. Lastly, a check with the technical requirements is given in Section 11.3.

11.1 Power Source

In general, there are three commonly used power sources in the space industry: primary batteries, solar arrays and radioisotope power generators [21]. A radioisotope power generator was discarded as a feasible option due to sustainability requirements. Next to that, batteries will not be feasible as a power source due to its mass characteristics. Each spacecraft requires more than $5,000[W]$ for a mission duration of at least 20 days, which is too much for batteries to supply. Hence, power generation with the use of solar energy is considered as the most feasible option.

The next step in the design of the power generator is to determine how much power is required by the spacecraft. table 11.1 provides the power, input voltage and type of current required for each subsystem. This sums up to a total required power of $5,424.5[W]$ for a single spacecraft.

Table 11.1: Required power for each subsystem

Subsystem	**Required Power** $[W]$	**Voltage Range** $[V]$	**AC/DC**
ADCS	559	24-51	DC
Propulsion System	4,400	80-160	DC
TCS	300	115	DC
C&DHS	45.5	1.5-3.3	DC
TT&CS	28	1-3	DC
Reflector Cleaning	92	1,500	AC
Total	**5,424.5**	**NA**	**NA**

The amount of power that can be produced by the solar arrays at the end of life is calculated using Equation 11.1.

$$P_{EOL} = SI * \eta * I_d * cos(\theta) * (1 - \kappa)^T \tag{11.1}$$

In Equation 11.1, SI, η, I_d, θ, κ, and T denote the solar irradiance, solar cell efficiency, inherent degradation, incidence angle, solar cell degradation and the mission duration respectively. Also it should be noted that P_{EOL} is the power density, in other words, the power that can be produced per square meter. It was assumed that the incidence angle of the solar beams is equal to 0 [rad]. With the use of Equation 11.1, the required solar array area was easily determined as given in Equation 11.2.

$$Area = P_{required}/P_{EOL} \tag{11.2}$$

In order to size the solar arrays, the right solar cells should be selected. Multi Junction Gallium Arsenide solar cells are considered to be the most feasible option, due to the high efficiency and low degradation characteristics. To be precise, Quadruple Junction Gallium Arsenide solar cells from AzurSpace will be used. These solar cells have an efficiency of 32% and a typical degradation of 0.5% per year[1]. With the use of Equation 11.1 and Equation 11.2, a total required solar array area was determined to be $20[m^2]$, which includes a power margin of 25%.

These solar cells will be attached to ten 2x1 $[m]$ solar panels and are placed in strings of $75[V]$. This means that each solar panel contains 25 strings of solar cells. Next to that, the solar panels will be divided into two deployment systems, each containing five panels, and will be placed in the Primary Reflector structure. As shown in Figure 11.1, five solar panels will be stacked on top of each other in undeployed form. This causes

[1]URL `http://www.azurspace.com/images/0005979-01-01_DB_4G32C_Advanced.pdf` [accessed 26 January 2021]

an effective area increase with a factor of five after deployment of the solar panels. The total solar panel mass was calculated to be $82[kg]$ [93].

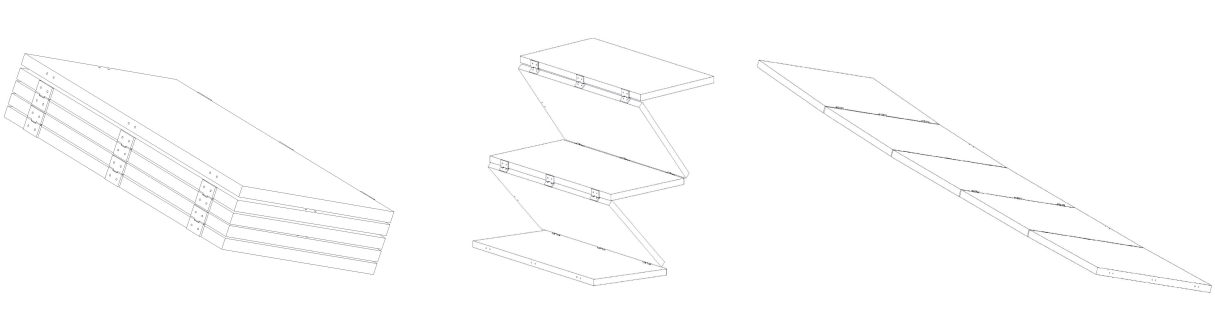

Figure 11.1: Deployment of the Solar Panels.

11.2 Power Control and Distribution

11.2.1 Batteries

The EPS design should also consider situations where the subsystems require more power than assumed for short durations. These situations are called power spikes. In order for the spacecraft to be able to cope with these power spikes, batteries will be designed that are able to deliver the required extra power during these power spikes [93]. It is assumed that the spacecraft should be able to handle power spikes of 50% of the total required power for a duration of five minutes. This results in a total required energy storage of around $850,000[J]$.

Considering the high energy density and its common usage, Lithium-ion batteries were selected to store the energy. The mass of these Lithium-ion batteries can be calculated using Equation 11.3.

$$m_{battery} = \eta * e * E/(DOD * n) \tag{11.3}$$

In Equation 11.3, η, e, E, DOD and n denote the battery efficiency, specific energy, energy, depth of discharge and transmission efficiency respectively. This results in a required battery mass of $10.3[kg]$ for common Lithium-ion batteries [93]. Next to that, the capacity of Lithium-ion batteries will decrease with 3% per month [21]. This results in a maximum decrease of 43% for a mission duration of 1.5 years. However, the batteries are only active in use during the final stage, only consisting of around 20 days.

11.2.2 PCDU

As there will be power generated by the solar arrays, the generated power should be supplied to the different subsystems. For this reason a power control and distribution unit (PCDU) was designed. This PCDU will control the power levels for different subsystems, it will distribute power with the right voltages to every subsystem and it will ensure that the right type of current is received by each subsystem. The aforementioned factors can be seen in Table 11.1 for each subsystem.

The power will be supplied to each subsystem with the use of wires. It should be noted that the resistance of the wires will cause a small power loss. This power loss can be calculated using Equation 11.4.

$$P_{loss} = R_{wire} * I^2_{transmission} = R_{wire} \frac{P^2_{transmission}}{V^2_{transmission}} \tag{11.4}$$

As can be seen, the lost power due to transmission can be reduced quadratically by increasing the voltage. For this reason, a combination of boost and buck converters will be used. In front of the PCDU, a boost converter will increase the incoming voltage from the solar arrays to a voltage of $1,500[V]$. As most subsystems require lower voltage levels, except for the secondary mirror cleaning system, a buck converter will be placed in front of those subsystems in order to reduce the voltage level. With the use of these boost and buck converters, the lost power will be minimized.

Next to that, the incoming power from the solar arrays will be DC power. Again, all subsystems, except for the secondary mirror cleaning system, require DC power. The secondary mirror cleaning system requires AC power. So, the incoming DC power should be converted to AC power. For this process, a DC-AC inverter will

be used.

A power tracker will be positioned at the solar arrays to ensure that the solar arrays produce maximum power. Also, the charge and discharge of the batteries will be controlled by a battery charge regulator and a battery discharge regulator. Lastly, it should be noted that the power levels of all other subsystems will be tracked and controlled. All aforementioned components of the PCDU are summarized in Figure 11.2.

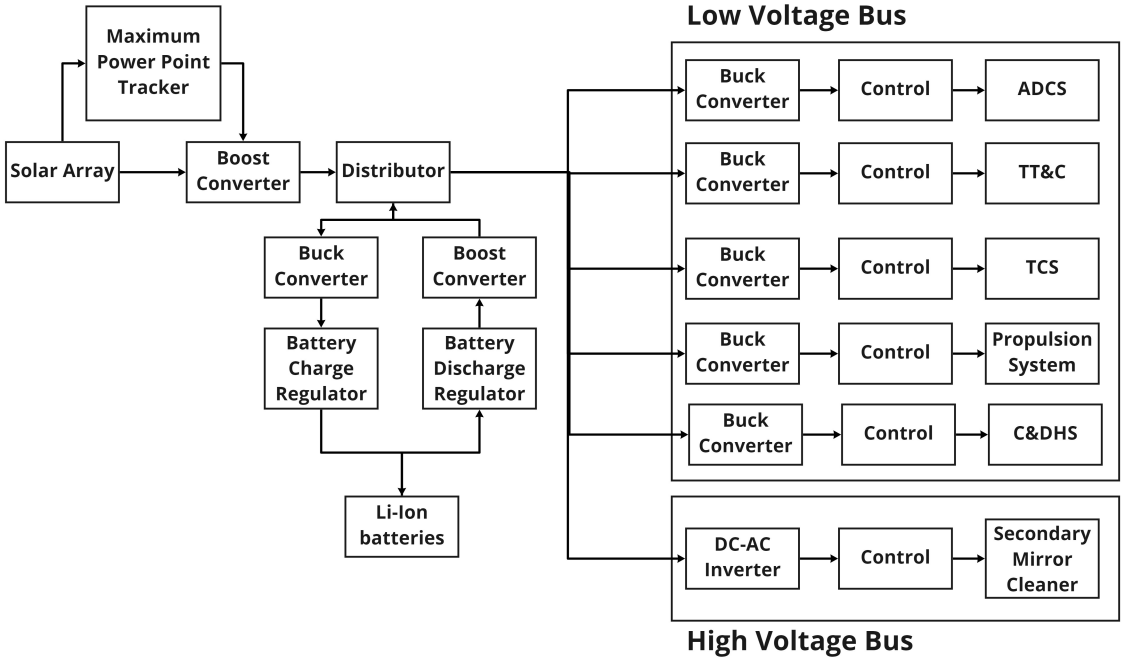

Figure 11.2: Electrical Block Diagram of the Power Control and Distribution Unit.

For the PCDU, an off the shelf product was selected. The required power of $5,424.5[W]$ was considered as a medium power level. The PCDU: Medium Power from Thales Alenia fits the power requirement and offers possibilities for the usage of boost and buck converters. It was estimated with data from Thales Alenia that the PCDU will have a mass of $10.45\ [kg]$.[2]

11.3 Requirements

Concluding, solar panels with a mass of $82[kg]$ will be designed that are capable of producing at least $5425[W]$ during the mission. The solar cells used for the solar panels will have an efficiency of 32%.

The generated power will be controlled, stored and distributed by the PCDU weighing $20.75[kg]$, including the battery mass. The capacity of the batteries will decrease with a maximum of 3% per month and are able to store a maximum energy of $1300\ [kWh]$.

[2]URL `https://www.terma.com/media/150039/modular_medium_power_unit.pdf` [accessed 26 January 2021]

Table 11.2: Power Requirements

Identifier	Requirement	MOC	Compliance
AD-SYS-TECH-POW-10	The power system shall provide power to all subsystems.	Demonstration	Y
AD-SYS-TECH-POW-10.1	The space system shall use no more than 3,000,000 kWh of energy.	Analysis	Y
AD-SYS-TECH-POW-10.2	The PSU shall supply the CPU with no less than 5,425 kW of power.	Analysis	Y
AD-SYS-TECH-POW-10.3	The power generation system shall have an efficiency of 32%	Inspection	Y
AD-SYS-TECH-POW-11	The power system shall store the required energy of the systems.	Analysis	Y
AD-SYS-TECH-POW-11.1	The power storage unit shall be able to store a maximum of 1300 kWh.	Analysis	Y
AD-SYS-TECH-POW-11.2	The energy storage system shall lose 43% of its maximum storage capacity over the course of 5 years.	Analysis	Y
AD-SYS-TECH-POW-4	The power unit shall weigh no more than 90 kg.	Analysis and Test	Y
AD-SYS-TECH-POW-5	The power storage unit shall weigh no more than 25 kg.	Analysis and Test	Y

12 Thermal Control System

This chapter discusses the design of the Thermal Control System (TCS). First, Section 12.1 discusses the model that is used to determine the equilibrium temperature of different components of the spacecraft. Section 12.2 gives the temperature ranges that the TCS should maintain. Then, Section 12.3 discusses the final design of the TCS. Finally, Section 12.5 lists the requirements for the TCS, and checks it meets them.

12.1 Thermal Model

All components within a spacecraft have their own operational and surviving temperatures. When the operational temperatures are exceeded, the subsystem will not function as it should. Exceeding the surviving temperatures of a component will result in a failure of the component or even a failure of the spacecraft itself. In order to prevent a spacecraft from failure, the temperature of all components should be controlled during the mission. This can be done by means of passive thermal control (e.g. coatings, insulation etc.) or active thermal control (e.g. heaters, louvers etc.). These different thermal control techniques will be further elaborated upon in Section 12.3. In order to design the thermal control system, the equilibrium temperatures of the different components should be modeled. This was done by setting up a heat balance for every component.

First step is to model the incoming heat from the Sun. Due to the high temperature of the Sun, a lot of heat gets distributed in space. This can be expressed by the SI (Solar Irradiance), which is a measure for the amount of power per square meter received by an object in space. The SI at varying points in space can be calculated using Equation 12.1.

$$SI = H_{SUN}\left(\frac{R_{SUN}}{R_{SUN-OBJ}}\right)^2 \tag{12.1}$$

Where H_{SUN} denotes the power density at the surface of the Sun, R_{SUN} the radius of the Sun and $R_{SUN-OBJ}$ the distance between the Sun and the object in space. From the set of possible asteroid encounters with Earth, a closest distance for the spacecraft of one AU was assumed. This resulted in a SI of $1,386.7$ $[W/m^2]$. Using this, the heat transfer from the Sun to an object in space can be calculated as followed [93]:

$$Q_{in} = SI * A_p * \alpha \tag{12.2}$$

In Equation 12.2, A_p is the projected area of the object towards the Sun and α is the absorptivity of the object. However, just as for the Sun, every object within space with a temperature larger than zero degrees K radiates energy. This can be calculated using Equation 12.3 [93].

$$Q_{out} = A_r * \epsilon * \sigma * T^4 \tag{12.3}$$

Where A_r is the radiating surface of the object, ϵ the emissivity of the object, σ the Stefan-Boltzmann constant and T the temperature of the object. Combining Equation 12.2 and Equation 12.3 leads to the equation that can be used to calculate the equilibrium temperature of an object in space. This equation is formulated as followed:

$$T = \sqrt[4]{\left(SI * \frac{\alpha}{\epsilon} * \frac{A_p}{A_r}\right)/\sigma} \tag{12.4}$$

It should be noted that heat transfer via conduction does not occur as there is no air present in space. Next to that, it was assumed that the heat transfer between different components via radiation and convection was negligible with respect to the incoming power from the Sun. Another important assumption is that the spacecraft will not be in eclipse, so it will receive a constant power from the Sun.

12.2 Design Goal

12.2.1 Temperature Ranges

As mentioned before in Section 12.1, all components within the spacecraft have different surviving and operational temperatures. These values are given in Table 12.1 and are based on the data given by the manufacturer of each component.

Table 12.1: Surviving and Operational Temperatures of different components.

Component	**Surviving Temperature Range** $[K]$	**Operational Temperature Range** $[K]$
Primary Reflector	NA - 673	NA - 673
Collimator	NA - 673	NA - 673
Secondary Reflector	NA - 648	NA - 648
PCDU	258.15 - 313	268 - 308
Solar Panel	73 - 403	123 - 383
On-board Computer	203 - 358	218 - 343
Steady State Recorder	233 - 348	248 - 333
Reaction Wheel	233 - 348	253 - 343
Star Senor	233 - 343	243 - 333
Sun Senor	No information found	223 - 358

From Table 12.1, some useful design decisions were made. As the PCDU, On-board Computer, Steady State Recorder, Reaction Wheels and Star Sensors will be positioned in the subsystem bus, a design temperature for the subsystem bus of $280\ [K]$ was decided on. Next to that, it should be noted that the Primary Reflector, Collimator and Secondary Reflector have a high maximum operational temperature. As these components will receive a lot of solar power, the high maximum operational temperatures are useful.

12.2.2 Equilibrium Temperatures without Thermal Control

For the determination of the equilibrium temperature, the spacecraft was divided in five parts: the Primary Reflector, Collimator, Secondary Reflector, Subsystem Bus and the Solar Panels. With the use of Equation 12.4, the following equilibrium temperatures were determined:

Table 12.2: Equilibrium Temperatures without Thermal Control

Subsystem	**Equilibrium Temperature** $[K]$	**Operational Temperature Range** $[K]$
Primary Reflector	125	NA-673
Collimator	568	NA-673
Secondary Reflector	345	NA-648
Subsystem Bus	NA	268-308
Solar Panels	333	123-383

As the Subsystem Bus will be positioned in the shadow of the Collimator, the Subsystem Bus will not receive any heat from the Sun. This results in a continuously decreasing temperature of the Subsystem Bus until it reaches equilibrium temperature relatively close to $0\ [K]$. When comparing Table 12.1 and Table 12.2, it can be seen that the equilibrium temperatures without thermal control for the Primary Reflector, Collimator, Secondary Reflector and Solar Panels are well within their operational limits. So, the thermal control system design will only focus on maintaining the operational temperatures for the Subsystem Bus.

12.3 Thermal Control System Design

As the Subsystem Bus lacks a heat source, Equation 12.3 was used to determine the amount of power needed to maintain an equilibrium temperature of $280\ [K]$. This resulted in required power source of $2.7\ [kW]$. As this required power is not desirable, the Thermal Control System design focused on two factors:

- **Emissivity** The ability of the Subsystem Bus to emit energy into space should be reduced.
- **Heat Source** The Subsystem Bus requires a heat source that can act as a substitution of the Sun.

12.3.1 Emissivity

In order to reduce the required power from the heat source, it was decided to reduce the emissivity of Subsystem Bus. In general, there are two possible options in the space industry to reduce the emissivity of a spacecraft [93]. Namely, applying coatings to the outside of the spacecraft or insulating the inside of the spacecraft. Coatings are not a viable option as they are effective when a spacecraft receives power from the Sun. However, insulation on the other hand will minimize the power that gets dissipated by the Subsystem Bus.

Insulation of the Subsystem Bus will be done with the use of Multilayer Insulation (MLI) blankets. These MLI blankets are common in the space industry and are made of multiple thin films of different low emissivity materials. It is proven that MLI blankets can reduce the emissivity of objects with a factor of 200, but in practice a factor of 33 is more applicable for common types of MLI blankets [93]. The usage of these MLI blankets to reduce the emissivity of the Subsystem Bus results in a required power source of $82[W]$, which is considered acceptable.

12.3.2 Heat Source

As the iterated required power is deemed acceptable, the heat source can be designed. In general there are also two options for the Subsystem Bus to add heat, namely with the use of heat pipes (passive thermal control) or heaters (active thermal control). Heat pipes use liquid to transfer heat between different components of a spacecraft. Keeping the low required power and the size of the spacecraft in mind, the heat piper were considered to be unfeasible.

Heaters for spacecraft applications can be divided into patch and cartridge heaters. Patch heaters use an electrical resistance element that is placed between two thin sheets of insulating material. Cartridge heaters use a wound resistor that is placed inside a metallic case [93]. As the patch heaters are really thin, they can be positioned against the walls of the Subsystem Bus. Hence, they require less space and are the more feasible option. Figure 12.1 shows such a patch heater.

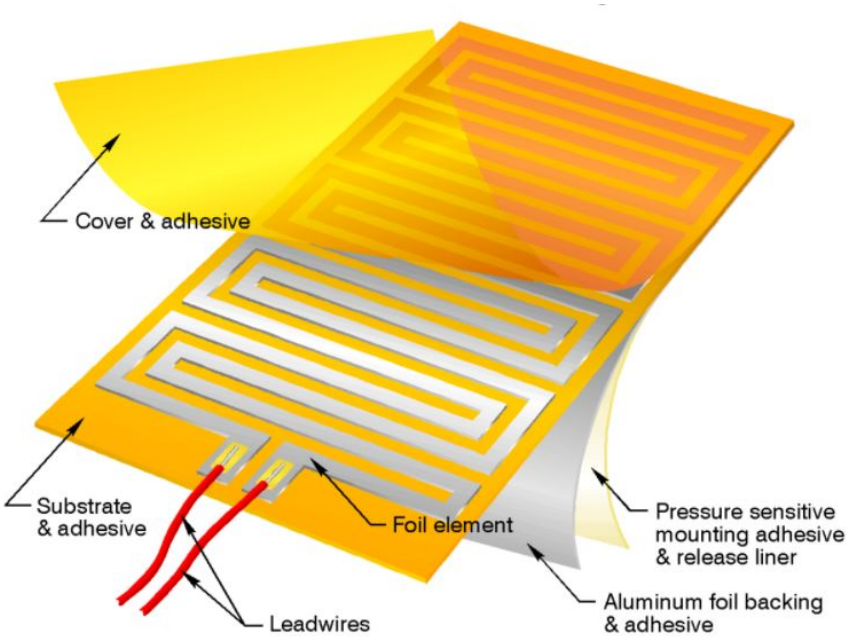

Figure 12.1: A visual representation of the patch heater manufactured by Minco[1]

These flexible patch heaters from Minco produce $5.4\ [kW/m^2]$ and are already used for different space applications. So, 10 heaters of $4x4\ [cm]$ are required to maintain the Subsystem Bus on the desired temperature of $280\ [K]$. Four heaters with the same size will be added to the design for the sake of redundancy. This results in a mass of $9.74\ [kg]$ for the heaters[2]. Next to that, these heaters will be controlled with the use of a thermal control processor. It was assumed that the mass of this thermal control processor was already included in the mass estimation for the PCDU.

[1]URL `http://bit.ly/mincoheaters` [accessed 26 January 2021]
[2]URL `http://bit.ly/mincoheaters` [accessed 26 January 2021]

12.4 Conclusion

Concluding, the thermal control system is designed to maintain the Subsystem Bus within the operational limits of the components in the bus. With the use of MLI blankets and patch heaters, the Subsystem Bus will be maintained at a desirable temperature of $280\ [K]$. All other subsystems, such as the Primary Mirror, Collimator, Secondary Mirror and the Solar Panels will maintain the equilibrium temperatures as given in Table 12.2.

Also, as mentioned in Section 12.3, the patch heaters require $300\ [W]$ of power, have a mass of $9.74\ [kg]$ and are already used in space. Lastly, it should be noted that the TCS design should be further researched for other environmental influences, such as magnetic fields or high speed particles. For this reason, the compliance with the requirements in Table 12.4 should still be determined.

12.5 Requirements

Table 12.3 gives the requirements for the thermal control system. All of these requirements have been met with this design. Table 12.4 gives the requirements for environmental control, such as protection from magnetic fields and high energy particles. At this stage of the design the effects of these were not assessed for the spacecraft, so it cannot be determined yet whether the system meets these requirements. Following the DSE, more research and analysis should be done on the environmental control to ensure the system will be operable under these conditions.

Table 12.3: Thermal Control Requirements

Identifier	Requirement	MOC	Compliance
AD-SYS-TECH-THERM-5	The thermal control system shall keep all subsystems within their operating temperatures.	Analysis	Y
AD-SYS-TECH-THERM-5.1	The thermal control system shall control the temperatures of the subsystems.	Demonstration	Y
AD-SYS-TECH-THERM-5.2	The space systems thermal control system shall use no more than 350 W throughout the entire mission.	Analysis	Y
AD-SYS-TECH-THERM-5.3	The thermal control system shall monitor the temperatures of all subsystems.	Demonstration	Y
AD-SYS-TECH-THERM-7	The thermal control system shall make use of technology that has a TRL 4 or higher.	Inspection	Y
AD-SYS-TECH-THERM-1	The space systems thermal control system shall weigh no more than 25 kg.	Demonstration	Y

Table 12.4: Environmental Requirements

Identifier	Requirement	MOC	Compliance
AD-SYS-TECH-ENV-2	The system shall be able to protect the subsystems against magnetic fields.	Analysis	TBD
AD-SYS-TECH-ENV-3	The system shall be able to protect the subsystems from high energy particles.	Analysis	TBD
AD-SYS-TECH-ENV-3.1	The system shall be able to withstand a total Radiation dose of <tbd>Gy, while it is in operation.	Analysis	TBD
AD-SYS-TECH-ENV-4	The system shall be able to function in the vacuum of space.	Test	TBD

13 Structures

Due to the novelty of the asteroid deflection system, the structural integrity of the design is a complex matter. The design must adhere to the performance requirements, which in turn defines structural requirements for the system [3]. Therefore the structures must be analyzed to ensure they meet these requirements, and are strong enough to withstand any loads on them. In Section 13.1 the analysis approach is presented. Following this, the bus design will be explored in Section 13.2 with its accommodation for the necessary subsystems. The dependency of subsystems will be identified, on a structural level, which helps to verify certain design choices throughout the detailed design procedure. In Section 13.3 the overall structures will be analyzed in the launch configuration, and in Section 13.4 they will be analyzed in the deployed configuration. Finally in Section 13.5 the requirements for the structures are listed, and it is checked whether or not the structures comply.

13.1 Analysis Method

To check that the structures meet the requirements, structural and vibrational analysis were performed on the spacecraft design. Firstly, the critical structural elements and their critical load case were identified. The structures were then idealized to make the analysis easier. Then the idealized structures were analyzed under the loads and checked to ensure they can withstand them. A rough estimate was originally done on paper, then the idealized structures were modeled in Catia and checked with finite element methods (FEM).

13.1.1 Validation of FEM Analysis

Validating the results of the FEM analysis is extremely difficult for entire structures with combined loading. However, the model was validated using much simpler cases to check that it held for these. The case of a cantilever beam with a point force on the end was analyzed both analytically and with FEM to check that the solutions matched. In this case the forward mast of the spacecraft was used, which was modeled as an $84.02\ [m]$ long cantilever beam, with cross section of an equilateral triangle with side length $1.070\ [m]$. A moment of $50\ [kNm]$ was applied around the x-axis, and $10\ [kNm]$ around the y. The results and error rate for various mesh sizes is presented in Table 13.1.

Table 13.1: Deflection in x- and y-direction for a cantilever beam from FEM compared to the expected value. Length = 84.02 $[m]$, Mass = 81 $[kg]$, Inertia = 0.0236 $[m^4]$.

Mesh Size [mm]	**dx [mm]**	**dy [mm]**	**Combined [mm]**	**% Error for combined deflection**
Expected Output	37.4	7.47	38.1	-
500	10.9	2.45	11.2	70.6
250	19.8	4.05	20.3	46.7
100	24.6	4.91	25.1	34.1
50	25.4	5.10	25.9	32.0

The % error from the FEM analysis is relatively high, even at lower mesh sizes. However, it is still in the correct order of magnitude. For the mast, which is the critical structure for the deployed case, the loads it will experience are quite small, and this error margin from the FEM analysis is still well within the amount of deflection allowed by the structure. The FEM analysis can therefore be said to be validated for this case. This will be explored more in Section 13.4. Due to time pressure, validity checks could not be done on the case of the full structure, but it is assumed that the model is valid for this case as well.

13.2 Bus Design

It was determined that the launch vehicle would assert the most critical forces on the bus structure during launch. This is due to an assessment of the load cases on the overall spacecraft during various stages of the mission. Due to the compaction of the vehicle for launch, the forces are more concentrated towards the center

of mass as opposed to the deployed structure; in free space, the force applications are consequential for larger structures of the vehicle.

To begin with, the applied launch forces are derived from the maximal accelerations derived from Figure 13.2. Based on this, and for the sake of idealization, the bus structure was designed to have a main support cylinder which could withstand the maximum acceleration of (0.5,6) [g] in the lateral and axial direction, respectively. Taking the magnitude and thus applying a safety margin, the design acceleration force applied to the structure is **6.5** [g]. Furthermore, the acceleration as a force is dependent on the overall vehicle mass (which is discussed and shown in Figure A.1). Thus, using 1167 [kg], the applied resultant force which the support cylinder will be designed for is 92964 [N].

13.2.1 Design Constraints

Certain constraints on the bus sizing must be presented, such as the subsystem sizes. For this, a spreadsheet containing all the necessary data of each subsystem was recorded and placed into Table 13.2 below. From this, design choices can be identified such as the minimum place-able length of 0.46 [m]. Furthermore, the mass summation of all subsystems & components within the bus are estimated. Knowing this, with the use of SMAD [93], an estimation can be made of the bus's structural and mechanical weight (Figure A.1). From this source, the 'Structures and Mechanisms' weight is estimated to be 20% of the overall Bus mass for a Spacecraft without a propulsion system. This assumes that the total Bus mass (excluding structures) is 80% of the design, thus the maximum Bus mass should not exceed 27.92 [kg]. This will act as a design constraint along with the aforementioned minimum place-able length.

Table 13.2: Mass and dimension data of all subsystems within spacecraft bus.

Subsystem	Number [#]	Total Mass [kg]	Total Volume [m^3]	Length [m]	Width [m]	Height [m]	Radius [m]
GNC & ADCS							
- Reaction Wheels	6	49.800	0.0670			0.118	0.174
-Star Sens EU	2	2.700	0.0035	0.171	0.156	0.065	
Power & TC							
- Heater	16	9.741	0.0000	0.039	0.039	0.000	
- Power Control Unit	1	10.450	0.0135	0.460	0.210	0.140	
- Batteries	10	10.800	0.0051			0.222	0.027
Structures							
- Bus Structure	1	27.920					
Comms & Data							
- Transponder	2	5.200	0.0069	0.151	0.151	0.151	
- Diplexer	1	2.000	0.0027	0.150	0.300	0.060	
- On-Board Computer	1	0.058	0.0000	0.005	0.091	0.091	
- Solid-State Recorder	1	15.000	0.0094	0.250	0.250	0.150	
- Data bus	1	5.000	0.0100				
Bus (Exc Structure)		110.749	0.1181	0.460	0.300	0.222	0.174
Total Bus Mass		138.669					

13.2.2 Preliminary Design

With the relevant information stated, a preliminary mock-up of the design could be made. This was evaluated in a spreadsheet first, due to the iterative nature of the design. After the figures were confirmed and deemed reasonable, the Bus could be drafted in CATIA V5, as well as the idealized form of each subsystem, for assembly. Another important design constraint, not mentioned earlier, was that the Bus could not exceed a total height of 1 [m]. Furthermore, the total diameter could not exceed 1.8 [m], this restriction depends on the free space within the Primary Reflector, indicated in Chapter 8.

The data shown in Table 13.3 identifies the necessary constraints to size the bus structure correctly. The material selection was not known exactly at the beginning of this procedure. But after the final design iteration (which will be presented shortly), these were the chosen materials for specified parts of the Bus structure. The Bus structure comprises of two parts, the Bus shell and the Bus support column, whereby the support column was designed to carry the critical loads that the bus structure experiences, both translational and rotational. The shell structure will serve as a housing unit for the subsystems and has been designed to withstand any

[1]URL `https://www.christinedemerchant.com/carbon-kevlar-glass-comparison.html`

Table 13.3: Bus design parameters and chosen material for structure[1].

Parameters			Material		
Description	**Value**	**Unit**	**Description**	**Value**	**Unit**
Open Width	0.3	m	Aluminium: Density	2710	kg/m^3
Height	1	m	Aluminium: E-modulus	70	GPa
Shell Diameter	1.2	m	Kevlar-49: Density	1440	kg/m^3
Structure Mass	27.92	kg	Kevlar-49: E-modulus	92	GPa

translational forces. It was determined that the Bus support column would weigh 70% and that the shell would weigh the remaining 30% of the structure mass, indicated in Table 13.3. Knowing that the shell is made of Aluminum and the support column of Kevlar-49, their respective volumes can be derived. These volumes can then be used to determine the shell thickness and the support column radius. For the shell thickness Equation 13.1 was used based on the values indicated in Table 13.3.

$$t = D_{out} - D_{in} = D_{out} - \sqrt{(D_{out})^2 - \frac{4 * V}{\pi * H}} \tag{13.1}$$

This resulted in a shell thickness of 1.65 mm, thus giving a thin-walled structure. As for the support column, a similar approach was used but instead was initially considered to be a solid cylinder.

$$R = \sqrt{\frac{V}{\pi * H}} \tag{13.2}$$

Equation 13.2 resulted in a minimum radius of 0.066 [m] which is rather small but this is to simply account for the volume, not the strength. Therefore, a backwards approach was used to account for the same volume but adjusted to counteract the longitudinal stress. In doing so, the support column could be idealized as a thick walled cylinder of radius 0.157 [m] with a wall thickness of 84.5 [mm]. To ensure that the design meets the loading criteria, various cross sectional areas of the design were taken and tested against the loading forces longitudinally and laterally using Equation 13.3.

$$\sigma = \frac{F}{A} \tag{13.3}$$

Using this equation, the highest stress case was determined to be 1.044 [MPa], which is well under the yield strength of the selected materials. It may be considered to be over-designed for this matter, but this will be analyzed and concluded in Section 13.3. A schematic representation of the bus structure is shown in Figure 13.1.

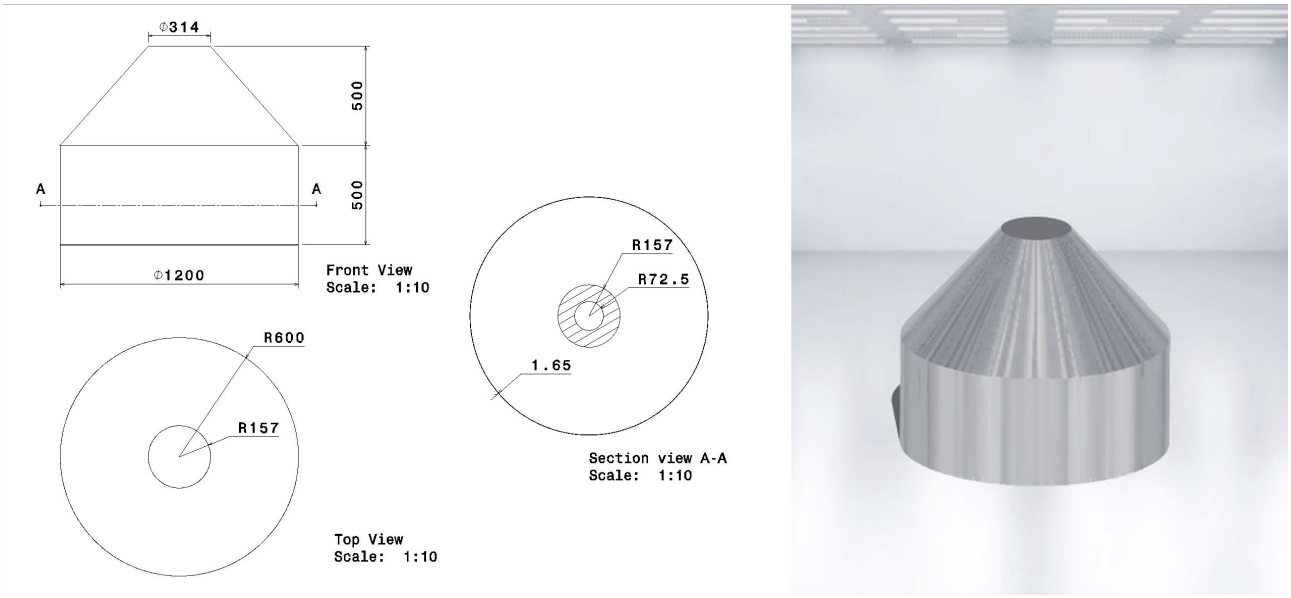

Figure 13.1: CAD drawing and visualization of Bus structure and its measurements.

13.3 Launch Configuration

To get into space, the system has to be carried by a launch vehicle (LV). The LV imparts a significant amount of force into the system so that it can lift the system off the ground. The structure will be much stiffer in the folded up launch configuration, however, it is still necessary to check that it can withstand the high loads during launch.

The LV in this case is SpaceX's Starship, and the acceleration during launch can be determined straight from the Starship user guide. This is shown in Figure 13.2. The point of maximum total acceleration is the critical load case, and here that is (0.5,6), i.e. $0.5\ [g]$ of acceleration in the lateral direction (perpendicular to main axis of the LV), and $6\ [g]$ of acceleration in the axial direction (along the main axis of the LV).

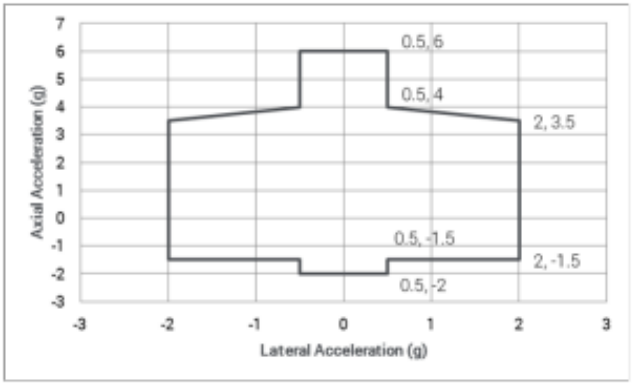

Figure 13.2: Acceleration experienced by the payload during Starship launch[2]. The critical load case is at the point (0.5,6).

The analysis was done using FEM in Catia v5 to analyze the stress on the structure. A simplified version of the launch configuration was modeled using solid cylinders or rings to approximate all the parts. The launch vehicle adapter (LVA) was not modeled and is assumed to be rigid compared to the spacecraft. For the bus itself only the support column was modeled as it is assumed to carry all of the loads. The aft truss and forward truss were assumed to be rigidly connected to the bus, and the primary reflector, collimator, and secondary reflector are in contact with their supports with no sliding, as they are assumed to be so densely packed that they cannot slide around. The model of the launch configuration is shown in Figure 13.3.

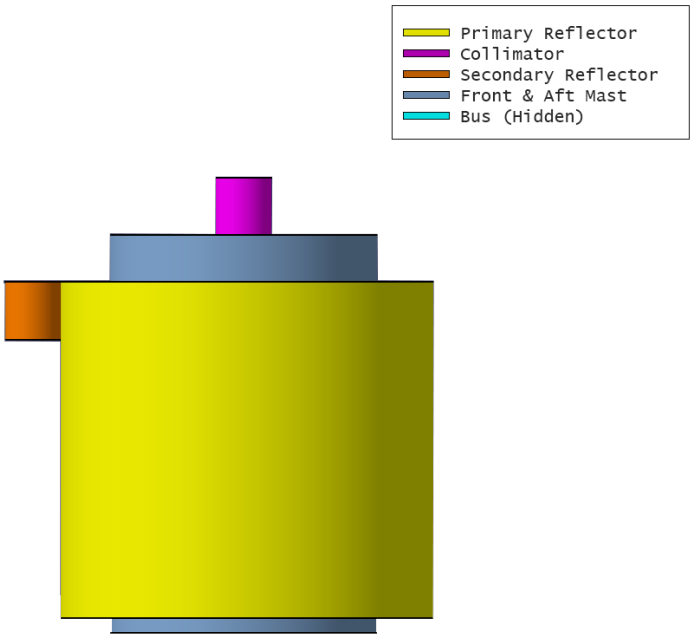

Figure 13.3: Simplified model of the launch configuration of the satellite, used for finite element analysis

The launch loads were applied to the model and the resulting stresses were computed. The results of this

[2]URL https://www.spacex.com/media/starship_users_guide_v1.pdf [accessed 4 January 2021]

analysis show that the max stress on each part should be less than the yield stress of the materials they are made of. This means that all the parts of the spacecraft should be able to withstand the loads without any permanent deformation.

Figure 13.4 shows the Von Mises stress in a cross section of the spacecraft during launch. The deformations are exaggerated for visibility. The max stress is on the forward mast, with a value of $1.24\ [GPa]$, the forward mast itself is made of carbon fiber, and has an ultimate strength of $200\ [GPa]$, so it should be able to withstand this stress. The stresses on the rest of the structure vary quite a bit, but overall all the parts are able to withstand the launch loads.

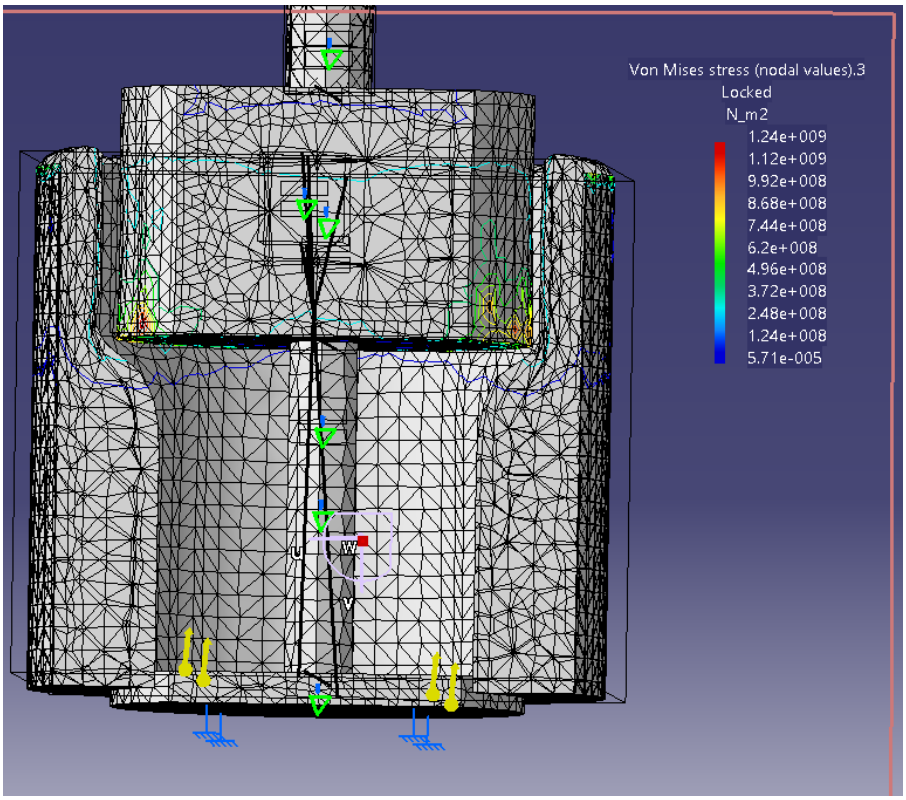

Figure 13.4: Von Mises stress in the structure in the launch configuration. The maximum stress is the red point on the left side of the image, located on the side of the forward truss.

No vibrational analysis was done of the launch configuration due to time constraints. Although the LV does induce a lot of vibrations in the spacecraft, and the loads are quite high, the structure is so much more stiff in the launch configuration than the deployed configuration that it was determined that the deployed case is more critical. Therefore, more time was spent on analyzing the deployed configuration instead, which is explored in Section 13.4. The launch configuration and the LVA design will be explored more in depth after the DSE.

13.4 Deployed Configuration

The front mast and the primary reflector were deemed as the crucial structural components. A hindrance to either component directly influences the ability of the system to perform. This was an initial assumption which has been proven through analysis of the entire system in both the launch and deployed configuration. In order to perform the structural analysis the satellite was idealized, which could then be simulated in a FEM analysis and then verified by both hand and program script. Finally, validation is done to ensure that the structural requirements are met, as stated in Section 13.5, without having a direct influence on the performance parameters.

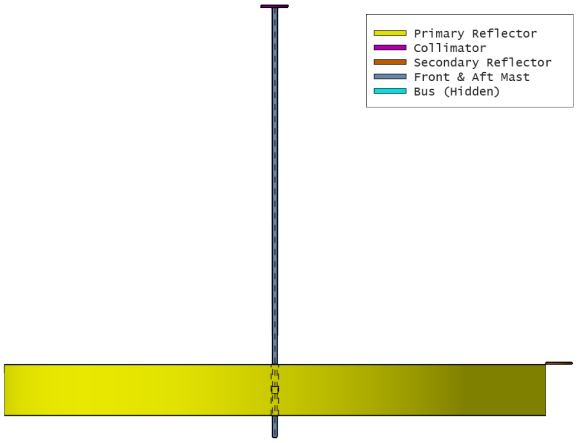

Figure 13.5: Side view of deployed structure in idealized form.

Figure 13.5 shows the idealized structure which is to be tested in the FEM model. The method for this is largely similar to the steps taken in Section 13.3. The loading cases to be assessed are derived from combined loads on the deployed structure which form both translation and rotation motion. However, these combined loads are deductible into the format of moments, which are in the critical case of using the RCS thrusters (discussed in Subsection 9.3.3). The highest possible range of thruster application has been modeled and the resulting moments about the center of mass have been put into Table 13.4. As previously mentioned, the critical structures, due to their length and size, are the front mast and the primary reflector. Therefore, the analysis will only occur for each of these components, individually and then together as a whole assembly.

Table 13.4: Critical load case for deployed structure as a consequence of firing differential RCS Thrusters simultaneously.

Moments			**Coordinates**		
Description	**Value**	**Unit**	**Description**	**Value**	**Unit**
M_x	260	Nm	x	0.408	m
M_y	89.2	Nm	y	0	m
M_z	175	Nm	z	7.96	m

13.4.1 Structural Analysis

Making use of the FEM tool in CATIA V5, the front mast was idealized as an equilateral triangle with side lengths of $1.07\ [m]$ and a beam length of $84.02\ [m]$. Furthermore, the front mast is made of carbon fiber (as stated in Section 8.4) with an E-modulus of $2 \cdot 10^{11}\ [Pa]$. Using the moments from Table 13.4, with the mast simply clamped at one end, the combined moments can be applied. The outcome of this is shown in Figure 13.6a & Figure 13.6b, with a the largest deflection at the tip of the beam being $0.144\ [mm]$. The verification of this result has already been discussed in Subsection 13.1.1, whereby it was deemed accurate enough, given the resources and time available.

As for the stress concentrations, they are depicted in Figure 13.7 where a peak stress of $1.11 \cdot 10^4 [N/m^2]$ is recorded at the points closest to the clamp. The results of the FEM analysis for the front mast are well below the critical points of failure in terms of material property or mission performance. Due to the margin of difference, no additional structural measures need to be taken to stiffen the front mast.

Due to the lack of time, it was not possible to yet show the structural analysis results for the Primary Reflector, as this depends on an additional support structure (presented in Figure 13.5). This still has to be implemented into the CAD Assembly for the FEM analysis.

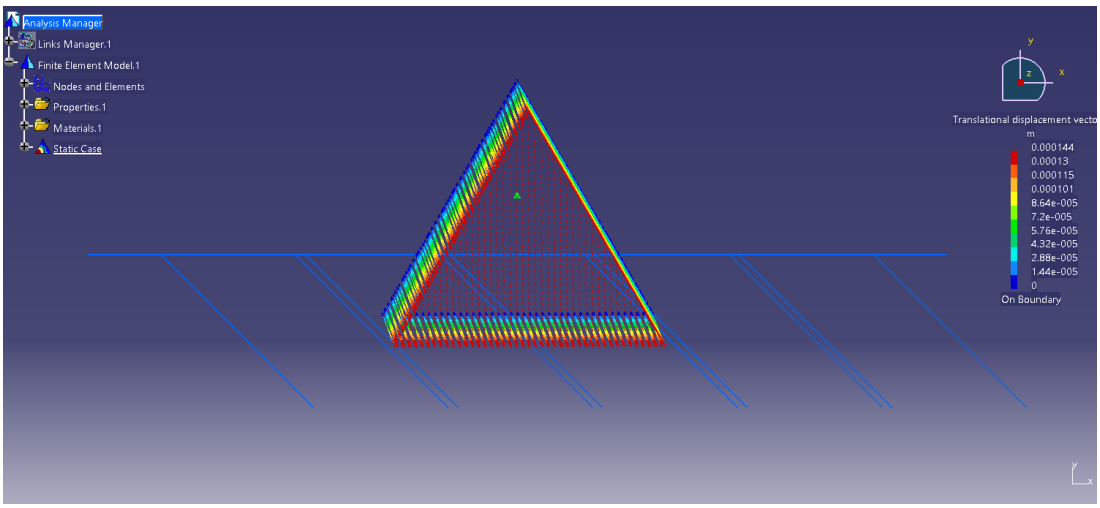

(a)

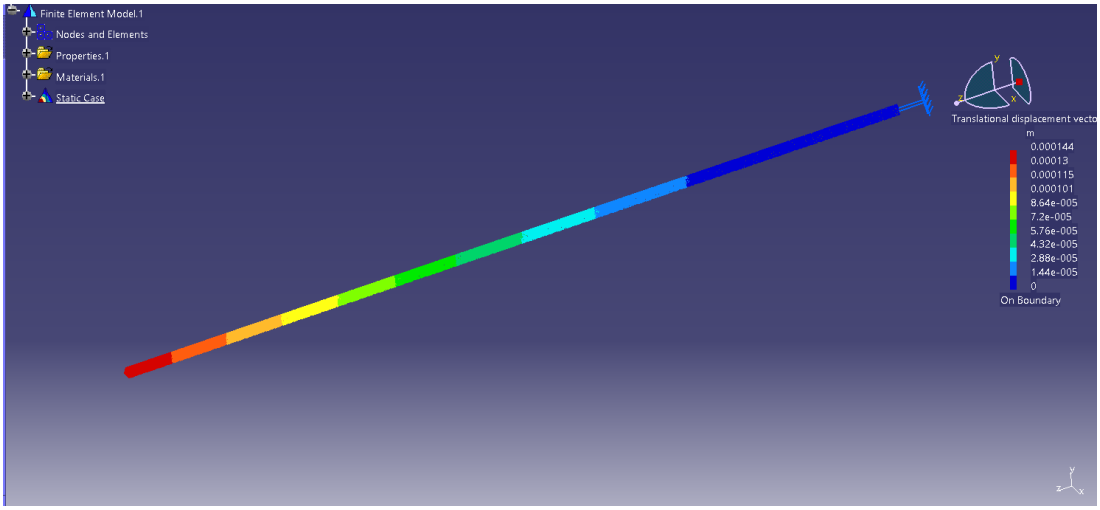

(b)

Figure 13.6: (a) Cross-sectional view of the deflection. (b) Longitudinal view of the deflection, under the applied moment. The values on the right side of both figures shows a total deflection of 0.144 [mm].

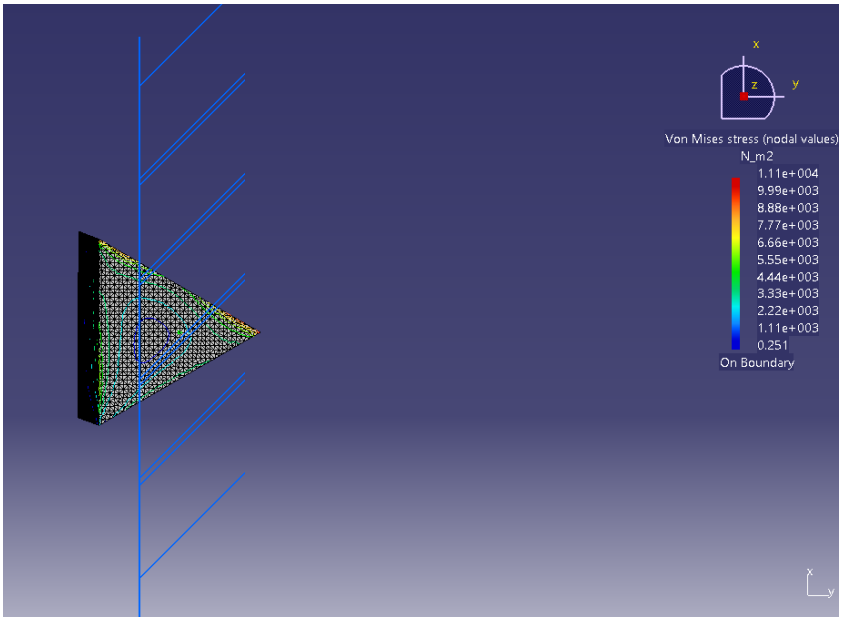

Figure 13.7: The highest point of Von Mises stress is located at the point of clamping for this idealized beam. The results on the right of the image show a peak stress of $1.11 * 10^4$ [N/m^2].

13.4.2 Vibrational Analysis

Due to the level of complexity a vibration model must be able to achieve logical results. The analysis was mostly performed using program calculations. CATIA V5 was used initially for the frequency analysis on the same front mast as analyzed in Subsection 13.4.1. The results shown in Figure 13.8 estimate the fundamental frequency to be approximately $40\ [Hz]$ at mode three. This is because it is the mode which closest resembles a periodic waveform. This result is based on the entered material properties and design of the part in CATIA, which is not a conventional vibrational analysis tool, therefore it must be analyzed and verified by other means.

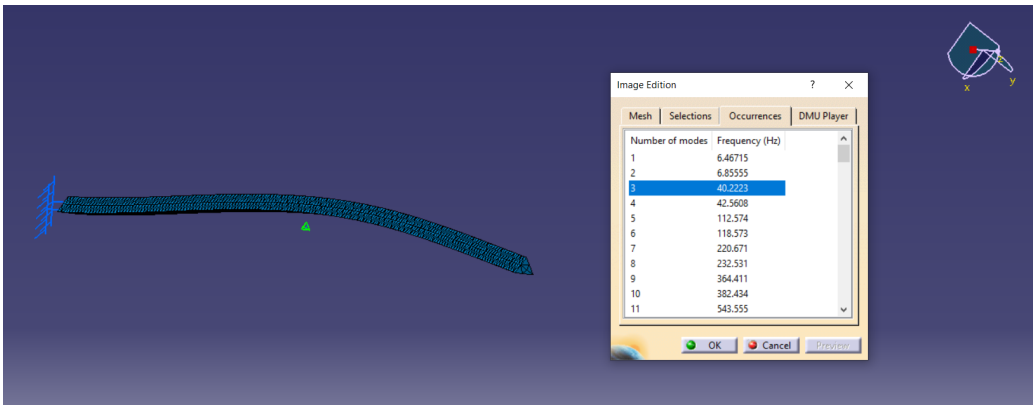

Figure 13.8: Front mast frequency simulation of 100 modes, with a stated fundamental frequency of 40 $[Hz]$.

To verify the frequency by hand the beam and collimator were further idealized to a cantilever beam with end mass, see Figure 13.9. From this the beam stiffness and natural frequency can be calculated.

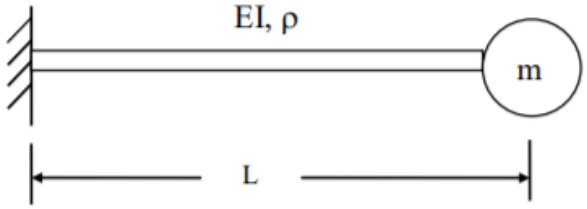

Figure 13.9: Idealization of front mast as point mass beam structure.

The beam stiffness formula is shown in Equation 13.4, where the E-modulus E and length L were stated at the beginning of Subsection 13.4.1. The area moment of inertia I is based on the equilateral triangular cross-section, with a value of $0.023617\ [m^4]$.

$$k = \frac{3 \cdot EI}{L^3} \tag{13.4}$$

The beam stiffness was calculated to be $23891.16[N/m]$. Furthermore, the effective mass m_e was calculated with Equation 13.5[3]. Where, ρ is equal to the beam mass per unit length and m defines the collimator mass.

$$m_e = 0.2235 \cdot \rho \cdot L + m \tag{13.5}$$

The effective point mass is found to be $37.44\ [kg]$. The fundamental frequency f_n can now be calculated with Equation 13.6, with all the parameters identified. This yields a frequency value of $4.02\ [Hz]$, which is the fundamental frequency of the front mast.

[3]URL `https://www.vibrationdata.com/tutorials2/beam.pdf`

$$f_n = \frac{1}{2\pi}\sqrt{\frac{k}{m_e}} \tag{13.6}$$

The question now is why this value differs by a multiple of 10 from what was shown in the CATIA results. This could possibly be related to the difference in idealization, as CATIA uses a very refined mesh, whereas the hand calculations account only for a simplified structure. This is something unfortunately there was not enough time to identify with the time constraints, but would certainly be analyzed in further detail beyond the DSE, for a proof of concept analysis. For the sake of the report, though, a clear discussion is made on the viability of the front mast design in terms of vibrational analysis, using the hand calculated data.

For the verification of the vibrational integrity, literature was studied to find a range of frequencies that the spacecraft may experience, during launch and operation. It was rather difficult to find exact frequency values for an orbiting spacecraft, let alone one chasing an asteroid. Therefore, the ranges were more easily found for launch vehicles, with values between $20 - 150[Hz]$ under the domain of 'random vibrations' [94]. Though the structure is collapsed in the launch phase, these values are used as an estimate due to their random nature to verify the deployed structure's integrity. As the value stated from Equation 13.6 falls below this range, the possibility of resonance is less likely. Furthermore, in the unlikely case of disturbance frequencies occurring at this value, a damping factor has been calculated for this structure, assuming critical damping.

$$c = 2 \cdot \sqrt{k \cdot m_t} \tag{13.7}$$

Equation 13.7 results in a damping value of $1891.47\ [Ns/m]$. This is regarded as a high value, but given the structural stiffness it is comparable. For this, a self-tuning compact vibrational damper, developed by NASA[4], would be used at the attachment point of the front mast.

Similar to Subsection 13.4.1, the results for the Primary Reflector vibrational analysis have not been included. Due to a lack of time, the deployable support structure has to still be implemented into the CAD Assembly.

13.5 Requirements

In the Midterm Report ([4]), the system requirements were defined in correspondence with the client and relevant stakeholders. An overview of these requirements, specifically the structural requirements, can be found in Table 13.5. This updated table now contains specific design values which have to be met, along with the method of compliance (MOC), and whether or not these requirements were in-fact met.

[4]URL `https://technology.nasa.gov/patent/LAR-TOPS-290`

Table 13.5: Structural Requirements

Identifier	Requirement	MOC	Compliance
AD-SYS-TECH-STRUC-8	The space structural system shall support the space subsystems.	Analysis	Y
AD-SYS-TECH-STRUC-8.1	The space system structure shall weigh no more than 3125 $[kg]$.	Analysis	Y
AD-SYS-TECH-STRUC-8.1.1	The primary mission payload shall weigh no more than 1300 $[kg]$.	Analysis	Y
AD-SYS-TECH-STRUC-9	The space structural system shall fit into the chosen launcher.	Analysis	Y
AD-SYS-TECH-STRUC-10	The structural system shall protect the other spacecraft subsystems.	Analysis	Y
AD-SYS-TECH-STRUC-10.1	The space structural system shall be able to withstand impacts of debris up to <TBD>$[kNs]$ impulse.	Test	TBD
AD-SYS-TECH-STRUC-10.2	The space structural system shall be able to tolerate temperature differences of at least 277.3 $[K]$.	Test	TBD
AD-SYS-TECH-STRUC-10.3	The spacecraft structural system shall be able to tolerate lateral vibrational frequencies of no less than 2 $[Hz]$ within the resonance frequency of the structure.	Analysis	Y
AD-SYS-TECH-STRUC-10.4	The structural system shall have a resonant frequency of no less than 4 $[Hz]$.	Analysis	Y
AD-SYS-TECH-STRUC-10.5	The spacecraft structural system shall be able to tolerate loads of no less than 4 [N].	Analysis	Y

Based on the findings in Chapter 13, it was possible to achieve a majority of the structural requirements outlines in Table 13.5. The specific values achieved can be found within the chapter, under their relevant sections. As for two which were not met: **AD-SYS-TECH-STRUC-10.1** and **AD-SYS-TECH-STRUC-10.2**, this was due to the MOC. The approach to proving compliance for these two requirements depends on a physical test. It is difficult to simulate such an environment due to the complexity of the design, therefore it cannot be easily determined the effect failure will have on the overall system performance. Thus, these design requirements are subject to further discussion and testing beyond the DSE.

14 Risk Engineering

14.1 Risk Management

Risks were identified and assessed following the guidelines laid out in the previous reports. Furthermore, the risk management presented in this chapter builds upon the previous work in these reports. [3, 4]

14.1.1 Risk Identification & Assessment

The technical risks were identified and assessed following the procedures laid out in the Baseline Report [3]. Table 14.2 shows all risks. Design and operational risks are examined using Probabilistic Risk Assessment (PRA), whereas all other risks were assessed quantitatively. The most important failure states are Loss of Vehicle (LOV) and Loss Of Mission (LOM).

Quantitative Risk Assessment

For many of the technical risks of this project Quantitative Risk Assessment is sufficiently accurate. Those risks have values filled in for the ”Probability” column in Table 14.2. Table 14.1 shows the definition of the probability and impact scale.

Table 14.1: Categories for Probability and Impact

Probability Categories	
>50%	5
>10%	4
>1%	3
>0.1%	2
>0.01%	1

Impact Categories	
LOM	5
LOV	4
Critical subsytem failure	3
Non-Critical Subsystem Failure	2
Negligible Influence	1

Table 14.2: Risk identification and assessment. In the ”Probability” column PRA indicates that the probability will be assessed in Section 14.1.1.

Risk ID	Description	Event	Impact	Prob. (1-5)	Impact (1-5)
AD-RISK-DV-01	Design Error	During the design process technical errors are made.	A component or system does not behave as expected.	4	5
AD-RISK-DV-02	Wrong Design Choice	During the design process a non-optimal design choice is taken.	The product quality will be be lower.	3	3
AD-RISK-DV-03	Design Impossible	It is impossible to design the product.	No design can be produced, thus no product can be produced.	2	5
AD-RISK-DV-04	Requirements Not Met	Requirements are not met.	The product does not fulfill its intended function and might not be accepted by the client.	2	5
AD-RISK-DV-05	Design Stuck	The design process becomes stuck.	The development is delayed or halted.	2	4
AD-RISK-DV-06	Better Rival	A competitor designs or produces a better system.	The product is inferior and thus might not be used.	2	4

Table 14.2 – *Continued on next page*

Table 14.2 – *Continued from previous page*

Risk ID	Description	Event	Impact	Prob. (1-5)	Impact (1-5)
AD-RISK-DV-07	Over Budget	Engineering budgets are not met	The product cannot be produced or operated.	3	5
AD-RISK-PRO-01	Assembly Impossible	It is impossible to assemble the system.	Product cannot be produced. Might require redesign.	3	5
AD-RISK-PRO-02	Production Error	During the production an error is made.	The system is not produced correctly. This might lead to failure, require new procedures or a redesign.	4	4
AD-RISK-PRO-03	Low Quality	The quality of the components or systems is too low.	The components or systems do not perform as expected.	3	4
AD-RISK-LOG-01	Material Shortage	Required materials are not available.	The production will be delayed or stopped. A severe shortage might require a design change.	2	4
AD-RISK-LOG-02	Supplier Delivery	A supplier does not deliver components or systems.	Required components are not available from that supplier. A new supplier might need to be identified. A design change mit be required.	2	4
AD-RISK-LOG-03	Supplier Delay	A supplier does not deliver components or systems in time.	The production will be delayed.	4	3
AD-RISK-LOG-04	LV Delay	The selected launch vehicle is delayed.	The begin of operation will be delayed. A new launch vehicle might need to be selected.	2	3
AD-RISK-LOG-05	LV Not Available	The selected launch vehicle is not available.	The begin of operation will be delayed. A new launch vehicle will need to be selected. A redesign might be necessary.	1	4
AD-RISK-LOG-06	Launch Delay	The launch is delayed.	A launch window might be missed. The begin of operation will be delayed.	3	3
AD-RISK-LOG-07	Complete Launch Failure	The launch vehicle fails and destroys the system.	The begin of operation will be delayed. The system will need to be produced again.	PRA	5
AD-RISK-LOG-08	Launch Failure	The launch vehicle fails and the system is not destroyed.	The begin of operation will be delayed. The system might be damaged.	PRA	4
AD-RISK-ENV-01	Natural Crisis	A natural disaster occurs that impacts the project.	The design, production or operation is interrupted, pause or stopped.	1	4
AD-RISK-ENV-02	Space Weather	A Space Weather event occurs.	The system fails or behaves unexpectedly.	3	5
AD-RISK-FIN-01	Economic Crisis	A economic crisis happens that impacts the project.	The design, production or operation might be delayed or stopped.	2	5

Table 14.2 – *Continued on next page*

Table 14.2 – *Continued from previous page*

Risk ID	Description	Event	Impact	Prob. (1-5)	Impact (1-5)
AD-RISK-FIN-02	Excessive Cost	The cost for the product design, production or operation is too large.	The project might be stopped or a redesign is needed.	3	4
AD-RISK-SOC-01	No Public Interest	There is no interest in developing the system.		2	5
AD-RISK-SOC-02	Not Accepted	The product is not acceptable to states or large organizations.	The system cannot be produced or operated. A redesign might be needed.	3	4
AD-RISK-SOC-03	Market Change	There is no longer a need for the product.	The project might be stopped.	2	5
AD-RISK-OP-08	Rendezvous Failure	The LV fails to rendezvous with the asteroid.	The mission fails as the spacecraft do not reach the asteroid.	PRA	5
AD-RISK-OP-09	Fatal FOD	The LV is fatally impacted by Foreign Object Debris	The mission fails as the spacecraft do not reach the asteroid.	PRA	5
AD-RISK-OP-10	Ground Segment Failure	The ground segments experiences some kind of failure.	The supervision of the spacecraft is temporarily interrupted.	2	4
AD-RISK-EPS-01	Solar String Failure	A number of solar strings fail.	Power collection is disrupted or fails completely.	PRA	4
AD-RISK-EPS-03	Power Storage Failure	The PSU fails.	Not enough power can be stored for power need spikes.	PRA	4
AD-RISK-CD-01	PCDU Failure	The PCDU fails.	Power needs cannot be assessed and power cannot be distributed.	PRA	4
AD-RISK-CD-02	Computer failure	The main computing unit fails.	The spacecraft can no longer be controlled.	PRA	4
AD-RISK-CD-03	Entire databus failure	The data bus fails.	The spacecraft behavior can no longer be monitored nor controlled.	PRA	4
AD-RISK-CD-04	All antenna fail	All antenna fail.	The spacecraft can no longer be communicated with.	PRA	4
AD-RISK-CD-08	HG antenna failure	The high gain antenna fails.	The spacecraft can no longer be communicated with when near the asteroid	PRA	4
AD-RISK-CD-09	LG antenna failure	The low gain antenna fail.	The spacecraft can no longer be communicated with by other spacecraft.	PRA	4
AD-RISK-CD-05	All transponder failures	All transponder fail.	The spacecraft can no longer be communicated with.	PRA	4
AD-RISK-CD-06	RF Unit failure	All RF Units fail.	The spacecraft can no longer be communicated with.	PRA	4
AD-RISK-CD-07	SSR failure	The SSR fail.	Power can no longer be distributed.	PRA	4

Table 14.2 – *Continued on next page*

Table 14.2 – *Continued from previous page*

Risk ID	Description	Event	Impact	Prob. (1-5)	Impact (1-5)
AD-RISK-TC-01	Heater failure	Heating elements fail.	The operational temperature of components can no longer be ensured.	PRA	4
AD-RISK-TC-02	Thermal Control unit failure	The thermal control unit fails.	The temperature of the spacecraft can no longer be controlled.	PRA	4
AD-RISK-ADCS-01	2 RW failures	2 RW fail on the same axis.	The spacecraft can no longer be accurately pointed.	PRA	4
AD-RISK-ADCS-34	RW precision loss	The reaction wheels lose precision.	The space craft can no longer point with high accuracy.	2	3
AD-RISK-ADCS-02	Electrical Units fail	Electrical units fail.	No power can be distributed to the ADCS components.	PRA	4
AD-RISK-ADCS-03	Sun sensors fail	Sun sensors fail.	The spacecraft can no longer determine its rough attitude.	PRA	4
AD-RISK-ADCS-04	Star sensors fail	Star sensors fail.	The spacecraft can no longer determine its precise attitude.	PRA	4
AD-RISK-ADCS-05 – AD-RISK-ADCS-010	Thruster Block Failure (1-5)	Thruster blocks fail.	The spacecraft can no longer perform rough attitude adjustments, translate or momentum dump.	PRA	4
AD-RISK-ADCS-10 – AD-RISK-ADCS-015	Thruster Block Failure (6-10)	Thruster blocks fail.	The spacecraft can no longer perform rough attitude adjustments, translate or momentum dump.	PRA	4
AD-RISK-ADCS-16 – AD-RISK-ADCS-21	Valve Failure (1-6)	Fluid distribution valves fail.	Fluid flow can no longer be controlled.	PRA	4
AD-RISK-ADCS-22	N2 Tank Failure	N2 tank fails.	No N2 is available. Momentum is transferred to the spacecraft.	PRA	4
AD-RISK-ADCS-23, AD-RISK-ADCS-24	RCS Pressure Sensor Failure 1,2	The pressure sensor in the RCS tank fails.	The pressure in the N2 tanks can no longer be monitored nor controlled.	PRA	4
AD-RISK-ADCS-25, AD-RISK-ADCS-25	RCS Level Sensor Failure 1,2	The level sensor in the RCS tank fails.	The level in the N2 tanks can no longer be monitored.	PRA	4
AD-RISK-ADCS-26, AD-RISK-ADCS-27	RCS Tank Failure 1,2	The RCS tanks fail.	No fluid is available for the RCS. Momentum is transferred to the spacecraft.	PRA	4
AD-RISK-ADCS-28, AD-RISK-ADCS-29	N2 Pressure Sensor Failure 1,2	The pressure sensor in the N2 tank fails.	The pressure in the RCS tanks can no longer be monitored nor controlled.	PRA	4
AD-RISK-ADCS-30, AD-RISK-ADCS-31	N2 Level Sensor Failure 1,2	The level sensor in the N2 tank fails.	The level in the RCS tanks can no longer be monitored.	PRA	4
AD-RISK-ADCS-32, AD-RISK-ADCS-33	N2 Tank Failure 1,2	The N2 tank fails.	No N2 is available. Momentum is transferred to the spacecraft.	PRA	4
AD-RISK-MI-01	Primary Reflector Rupture	The primary reflector ruptures.	Sunlight can no longer be collected	PRA	4

Table 14.2 – *Continued on next page*

Table 14.2 – *Continued from previous page*

Risk ID	Description	Event	Impact	Prob. (1-5)	Impact (1-5)
AD-RISK-MI-02	Secondary Reflector Rupture	The secondary reflector ruptures.	Sunlight can no longer be projected at the asteroid.	PRA	4
AD-RISK-MI-03	Collimator Rupture	The collimator ruptures.	The sunlight can no longer be collimated.	PRA	4
AD-RISK-MI-04	Primary Reflector Truss Deployment Mechanisms Failure	The mechanisms for deploying the primary reflector truss fail.	The primary reflector does not deploy.	PRA	4
AD-RISK-MI-05	Secondary Reflector Truss Deployment Mechanisms Failure	The mechanisms for deploying the collimator truss fail.	The secondary reflector does not deploy.	PRA	4
AD-RISK-MI-06	Collimator Truss Deployment Mechanisms Failure	The mechanisms for deploying the secondary reflector truss fail.	The collimator does not deploy.	PRA	4
AD-RISK-MI-07	Front Mast Failure	The front mast fails or fails to deploy.	The collimator does not deploy.	PRA	4
AD-RISK-MI-08	Collimator Holder Failure	The collimator fails or fails to deploy.	The collimator does not deploy.	PRA	4
AD-RISK-MI-09	Aft Mast Failure	The aft mast fails or fails to deploy.	The primary reflector can not hold its shape.	PRA	4
AD-RISK-MI-10	Secondary Reflector Gimbal Failure	The gimbal of the secondary reflector fails.	The secondary mirror can only be aimed by repositioning the entire spacecraft.	PRA	4
AD-RISK-MI-11	Primary Reflector Harness Failure	The harness of the primary reflector fails or fails to deploy.	The primary reflector can not hold its shape.	PRA	4
AD-RISK-MI-12	Secondary Reflector Harness Failure	The harness of the secondary reflector fails or fails to deploy.	The secondary reflector can not hold its shape.	PRA	4
AD-RISK-MI-13	Collimator Harness Failure	The harness of the collimator fails or fails to deploy.	The collimator can not hold its shape.	PRA	4
AD-RISK-MI-14	Optical Train Misalignment	The optical train is misaligned.	The light is not projected accurately at the asteroid	PRA	4
AD-RISK-MI-15	Electrical Junction Box Failure	The electrical junction box of the active cleaning mechanism fails.	The secondary reflector can no longer be actively cleaned.	PRA	4
AD-RISK-MI-16	Connection Wires failure	The connection wires of the active cleaning mechanism fails.	The secondary reflector can no longer be actively cleaned.	PRA	4
AD-RISK-ST-01	Structural Failure	Some other part of the spacecraft structure fails.	The spacecraft can no longer support the reflectors or hold its pointing.	PRA	4

Some of the risks already have mitigation strategies in place and will not be discussed again (see the Baseline and Mid-Term report [3, 4]). Mitigation for new risks that are not assessed using PRA and risks which have changed in some way are presented in Table 14.3.

Table 14.3: Risk mitigation for new or updated risks not assessed by PRA. See the Baseline and Mid-Term report for other mitigation strategies [3, 4].

Risk ID Requirement ID	**Descriptor**	**Probability Mitigation**	**Impact Mitigation**	**New Prob. (1-5)**	**New Impact (1-5)**
AD-RISK-ADCS-34 REQUIREMENT	RW precision loss	Redundant reaction wheels.	Implement a gimbal for the secondary reflector.	1 (-1)	2 (-1)
AD-RISK-OP-10 REQUIREMENT	Ground Segment Failure	Redundant ground segment systems.	The space craft have to be able to communicate and coordinate locally.	1 (-1)	2 (-2)

Probabilistic Risk Assessment

Following AD-RISK-DV-8 based on the requirements of ESA and NASA for planetary defense missions a PRA was performed for technical risks relating to design and operation of the system that lead to LOV or LOM.

For this sub-system specific failure modes were identified, either at subsystem or component level, by the responsible engineers. System level failure modes were identified by the risk engineer.

For each failure mode literature was consulted for its probability rate. If other metrics for the failure mode or related failure modes were given those were used and converted to probability rates. If neither was possible a Rough Order-of-Magnitude (ROM) estimation was performed by the engineer as explained in the Mid-Term [4]. In cases where no probability rates but rather probability or Mean Time To Failure (MTTF) data was given it was converted to a probability rate under the following assumptions. These assumptions were applied for the entire risk assessment:

1. The probability of failure or reliability was measured at the End Of Life (EOL) of a component or system. The EOL was either taken as the given lifetime of a component or system or was estimated from similar components or systems. This is a reasonable assumption for reported failure probabilities [48].
2. The failure rate of each component or system is constant. The failure rate of real components or systems follows often a ”bath-tub” curve or more exotic curves that are component specific. However, without this assumption the resources required for a PRA would exceed the available ones [38].

Using this data the failure rate of a component or system is calculated using Equation 14.1 and Equation 14.2 [38]:

$$\lambda = \frac{ln\,(R)}{-t} = \frac{ln\,(1-F)}{-t} \tag{14.1}$$

$$\lambda = 1/MTTF \tag{14.2}$$

Where λ is the constant failure rate, R is the reliability, F is the failure probability and t is the time at which the probabilities were measured.

Failures in spacecraft occur when vital components or systems fail. However, some component or system failure only lead to LOV if other components also fail. This can either be because the system is redundant or because the system is not vital itself. PRA identifies failure paths, e.g. an event chain of failures that lead to some failure state. The failure states of interest in this analysis in this case are LOV and LOM. Since each vehicle can operate independently of the others LOM only occurs when the number of spacecraft drops below the number required for sublimating the asteroid, assuming the spacecraft deployed successfully around the asteroid. However, the LOV event can occur in a number of ways or after a number of failure event chains. Generally speaking the analysis of these event chains can be restricted to each subsystem independently if the outcome of each event chain is chosen conservatively and it is assumed that the failure of a subsystem leads to LOV. [48] The failure paths leading to LOV were identified for each subsystem by the responsible engineer. The risk engineer identified the failure paths leading to LOM.

When components or sub-systems can have active (m out of n must be working) redundancy, the failure rate of the total system is [55]:

$$R(t) = \sum_{n}^{k=m} \frac{n!}{k!(n-k)!} p^k (1-p)^{n-k} \quad where \quad p = e^{-\lambda t} \tag{14.3}$$

Here n, the total number of components or systems, is a design variable and m is the minimum number of working systems to not lead to LOV. Both are supplied by the responsible engineer. When high failure probabilities for a system were identified during the design by the risk management this was communicated to the engineer. Possible solutions are either increasing n or choosing components or systems with higher reliability.

The probability of a certain failure path occurring is the product of the individual probabilities of the events in the path, assuming they are independent. This assumption is generally valid for high level analysis [48], and thus:

$$P_{LOV_{failure\ path}} = \prod \left(1 - R_{subsystem}(t)\right) \tag{14.4}$$

where $R_{subsystem}(t)$ is the reliability of a subsystem or component from Equation 14.3.

The probability of LOV is the sum of all event chains leading to LOV:

$$P_{LOV} = \sum P_{LOV_{failure\ path}} \tag{14.5}$$

Since each spacecraft is part of a system with active redundancy the probability for LOM due to space craft failure can be calculated using Equation 14.3. A conservative estimation of the minimum number of operating spacecraft for sublimation is 20.

The probability for LOM is the sum of all event leading to LOM:

$$P_{LOM} = \sum P_{LOM_{event}} \tag{14.6}$$

In order to assess the certainty and sensitivity of the result a sensitivity analysis was conducted. For each component or system failure rate the uncertainty of it was also taken from the relevant literature, or ROM estimated. It was assumed that the failure rate was normally distributed around its mean. Hence the normally distributed failure rate λ could be sampled using a large number of random parameters.

This sampling and subsequent computation of Equation 14.3 to Equation 14.5 was implemented in python using the standard libraries `numpy.random` for random number generation and `scipy.stats` for the probability mass function (Equation 14.3) and data evaluation. Since the process was multi-threaded using `multiprocessing`, care was taken to sample from independent random number generation streams for each thread using the `numpy.random.SeedSequence()` class as recommended by the `numpy` API reference[1]. Multi-threading the process allowed 20,000 samples of the overall LOV probability to be taken with independently varying component or system failure rates.

In total 71 components or subsystems were identified whose failure could lead to LOV. Table 14.4 shows the inputs for the component or system data. 73 failure paths of varying lengths were identified that lead to LOV. The risks associated with each failure paths can be seen in Table 14.2. Not all failure paths can be adequately shown in the report as they span a 71x73 sparse block matrix or 9 non-sparse system level matrices with sizes up to 36x40 for the ADCS.

Table 14.4: Components or systems, redundancy, failure rates and uncertainties for the PRA. Sources are accessed as [XX] for direct citations, ([XX]) for extrapolations or references and an empty cell indicates ROM estimation.

System / Component Name	n	m	Failure Rate $[1/yr]$	Relative uncertainty	Confidence interval width [xσ]	Source
EPS						
Solar Cell String	250	167	8.02E-04	1.30E-01	2	[19]
Battery	15	10	1.00E-03	2.45E-01	2	[19]
Power Control	1	1	4.00E-04	1.13E-01	2	[19]

Table 14.4 – *Continued on next page*

[1] Parallel Random Number Generation: `https://numpy.org/devdocs/reference/random/parallel.html` [accessed 18 January 2021]

Table 14.4 – *Continued from previous page*

System / Component Name	n	m	Failure Rate [$1/yr$]	Relative uncertainty	Confidence interval width [xσ]	Source
Comms & Data						
LEON3-FT SPARC V8 Processor	1	1	3.40E-04	2.00E-01	2	[19]
Watchdog Timer	1	1	3.40E-04	2.00E-01	2	[19]
Airbus Basic SSR	1	1	1.44E-03	3.37E-01	3	[25]
SpaceWire Databus	1	1	1.00E-03	5.03E-02	1	[98]
Low-Gain Patch Antenna	2	1	2.01E-03	1.01E-01	2	[19]
High-Gain Antenna	1	1	2.01E-03	1.01E-01	2	[19]
Transponder	2	1	3.40E-04	2.00E-01	2	[19]
Diplexer	1	1	2.01E-03	1.01E-01	2	[19]
RF Distribution Unit	2	1	2.01E-03	1.01E-01	2	[19]
Thermal Control						
Heater	16	12	1.00E-03	4.02E-02	2	[19]
Thermal Control Unit	1	1	4.00E-04	2.50E-02	2	[19]
ADCS						
Reaction wheel 1	3	2	6.67E-03	1.67E-01	1	[26]
Reaction wheel 2	3	2	6.67E-03	1.67E-01	1	[26]
Sun sensor	4	1	6.01E-04	1.60E-01	1	[31]
Star sensor	8	1	2.11E-03	1.21E-01	1	([84])
Electrical Unit	2	1	7.59E-03	2.76E-01	1	[84]
Xenon Thruster	1	1	3.36E-03	2.00E-01	1	[78]
Xenon Tank	1	1	6.00E-06	2.00E-01	1	[29]
Xenon Valve	1	1	1.00E-05	2.00E-01	1	[29]
Xenon Tank Pressure Sensor	1	1	1.00E-04	2.00E-01	1	[29]
Xenon Level Sensor	1	1	1.00E-04	2.00E-01	1	[29]
Thruster Set 1, 4	8	2	1.00E-03	2.00E-01	2	[19]
Thruster Set 2, 3, 5, 6	4	2	1.00E-03	2.00E-01	2	[19]
Thrust Valve Set 1, 4	8	2	1.00E-05	2.00E-01	1	[29]
Thrust Valve Set 2, 3, 5, 6	4	2	1.00E-05	2.00E-01	1	[29]
N2 Tank Set 1, 2	2	1	3.00E-05	2.00E-01	1	[29]
RCS Valve Set 1, 2	2	1	1.00E-05	2.00E-01	1	[29]
RCS Tank Pressure Sensor Set 1, 2	2	1	1.00E-04	2.00E-01	1	[29]
RCS Tank Level Sensor Set 1, 2	2	1	1.00E-04	2.00E-01	1	[29]
RCS Tank Set 1, 2	2	1	6.00E-06	2.00E-01	1	[29]
RCS Tank Pressure Sensor Set 1, 2	2	1	1.00E-05	2.00E-01	1	[29]
N2 Tank Valve Set 1, 2	2	1	1.00E-05	2.00E-01	1	[29]
Pressure Sensor N2 Tank Set 1, 2	2	1	1.00E-04	2.00E-01	1	[29]
N2 Tank Level Sensor Set 1, 2	2	1	1.00E-04	2.00E-01	1	[29]
Mission Implementation						
Main Reflector	12	10	4.00E-03	2.00E-01	1	([61])
Secondary Reflector	6	5	2.00E-03	2.00E-01	1	([61])
Collimator	6	5	2.00E-03	2.00E-01	1	([61])
Main Reflector Support Deployment Mechanisms	162	122	1.00E-03	2.00E-01	1	([60, 85])
Secondary Reflector Support Deployment Mechanisms	48	36	1.00E-03	2.00E-01	1	([60, 85])
Collimator Support Deployment Mechanisms	48	36	1.00E-03	2.00E-01	1	([60, 85])
Front Mast	1	1	5.00E-03	2.00E-01	1	([33, 72])
Front Collimator Holder	1	1	2.00E-03	2.00E-01	1	([72])

Table 14.4 – *Continued on next page*

Table 14.4 – *Continued from previous page*

System / Component Name	n	m	Failure Rate [$1/yr$]	Relative uncertainty	Confidence interval width [xσ]	Source
Aft Mast	1	1	5.00E-03	2.00E-01	1	([33, 72])
Secondary Reflector Gimbal	1	1	1.00E-03	2.00E-01	1	([52, 67])
Main Reflector Harness	30	23	1.00E-05	2.00E-01	1	([90])
Secondary Reflector Harness	12	9	1.00E-05	2.00E-01	1	([90])
Collimator Harness	12	9	1.00E-05	2.00E-01	1	([90])
Optical Train	1	1	1.00E-06	2.00E-01	1	([32, 41])
Electrical Junkion Box	4	2	4.80E-03	1.00E-01	1	([29])
Connection wires	4	2	1.00E-03	1.00E-01	1	([29, 90])
Structures						
Entire structure	1	1	1.37E-04	1.94E-01	1	[90]

There are several events that can lead to LOM apart from several LOV. During the launch, stand-by in LEO and transfer to the asteroid the spacecraft will be supported by a single space transport system. The failure modes that result from this are presented in Table 14.5. It is assumed that the probability for failures of the ground segment resulting in permanent LOV or LOM is negligible [89].

Table 14.5: LV related failure modes, failure rates and uncertainties for the PRA. Sources are accessed as [XX] for direct citations, ([XX]) for extrapolations or references and an empty cell indicates ROM estimation.

Failure Mode	n	m	Failure Probability	Relative uncertainty	Confidence interval width [xσ]	Source
AD-FM-LV.1 Catastrophic Launch Failure	1	1	1.00E-02	NA	NA	([35, 45, 93]) Difficult to predict for Starship. Depends on launch cadence before 2030. 1% LOV probability should be conservative.
AD-FM-LV.2 Failure to Rendezvous	1	1	2.00E-02	NA	NA	([35]) See above.
AD-FM-FOD.1 Foreign Object Debris Collision (Fatal)	1	1	1.00E-05	NA	NA	assumed small due to maneuvering capabilities

Table 14.6 shows the results of the PRA. Figure 14.1 shows the failure paths leading to LOV that have a probability of occurring of more than 0.1%. As is expected the highest spacecraft failure probabilities come from the extremely expandable structures and the ADCS. As can be seen from the probability of AD-FM-LOM.1 however, the decision to have multiple actively redundant spacecraft is beneficial with more than 99.6% of all sampled cases having a LOM probability of less than 0.496%.

Table 14.6: Results of the PRA.

Failure Mode ID	Event Name	Probability	Note
AD-FM-LOV.1	LOV (single SC)	1.64E-01	99.6% interval: [1.62E-01, 1.67E-01]
AD-FM-LOM.1	LOM through successive LOV	3.96E-03	99.6% interval: [2.93E-03, 4.96E-03]
AD-FM-LOM.2	LOM total	3.41E-02	

As can be seen from Table 14.6 and Table 14.5 the LV associated failure modes have an order of magnitude difference to the spacecraft swarm associated LOM probabilities. This is because the LV is still in development

and no figures are available. Hence, very conservative values for both AD-FM-LOM.1 and AD-FM-LOM.2 were chosen. Since Starship is supposed to be human rated and intended for interplanetary human transport the reliability and accuracy of it will need to be very high [2]. Additionally, the recent track record of SpaceX with regards to Falcon 9 launches shows that the company might archive a much higher success rate than what is estimated here[3]. Nevertheless, as the program is still in development without attempted orbital launches and without announced reliability target the conservatives values given above are used.

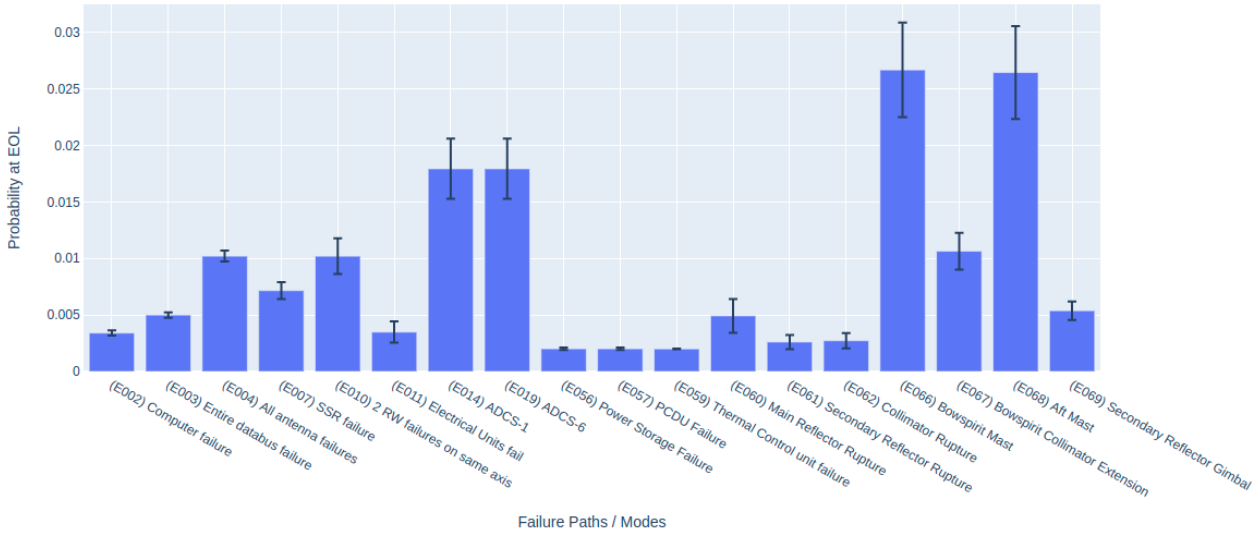

Figure 14.1: Failure paths and associated probabilities for failure paths with probabilities higher than 0.1%. Error bars are for 99.6% confidence interval.

The PRA results in an overall probability for LOM of 3.41% of which 0.4% is due to spacecraft swarm failures. The spacecraft swarm failure probability is below 0.496% with a certainty of 99.6%. This risk is acceptable because of the likelihood of overestimating the actual LV failure probability. It is desireable to increase the certainty of the estimation LV failure probability. Overall, the probability of mission failure is similar to interplanetary missions.

14.2 Reliability, Availability, Maintainability & Safety

In this section the implications of Section 14.1 on the reliability of the system are discussed, the availability of the system is analyzed, the maintainability is examined and safety aspects are presented.

14.2.1 Reliability

As presented in Section 14.1 the reliability of the entire system is high. If the reliability needs to be increased in the future it is necessary to focus on the high probability failure modes shown in Figure 14.1. A 10% decrease in single LOV probability decreases the probability for AD-FM-LOM.1 by more than a third and has hence very desirable scaling. As discussed in Section 14.1 the highest probability items for LOM are AD-FM-LV.1 and AD-FM-LV.1 which are both dependent on the LV. If the reliability of Starship is less than expected the reliability of the system can decrease significantly. Furthermore, since no other existing or proposed LV offers equivalent capabilities as Starship, this might be a significant risk for the mission which can hardly be influenced even when the mitigation procedures are correctly applied.

14.2.2 Availability

According to AD-SH-PFM-5 the system shall be operational before November 2030. Based on Chapter 15 this deadline can be met. Furthermore, the system must be continuously in a stand-by state for the duration of five

[2]URL `https://www.spacex.com/media/starship_users_guide_v1.pdf` [accessed 26 January 2021]
[3]Space Launch Report: SpaceX Falcon 9 v1.2 Data Sheet: `http://spacelaunchreport.com/falcon9ft.html` [accessed 18. January 2021]

years and must be able to operate around an asteroid for a maximum of two years[4]. Based on Chapter 5 and Section 14.1 this availability can be guaranteed.

14.2.3 Maintainability

Generally speaking it is not intended to perform active hardware maintenance on the space segment once it has been launched. However, in cases where it is absolutely required the system could be maintained by servicing it using another Starship, see Chapter 5 for more details.

14.2.4 Safety

The safety aspects split into three categories: Launch, stand-by and EOL related. Of which launch related safety concerns are the most serious ones.

Launch Safety

Launch safety is typically required of and performed by launch providers. Additionally, the spacecraft characteristics important for launch (e.g. structural response to launch loads and acoustics) need to be verified to meet the requirements of the LV. See [4] for more details.

Stand-By Safety

Since the spacecraft will remain in the Starship payload bay during the entire stand-by phase the launch provider is again responsible for safety during that time.

EOL Safety

At EOL the spacecraft might make a close pass by earth. While the probability of them being captured by earth is low (see Chapter 7 due to the large relative velocities the position of the spacecraft will need to be monitored during approach. Nevertheless, due to their high cross-section to mass ratio the space craft pose little threat even if they re-enter Earth's atmosphere as they would burn up during re-entry.

14.3 Requirements

Table 14.7 to Table 14.11 show the risk related requirements. Some of the requirements apply to the launch vehicle and not the system itself.

[4] The expected operational period near the asteroid is much lower, on the order of 6 to 12 months (Chapter 8)

Table 14.7: Design Risk Requirements

Identifier	Requirement	MOC	Compliance
AD-RISK-DV-1.1	All design tools shall be verified.	Analysis	Y
AD-RISK-DV-1.2	All design tools shall be validated.	Analysis	Y
AD-RISK-DV-1.3	An integrated design sheet shall be developed.	Inspection	-
AD-RISK-DV-2.1	Design decisions shall be based on a techno-financial trade-off.	Inspection	Y
AD-RISK-DV-2.2	A general trade-off tool shall be developed and used for every trade-off.	Inspection	Y
AD-RISK-DV-2.3	A sensitivity analysis shall be performed for every trade-off.	Inspection	Y
AD-RISK-DV-2.4	The selected design shall win the trade-off with a certainty of at least 80%.	Analysis	Y
AD-RISK-DV-2.5	At least 20 000 cases shall be analyzed for each sensitivity study.	Inspection	Y
AD-RISK-DV-2.5	The sensitivity study shall independently vary its input parameters.	Analysis	Y
AD-RISK-DV-3	Sanity Checks shall be performed before every major design decision.	Inspection	Y
AD-RISK-DV-4	Requirement fulfillment shall be continuously monitored.	Inspection	Y
AD-RISK-DV-6.2	A SWOT analysis shall be performed for a selected competitor concepts.	Inspection	N
AD-RISK-DV-7	The engineering budgets shall be monitored continuously by the Chief Engineer.	Inspection	Y
AD-RISK-DV-8	Probabilistic risk assessment shall be used for concepts at least at a subsystem level.	Inspection	Y
AD-RISK-DV-9	Fever maps shall adhere to the ECSS standards.	Inspection	Y

Table 14.8: Production Risk Requirements

Identifier	Requirement	MOC	Compliance
AD-RISK-PRO-1.1	It shall be possible to produce the design.	Analysis	TBD
AD-RISK-PRO-1.2	It shall be possible to assemble the design.	Analysis	TBD
AD-RISK-PRO-3	A Design Margin of [35%, 25% or 10% for Baseline, Midterm or Final] shall be chosen for each to be produced part to keep the part operational for a lifetime of 5 years	Inspection	Y

Table 14.9: Operation Risk Requirements

Identifier	Requirement	MOC	Compliance
AD-RISK-OP-1.1	Critical systems shall have a level of redundancy of at least 1.	Analysis	Y
AD-RISK-OP-1.2	Digital systems shall have at least triple modular redundancy.	Demonstration	Y
AD-RISK-OP-5.1	The software of the system shall have an automatically triggered ”safe” state in which the software shall be able to be modified.	Test	Y
AD-RISK-OP-5.2	The ”safe” state shall trigger when a communication loss is detected by the system.	Test	Y
AD-RISK-OP-5.3	The ”safe” state shall trigger when a control loss is detected by the system.	Test	Y
AD-RISK-OP-6	The secondary reflector shall be able to gimble around 2 axes.	Demonstration	Y
AD-RISK-OP-7	Each spacecraft shall be able to communicate with each spacecraft in the swarm after being deployed.	Test	Y

Table 14.10: Logistic Risk Requirements

Identifier	Requirement	MOC	Compliance
AD-RISK-LOG-1	The system shall use materials with a NASA Technology Readiness Level of at least 4.	Inspection	Y
AD-RISK-LOG-2.1	Supplier progress shall be monitored.	Inspection	-
AD-RISK-LOG-2.2	Secondary supply lines shall be identified.	Demonstration	-
AD-RISK-LOG-2.3	Critical processes or systems shall be insured.	Demonstration	-
AD-RISK-LOG-4	The selected launch provider shall have flown at least 100 successful missions in the past.	Inspection	Y
AD-RISK-LOG-7	The launch vehicle shall have a reliability of at least 99%.	Analysis	-

Table 14.11: Environmental Risk Requirements

Identifier	Requirement	MOC	Compliance
AD-RISK-ENV-1	The design process shall be saved in an online secured environment.	Inspection	Y
AD-RISK-ENV-2	The design of the system shall be performed in an environmentally sustainable way.	Analysis	Y
AD-RISK-ENV-3	The production of the system shall be performed in an environmentally sustainable way.	Analysis	-
AD-RISK-ENV-2	The operation of the system shall be performed in an environmentally sustainable way.	Analysis	-

15 Satellite Production

A reliable production process is integral to the success of the mission. The design calls for 32 identical spacecraft to be produced. Each spacecraft has a mix of outsourced components and highly custom components. Manufacturing a run of 32 spacecraft does not call for a fully automated assembly line. Instead automation should be used strategically on components that find themselves made over and over again even in a single spacecraft. This chapter will take a short look at what such a production process would look like.

For production purposes the spacecraft can be segmented between commercially available components, high volume components and low volume components. Commercially available components would be electrical devices such as star sensors. High volume components mainly refer to the components in the deployable structures where there are hundreds of the same component per satellite. Low volume components refer to items that have low part counts per spacecraft such as the main reflector sheet.

The commercial components require that they be tested properly to ensure that they work correctly with the entire system. It is not as critical to individually test each component as long as the original manufacturer provides its own validation.

The production of high volume components will take advantage of automation such as computer numerical controlled (CNC) machines. Setting up a fully automated assembly line is not worth it as the number of parts is not that high, but it is important to ensure the process is efficient and repeatable with minimal personnel involvement. It will also be critical to have efficient and effective quality control processes in place.

Producing the low volume components is very dependent on the type of component. Components like the reflectors that are very custom and very specialized are likely to become bottlenecks in the production process so putting different timeline checks in place is critical to keeping the production line from having major hangups.

An overview of the production process is given in Figure 15.1. Due to the need for the production of at least 32 spacecraft the production should be serialized as much possible once assembly begins. For example large aircraft are produced serially where at each station a new component is fitted. This concept would work well for the production of the spacecraft. The assembly stage should also start as soon as sufficient components are available. This will allow for one spacecraft to be assembled while another is being manufactured, thus keeping assembly lines open for the minimum amount of time and reducing the cost of storing finished components. This concept is also known as ’just-in-time’ manufacturing.

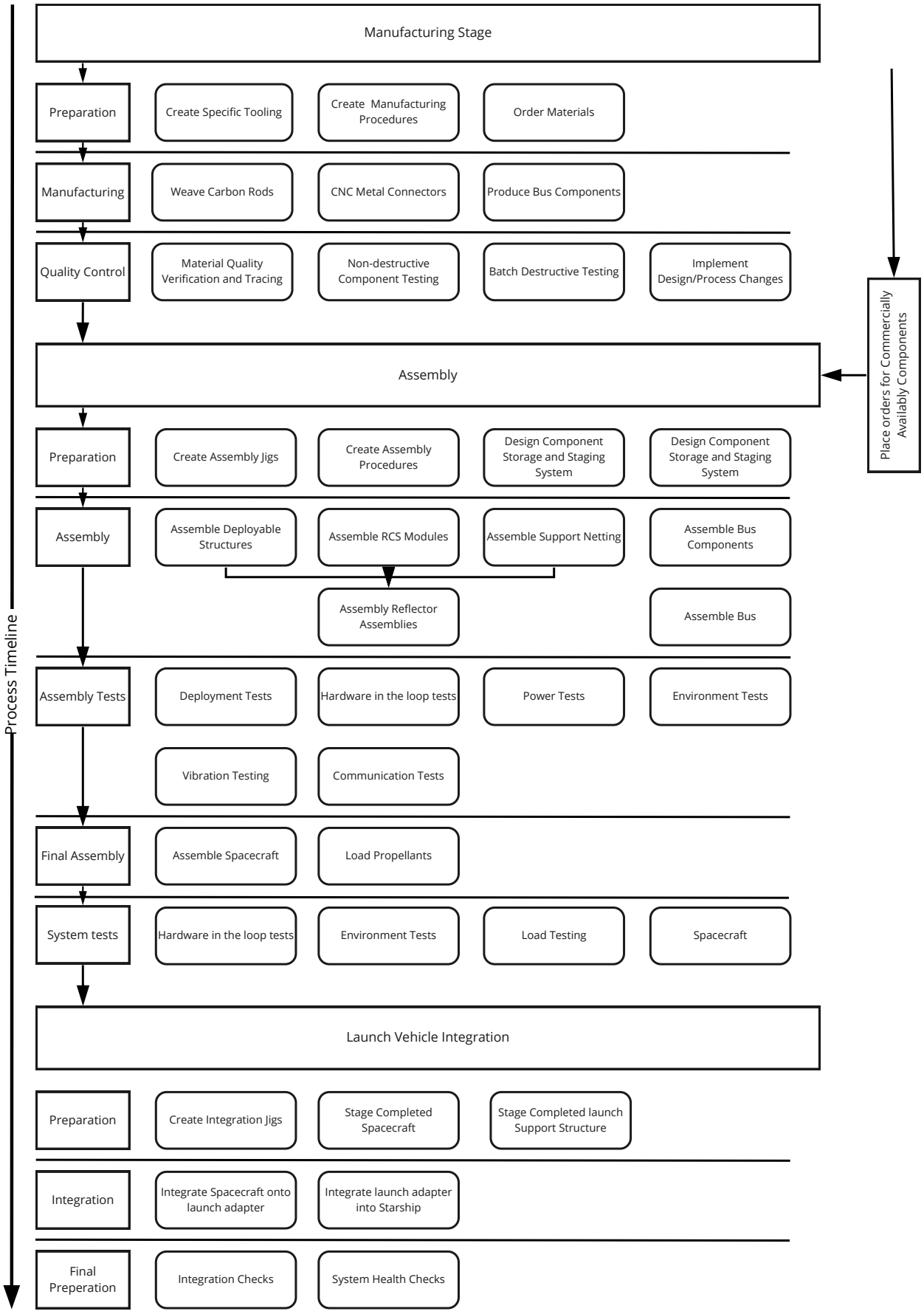

Figure 15.1: Process Timeline for the manufacturing, assembly and integration of the system

16 Cost Analysis

This chapter discusses the cost analysis of the mission. Firstly, non-recurring costs will be discusses in Section 16.1. Section 16.2 will analyze the recurring costs more in depth. And lastly, Section 16.3 will present the total cost breakdown of the mission.

16.1 Non-recurring Costs

Firstly, the non-recurring costs will be discussed. It is assumed that these costs will not increase for an increasing number of units produced. Such costs are for example the costs of building a factory where the units will be produced. All different non-recurring costs will be discussed in this section.

16.1.1 Office and Factory space

During the Research and Development phase of this project, suitable office space should be provided to the employees. It was assumed that 200 employees will work on the Research and Development of this project for a period of six years. In order to calculate the total required office area, an average area of $23.5\ [m^2]$ per employee was considered [1]. This results in a total required office area of $4700\ [m^2]$. Against a rate of $1,323.5\ [€/m^2]$ [2], the total costs for the construction of suitable office area was estimated to be $€6.3M$.

After the research and development phase, the spacecraft will be produced. For this production phase, a suitable factory will be constructed. It was estimated that a factory with a size of $40,000\ [m^2]$ is needed to produce the 32 systems. For the construction of the factory, a rate of $213.2\ [€/m^2]$ was accounted for [3]. It was assumed that the costs for tooling equipment increases the aforementioned rate with a factor of five. Overall, it is estimated that the construction of the factory will cost $€25.6M$.

16.1.2 Research and Development Phase

As mentioned before, 200 employees will work for six years on the Research and Development of the space system. Using an average salary of $€73,737$ per year of an aerospace engineer in The Netherlands, a total cost of the research and development phase was estimated to be $€89M$[4]. Next to these costs, it was assumed that another 10% of these costs should be accounted for legal fees and promotion. This results in a estimated cost of $€97.9M$ for the research and development combined with a budget for legal fees and promotion.

16.1.3 Launch, Ground Segment and Operations

The SpaceX Starship will be used for the launch of the space system. As the Starship will not be able to take enough fuel to return to Earth from the asteroid, the Starship should be bought from SpaceX. It was assumed that a Starship will cost around $€205M$, including the costs of required fuel and launch insurance[5]. Next to that, it was estimated that the cost of the ground segment and operations will be $€98M$ [93]. Overall, a total cost of $€303M$ is accounted for the launch, ground segment and operations.

16.1.4 Testing and Contingency

Testing of the spacecraft should be done in order to ensure that the spacecraft will operate in space properly. For example, the spacecraft should be tested if it operates properly in vacuum. Other examples are testing the temperature and vibrational characteristics. It is estimated that the testing of the spacecraft costs 10% of the total cost budget [93]. This results in a testing budget of $€100M$.

[1] URL `http://bit.ly/needed_office_space` [accessed 17 January 2021]
[2] URL `https://proest.com/office-building-construction-costs` [accessed 17 January 2021]
[3] URL `https://www.centralbuild.com.au` [accessed 17 January 2021]
[4] URL `https://interestingengineering.com/a-look-at-aerospace-engineering-salaries-worldwide` [accessed 18 January 2021]
[5] URL `https://www.fool.com/investing/2020/02/16/are-elon-musks-spacex-promises-even-possible.aspx` [accessed 16 January 2021]

Also, the average cost growth from detailed design to system delivery is 30% [83]. This percentage will be accounted for in the contingency budget. This leads to a budget of $€207M$, which can be used to finance any unforeseen costs.

16.2 Recurring Costs

16.2.1 Labor

For the production of the space system, it is assumed that 500 production employees are required to produce 32 spacecraft such a limited production time. It was assumed that these production employees earn 10% less than the research and development employees. This results in an annual salary of $€66,363$. It is assumed that the 500 production employees are capable of producing 10 units per year at the beginning of the production phase. Next to that, learning rates for the different industries may vary between 54% and 108% with an average learning rate across different industries of 82%. As the aerospace industry is a more challenging industry, a learning rate of 95% was assumed per doubling of the produced units. As the system is a novel design with a relative low TRL, a maximum total learning rate of 80% was assumed. [9]

All aforementioned assumptions lead to a production time for the 32^{rd} unit of $0.08[years]$ and labor cost of $€2.7M$. Adding the labor costs of all previous units results in a total labor cost of $€90M$ for the space system.

16.2.2 Material Costs

For the production of 32 spacecraft, it was assumed that there will be a bulk discount of 30% when all materials are bought at the same time. This resulted in a total material cost of $€66M$. The estimation of the materials costs are discussed in this section per subsystem. The estimation of the material costs per subsystem are mostly based on prices from off the shelf products. However, for some subsystems, an estimation was done with the use of market prices of the materials that are used for that subsystem. The estimated material costs will be discussed per subsystem.

Mission Implementation

For the mission implementation, an estimation was performed based on the materials that are used. These materials are for example aluminum, carbon fiber composites, Kapton and in lower amounts silver and polydimethylsiloxane. The costs for the usage of these materials can be seen in Table 16.1[6,7,8,9].

Table 16.1: Material Costs for the Mission Implementation subsystem

Material	**Mass [kg]**	**Price** $[€/kg]$	**Cost** $[€]$
Aluminum	5	2	10
Carbon Fiber composites	150	85	12,750
Kapton	1,000	143.25	143,254
Silver	0.02	671	13.42
Polydimethylsiloxane	0.03	2.25	0.07
Total			**156,027.49**

Electrical Power System and Thermal Control System

For the electrical power system, solar panels were used. The cost of the solar cells present in the solar panels is approximated by the amount of power that should be produced. As it costs $10[€/W]$, the solar cells are estimated to cost $€51,250$ [10]. Next to these solar cells, $80[kg]$ of carbon fiber composites were used for the structure of the solar panels. Using the same value as given in Table 16.1, a cost of $€6,870$ was estimated [74]. This results in a total cost of the solar panels of $€58,120$. Next to that, an off the shelf power control and

[6]URL `https://markets.businessinsider.com/commodities/aluminum-price` [accessed 16. January 2021]
[7]URL `http://bit.ly/kapton_price` [accessed 15 January 2021]
[8]URL `https://www.bullionbypost.eu/silver-price/silver-price-per-kilo/` [accessed 15 January 2021]
[9]URL `http://www.satsusilicones.com/polydimethylsiloxane-pdms-4072753.html` [accessed 15 January 2021]
[10]The Case for Solar Power From Space `https://space.nss.org/the-case-for-solar-power-from-space/` [accessed 17. January 2021]

distribution unit including batteries was estimated to cost $€20,000$ [59].

For the thermal control system, heaters are used that cost approximately $90,000[€/m^2]$[11]. This results in an estimated cost for the heaters of $€2,250$. Next to that, there is $€10,000$ accounted for the MLI blankets. Also, it is assumed that the thermal control unit will be bought for the same price as the power control and distribution unit. This leads to the cost breakdown for the electrical power system and the thermal control system as given in Table 16.2.

Table 16.2: Material Costs for the EPS and TCS.

Component	**Cost** [€]
Solar Panels	58,120
Power Control and Distribution Unit	20,000
Total EPS	**78,120**
Heaters	2,250
MLI blankets	10,000
Thermal Control Unit	20,000
Total TCS	**32,250**

ADCS and Propulsion System

The ADCS uses reaction wheels, sun sensors and star sensors to control the orientation of the spacecraft. In total it uses six reaction wheels, eight sun sensors and six star sensors. All price estimations are based on off the shelf products and are $€80,000$, $€12,000$ and $€45,000$ for the reaction wheels, sun sensors and star sensors respectively[12].

The propulsion system uses 16 RCS thrusters with a cost per unit of $€15,000$[13]. In total, these RCS thrusters use 22.09 [kg] of Xenon, which gets sold for 850 $[€/kg]$[14]. The propulsion system also uses an Ion thruster that is estimated to cost $€1.1M$ [57]. This Ion thruster uses 30 [kg] of the propellant LMP-103S, which costs $2,000$ $[€/kg]$ [20]. Table 16.3 gives the material costs for the ADCS and propulsion system.

Table 16.3: Material Costs for the ADCS and Propulsion System.

Component	**Cost** [€]
Reaction Wheels	480,000
Sun Sensors	96,000
Star Sensors	270,000
Total ADCS	**846,000**
RCS Thrusters	240,000
Ion Thruster	1,140,000
LMP-103S	60,000
Xenon	18,800
Total TCS	**1,458,800**

TT&CS and C&DHS

The design of the TT&CS uses two transponders, one high gain antenna and two low gain antennas. The transponders are estimated to cost $€30,000$ per unit[15]. From the same source. it was estimated that the low gain antenna's cost $€5,000$ per unit. Lastly, it is assumed that the high gain antenna will cost 10 times as much as a single low gain antenna.

The C&DHS uses an On-board Computer, a solid-state recorder and a diplexer. The On-board Computer is responsible for the largest part of this subsystem cost, with an estimated cost of $€200,000$[16]. Next to that, the

[11] Minco Heater Price `https://www.distrelec.nl/nl/polyimide-thermofoiltm-heater` [accessed 14. January 2021]
[12] CubeSatShop `https://www.cubesatshop.com/` [accessed 14. January 2021]
[13] Thruster Cost `https://space.stackexchange.com/questions/26676/` [accessed 17. January 2021]
[14] Xenon Cost `https://space.stackexchange.com/questions/8698/` [accessed 17. January 2021]
[15] CubeSatShop `https://www.cubesatshop.com/` [accessed 16. January 2021]
[16] Space-grade CPUs `https://arstechnica.com/science/2019/11` [accessed 18. January 2021]

diplexer will cost $€1,000$[17].

Table 16.4: Material Costs for the TT&CS and C&DHS.

Component	**Cost** [€]
Transponders	60,000
High Gain Antenna	50,000
Low Gain Antennas	10,000
Total TT&CS	**120,000**
On-board Computer	200,000
Solid-State Recorder	30,000
Diplexer	1,000
Total C&DHS	**231,000**

16.3 Cost Analysis Summary

Adding all factors mentioned in the cost analysis resulted in a total mission cost of $€896M$ and satisfies **AD-SH-CST-01**, which required a maximum total mission cost of $€1B$ [3]. Figure 16.1 summarizes the total cost analysis.

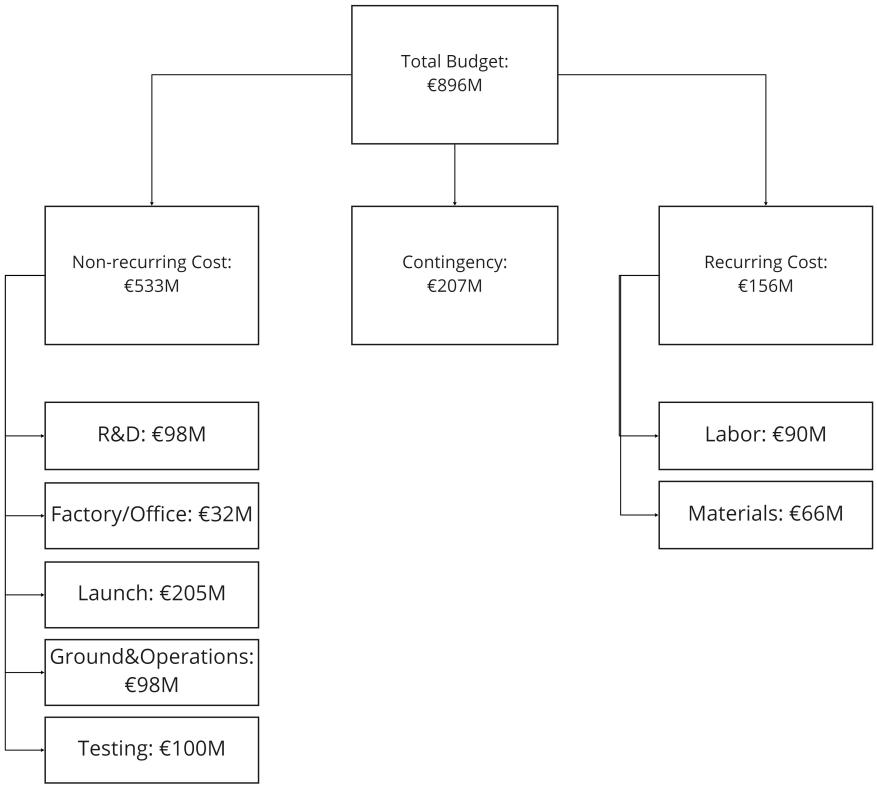

Figure 16.1: Breakdown of the total cost budget.

[17]Twin Diplexer `https://www.talleycom.com/` [accessed 16. January 2021]

17 Sustainability Engineering

Throughout the mission design phases, sustainability aspects, goals and requirements have been presented in order to implement a sustainable approach throughout the entire mission. The ultimate goal of this approach is to fulfill our own needs without preventing future generations to also be able to do this. Therefore, four different sustainability pillars have to be considered, namely human, social, environmental and economic sustainability. In this section, further elaboration on the sustainability analysis from the Baseline and Midterm reports is presented [3, 4].

17.1 Social and Human

Compared to the overall system social and human sustainability aspects, not much divergence can be found when looking at the individual subsystems presented in this report. The selection of existing, up-to-date ground facilities does bring a new factor of cohesion with itself; since both ESA and NASA facilities will be used, a need for cooperation between these two agencies has arisen, which will enhance social sustainability.

The investigation and development of the cleaning mechanism of the secondary reflector also bring along an increase in human sustainability, since this is a technique that had only been used in labs and never been put to practice on actual space missions. Future space engineers can use this technique if it proves successful in the mission at hand.

17.2 Spacecraft Design

17.2.1 Materials

To make an objective comparison between the sustainability of the various materials used within the different subsystems, the total production carbon footprint, and energy consumption have been calculated based on material data from CES Edupack. With the amount of material present in each subsystem, Table 17.1 has been set up so a clear overview is provided of the emission costs due to manufacturing of the different subsystems.

Table 17.1: Total material production emission and energy consumption comparison for each subsystems.

Subsystem	Total material emission (kg CO2)	Total material energy consumption (kWh)
ADCS	12,400	16,967
Propulsion	81.4	26
Power	1,856	1,137
Thermal	219	25.7
Solar concentrator	3,110	1,240
S/C bus	220	594
TT&C	618	1,235
C&DH	533	111

It can be seen that especially the ADCS is emitting a lot of CO_2 due to its production, mainly due to the presence of Platinum.

17.2.2 Propellants

The propulsion chosen for the on-board thrusters is High-Performance Green Propulsion (HPGP, an alternative to the environmentally-damaging hydrazine. A different name for this propellant type is LMP-103S. It has numerous advantages, like increased performance, responsiveness and reduced costs. About 64 % of the

total propellant is saved by choosing this green alternative. Some key specifications are tabulated in Table 17.2 below, where hydrazine is compared to HPGP.[1]

Table 17.2: Key specifications for Hydrazine and HPGP comparison.

Specification	**Hydrazine**	**HPGP (LMP-103S)**
Specific impulse	$220\ [s]$	$6\ [\%]$ higher than hydrazine
Density	$1.02\ [g/mL]$	$24\ [\%]$ higher than hydrazine
Toxicity	Highly toxic	Low toxicity
Carcinogenic	Yes	No
Corrosive	Yes	No
Flammable vapors	Yes	No
Environmental Hazard	Yes	No
Sensitive to air & humidity	Yes	No
Storable	Yes	Yes (>8.5 years)
Freezing point	$1\ [^{\circ}C]$	$-90[^{\circ}C]$
Boiling point	$114\ [^{\circ}C]$	$120\ [^{\circ}C]$
Exhaust gases	Ammonia, nitrogen, hydrogen	H_2O, N_2, H_2, CO, CO_2

After having contacted Bradford ECAPS, the company that produces HPGP and is also situated in The Netherlands, about more information on this propellant type, their system engineer, William Meerbeeck, responded with additional information. The propellant is made out of ADN, a highly energetic type of salt, ultra-pure water, methanol and ammonia. The last three of these are readily available and are produced on a large scale, meaning their production is very efficient and they are acquired locally, reducing transportation costs.

In comparison to hydrazine, a couple of benefits are acquired with the usage of HPGP due to its lower toxicity, namely:

1. The air transportation can be done along with different types of cargo; no special aircraft has to be used to transport the HPGP.
2. The inherent safety of the propellant results in a much easier fueling of the spacecraft; no additional measures have to be taken, which saves material and staff costs.
3. At spacecraft EOL, the propellant that is still left in the tank can easily be destroyed. For hydrazine, very strict protocols and thorough measures have to be taken for this process, which also comes along with more material use and more costs.

All in all, HPGP has been validated as a proper alternative to hydrazine mainly due to its lower toxicity and therefore ease of use.[2]

17.2.3 End of Life

For the End of Life procedures of the system, two possible scenarios are realistic. The first one is when the spacecraft are actually sent towards the asteroid in order to deflect it. Due to the propellant that is then used and the distance the constellation will be from the Earth, it is not realistic to bring the spacecraft back in the way the system has been designed right now. Therefore, the spacecraft will be lost in space forever but luckily at a far distance from the Earth, so that no future space missions will be harmed. The second scenario is that the spacecraft will be in orbit for 5 years and no asteroid is coming towards the Earth, meaning they will not have a clear purpose. In this case, the spacecraft can be deployed from Starship to perform additional tasks, such as removing space debris or transferring solar power back to the Earth. When this task has been finished, the spacecraft can be de-orbited such that it partially burns up in the atmosphere and can partially be recollected by ground operations.

[1] URL `https://www.ecaps.space/assets/pdf/Bradford_ECAPS_Folder_2017.pdf` [accessed 19 January 2021]
[2] (Meerbeeck, W. (20 January 2021). Personal interview [E-mail].)

17.3 Launcher Comparison

In the Midterm Report, a total of 13 different launch vehicles were compared based on multiple aspects. One of the most important aspects was the reusability of the launcher, where a reusable launcher would always be preferred over non-reusable launchers. Bearing this in mind, SpaceX's Starship launch vehicle was selected for bringing the spacecraft into orbit. Previously, only the Falcon 9 Full Thrust and the Falcon Heavy were considered but since Starship is the most state-of-the-art reusable launch vehicle, this was chosen initially. [4]

The criteria that the launch vehicles in the Midterm Report were compared with, have now also been found and tabulated for Starship in Table 17.3 below.

Table 17.3: Starship launcher sustainability analysis based on 7 different criteria.[3]

Parameter	Value
Reusable [Yes/No]	Yes
Maximum payload to LEO [kg]	>100,000
Launch cost / Payload mass [US$/kg]	20
Propellant mass / Payload mass [kg/kg]	46
Fuel type(s)	CH4/LOX
Toxic exhaust components	CO CO2
Reliability [%]	tbd

Compared to the values found for the different launchers in the Midterm Report, it can be seen that Starship is by far the most sustainable one when looking at the launch costs and propellant mass per payload mass. This is largely due to the fact that a relatively large payload mass can be taken to LEO, a lot more than needed for the mission. In order to make this more sustainable, ride sharing can be applied with for example multiple CubeSats that will fit in the cargo bay next to the spacecraft. In this way, the excessive payload-to-LEO availability of Starship is optimally used.[4]

As mentioned previously, Starship can entirely be reused which will save production and assembly costs. It uses subcooled methane and liquid oxygen as its propellant which only produces carbon monoxide and carbon dioxide as its exhaust components, which harms the atmosphere but not as much as the exhaust fumes of hydrazine-type of fuels that is commonly used on different launcher types. As mentioned previously, the entire spacecraft communication system can be coupled to the Starship interface so that an additional communication device is not needed when integrated as a payload. Starship's reliability is yet to be determined.[5]

17.4 Ground Segment

facilities have been selected to support the mission at hand. First of all, the only two facilities that SpaceX's Starship can launch from are Kennedy Space Center in Florida and Boca Chica launch pad in Texas.[6] Boca Chica is chosen as the launch site since it will be closest to the $0\,\mathrm{deg}$ inclination orbit that the spacecraft will be in during parking. Over the last few months, however, the Federal Aviation Administration (FAA) has required SpaceX to do an Environmental Assessment, in which they will analyze their environmental impact on the surroundings of Boca Chica, for them to obtain Starship launch clearance. If this Environmental Assessment is successful, Starship can launch from this site within the environmental boundaries set by the FAA so a sufficient degree of environmental sustainability will be achieved.[7] If this assessment is not successful, Kennedy Space Center will have to be used as launch site, where sustainable facilities such as carbon-neutral buildings, a 1 $[MW]$ PV system and electric personal transportation vehicles are present.[8]

[3]URL https://www.spacex.com/media/starship_users_guide_v1.pdf [accessed 26 January 2021]
[4]URL https://www.spacex.com/media/starship_users_guide_v1.pdf [accessed 26 January 2021]
[5]URL https://www.spacex.com/media/starship_users_guide_v1.pdf [accessed 26 January 2021]
[6]URL https://www.spacex.com/media/starship_users_guide_v1.pdf [accessed 26 January 2021]
[7]URL https://bit.ly/2Kpsapo [accessed 18 January 2021]
[8]URL https://go.nasa.gov/2M47p2R [accessed 18 January 2021]

The communications ground stations that are chosen are the Redu station, which is part of ESA's ESTRACK network, and NASA's Deep Space Network.[9] [10] The latter consists of 3 different ground stations, each located 120 degrees apart in longitude, so that constant communication is possible with deep space missions. All control rooms send their information through to NASA's Jet Propulsion Laboratory.

17.5 Sustainability goals compliance

In the Baseline Report, sustainability goals were set up for the entire mission. After having finalized the design, the number of goals that were actually achieved can be determined. In Table 17.4, a sustainability goal compliance matrix has been created. In this table, all sustainability goal identities are presented along with their Means of Compliance (MOC), or the validation method applied to determine whether the goal was achieved or not. Finally, a Yes/No statement is presented for the goals that were actually achieved. [3]

Table 17.4: Sustainability goals compliance matrix.

Goal ID	MOC	Compliance	Goal ID	MOC	Compliance
AD-SAB-SO-01	Inpection	Y	**AD-SAB-GRE-02**	Demonstration	Y
AD-SAB-SO-02	Inspection	Y	**AD-SAB-GRE-03**	Inspection	Y
AD-SAB-HM-01	Analysis	Y	**AD-SAB-GRE-04**	Analysis	Y
AD-SAB-HM-02	Analysis	Y	**AD-SAB-GRE-05**	Analysis	Y
AD-SAB-SPE-01	Analysis	N	AD-SAB-GRE-06	Inspection	Y
AD-SAB-SPE-02	Test	Y	AD-SAB-GRC-01	Analysis	Y
AD-SAB-SPE-03	Analysis	Y	AD-SAB-GRC-02	Analysis	Y
AD-SAB-SPE-04	-	-	AD-SAB-GRC-03	Inspection	Y
AD-SAB-SPE-05	Analysis	N	AD-SAB-GRC-04	Inspection	Y
AD-SAB-SPE-06	Test	Y	AD-SAB-GRC-05	Analysis	Y
AD-SAB-SPC-01	Analysis	Y	AD-SAB-OPE-01	Analysis	Y
AD-SAB-SPC-02	Analysis	Y	AD-SAB-OPE-02	Analysis	Y
AD-SAB-SPC-03	Inspection	Y	AD-SAB-OPE-03	Inspection	Y
AD-SAB-SPC-04	Analysis	N	AD-SAB-OPE-04	Analysis	Y
AD-SAB-GRE-01	Inspection	N	AD-SAB-OPE-05	Inspection	Y
AD-SAB-OPC-01	Analysis	Y	**AD-SAB-OPC-02**	Analysis	Y

As can be seen, not all goals were achieved. Starting with **AD-SAB-SPE-01**, which stated that the mission would prevent the addition of the amount of pollution in space, is not achieved since we will not be able to deorbit the spacecraft constellation along with Starship back to Earth. The reason for this is that all propellants will be spent during the deflection phase, making it impossible for the systems to return home. This can, however, be justified by the fact that the orbit the spacecraft will remain in, does not interfere with other satellites, because they are at a significantly long distance from Earth. The same goes for **AD-SAB-SPE-05**, as the spacecraft waste will not be treated at all, just leaving it in space. Concerning **AD-SAB-SPC-04**, no additional payload has been added since this would not fit within the design budgets of the spacecraft. This can still be applied for future recommendations. Finally, **AD-SAB-GRE-01** states that renewable power sources will be used for all ground stations. This is unfortunately not the case, since for example, the Redu-1 Antenna uses diesel generators for its power supply.[11] This can in future improvements also be replaced by renewable energy sources such as a solar park.

17.5.1 Sustainability Factor

The Sustainability Factor that was also presented in the Baseline Report can now be computed using the equation below. [3]

$$SF = \frac{\sum_i w_i}{77} \tag{17.1}$$

[9] URL `https://bit.ly/35QTOTD` [accessed 18 January 2021]
[10] URL `https://go.nasa.gov/3nUifG9` [accessed 18 January 2021]
[11] URL `https://bit.ly/3pkCka9` [accessed 26 January 2021]

This gives an overall indication on how well all 4 pillars of sustainability have been adhered to. A total of 65 points have been achieved, meaning the total Sustainability Factor has become 0.844. Compared to the value that was estimated in the Midterm Report, namely 0.826, this is an improvement, which means the team has performed better than initially expected for the sustainability criteria. [4]

18 Performance Analysis

This chapter will serve to analyze the performance of the final system. Firstly it will find whether the asteroids can be reached by confirming the ΔV goal in Section 18.1. Secondly it will test these capabilities against a range of known asteroids to determine if its performance is sufficient in Subsection 18.2.1.

18.1 Reaching the asteroid

As was mentioned in Section 7.2, a high ΔV budget is needed in order to reach as many asteroids as possible. In the same section a goal was set of $8\ [km/s]$ of ΔV available from the system's parking orbit. This goal was to be achieved by the use of an in orbit refueled kick stage, specifically SpaceX's Starship as it has a high payload and propellant capacity.

Verification of the ΔV goal can easily be done by the use of Tsiolkovsky's rocket equation, see Equation 18.1. Here I_{sp} is the specific impulse of the kick stage's engines, which is $380\ [s]$[1] for the vacuum optimized version of the raptor engine, and g_0 is the standard gravity, which is $9.80665\ [m/s^2]$. Next, m_0 is the wet mass and m_f is the dry mass. The dry mass is the Starship's empty mass of $120,000\ [kg]$ combined with our payload of 32 satellites weighing $1166\ [kg]$ each for a total of $157,312\ [kg]$[2]. As for the wet mass it is simply the dry mass plus the propellant mass, which is $1,200,000\ [kg]$. This results in a total wet mass of $1,357,312\ [kg]$. This then results in an achieved ΔV of $8.033\ [km/s]$ and thus satisfies the design goal.

$$\Delta V = I_{sp}\ g_0 \ln\left(\frac{m_0}{m_f}\right) \tag{18.1}$$

While having a sufficient ΔV budget to reach an asteroid is the most limiting part, there is also a chance of missing the rendezvous with asteroid. From Section 14.1.1, the chance of a successful rendezvous and deployment was found to be in excess of 96.59% with a certainty of more than 99.6%. The kick stage failing to rendezvous is responsible for 3.0% of the failures and failures due to deployment are responsible for the remaining 0.41%.

18.2 Performance Analysis of Known Asteroids

In order to find out whether the system is capable of deflecting the asteroids it is able to reach, the system has been simulated on an envelope of asteroids using the solar system model. The solar system model is described in more detail in the Midterm Report [4]. The asteroid envelope is the same as the one used in Section 7.2. However, all unreachable asteroids where a ΔV greater than $8\ [km/s]$ is required were filtered out. The resulting database counts 888 asteroids within our size range that have a close approach with Earth of less than $0.05\ [AU]$.

Unfortunately, while the orbital data of each asteroid is fairly accurately mapped, the size and mass are almost always unknown. Hence, some assumptions must be made. For sizing one can retrieve an equivalent diameter from the absolute magnitude according to Equation 18.2[3]. Here D is the estimated diameter of the asteroid, H is the absolute magnitude and p is the asteroid's albedo which was assumed to be 0.15, which is a typical value.

$$D = \frac{1329}{\sqrt{p}}\ 10^{-0.2 \cdot H} \tag{18.2}$$

With the use of the diameter, the mass can simply be found with the density. The density however is also usually unknown. However, for some asteroids the densities are known and an estimation can be drawn from this. For different asteroids, estimated densities were found and ranked from A–E, indicating the level of confidence at which the densities are determined [18]. Figure 18.1 shows the estimated densities for different ranks. A high end density of $4\ [g/cm^3]$ was chosen as estimate for all asteroids in the simulation. This was done to increase the confidence of the results. A density of $4\ [g/cm^3]$ covers 100% of the asteroids if only rank A estimates are

[1] URL `https://www.youtube.com/watch?v=zu7WJD8vpAQ` [accessed 7 January 2021]
[2] URL `https://www.spacex.com/vehicles/starship/` [accessed 7 January 2021]
[3] URL `https://cneos.jpl.nasa.gov/tools/ast_size_est.html`[accessed 20 January 2021]

included, 93% of the asteroids if rank A & B estimates are included and 89% of the asteroids if rank A, B & C estimates are included.

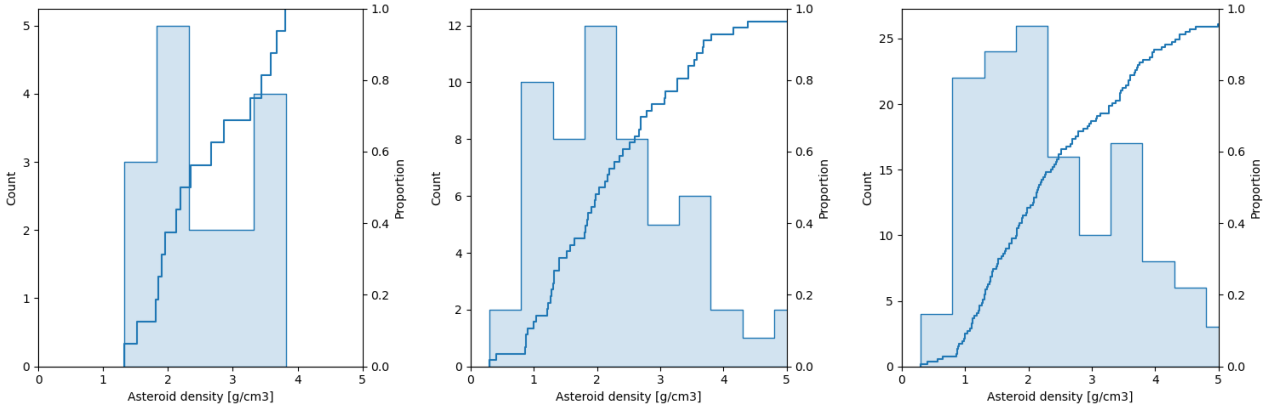

(a) Estimated densities only including rank A (b) Estimated densities including rank A & B (c) Estimated densities including rank A,B & C

Figure 18.1: Estimated densities of a selection of asteroids

18.2.1 Deflection of Known Asteroids

Depending on how reachable the asteroid is, the simulation was done for each asteroid starting either one or half a year before the asteroids closest approach. It used an estimation of the degrading force of the system which started at F_0 being the full $10000\ [N]$ of thrust and degraded according to Equation 18.3.

The simulation was done with the force applied both along and against the asteroids velocity vector. These directions of force are deliberately chosen as this is the best way to add or remove velocity from the asteroid. Adding or removing velocity raises or lowers it's orbit respectively. This results in a biggest change of orbit and thus deflection. Applying velocity perpendicular to the asteroid's orbital velocity does not work for long term deflection as it would merely result in the asteroid oscillating within it's original orbit thus not only failing to achieve a guaranteed deflection but also making it more unpredictable. [79]

Whichever direction of force applied granted the most deflection was kept. Results can be found in Figure 18.2.

$$F = F_0 \cdot e^{-2.58268 \cdot 10^{-7} \cdot t} \tag{18.3}$$

From Figure 18.2a, it can be seen that there is a large spread in the distance the asteroids are deflected with some asteroids being deflected extreme distances. This is not wholly unexpected due to the size differences of the asteroids: as per requirements **AD-SH-PFM-1** and **AD-SH-RISK-1**, the system must be able to deflect asteroids in the range of $10-100\ [m]$. This results in a range of mass differences of three orders of magnitude. Figure 18.2b shows the same graph but zoomed in. It displays the low end of the deflections from $0-10$ times the Earth's radius. At minimum the asteroid should be deflected with one time the Earth's radius, this happens in 97% of the cases. Due to the assumptions made, inaccuracies occur in the model and orbit predictions etc. So, it would be preferred to have a greater deflection than only one times the Earth's radius. For example, 83% of the asteroids are deflected more than ten times the Earth's radius.

It should be noted that in 6 of the 888 cases the deflection came out negative, i.e. the asteroid came closer to Earth, no matter whether the asteroid was accelerated or decelerated along it's velocity vector. Upon closer examination the cause of this was that initially the deflection was effective, but due to the deflection the asteroid would return to Earth at a later date and make a closer approach. Nevertheless, in these cases it would likely be possible to circumvent this problem by simply deflecting it a bit less. Actual deflection must thus be carefully examined on a per asteroid basis to make sure this problem does not occur. It is also likely that some other asteroids had this problem resulting in a lower deflection value, albeit not negative, then actually achieved. Thus, actual deflections could be higher and the system would then be able to deflect more than 97% and 83% of the asteroids with a distance of one and ten times the Earth's radius respectively. For all manually reviewed cases where this problem occurred, the asteroid was actually deflected extremely large amounts.

A visualization of the above mentioned problem, in which the deflection is underestimated, is given in Figure 18.3. The blue dot is Earth, the gray dot is the undeflected asteroid and the green and purple dots are the asteroid deflected along and against its velocity vector respectively. In Figure 18.3a, the moment of closest

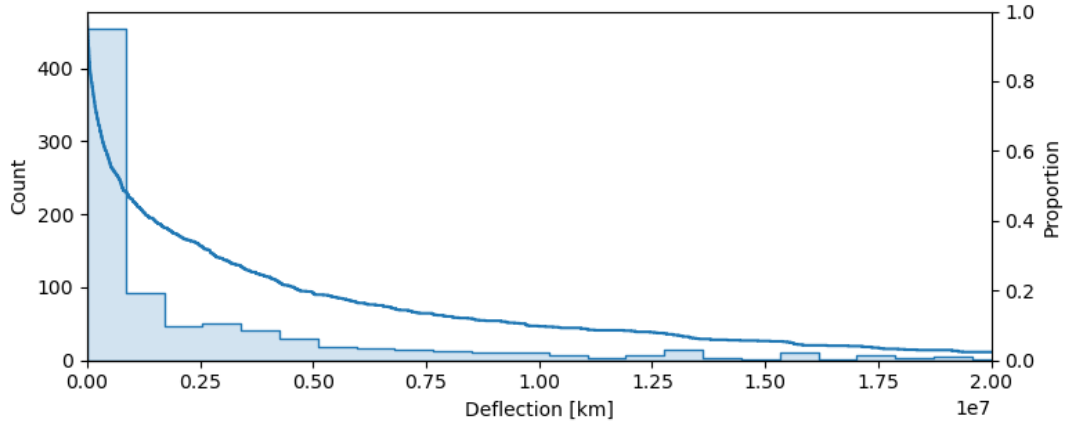

(a) Full histogram

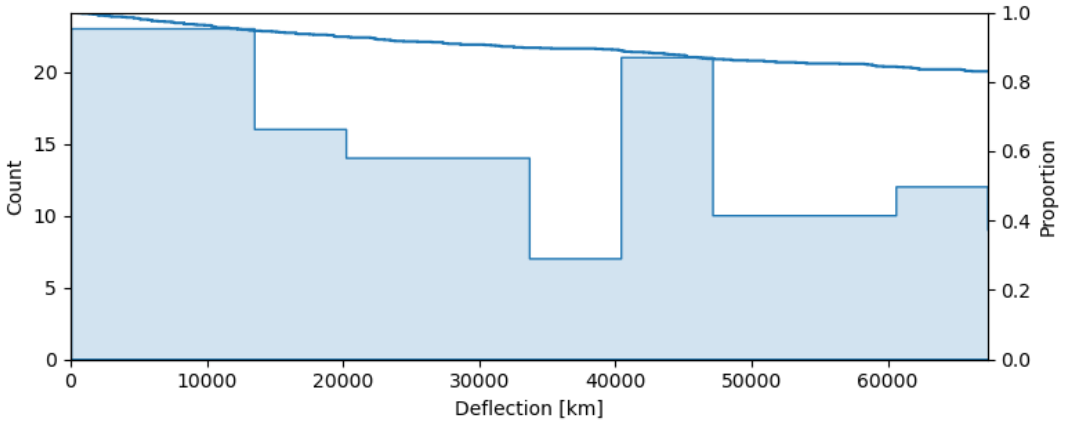

(b) Zoomed in on deflections of $0 - 10$ times the Earth's radius

Figure 18.2: Deflection distance of known asteroids

approach of the undeflected asteroid can be seen. Note that the asteroids where the system is applied are both extremely deflected. Figure 18.3b gives the situation about a month earlier, here the asteroid that was accelerated along it's velocity vector makes an approach closer than the undeflected asteroid does. Figure 18.3b gives the situation about a month later, here the asteroid that was accelerated against it's velocity vector makes an approach closer then the undeflected asteroid does. The result is a seemingly lower deflection than the actual case.

18.2.2 Trends from known asteroids

While being able to deflect most known asteroids that come close to Earth is a great achievement, most of these asteroids are unlikely to actually impact Earth in our time frame. It are the currently unknown asteroids that can form a real danger to Earth. As such, it is desired that one could quickly see whether the system would be a good candidate for the deflection at the moment an asteroid on collision course with Earth is discovered. This section hopes to find trends from the deflection of known asteroids, so a general idea of what type of asteroids can be deflected can be formed. Please note that, while it should be clear from the results, the actual deflection can vary extremely from these trends and thus they should only be taken as a general impression rather then drawing any conclusions from them.

Figure 18.4 shows the deflection of known asteroids plotted against their absolute magnitude. Exponential trend lines are added, these are $y = 3.9953 \cdot 10^{-4} \cdot e^{0.8542 \cdot x}$ and $y = 7.8420 \cdot 10^{-11} \cdot e^{1.4596 \cdot x}$ for 1 year and 0.5 years of deflection respectively. It is clear from the figure that the actual deflection values can vary greatly with even some large asteroids (low absolute magnitude) being deflected for distances far greater than the trend line indicates.

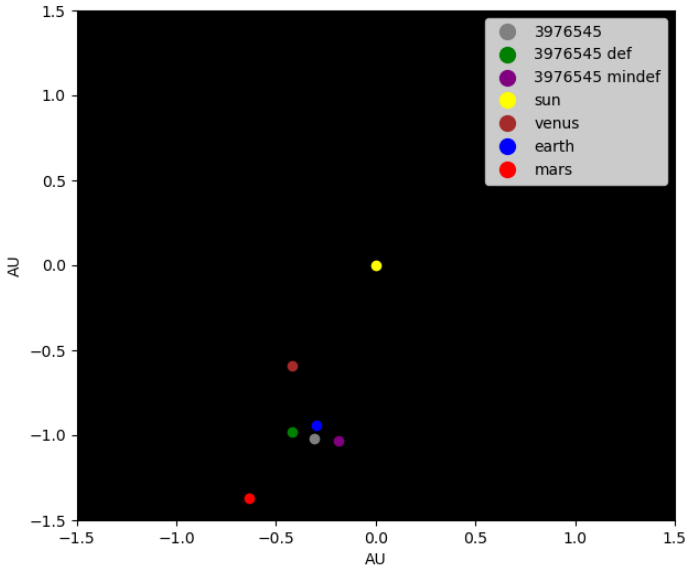

(a) Closest approach of the undeflected asteroid

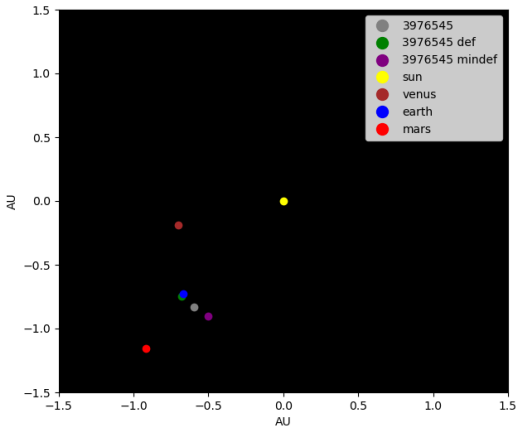

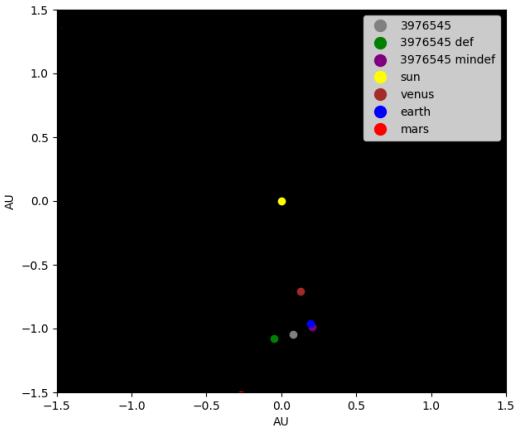

(b) Closest approach of the asteroid deflected along it's velocity vector (c) Closest approach of the asteroid deflected along it's velocity vector

Figure 18.3: A visualization of the underestimation of the deflection: closest approaches of the asteroid 3976545

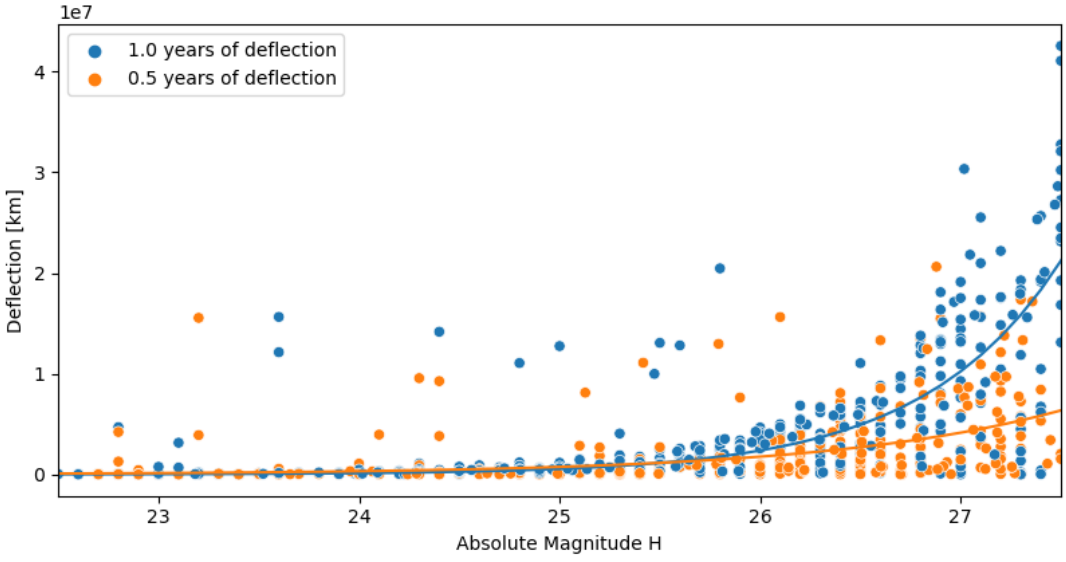

Figure 18.4: The deflection of known asteroids plotted against their absolute magnitude for both 1 year and 0.5 years of deflection

Figure 18.5 shows the deflection of known asteroids plotted against their specific orbital energy and their semi-major axis. From Figure 18.5a, it is clear that the best candidates for deflection have an semi major axis similar to that of Earth, i.e. around $0.5 - 1.5$ $[AU]$. Specific orbital energy is calculated according to Equation 18.4. Here ϵ is the specific orbital energy, G is the gravitational constant, a is the semi major axis of the orbiting bodies and m_s and m_a are the masses of the Sun and the asteroid respectively. As the mass of the Sun is far greater than the mass of the asteroids, the specific orbital energy is largely determined by the semi-major axis. So, similar results are observed as in Figure 18.5a, where the best candidates for deflection have a specific orbital energy similar to that of Earth.

$$\epsilon = \frac{G(m_s + m_a)}{2 \cdot a} \tag{18.4}$$

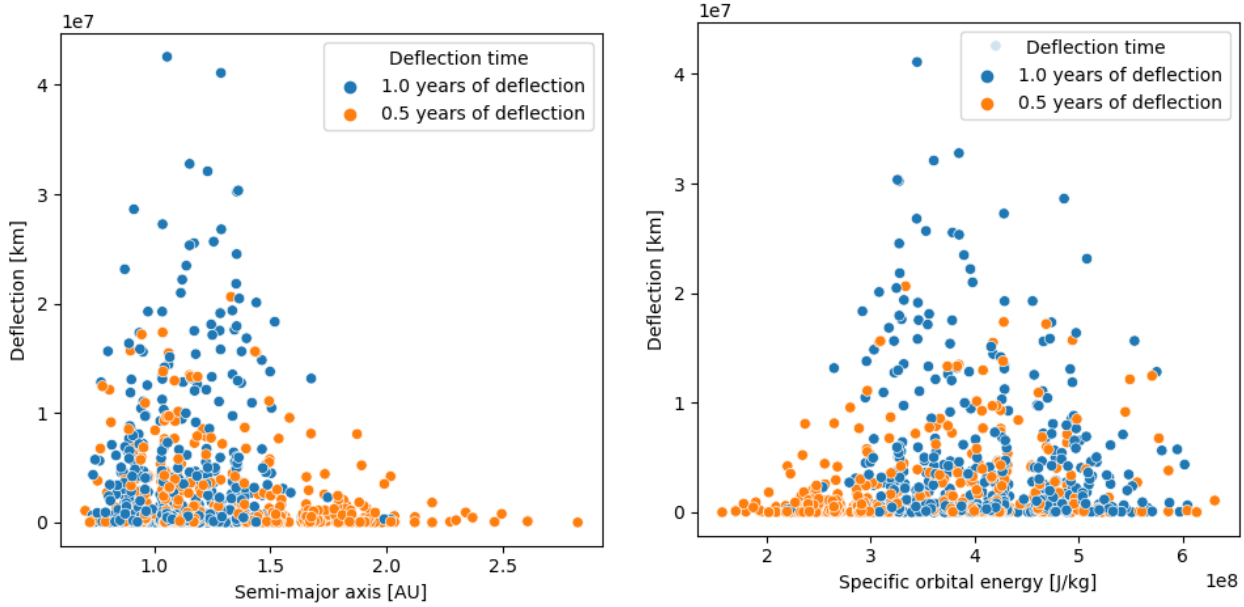

(a) The deflection of known asteroids plotted against their semi-major axis

(b) The deflection of known asteroids plotted against their specific orbital energy

Figure 18.5: The deflection of known asteroids plotted against their specific orbital energy and their semi-major axis

Figure 18.6 shows the deflection of known asteroids plotted against their orbital eccentricity for both 1 year and 0.5 years of deflection. Perhaps somewhat surprising is that the best candidates for deflection seem to have an eccentricity between 0.1 and 0.4, Somewhat circular orbits with a relatively low eccentricity are thus suitable for deflection but near circular orbits with extremely low eccentricity are less so. Unsurprising is that highly elliptical orbits with high eccentricities are harder to deflect. This is most likely caused by the high velocity the asteroids arrive at if their semi-major axis is larger than 1 $[AU]$, which is the case for almost all highly elliptical asteroids discovered.

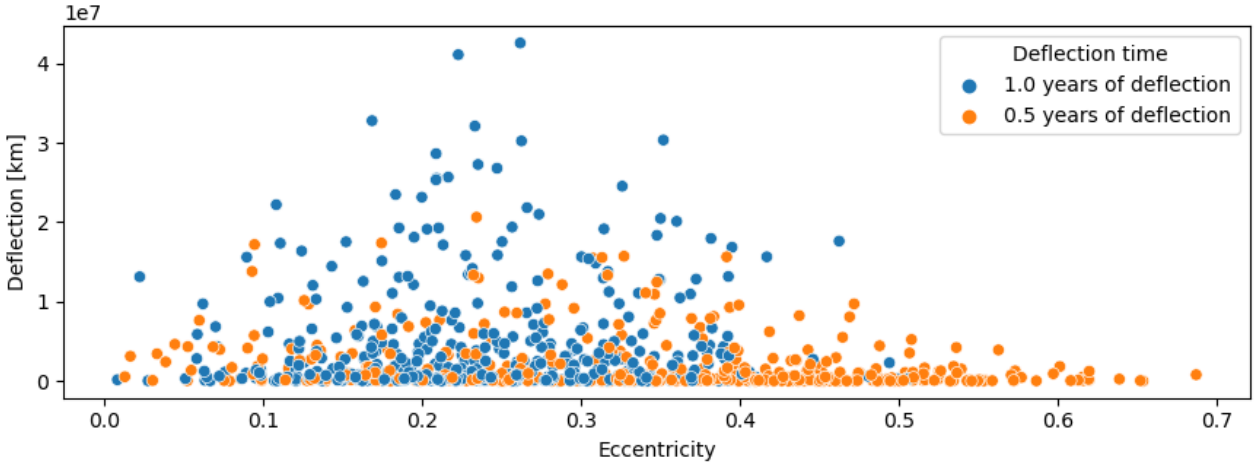

Figure 18.6: The deflection of known asteroids plotted against their orbital eccentricity for both 1 year and 0.5 years of deflection

Figure 18.7 shows the deflection of known asteroids plotted against their orbital inclination for both 1 year and 0.5 years of deflection. The inclination is relative to the plane of the Earth's orbit, so $0\,\mathrm{deg}$ means the asteroid's orbit is not inclined at all relative to the Earth's. The graph shows that asteroids with higher inclination are harder to deflect.

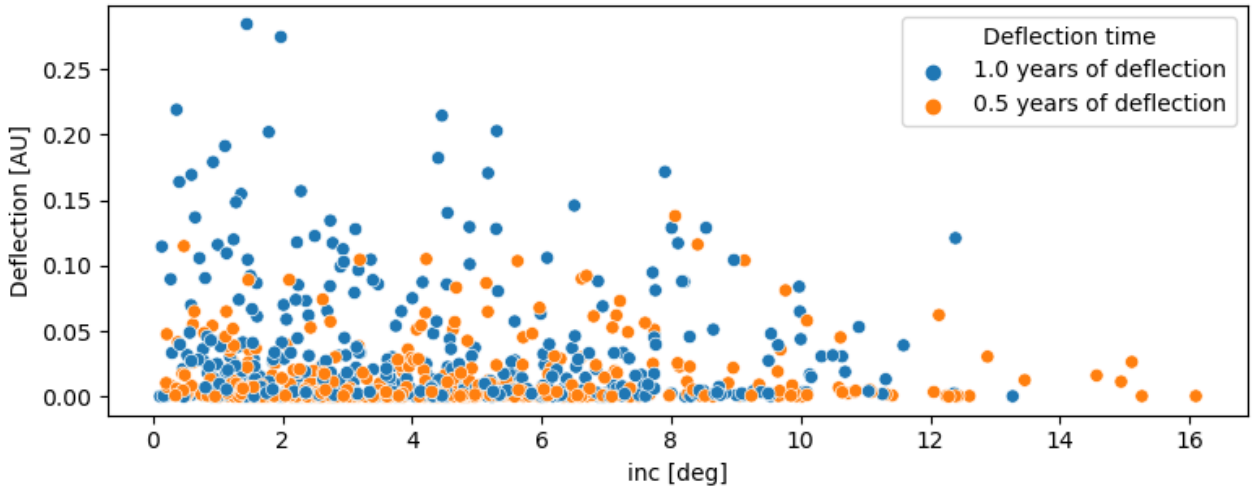

Figure 18.7: The deflection of known asteroids plotted against their orbital inclination for both 1 year and 0.5 years of deflection

It is worth noting that all of these deflections are relative to the undeflected close approach distance of the asteroid. That is, the distance the asteroid would be from the Earth at its closest approach if it were not deflected. However, none of these asteroids are on a collision course with the Earth, so they all have an undeflected close approach distance greater than $0\ [km]$. It is worth checking to make sure that this performance data will still hold for asteroids that are on a collision course. Figure 18.8 shows the deflection of known asteroids plotted against their undeflected close approach distance for 1 year and 0.5 years of deflection. The data points are randomly scattered, and there is clearly no correlation between the deflection and undeflected close approach distance. This means that this performance data will still hold for a hypothetical asteroid that is on a collision course with the Earth.

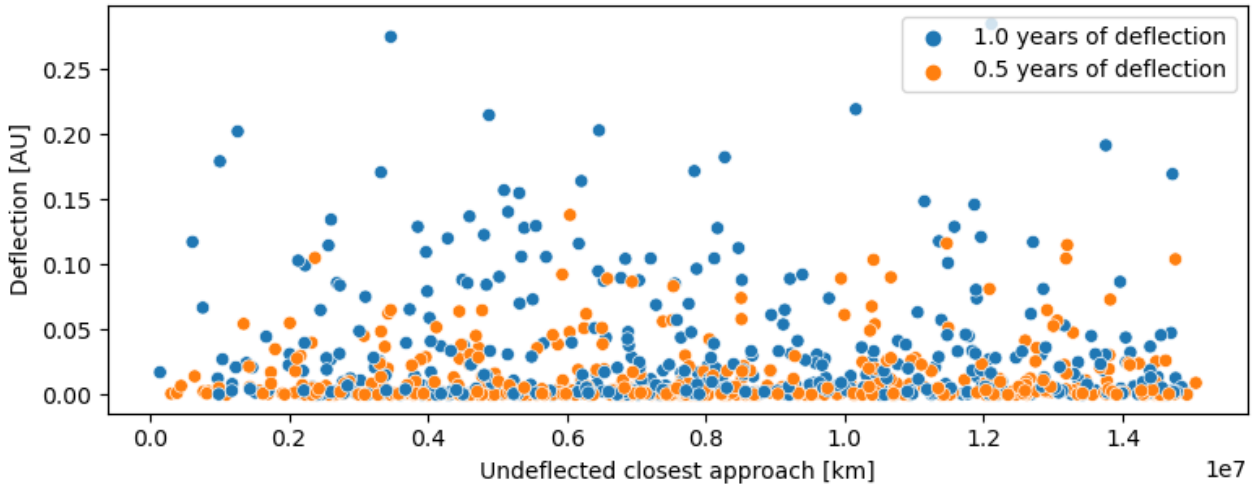

Figure 18.8: The deflection of known asteroids plotted against the undeflected close approach distance for both 1 year and 0.5 years of deflection

In conclusion, asteroids with low eccentricity, low inclination, an Earth like semi-major axis, and a small size are easier to deflect. However, measure of deflection can vary extremely per asteroid and thus these "rules of thumb" can only be described as inaccurate at best. If an asteroid is discovered it should be simulated to see its actual deflection. Additionally, large deflections are usually not needed as the asteroid only needs to miss Earth which has a relatively small radius of only $6731\ [km]$.

18.3 Overview of deflection chances

This section aims to give a quick overview of the chance of deflecting an asteroid and can be found in Table 18.1. The chances come from analysis of the database of known asteroids with data taken for all asteroids within the relevant size limit (an absolute magnitude of $22.5 < H < 27.5$, which roughly translates to $10 - 100$ $[m]$ in diameter), with a MOID with Earth of less than 0.05 $[AU]$ and a close approach within the years $2030 - 2040$. Please note that a lot of assumptions had to be made, thus the chances are inaccurate and should only serve as an indication. Often assumptions were made to be more limiting rather than less limiting and due to the deflection underestimation described in Subsection 18.2.1, one could expect the actual chances of deflecting an asteroid to be higher. Finally, having a longer period to reach the asteroid would greatly increase the amount asteroids that are reachable.

Table 18.1: Chance of successful deflection of asteroid

Event	**Chance [%]**	**See**
Asteroid is reachable within 1.5 years	47.9	Section 7.2
Successful rendezvous and deployment	96.59	Section 14.1.1
Deflection of at least one Earth radius	97	Subsection 18.2.1
Deflection of at least ten Earth radii	83	Subsection 18.2.1
Total		
Deflection of at least one Earth radius	45	
Deflection of at least ten Earth radii	38	
Generally higher success chance if		
Absolute magnitude is	larger	Subsection 18.2.2
Semi-major axis is	Earth like	Subsection 18.2.2
Eccentricity is	lower	Subsection 18.2.2
Inclination is	lower	Subsection 18.2.2

19 Conclusion and Recommendations

19.1 Conclusion

This report has presented the detailed design of an asteroid deflection system consisting of a swarm of solar concentrator spacecraft. The swarm will contain a total of 32 spacecraft. Each spacecraft will be equipped with a $60\ [m]$ radius parabolic primary reflector, which will reflect sunlight onto a collimator. This will collimate the light and reflect it to a flat secondary reflector. The secondary reflector will then aim the beam of light onto the asteroid. This will heat up the asteroid and cause sublimation, which will produce thrust to redirect the asteroid.

The spacecraft does not expose the primary reflector to the ejecta, preventing its degradation. The secondary reflector will be actively cleaned using an electrodynamic screen to maintain a high efficiency. This optical arrangement combined with the active cleaning is a novel solution to solar concentrator design.

A single kickstage is used to transport the swarm to a threatening asteroid. In this case the upper stage of the SpaceX Starship is used, which is able to impart a ΔV of $8\ [km/s]$ from LEO. This performance allows the system to reach an estimated 29.8% of NEA at least one year before a potential impact and a further 18.1% at least half a year before a potential impact, when the asteroid is detected two years prior to impact. However, for asteroids detected further in advance, more optimal transfers may be used, allowing to reach more of the asteroids. This means it is of utmost importance to continue on programs scanning for NEA, so that threatening asteroids can be found in time.

Upon rendezvous, the system can move the closest approach distance of 97% of the asteroids at least one Earth radius away, meaning successful deflection. The system can be said to be characterized by a 45% effectiveness at deflecting asteroids $10 - 100\ [m]$ in size when detected two years before a potential impact. However, further simulations and sensitivity analysis should be done on this performance envelope to account for the large degree of uncertainty in asteroid mass and orbits.

This design will hopefully be useful for continued research into asteroid deflection. This represents a completely novel concept for rapid deflection of small asteroids. Continued research into this field may prove crucial in preventing a future impact. This system can easily be scaled up by adding additional spacecraft to the swarm, allowing deflection of larger targets. With the invention of larger, more efficient launch vehicles, the system may be able to reach even more asteroids within time. Solar concentrators of this type may also prove useful for other applications such as space-based solar power or de-orbiting of space debris, and researchers should continue to investigate such opportunities.

19.2 Recommendations

In order to continue the development of this project, several recommendations were generated in order to detail some areas that required further development. These recommendations detail not only several recommendations to refine the subsystem designs, but to also expand upon the concept of asteroid redirection as a whole. With the mission implementation of this concept being the most important aspect of this project. Further testing would have to be conducted on the general physics behind what makes this concept feasible. This includes tests to determine the physical properties of asteroids, optical models and tests, ejecta modeling and structural tests. This collection of actions and tests would help bring this asteroid redirection concept to a better level of resolution, so as to improve not only the technology readiness levels of the concept, but to also gain important knowledge on the physical characteristics of asteroids as well.

With this asteroid redirection concept revolving around the physics and physical properties of asteroids, it is important to gather as much information in these fields as possible. The physics surrounding the heat transfer between the sunlight beam and the asteroid material would have to be examined, as well as the mass flow of material generated through the variation in sizing of the sunlight spot on the asteroid. A solar oven is then used to create similar conditions as would exist on the surface of the asteroid. After this environment is generated, the sublimation characteristics of lunar regolith and asteroid dust are analyzed and compared to the same characteristics of rocks of differing compositions sourced on Earth. In order to check the validity and applicability

of these tests, further asteroid observations are also required to determine the composition of target asteroids with more precision.

Tests involving the feasibility of the solar reflector optics used in the concept are also necessary. This starts with the creation of a more accurate model, which can be done with proper optical analysis of the mirrors proposed, particularly through the use of non-classical treatments and Fourier optics models. This modeling then leads to a better optimized sizing of the reflectors used in the concept. Ray-tracing technology can also be used to further realize the concept, as it would lead to a model of a more realistic light envelope. After this is modeled, engineering models are required to be produced so as to test the real world outcomes of the optical system. These test would have to be conducted in laboratories and space to produce applicable results.

Further ejecta modeling is also required, as it poses a large threat to the efficiency of the system. This can be done by first creating a better ejecta cone model. Once this is done, further real life tests can be conducted to observe the sorts of ejecta paths that take shape in a vacuum and in zero-g environments. Tests are also required to see how this ejecta is deposited on the mirrors as well as how it moves around the primary reflector if it is facing away from the asteroid.

Due to the complexity of the structural components involved in the SHARD system, a more detailed analysis must be performed on each individual complex component. With verification that each component meets the necessary rigidity and strength, based on the critical loads, the entire system should then be analyzed. This is to ensure that the interaction between the structural components interfaces are not detrimental to the overall system performance. For clarity, the main components of interest are the Deployable Mast, Primary Reflector Deployable Structure, Collimator & Secondary Reflector Deployable Structure. In terms of performed analysis, it would be similar to the approach given in Chapter 13 for the Front Mast. First, the critical loads on the given sub-structure are determined, followed by a structural and vibrational analysis for an idealized version of the sub-structure. Once it is verified that it withstands the given loads or frequencies and the necessary adjustments are made to support the structure, a detailed version of the design should be analyzed. This iterative process would be applied to all the stated main components, after which a full system analysis can be performed. This of course only proves the concept structures in theory; real-life tests and experiments would follow to validate the results of the calculations. For example, in launch configuration, the undeployed structures could be tested for launch vibrations using ESA ESTEC's Electrodynamic Shakers [1]. Following these tests, clear optimizations to the sub-structures may surface, which could help to lower the overall spacecraft weight. This can only be determined through future activity, after the DSE.

Structural tests are also necessary as these large space structures have only been tested in lab conditions and have also never been applied in combination with one another. Further tests are necessary to see how the shape of the reflector sheet can be held when it is stationary, when it experiences translational, and rotational motions. The folding mechanics also require zero gravity testing, as testing on Earth would result in a torn mirror due to the overall loading, thus preventing proper testing. Tests are also required to check the overall mechanics of the expandable structures to be used in general. These tests would have to be conducted numerous times in order to certify the function of the most mechanical portions of the system. The deployment sequence requires multiple test runs as well in order to make sure the expandable structures are reliable. Since the primary reflector is held open by a system of cables, these cables also require further testing to determine the proper deployment procedures for the system so as not to allow for any deployment issues to occur.

Aside from this set of tests and models, comparisons to alternate methods are still required, such as a deeper investigation into the usage of laser systems as opposed to collimator systems in order to reduce the amount of complexity in the deployment system. A risk assessment on a component level is also required. This assessment would be done through the use of Probalisitc Risk Assessment. However, Before this entire design and test phase begins, a call to the Space Situational Awareness team at ESA is necessary as a first step. This conversation could be conducted as a way to gain more knowledge on the asteroids that pose a potential threat to the Earth.

As for specific subsystems such as the Communications and Data Handling, Thermal Control and Electrical Power Systems, further design research would help to apply novel solutions. As oppose to generic telemetry methods, a novel application of laser communication between the spacecraft swarm can be applied. It is currently under research by a TU Delft Aerospace Master's student: Joshua Spaander, who was kind enough to give the relevant team members insight into his research and findings. Furthermore, it is believed that more

[1] URL `https://www.esa.int/Enabling_Support/Space_Engineering_Technology/Test_centre/Electrodynamic_shakers` [accessed 26 January 2021]

intelligent methods can be used for data recognition and how it is handled in terms of what is transmitted back to earth. As for the Thermal Control System, a better understanding of the environment the spacecraft swarm will be subjected to is needed. The magnetic fields, high energy particles and radiation levels greatly influence the necessary shielding which is required for the housing units, in order for the system to operate correctly. Therefore, given the systems operational parameters, an in-depth study can reveal the steps needed to protect the spacecraft optimally from the harsh space environment.

The ADCS subsystem requires some extra research and testing in order to be fully integrated with the concept as a whole. Extra modeling is also required so as to check the results found within this report. These models include checking the dynamics of different reaction wheel configurations such as a tetrahedral configuration compared to the chosen three axis configuration. After this modeling has taken place, materials tests for the reaction wheel bearings can be conducted. This test regime notably includes durability tests of ceramic bearings as this type of bearing was found to not only improve durability, but also improve momentum storage capabilities [6]. As for the thrusters used within the ADCS system, the creation of a dynamic model is required to better understand the forces generated on the system when presented with certain position changes. Physical testing is also necessary in order to see the physical effects of exhaust plume impingement on the systems in order to assess the overall severity of this occurring due to the tight packing of the systems.

Overall, the threat of an asteroid impact still looms, yet the public has little understanding of how serious of an issue this actually is. This can be solved by raising the awareness of the public to this issue through the use of publicity campaigns. This may also offer some return on investment in the form of not only an increase in public knowledge on the topic, but also in the form of better funding for asteroid redirection projects as well. Furthermore, locating potentially hazardous asteroids is also an issue. This can be addressed through the creation of a Cubesat swarm, which can be sent out beyond Earth's gravitational sphere of influence towards the asteroid belt (located between the Earth and Mars) to better image and locate potential redirection candidates. This swarm could also be sent inward in order to better image asteroids with orbits closer to the Sun than the Earth. This would allow for a much more advanced sensitivity analysis on the performance envelope. This will allow for a better understanding of the system capabilities and thus improve the level of confidence about what it can achieve.

One limitation to the overall spacecraft swarm system is the launcher capabilities available. Due to the strict time-frame for redirecting asteroids, it is necessary to be able to deliver the entire system to its operational position as quickly as possible. Therefore, achieving this in one launch is ideally necessary for the operation, in the sense of performance as well as sustainability. Which brings this discussion to a final point: the end-of-life disposal strategy. This was a necessary requirement stated by the stakeholder, as the mission philosophy is geared towards a sustainable one. For this, there are the two considered scenarios stated in Chapter 17. One is where after a successful asteroid deflection, the swarm cannot be recovered. Whereas the second scenario, where the systems have not been used for their intended purpose, can be operated to de-orbit space debris or a space-based solar power system. These options offer a promising and sustainable utilization of the system, therefore would be researched after the DSE. The spacecraft swarm system offers a variety of opportunities, the biggest being asteroid deflection, as it's design raises the benchmark on sustainable applications across the solar system.

Bibliography

[1] K Anflo, S Moore, and P King. Expanding the adn-based monopropellant thruster family. In *23rd Annual AIAA/USU conference on Small Satellites*, 2009.

[2] Anomet. Fine aluminum surfaces: Interior non-corrosive applications. Data Sheet Anomet Standard 2020, Anomet, 2020.

[3] Amir Anwar-Hameed, Zachary Burr, Luke Chin A Foeng, Pieter de Lange, Nicolaas Petit dit de la Roche, Andres Sanders, Nathaniel Stebbins Dahl, Tijn van Eil, and Lukas Welzel. *Baseline Report: Save the Earth from Asteroids*. Faculty of Aerospace Engineering, TU Delft, Delft, The Netherlands, nov 2020.

[4] Amir Anwar-Hameed, Zachary Burr, Luke Chin A Foeng, Pieter de Lange, Nicolaas Petit dit de la Roche, Andres Sanders, Nathaniel Stebbins Dahl, Tijn van Eil, and Lukas Welzel. *Mid-Term Report: Save the Earth from Asteroids*. Faculty of Aerospace Engineering, TU Delft, Delft, The Netherlands, dec 2020.

[5] Amir Anwar-Hameed, Zachary Burr, Luke Chin A Foeng, Pieter de Lange, Nicolaas Petit dit de la Roche, Andres Sanders, Nathaniel Stebbins Dahl, Tijn van Eil, and Lukas Welzel. *Project Plan: Save the Earth from Asteroids*. Faculty of Aerospace Engineering, TU Delft, Delft, The Netherlands, nov 2020.

[6] William Bialke and Eric Hansell. A newly discovered branch of the fault tree explaining systemic reaction wheel failures and anomalies.

[7] Julio Chaves Brian J. Thompson et al. *Introduction To Nonimaging Optics*. Optical Science And Engineering. CRC Press, 2008.

[8] Michael A. Brown. A deployable mast for solar sails in the range of 100–1000 m. *Advances in Space Research*, 48:1747–1753, jan 2011.

[9] Nichols F. Brown and Timothy P. Anderson. Learning rate sensitivity model. Technical report, ICEAA, 2018.

[10] Jared T. Bruton, Todd G. Nelson, Trent K. Zimmerman, Janette D. Fernelius, Spencer P. Magleby, and Larry L. Howell. Packing and deploying soft origami to and from cylindrical volumes with application to automotive airbags. *Royal Society Open Science*, 3(9), Sep 2016. doi: 10.1098/rsos.160429.

[11] Carlos Calle, M.K. Mazumder, C.D. Immer, C.R. Buhler, J. Clements, P. Lundeen, A. Chen, and João Mantovani. Electrodynamic dust shield for surface exploration activities on the moon and mars. *AIAA 57th International Astronautical Congress, IAC 2006*, 2006.

[12] C.I. Calle, C.R. Buhler, J.L. McFall, and S.J. Snyder. Development of an active dust mitigation technology for lunar exploration. *AIAA SPACE 2008 Conference & Exposition*, 2008.

[13] C.I. Calle, C.R. Buhler, J.L. McFall, and S.J. Snyder. Particle removal by electrostatic and dielectrophoretic forces for dust control during lunar exploration missions. *Journal of Electrostatics*, 2009.

[14] C.I. Calle, C.R. Buhler, M.R. Johansen, M.D. Hogue, and S.J. Snyder. Active dust control and mitigation technology for lunar and martian exploration. *Acta Astronautica*, 2011.

[15] G. Camino, S. M. Lomakin, and M. Lazzari. Polydimethylsiloxane thermal degradation part 1. kinetic aspects. *Polymer*, 42(6):2395 – 2402, 2001.

[16] Carlos Jorge Rodrigues Capela. Protocol of communications for vorsat satellite - link budget. Master's thesis, Universidade do Porto, apr 2012.

[17] Carlos Jorge Rodrigues Capela. Protocol of communications for vorsat satellite - transmission losses. Master's thesis, Universidade do Porto, apr 2012.

[18] B. Carry. Density of asteroids. *Planetary and Space Science*, 73, 2012.

[19] Jean-Francois Castet and Joseph H. Saleh. Satellite and satellite subsystems reliability: Statistical data analysis and modeling. *Reliability Engineering and System Safety*, 94:1718–1729, 2009. doi: 10.1016/j.ress.2009.05.004.

[20] Daniel Cavender. Emerging low toxicity “green” chemical propulsion technologies for smallsats, 9 2020. Online Webinar.

[21] A. Cervone and B.T.C. Zandbergen. Ae2230-ii: Propulsion and power. electrical power systems for aerospace vehicles. Technical report, Faculty of Aerospace Engineering, TU Delft., 2017.

[22] B. Cook, M. Dennis, S. Kayalar, J. Lux, and N. Mysoor. Development of the advanced deep space transponder. *Interplanetary Network Progress Report*, 1(1):1–41, feb 2004.

[23] Barry M. Cook and Paul H. Walker. Low-latency packet delivery in spacewire networks. *Networks and Protocols*, 1, sep 2011.

[24] N.H. Crisp, K. Smith, and P. Hollingsworth. Launch and deployment of distributed small satellite systems. *Acta Astronautica*, 114:65 – 78, 2015. ISSN 0094-5765. doi: https://doi.org/10.1016/j.actaastro.2015.04.015.

[25] Airbus Defence and Space:. Space equipment payload products: Ssr solid state recorders for space applications. Data Sheet SPE-DS-SSR, Airbus Defence and Space, apr 2018.

[26] Rockwell Collins Deutschland. Rsi 68 momentum and reaction wheels 14 – 68 nms with integrated wheel drive electronics. Technical Report 147-0717-000-GS 06/07, Rockwell Collins, 2007.

[27] Buwaneth Y. Dharmadasa, H.M.Y. C. Mallikarachchi, and Francisco Lopez Jimenez. Characterizing the mechanics of fold-lines in thin kapton membranes. In *2018 AIAA Spacecraft Structures Conference*, 2008. doi: 10.2514/6.2018-0450.

[28] Simulink Documentation. Simulation and model-based design, 2020.

[29] M. J. Downey. Satellite reliability. *Microelectronics Reliability*, 9(3):271–282, 1970. doi: doi.org/10.1016/0026-2714(70)90115-0.

[30] DuPoint. DuPoint Kapton PST Polyimide Film. Technical Report EI-10150, DuPoint, 2020.

[31] Bradford Engineering. Fine sun sensor. Technical report, Bradford Engineering, jan 2017.

[32] C. Escolle, V. Michau, M. Ferrari, T. Fusco , and E. Hugot. Misalignment estimation for active telescopes. *CEAS Space Journal*, 11:553–559, 2019. https://doi.org/10.1007/s12567-019-00272-w.

[33] Juan M. Fernandez. Advanced deployable shell-based composite booms for small satellite structural applications including solar sails. Conference Paper (International Symposium on Solar Sailing 2017) NF1676L-25486 (NTRS: 201700015699, NASA, jan 2017.

[34] Robert L. Forward. Statite - a spacecraft that does not orbit. *Journal of Spacecraft and Rockets*, 28(5): 606–611, 1991. doi: 10.2514/3.26287.

[35] Susie Go, Scott L. Lawrence, Donovan L. Mathias, and Ryann Powell. Mission success of u.s. launch vehicle flights from a propulsion stage-based perspective: 1980-2015. Technical Report NASA/TM-2017-219497, NASA, apr 2017.

[36] Joseph W. Goodman. *Introduction to Fourier optics*. Roberts and Co., 2005. 0974707724.

[37] Jian Guo. *Project Guide Design Synthesis Exercise Save the Earth from Asteroids*. Faculty of Aerospace Engineering, TU Delft, Delft, The Netherlands, Nov 2020.

[38] Yacov Y. Haimes. *Risk Modeling, Assessment and Management*. Systems Engineering and Management. Wiley, third edition, 2009.

[39] Joseph Haring and Natalie Pastuszka. CPC Essentials: Design Considerations For Compound Parabolic Concentrators. Design report, optiforms, 2015.

[40] Wei He, Philippe Goudeau, Eric Le Bourhis, Pierre-Olivier Renault, Jean Christophe Dupré, Pascal Doumalin, and Shibin Wang. Study on young’s modulus of thin films on kapton by microtensile testing combined with dual dic system. *Surface and Coatings Technology*, 308:273 – 279, 2016. ISSN 0257-8972. doi: https://doi.org/10.1016/j.surfcoat.2016.07.114. The 43rd International Conference on Metallurgical Coatings and Thin Films.

[41] Hennes Henniger and Otakar Wilfert2. An introduction to free-space optical communications. *Radioengineering*, 19(2), jun 2010.

[42] Sighard F. Hoerner. *Fluid Dynamic Drag*. Sighard F. Hoerner, 2 edition, 1965.

[43] R.E. Hummel. Reflectivity of silver- and aluminium-based alloys for solar reflectors. *Solar Energy*, 27(6): 449 – 455, 1981. ISSN 0038-092X. doi: https://doi.org/10.1016/0038-092X(81)90040-2.

[44] Muhammad Iqbal. *An Introduction To Solar Radiation*. Science. Elsevier, dec 2012.

[45] M. Ireland and J. Gonzales. Bayesian reliability analysis with slice sampling in launch vehicle applications. In *2020 Annual Reliability and Maintainability Symposium (RAMS)*, pages 1–6, 2020. doi: 10.1109/RAMS48030.2020.9153710.

[46] Shahrokh Jalilian, Fatemeh SalarKaleji, and Tofig Kazimov. Fault detection, isolation and recovery (fdir) in satellite onboard software. In *Proqram mühəndisliyinin aktual elmi-praktiki problemləri*, pages 329–332, 05 2017. doi: 10.25045/NCSoftEng.2017.87.

[47] Ralph Kahle, Ekkehard Kührt, Gerhard Hahn, and Jörg Knollenberg. Physical limits of solar collectors in deflecting earth-threatening asteroids. *Aerospace Science and Technology*, 10(3):256 – 263, 2006. ISSN 1270-9638. doi: https://doi.org/10.1016/j.ast.2005.12.004.

[48] Hiromitsu Kumamoto and E. J. Henley. *Probabilistic Risk Assessment and Management for Engineers and Scientists*. IEEE Press, second edition, 1996.

[49] S. Kumar, D. Sahay, S. R. Hegde, S. Sandya, A. K. Jha, and T. C. Mahalingesh. Design and development of 3-axis reaction wheel for studsat-2. In *2015 IEEE Aerospace Conference*, pages 1–13, 2015. doi: 10.1109/AERO.2015.7119181.

[50] Ralf Leutz and Akio Suzuki. *Nonimaging Fresnel Lenses: Design and Performance of Solar Concentrators*, volume 83 of *Springer Series in Optical Sciences*. Springer-Verlag Berlin Heidelberg, first edition, 2001.

[51] Takashi Lida and Hiromitsu Waken. *Communications Satellite Systems*. Encyclopedia of Physical Science and Technology. Elsevier, third edition, jan 2003.

[52] Michael Locke, Mariusz Czarnomski, Ashraf Qadir, Brock Setness, Nicolai Baer, Jennifer Meyer, and William H. Semke. High-performance two-axis gimbal system for free space laser communications onboard unmanned aircraft systems. In Hamid Hemmati, editor, *Free-Space Laser Communication Technologies XXIII*, volume 7923, pages 141 – 148. International Society for Optics and Photonics, SPIE, 2011. doi: 10.1117/12.873938.

[53] Seamus Lombardo and John Crassidis. A low-cost method for reaction wheel torque characterization in small satellites. In *A Low-Cost Method for Reaction Wheel Torque Characterization in Small Satellites*, 2016.

[54] M Louwerse, H.V. Jansen, M Groenendijk, and M. Elwenspoek. Nozzle fabrication for micropropulsion of a microsatellite. *Journal of Micromechanics and Microengineering*, 19:045008, 03 2009. doi: 10.1088/0960-1317/19/4/045008.

[55] Preston R. MacDiarmid and John J. Bart. *Reliability Toolkit: Commercial Practices Edition - A Practical Guide for Commercial Products and Military Systems Under Acquisition Reform*. Reliability Analysis Center, jan 1988.

[56] Tapas K. Mallick, Philip C. Eames, and Brian Norton. Non-concentrating and asymmetric compound parabolic concentrating building façade integrated photovoltaics: An experimental comparison. *Solar Energy*, 80(7):834 – 849, 2006. ISSN 0038-092X. doi: https://doi.org/10.1016/j.solener.2005.05.011.

[57] David Manzella. Low cost electric propulsion thruster for deep space robotic missions. Technical report, NASA Glenn Research Center, 2007.

[58] Doug May. Amsat phase IV propulsion and attitude control systems conceptual design. Technical report, Thiokol Corporation, 1989.

[59] David Miller. Space systems cost modeling. Technical report, Massachussets Institute of Technology, 2018.

[60] Y. Miyazaki. Deployable techniques for small satellites. *Proceedings of the IEEE*, 106(3):471–483, 2018. doi: 10.1109/JPROC.2018.2799608.

[61] John Moery. Development of robust thermo-optical thin-film membranes for the James Webb Space Telescope sunshield. In John C. Mather, Howard A. MacEwen, and Mattheus W. M. de Graauw, editors, *Space Telescopes and Instrumentation I: Optical, Infrared, and Millimeter*, volume 6265, pages 1086 – 1095. International Society for Optics and Photonics, SPIE, 2006. doi: 10.1117/12.672343.

[62] A. Mostafa, M. I. El-Saftawy, Elbaz I. Abouelmagd, and Miguel A. López. Controlling the perturbations of solar radiation pressure on the lorentz spacecraft. *Symmetry*, 12(9):1423, Aug 2020. ISSN 2073-8994. doi: 10.3390/sym12091423.

[63] Mahajan V. N. *Optical Imaging and Aberration: Ray Geometrical Optics*, volume 1. Издательство SPIE Press, 1998.

[64] Khashayar Khorasani Nader Meskin. *Fault Detection and Isolation: Multi-Vehicle Unmanned Systems*. Springer Science+Business Media, 2011.

[65] B. Norton and D. E. Prapas. *Thermal Analysis of Compound—Parabolic Concentrating Solar Energy Collectors*, pages 109–135. Springer Netherlands, Dordrecht, 1987. ISBN 978-94-009-3939-4. doi: 10.1007/978-94-009-3939-4_6.

[66] E. E. Ortelli, F. Geiger, T. Lippert, J. Wei, and A. Wokaun. UV-Laser-Induced Decomposition of Kapton Studied by Infrared Spectroscopy. *Macromolecules*, 33(14):5090–5097, jun 2000.

[67] Bo Pan, Shuyang Zhang, Lin Li, Fanxin Sun, and Yongqiang He. Development of an integrative pointing gimbal mechanism for space application. In Bo Huang and Yufeng Yao, editors, *Proceedings of the 5th International Conference on Electrical Engineering and Automatic Control*, pages 817–826. Springer Berlin Heidelberg, 2016. ISBN 978-3-662-48768-6.

[68] S. Pellegrino. *Deployable Structures*. CISM Courses and Lectures (CISM International Centre for Mechanical Sciences). Springer-Verlag Wien, 2001. doi: 10.1007/978-3-7091-2584-7.

[69] Mathias Persson, Kjell Anflo, Aaron Dinardi, and J. Bahu. A family of thrusters for adn-based monopropellant lmp-103s. In *48th AIAA/ASME/SAE/ASEE Joint Propulsion Conference & Exhibit*, 2012. doi: 10.2514/6.2012-3815.

[70] Michael Porter. The five competitive force that shape strategy. *Harvard Business Review*, R0801E, jan 2008.

[71] V. Pranesh, R. Velraj, S. Christopher, and V. Kumaresan. A 50 year review of basic and applied research in compound parabolic concentrating solar thermal collector for domestic and industrial applications. *Solar Energy*, 187:293 – 340, 2019. ISSN 0038-092X. doi: https://doi.org/10.1016/j.solener.2019.04.056.

[72] Xiaozhi Qi, Hailin Huang, Bing Li, and Zongquan Deng. A large deployable mechanism for space satellite antenna. *Aerospace Science and Technology*, Jun 2016.

[73] Darshan Ramasubramanian and Cayuela Vicenç Puig. *Identification and control of DC motors*. PhD thesis, Universitat Politècnica de Catalunya, 2016.

[74] Shama Rao. Carbon composites are becoming competitive and cost effective. Technical report, Infosys, 2018.

[75] V. Sambasiva Rao and Surendra Pal. High bit rate data transmitting system for remote sensing satellites. *High Frequency Electronics*, 1(1):18–26, apr 2009.

[76] W. M. Rowe. Sail film materials and supporting structure for a solar sail, a preliminary design. Contractor Report 19790007869, NASA Jet Propulsion Lab, 1978.

[77] Phillip A. Sabelhaus and John E. Decker. An overview of the James Webb Space Telescope (JWST) project. In John C. Mather, editor, *Optical, Infrared, and Millimeter Space Telescopes*, volume 5487, pages 550 – 563. International Society for Optics and Photonics, SPIE, 2004. doi: 10.1117/12.549895.

[78] Joseph Homer Saleh, Fan Geng, Michelle Ku, and Mitchell L. R. Walker II. Electric propulsion reliability: Statistical analysis of on-orbit anomalies and comparative analysis of electric versus chemical propulsion failure rates. *Acta Astronautica*, 139:141–167, jul 2017.

[79] Daniel Scheeres and Russell Schweickart. The mechanics of moving asteroids. In *Planetary Defense Conference: Protecting Earth from Asteroids*, 2004. doi: 10.2514/6.2004-1446.

[80] W.A. Schneider, J.L. Moore, T.L. Blakney, D.D. Smith, and J.D. Vacchione. An ultra-lightweight high gain spacecraft antenna. In *Proceedings of IEEE Antennas and Propagation Society International Symposium and URSI National Radio Science Meeting*. IEEE, jun 1994.

[81] D. Schrunk, B. Sharpe, B.L. Cooper, and M. Thangavelu. *The Moon: Resources, Future Development and Colonization*. Praxis Publishing Ltd.: Chichester, 1999.

[82] L. Scialino, A. Ihle, M. Migliorelli, N. Gatti, L. Datashvili, K. van 't Klooster, and J. Santiago Prowald. Large deployable reflectors for telecom and earth observation applications. *CEAS Space Journal*, 5(125), Jul 2013. doi: 10.1007/s12567-013-0044-7.

[83] Stephen Sinn. Historical mass, power, schedule & cost growth for nasa instruments & spacecraft, aug 2016.

[84] Sodern. Hydra: Multiple heads star tracker with high performance. Technical report, arianeGroup, may 2019.

[85] Witold M. Sokolowski and Seng C. Tan. Advanced self-deployable structures for space applications. *Journal of Spacecraft and Rockets*, 44(4):750–754, 2007. doi: 10.2514/1.22854.

[86] A. V. G. Subramanyam, D. Sivareddy, V. V. Srinivasan, and V. K. Hariharan. Multipaction-free combline diplexer for deep space applications. In *International Microwave and RF Conference (IMaRC)*. IEEE, dec 2014.

[87] Walter Tam, Arthur Jackson, Eiji Nishida, Yukikazu Kasai, Akio Tsujihata, and Kenichi Kajiwara. Design and manufacture of the ets viii xenon tank. In *36th AIAA/ASME/SAE/ASEE Joint Propulsion Conference and Exhibit*, 07 2000. doi: 10.2514/6.2000-3677.

[88] Marco Tantardini, Louis Friedman, John Brophy, Fred Culick, carlton allen, David Baughman, Julie Bellerose, Bruce Betts, Mike Brown, Michael Busch, John Casani, Marcello Coradin, John Dankanich, Paul Dimotakis, Martin Elvis, Ian Garrick-Bethel, Bob Gershman, Tom Jones, Damon Landau, and Donald Yeomans. Asteroid retrieval feasibility study. Technical report, Keck Institute for Space Studies, California Institute of Technology, Jet Propulsion Laboratory, 04 2012.

[89] Mr. Alberto Torre, Dr. Jesus Gonzalo, Ms. Rosa María Pulido, and Dr. Ramón Martínez. New generation ground segment architecture for leo satellites. In *57th International Astronautical Congress*, 2006. doi: 10.2514/6.IAC-06-B3.1.08.

[90] Viet-Hung Truong and Seung-Eock Kim. An efficient method of system reliability analysis of steel cable-stayed bridges. *Advances in Engineering Software*, 114:295–311, dec 2017. doi: https://doi.org/10.1016/j.advengsoft.2017.07.011.

[91] J. Tuttle, M. DiPirro, E. Canavan, and T. Hait. Thermal properties of double-aluminized kapton at low temperatures. In *AIP Conference Proceedings*, 2008. doi: https://doi.org/10.1063/1.2900367.

[92] W.T. Welford. *High Collection Nonimaging Optics*. Academic Press, 1989. 978-0-12-742885-7.

[93] James R. Wertz, David F. Everett, and Jeffery J. Puschell. *Space Mission Engineering: The New SMAD*. Space Technology Library, 2011.

[94] J. Jaap Wijker. *Spacecraft Design Loads*, pages 27–69. Springer Berlin Heidelberg, Berlin, Heidelberg, 2008. ISBN 978-3-540-75553-1. doi: 10.1007/978-3-540-75553-1_6.

[95] Jerome L. Wright. *Space Sailing*. Science. Taylor & Francis, 1992.

[96] Feng Xu and Yong Zhu. Highly conductive and stretchable silver nanowire conductors. *Advanced Materials*, 24(37):5117–5122, 2012.

[97] Longhai Zhao, Hao Wang, Genliang Chen, and Shunzhou Huang. Sequentially assembled reconfigurable extended joints: Self-lockable deployable structure. *Journal of Aerospace Engineering*, 31(6):04018103, 2018. doi: 10.1061/(ASCE)AS.1943-5525.0000877.

[98] Qiang Zhou, Longjiang Zhu, Haidong Fei, and Xingyou Wang. A reliability analysis tool for spacewire network. *AIP Conference Proceedings*, 1834(1):020008, 2017. doi: 10.1063/1.4981547.

[99] Shannon A. Zirbel, Robert J. Lang, Mark W. Thomson, Deborah A. Sigel, Phillip E. Walkemeyer, Brain P. Trease, Spencer P. Magleby, and Larry L. Howell. Accommodating thickness in origami-based deployable arrays. *Journal of Mechanical Design*, MD(13), Oct 2013. doi: 10.1115/1.4025372.

Appendix

Table 14-18. Average Mass by Subsystem as a Percentage of Dry Mass for 4 Types of Spacecraft. Types include those with no propulsion, those in Low-Earth Orbit with propulsion, those in high-Earth orbit, and planetary missions. See App. A for more information.

Subsystem (% of Dry Mass)	No Prop	LEO with Prop	High Earth	Planetary
Payload	41%	31%	32%	15%
Structure and Mechanisms	20%	27%	24%	25%
Thermal Control	2%	2%	4%	6%
Power (incl. harness)	19%	21%	17%	21%
TT&C	2%	2%	4%	7%
On-Board Processing	5%	5%	3%	4%
Attitude Determination and Control	8%	6%	6%	6%
Propulsion	0%	3%	7%	13%
Other (balance + launch)	3%	3%	3%	3%
Total	100%	100%	100%	100%
Propellant	0%	27%	72%	110%

Figure A.1: SMAD mass percentage estimation for a spacecraft bus without a propulsion system.


NAME
November, 2020
Nov 15
Nov 16
Nov 17
Nov 18
Nov 19
Nov 20
D Concept Generation
D.1 Discover Design Options
D.1.1 Discover Obvious Concepts
D.1.1.1 Brainstorm Concepts
D.1.1.2 Trigger-Word Concept Generation
D.1.1.3 Perform Morphological Analysis
D.1.1.4 Perform Synectics for Concept Generation
D.1.1.5 Find Known Concepts (from Lit. Study)
D.1.1.6 Create Sketches of Concepts (optional)
D.1.2 Discover Abstruse Concept
D.1.2.1 Brainstorm Abstruse Concepts
D.1.2.2 Check Sci-Fi Literature for Concepts
D.1.2.3 Create Sketches of Concepts (Optional)
D.1.3 Create Straw Man Concepts
D.1.4 Create DOT
D.1.4.1 Set-Up DOT
D.1.4.2 Include all Concepts in the DOT
D.2 Eliminate Obvious Unfeasible
D.2.1 Identify Obvious Unfeasible
D.2.1.1 Assess Technical Feasibility
D.2.1.2 Assess Economic Feasibility
D.2.1.3 Assess Planning Feasibility
D.2.1.4 Assess Legal Feasibility
D.2.1.5 Assess Operational Feas
D.2.2 Remove Obvious Unfeasible Concepts
D.3 Iterate DOT
D.3.1 Update DOT
D.3.1.1 Remove Eliminated Concepts
D.3.1.2 Format DOT
D.3.2 Present Design Options to
D.3.2.1 Go through Meeting Process [M]
D.3.3 Implement Customer Feed
D.3.3.1 Remove Eliminated Concepts
D.3.3.2 Include Additional Concepts
D.3.3.3 Format DOT
+ Add List
+ Add Folder
Productivity by ClickUp
NAME
28 NOV - 04 DEC
30 NOV - 06 DEC
07 DEC - 13 DEC
14 DEC - 20 DEC
21 DEC - 27 DEC
28 DEC - 03 JAN
F Concept Selection
F.1 Select Best Concept(s) based
F.1.1 Select Best Concept
F.1.1.1 Compare Trade-Off Results
F.1.1.2 Select Best Overall Design Concept
F.1.2 Present Chosen Concept
F.1.2.4 Present Concept
F.1.2.1 Create Presentable Overview of Concepts
F.1.2.2 Create Presentable Overview of the Trade-Off Proces
F.1.2.3 Go through Meeting Process [M]
F.1.3 Integrate Customer Feed
F.1.3.1 Analyse Customer Feedback Implications
F.1.3.2 Make Adjustments to Requirements
F.1.4 Review Concept
F.1.4.1 Review Requirements
F.1.4.2 Adjust Concepts
F.1.4.3 Review Adjusted Concepts
F.1.5 Accept/Reject Concept
F.1.5 Accept/Reject Concept
+ Add List
+ Add Folder

Functional Flow Diagram

Legend

- Top Level Function — 01.0
- Second Level Function — 01.1
- Third Level Function — 01.1.1

Top Level

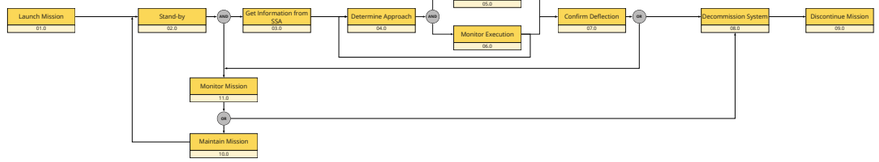

Second Level

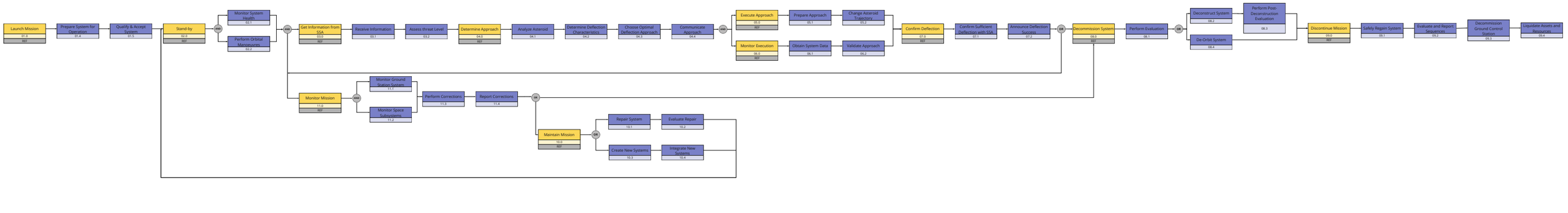

Third Level

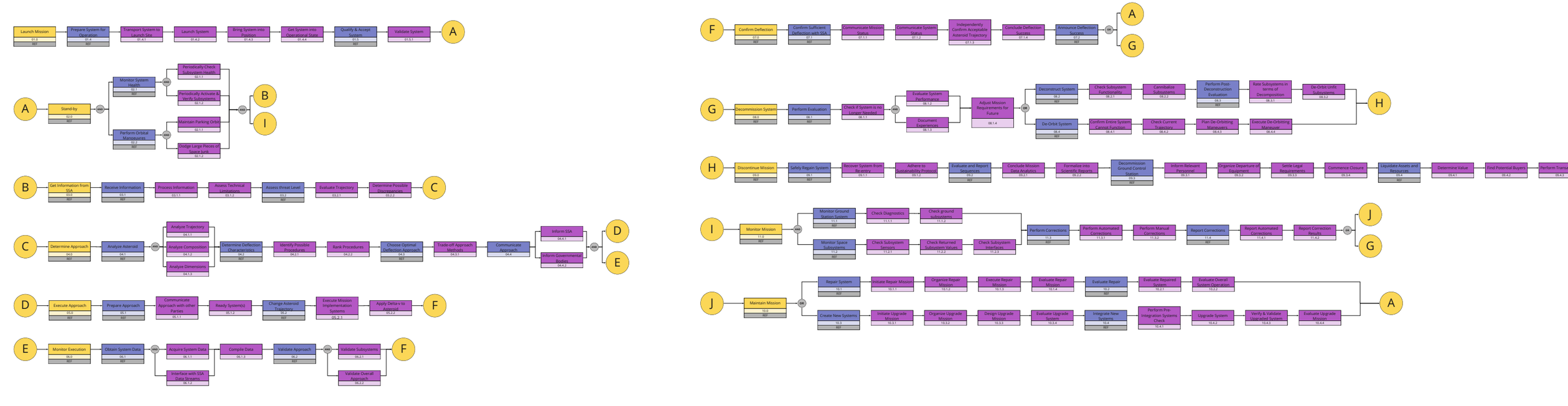

Functional Breakdown Structure

Legend

- Top Level Function — 01.0
- Second Level Function — 01.1
- Third Level Function — 01.1.1
- 01.1.1.1 Fourth Level Function

Launch Mission (01.0)

- Prepare System for Operation (01.4)
  - Transport System to Launch Site (01.4.1)
    - 01.4.1.1 Determine Launch Window
    - 01.4.1.2 Secure Payload for LV Integration
    - 01.4.1.3 Load Payload into Launch Vehicle
    - 01.4.1.4 Transport to Launch Position
  - Launch System (01.4.2)
    - 01.4.2.1 Set-up Launch
    - 01.4.2.2 Perform Weather and Visibility Check
    - 01.4.2.3 Initiate Launch Sequence
  - Bring System into Position (01.4.3)
    - 01.4.3.1 Initiate Separation Stages
    - 01.4.3.2 Achieve Desired Orbital Position
    - 01.4.3.3 Perform Diagnostics Check
  - Get System into Operational State (01.4.4)
    - 01.4.4.1 Deploy Structure
    - 01.4.4.2 Deploy Subsystems
    - 01.4.4.3 Initiate Mission Sequence
- Qualify & Accept System (01.5)
  - Validate System (01.5.1)
    - 01.5.1.1 Validate System Enviornment
    - 01.5.1.2 Correlate with Previous Missions
    - 01.5.1.3 Compare with Mission Simulation

Stand-by (02.0)

- Monitor System Health (02.1)
  - Periodically Check Subsystem Health (02.1.1)
    - 02.1.1.1 Acquire Status of Each Subsytem
    - 02.1.1.2 Ping Ground Station with Status
  - Periodically Activate & Verify Subsystems (02.1.2)
    - 02.1.2.1 Activate & Monitor Seperate Subsystem
    - 02.1.2.2 Send Data to Ground Station
    - 02.1.2.3 Verify Data & Perform Sanity Check
- Perform Orbital Manoeuvres (02.2)
  - Maintain Parking Orbit (02.2.1)
    - 02.2.1.1 Periodically Evaluate if Parking Orbit has been Maintained
    - 02.2.1.2 Boost System back into Parking Orbit when Necessary.
  - Dodge Large Pieces of Space Junk (02.2.2)
    - 02.2.2.1 Receive Information on Incoming Space Junk from SSA
    - 02.2.2.2 Raise or Lower Parking Orbit
    - 02.2.2.3 Await Space Junk Flyby
    - 02.2.2.4 Return to Original Parking Orbit

Get Information from SSA (03.0)

- Receive Information (03.1)
  - Process Information (03.1.1)
    - 03.1.1.1 Ensure all relevant information is handed over
    - 03.1.1.2 Establish clear communication line for mission development
  - Assess Technical Limitations (03.1.2)
    - 03.1.2.1 Process Technical Data
    - 03.1.2.2 Determine Clear Threat Level
- Assess threat Level (03.2)
  - Evaluate Trajectory (03.2.1)
    - 03.2.1.1 Check for Hazardous Intersections
    - 03.2.1.2 Check for gravitational influences on asteroid
  - Determine Possible Discrepancies (03.2.2)
    - 03.2.2.1 Assess given discrepancies
    - 03.2.2.2 Determine range of possible masses
    - 03.2.2.3 Determine range of possible trajectories
    - 03.2.2.4 Select worst case scenario

Determine Approach (04.0)

- Analyze Asteroid (04.1)
  - Analyze Trajectory (04.1.1)
    - 04.1.1.1 Compile Trajectory Data
    - 04.1.1.2 Determine Uncertainties
    - 04.1.1.3 Simulate Possible Asteroid Paths
    - 04.1.1.4 Rank Trajectories for Probability
    - 04.1.1.5 Rank Trajectories for Impact
    - 04.1.1.6 Determine Critical Trajectory / -ies
  - Analyze Composition (04.1.2)
    - 04.1.2.1 Determine Type of Asteroid
    - 04.1.2.2 Determine Uncertainties
    - 04.1.2.3 Determine Possible Asteroid Compositions
    - 04.1.2.4 Rank Compositions for Probability
    - 04.1.2.5 Rank Compositions for Impact
    - 04.1.2.6 Rank Compositions for Risk
    - 04.1.2.7 Determine Critical Composition
  - Analyze Dimensions (04.1.3)
    - 04.1.3.1 Determine Dimensions of Asteroid
    - 04.1.3.2 Determine Uncertainties
    - 04.1.3.3 Rank Dimensions for Probability
    - 04.1.3.4 Rank Dimensions for Impact
    - 04.1.3.5 Rank Dimensions for Risk
    - 04.1.3.6 Determine Critical Dimensions
- Determine Deflection Characteristics (04.2)
  - Identify Possible Procedures (04.2.1)
    - 04.2.1.1 Determine Approach Methods
    - 04.2.1.2 Trade-off Sustainability/Efficiency
  - Rank Procedures (04.2.2)
    - 04.2.2.1 Determine Probability of Failure
    - 04.2.2.2 Determine Impact of Failure
    - 04.2.2.3 Rank Procedures for Risk
- Choose Optimal Deflection Approach (04.3)
  - Trade-off Approach Methods (04.3.1)
    - 04.3.1.1 Assess Ranking Procedure (04.2.2)
    - 04.3.1.2 Check Compliance with Budget
    - 04.3.1.3 Determine Most Feasible Methods
- Communicate Approach (04.4)
  - Inform SSA (04.4.1)
  - Inform Governmental Bodies (04.4.2)

Execute Approach (05.0)

- Prepare Approach (05.1)
  - Communicate Approach with other Parties (05.1.1)
    - 05.1.1.1 Communicate with ESA
    - 05.1.1.2 Communicate with Nation of Asteroid Impact location
    - 05.1.1.3 Press Release with Media
  - Ready System(s) (05.1.2)
    - 05.1.2.1 Confirm all Subsystems are Online
    - 05.1.2.2 Manouver System into Position
    - 05.1.2.3 Ready Subsystems
- Change Asteroid Trajectory (05.2)
  - Execute Mission Implementation Systems (05.2.1)
    - 05.2.1.1 Review Approach Plan
    - 05.2.1.2 Activate Mission Implementation Subsytems
  - Apply Delta-v to Asteroid (05.2.2)
    - 05.2.2.1 Keep Mission Implementation Systems Activated
    - 05.2.2.2 Confirm with SSA sufficient Delta-v has been Applied
    - 05.2.2.3 Deactivate Mission Implementation Systems

Monitor Execution (06.0)

- Obtain System Data (06.1)
  - Acquire System Data (06.1.1)
    - 06.1.1.1 Uplink Sensor Data Request
    - 06.1.1.2 Compile Data for Downlink
    - 06.1.1.3 Recieve Sensor Data from Downlink
  - Interface with SSA Data Streams (06.1.2)
    - 06.1.2.1 Request Relevant Data from SSA
    - 06.1.2.2 Establish Data Stream Download
    - 06.1.2.3 Store Data
  - Compile Data (06.1.3)
    - 06.1.3.1 Compile Data with the use of Tools
    - 06.1.3.2 Display Data in a Clear Way
    - 06.1.3.3 Analyze Data
    - 06.1.3.4 Perform Sanity Check
- Validate Approach (06.2)
  - Validate Subsystems (06.2.1)
    - 06.2.1.1 Gather Data of each Subsystem
    - 06.2.1.2 Confirm each Subsystem is Nominal
  - Validate Overall Approach (06.2.2)
    - 06.2.2.1 Gather Data of Relevant Subsystems
    - 06.2.2.2 Gather Relevant Data of SSA Stream
    - 06.2.2.3 Comfirm Approach is Nominal

Confirm Deflection (07.0)

- Confirm Sufficient Deflection with SSA (07.1)
  - Communicate Mission Status (07.1.1)
    - 07.1.1.1 Check status of space system
    - 07.1.1.2 Check status of asteroid trajectory
    - 07.1.1.3 Prepare system information for transmission
    - 07.1.1.4 Relay information to ground station
    - 07.1.1.5 Perform sanity check on information
  - Communicate System Status (07.1.2)
    - 07.1.2.1 Check all subsystems
    - 07.1.2.2 Prepare information for transmission
    - 07.1.2.3 Relay information to ground station
    - 07.1.2.4 Perform sanity check on information
  - Independently Confirm Acceptable Asteroid Trajectory (07.1.3)
    - 07.1.3.1 Process information received
    - 07.1.3.2 Simulate possible post-deflection asteroid trajectories
    - 07.1.3.3 Perform analysis of the simulations
    - 07.1.3.4 Compare best possible outcome to current deflection outcome
    - 07.1.3.5 Relay outcome to approved parties
  - Conclude Deflection Success (07.1.4)
    - 07.1.4.1 Verify deflection is successful with approved parties
    - 07.1.4.2 Confirm stakeholder approval
- Announce Deflection Success (07.2)

Decommission System (08.0)

- Perform Evaluation (08.1)
  - Check if system is no longer needed (08.1.1)
    - 08.1.1.1 Evaluate set of other possible candidate asteroids
    - 08.1.1.2 Compare previous mission timeline to that required for other candidates
    - 08.1.1.3 Confirm possible new timelines do not overlap
  - Evaluate System Performace (08.1.2)
    - 08.1.2.1 Review system executions during previous mission
    - 08.1.2.2 Compare to validation set
    - 08.1.2.3 Check performance of subsystems with a validation set
  - Document Experiences (08.1.3)
    - 08.1.3.1 Review all mission events
    - 08.1.3.2 Review all system executions
    - 08.1.3.3 Document outcome of executions
  - Adjust Mission Requirements for Future (08.1.4)
    - 08.1.4.1 Filter out expected execution and outcome pairs
    - 08.1.4.2 Generate list of possible solutions to unexpected events
    - 08.1.4.3 Simulate previous mission with possible solutions
    - 08.1.4.4 Keep solutions with best outcomes
- Deconstruct System (08.2)
  - Check Subsystem Functionality (08.2.1)
    - 08.2.1.1 Perform subsystem tests
    - 08.2.1.2 Send test outcomes to ground station
    - 08.2.1.3 Verify test results
    - 08.2.1.4 Validate subsystems
  - Cannibalize Subsystems (08.2.2)
    - 08.2.2.1 Determine remaining lifecycle of subsystems
    - 08.2.2.2 Perform subsystem tests
    - 08.2.2.3 Determine reusability of subsystems
    - 08.2.2.4 Sequester reusable subsystems
- Conduct Post Deconstruction Assessment (08.3)
  - Rate Subsystems in terms of Decomposition (08.3.1)
    - 08.3.1.1 Develop a suitable rating system
    - 08.3.1.2 Perform a visual check on subsystems
    - 08.3.1.3 Compare to images from construction
    - 08.3.1.4 Review previous verifications
  - De-Orbit Unfit Subsystems (08.3.2)
    - 08.3.2.1 Simulate possible de-orbiting process
    - 08.3.2.2 Select least harmful process
    - 08.3.2.3 Execute chosen process
    - 08.3.2.4 Review outcome of the process
- De-Orbit System (08.4)
  - Confirm Entire System Cannot Function (08.4.1)
    - 08.4.1.1 Confirm total decomposition of all subsystems
    - 08.4.1.2 Check if subsystems no longer fulfill any requirements
    - 08.4.1.3 Notify stakeholders about status
  - Check Current Trajectory (08.4.2)
    - 08.4.2.1 Check orbits of all satellites
    - 08.4.2.2 Confirm there would be no collisions
  - Plan De-Orbitting Maneuvers (08.4.3)
    - 08.4.3.1 Generate de-orbitting options
    - 08.4.3.2 Simulate all options
    - 08.4.3.3 Select options with no ground impact
    - 08.4.3.4 Select most efficient option
  - Execute De-Orbitting Maneuver (08.4.4)

Discontinue Mission (09.0)

- Safely Regain System (09.1)
  - Recover System from Re-entry (09.1.1)
    - 09.1.1.1 Assess Touch Down Location
    - 09.1.1.2 Determine legal Implications
    - 09.1.1.3 Determine System Recovery Method
  - Adhere to Sustainability Protocol (09.1.2)
    - 09.1.2.1 Assess any possible leaks
    - 09.1.2.2 Remove waste from landing site
- Evaluate and Report Sequences (09.2)
  - Conclude Mission Data Analytics (09.2.1)
    - 09.2.1.1 Perform Data Extraction Method
    - 09.2.1.2 Verify if Data is Logical
  - Formalize into Scientific Reports (09.2.2)
    - 09.2.2.1 Report Mission Data
    - 09.2.2.2 Adhere to correct formatting
- Decommission Ground Control Station (09.3)
  - Inform Relevant Personnel (09.3.1)
    - 09.3.1.1 Notify Management
    - 09.3.1.2 Prepare Notification of other Personnel
  - Organize Departure of Equipment (09.3.2)
    - 09.3.2.1 Deconstruct Equipment
    - 09.3.2.2 Package equipment
    - 09.3.2.3 Organize by Department
  - Settle Legal Requirements (09.3.3)
    - 09.3.3.1 Contact Relevant Parties
    - 09.3.3.2 Organize meetings
  - Commence Closure (09.3.4)
    - 09.3.4.1 Determine Date of Closure
    - 09.3.4.2 Adhere to Security Protocol
- Liquidate Assets and Resources (09.4)
  - Determine Value (09.4.1)
    - 09.4.1.1 Generate list of all items in inventory
    - 09.4.1.2 Research approximate price of each item
    - 09.4.1.3 Determine depreciation of all items
  - Find Potential Buyers (09.4.2)
    - 09.4.2.1 Announce Liquidation
    - 09.4.2.2 Interview potential buyers
    - 09.4.2.3 Generate list of buyers
  - Perform Transactions (09.4.3)
    - 09.4.3.1 Sign relevant documents
    - 09.4.3.2 Generate list of bank account numbers

Maintain Mission (10.0)

- Repair System (10.1)
  - Initiate Repair Mission (10.1.1)
  - Organize Repair Mission (10.1.2)
    - 10.1.2.1 Identify Requirements
    - 10.1.2.2 Design Repair System
    - 10.1.2.3 Schedule Mission
    - 10.1.2.4 Allocate Resources
    - 10.1.2.5 Determine if Overall Mission has to be Paused
  - Execute Repair Mission (10.1.3)
    - 10.1.3.1 Prepare for Executing Repair
    - 10.1.3.2 Execute Repair
    - 10.1.3.3 Monitor Repair
    - 10.1.3.4 Monitor Schedule
    - 10.1.3.5 Monitor Resources
  - Evaluate Repair Mission (10.1.4)
- Evaluate Repair (10.2)
  - Evaluate Repaired System (10.2.1)
    - 10.2.1.1 Validate repaired subsystems
    - 10.2.1.2 Note discrepancies
    - 10.2.1.3 Make adjustments for future repairs
  - Evaluate Overall System Operation (10.2.2)
    - 10.2.2.1 Run a systems check
    - 10.2.2.2 Monitor repaired system
    - 10.2.2.3 Correct repair procedures for future
- Create New Systems (10.3)
  - Initiate Upgrade Mission (10.3.1)
    - 10.3.1.1 Analyze previous upgrades
    - 10.3.1.2 Generate Launch Procedures
  - Organize Upgrade Mission (10.3.2)
    - 10.3.2.1 Identify Requirements
    - 10.3.2.2 Schedule Mission
    - 10.3.2.3 Allocate Resources
  - Design Upgrade Mission (10.3.3)
    - 10.3.3.1 Design Upgrade System
    - 10.3.3.2 Determine if Overall Mission has to be Paused
    - 10.3.3.3 Develop Procedures for Executing Upgrade
  - Evaluate Upgrade System (10.3.4)
    - 10.3.4.1 Verify & Validate Subsystems
    - 10.3.4.2 Verify Upgrade System
- Integrate New Systems (10.4)
  - Perform Pre-Integration Systems Check (10.4.1)
  - Upgrade System (10.4.2)
    - 10.4.2.1 Adhere to 'Execute Repair Mission' (10.1.3) for Similar Approach
  - Verify & Validate Upgraded System (10.4.3)
    - 10.4.3.1 Perform System Functionality Check
    - 10.4.3.2 Compare Output with Desired Result
  - Evaluate Upgrade Mission (10.4.4)
    - 10.4.4.1 Advance with Mission Protocol

Monitor Mission (11.0)

- Monitor Ground Station System (11.1)
  - Check Diagnostics (11.1.1)
    - 11.1.1.1 Review efficiency of previous missions
    - 11.1.1.2 Perform stress tests
    - 11.1.1.3 Adjust procedures
    - 11.1.1.4 Check system needs
    - 11.1.1.5 Adjust resources to fulfill needs
  - Check ground subsystems (11.1.2)
    - 11.1.2.1 Review incoming subsystem data
    - 11.1.2.2 Perform performance tests
    - 11.1.2.3 Compare to validation set
- Monitor Space Subsystems (11.2)
  - Check Subsystem Sensors (11.2.1)
    - 11.2.1.1 Perform sanity checks on sensors
    - 11.2.1.2 Generate list of possible errors
    - 11.2.1.3 Correct errors where necessary
  - Check Returned Subsystem Values (11.2.2)
    - 11.2.2.1 Check incoming values for errors
    - 11.2.2.2 Require repairs for any errors
  - Check Subsystem Interfaces (11.2.3)
    - 11.2.3.1 Feed subsystems predefined values
    - 11.2.3.2 Check outputs of subsystems
    - 11.2.3.3 Compare example outputs to current outputs
    - 11.2.3.4 Correct for errors
- Perform Corrections (11.3)
  - Perform Automated Corrections (11.3.1)
    - 11.3.1.1 Execute on-board error management
    - 11.3.1.2 Implement automated corrections
  - Perform Manual Corrections (11.3.2)
    - 11.3.2.1 Draft Corrections
    - 11.3.2.2 Simulate correction outcomes
    - 11.3.2.3 Send selected corrections to space system
    - 11.3.2.4 Interpret Corrections
- Report Corrections (11.4)
  - Report Automated Corrections (11.4.1)
    - 11.4.1.1 Record all executed corrections
    - 11.4.1.2 Prepare for transmission
    - 11.4.1.3 Send to ground system
  - Report Correction Results (11.4.2)
    - 11.4.2.1 Observe satellite corrections with ground system
    - 11.4.2.2 Observe corrections with space system
    - 11.4.2.3 Compile both sets of observations
    - 11.4.2.4 Compare Observations
    - 11.4.2.5 Note Discrepancies